

UNIVERSITY OF SOUTHAMPTON
Faculty of Engineering, Science and Mathematics
School of Chemistry

**Development & Application
of UV-Visible Microspectrometry
to Solid Phase Organic Chemistry**

By

Lu Shin Wong

Doctor of Philosophy

May 2005

UNIVERSITY OF SOUTHAMPTON

ABSTRACT

Faculty of Engineering, Science and Mathematics

School of Chemistry

Doctor of Philosophy

Development & Application of UV-Visible Microspectrometry to Solid Phase Organic Chemistry

by Lu Shin Wong

The development and initial testing of a custom built UV-Visible microspectrometer for the analysis of materials supported on resins at the single-bead level is described with qualitative, quantitative and time-resolved UV-Vis spectroscopy being demonstrated with a variety of resins and supported chromophores.

On-bead UV-Vis spectroscopy was extended to a variety of applications including the development of fibre-optic pH sensors utilising indicator dyes covalently attached to macroporous controlled pore glass beads and procedures for the attachment of carboxyl- and aniline-functionalised dyes to glass beads and for interfacing a single sensor bead to a UV-Vis spectrometer are described.

Analysis of solid-supported chromophoric metal ligands was conducted for the detection and assessment of solid-supported tripeptides with high affinity for Cu, Ni and Co from a combinatorial “split-and-mix” library. The affinity of the various actively binding peptide sequences were estimated by quantifying the amount of chromophore produced within individual beads when exposed to an appropriate staining reagent.

On-bead e.e. determination of polystyrene-supported leucine and phenylalanine was also demonstrated by parallel kinetic chiral resolution using pseudoenantiomeric chromophore probes, followed by on-bead UV-Vis microspectrometric quantification of the attached probes. The e.e. measurement was conducted without the need for cleavage of the substrates from the resin at any stage and was successful even with low resin loadings.

For Dad, Kuma and Lu Kenn

Declaration of Authorship

I, Lu Shin Wong, declare that the thesis entitled *Development & Application of UV-Visible Microspectrometry to Solid Phase Organic Chemistry* and the work presented within it are my own. I further confirm that:

- The research described was conducted wholly at the University of Southampton under the supervision of Prof. Mark Bradley between October 2001 and November 2004;
- No part of this thesis has been previously submitted at this or any other university;
- Where I have consulted the published work of others, this is always clearly attributed and where I have quoted from the work of others, the source is always given. With the exception of such quotations, this thesis is entirely my own work;
- I have acknowledged all main sources of help and where the thesis is based on work done by myself jointly with others, I have made clear exactly what was done by others and what I have contributed myself (see acknowledgements section);
- Parts of this work have been published as:
 - 1) J. K. Cho, L. S. Wong, T. W. Dean, O. Ichihara, C. Muller, M. Bradley: pH Indicating Resins. *Chem. Commun.*, 2004, 1470-1471.
 - 2) L. S. Wong, F. Birembaut, W. S. Brocklesby, J. G. Frey, M. Bradley: Resin Bead Micro-UV-Visible Absorption Spectroscopy. *Anal. Chem.*, 2005, **77**, 2247-2251.
 - 3) L. S. Wong, W. S. Brocklesby, M. Bradley: Fibre Optic pH Sensors Employing Tethered Non-Fluorescent Indicators on Macroporous Glass. *Sens. Actuators B. Chem.*, 2005, **107**, 957-962 (Initial results presented at the Colorchem 2004 Conference)
 - 4) L. S. Wong, M. Bradley: Immobilisation and Assessment of Aniline-Functionalised Dyes for Non-Fluorescent pH Sensing Applications. *Tetrahedron Lett.*, 2005, **46**, *Accepted*.

Lu Shin Wong

20 July 2005

Acknowledgements

Over the course of this PhD, there are so many I would like to thank for having helped me in so many ways to run/walk/crawl/stagger the whole distance. It is my regret that I can only name but a few in the small space I have here.

First of all, I wish thank my supervisor, Prof. Mark Bradley, for providing me with the opportunity to carry out this work and for his guidance throughout the research described in this thesis.

Equally importantly, this research was made possible in part by collaboration with a number of capable scientists to whom I would like to express my appreciation: Dr. Fabrice Birembaut who constructed the UV-Vis microspectrometer and Dr. Jeremy Frey, his supervisor, with whom I have had many informative discussions; Dr. Jin Ku Cho, who provided the (4-carboxyphenyl)-Bromophenol Blue and the pH indicating resins described in Chapter 2; And also Dr. William Brocklesby and members of his research group at the Optoelectronics Research Centre, for teaching me the skills for handling optical fibres necessary for building the sensors in Chapter 3.

I also offer my unreserved gratitude to the numerous members of the Bradley research group between 2001 and 2005, and in particular the members of Lab 4009 (and previously 4005), for putting up with me through the highs and lows of PhD-hood, both in and outside of work. All those discussions we have had about the Thursday meeting problems, all aspects of chemistry and life in general have formed a major part of my education.

To members of the wardenal team of Glen Eyre and Chamberlain Halls from 2001 to 2005 and especially the veterans of the hall dinner table, thank you all for being part of my Southampton experience, for all the social outings and for being a source of some terrific conversations. I shall miss being part of the team.

Finally but perhaps most importantly, I wish to express my gratitude to friends and family, near and far, for their unwavering support, encouragement and belief in me.

Lu Shin Wong
Southampton
July 2005

Abbreviations

Standard IUPAC nomenclature used for elements, units of measurement and 3-letter abbreviations for amino acids.

| | |
|-----------------|---|
| Ac | Acetyl |
| ϵ Ahx | 6-Aminohexanoyl |
| AM-PS | Aminomethyl polystyrene |
| AP-CPG | Aminopropyl controlled pore glass |
| aq. | Aqueous |
| Ar | Aryl |
| ATR | Attenuated total reflectance |
| Bn | Benzyl |
| Boc | <i>tert</i> -Butyloxycarbonyl |
| ^t Bu | <i>tert</i> -Butyl |
| 4CBCP | (4-carboxyphenyl)-Bromocresol Purple |
| 4CBPB | (4-Carboxyphenyl)-Bromophenol Blue |
| 4CBTB | (4-carboxylphenyl)-Bromothymol Blue |
| Cbz | Benzyloxycarbonyl |
| CD | Circular dichroism |
| CgR | Congo Red |
| CIE | Commision Internationale de L'Eclairage |
| Cl-PS | Chloromethyl polystyrene |
| Clt | 2-Chlorotrityl (linker) |
| CPG | Controlled Pore Glass |
| DB3 | Disperse Black 3 |
| DBU | 1,8-Diazabicyclo(5.4.0)undec-7-ene |
| DCCI | <i>N,N'</i> -Dicyclohexylcarbodiimide |
| DCM | Dichloromethane |
| Dde | (4,4-Dimethyl-2,6-dioxocyclohex-1-ylidene)ethyl |
| DIC | <i>N,N'</i> -Diisopropylcarbodiimide |
| DIPEA | <i>N</i> -Ethyl-diisopropylamine |
| DMAP | 4-Dimethylaminopyridine |

| | |
|-----------------|---|
| DMF | <i>N,N</i> -Dimethylformamide |
| DMSO | Dimethylsulfoxide |
| Dmt | 4,4'-Dimethoxytrityl |
| DNP | 2,4-Dinitrophenylhydrazine |
| DRIFTS | Diffuse reflectance infrared Fourier transform spectroscopy |
| DTNB | 5,5'-Dithio-bis(2-nitrobenzoic acid) |
| e.e. | Enantiomeric excess |
| Et | Ethyl |
| FDPP | Pentafluorophenyl diphenylphosphinate |
| Fmoc | 9-Fluorenylmethoxycarbonyl |
| FT-IR | Fourier transform infrared (spectroscopy) |
| HOBt | 1-Hydroxybenzotriazole |
| HOPfp | Pentafluorophenol |
| HOSu | <i>N</i> -Hydroxysuccinimide |
| HPLC | High pressure liquid chromatography |
| IR | Infrared (spectroscopy) |
| MAS | Magic angle spinning |
| Me | Methyl |
| MO1 | Mordant Orange 1 |
| mol. eq. | Molar equivalent(s) |
| MS | Mass spectrometry |
| NMM | <i>N</i> -Methylmorpholine |
| NMP | <i>N</i> -Methyl-2-pyrrolidinone |
| NMR | Nuclear magnetic resonance (spectroscopy) |
| Np | 4-Nitrophenyl |
| PEG | Polyethylene glycol |
| Pfp | 4-Pentafluorophenyl |
| Ph | Phenyl |
| <i>p</i> MR | <i>para</i> -Methyl Red |
| PNBP | <i>para</i> -Nitrobenzylpyridine |
| POEPOP | Polyoxyethylene-polyoxypropylene (resin) |
| ⁱ Pr | <i>iso</i> -Propyl / isopropyl |
| PS | Polystyrene |

| | |
|--------|---|
| PyBOP | Benzotriazole-1-yl-oxy-tris-pyrrolidino-phosphonium hexafluorophosphate |
| PyBroP | bromo-tris-pyrrolidino-phosphonium hexafluorophosphate |
| Pyr | Pyroglutamate |
| RT | Room temperature |
| SPOS | Solid phase organic synthesis |
| TFA | Trifluoroacetic acid |
| TFFH | <i>N,N,N',N'</i> -Tetramethylfluoroformamidinium hexafluorophosphate |
| TG | TentaGel® (amino functionalised) |
| THF | Tetrahydrofuran |
| TIPS | Tri(isopropyl)silane |
| TLC | Thin-layer chromatography |
| TNBS | 2,4,6-Trinitrobenzenesulfonic acid |
| TPM | Two-photon microscopy |
| Trt | Trityl |
| Ts | <i>para</i> -Toluenesulfonyl / Tosyl |
| UV | Ultraviolet |
| UV-Vis | Ultraviolet-visible (spectroscopy) |
| Xaa | Unspecified amino acid residue |

Permissions sought and granted from the publishers for the following copyrighted materials:

Figure 1.6: Image & inset from Fig. 2 in ref. 47 (American Chemical Society)

Figure 1.7: Image from Fig. 2 in ref. 52 (American Chemical Society)

Figure 1.8: Spectra from Fig. 2 in ref. 59 (Wiley-VCH)

Figure 1.9: Spectra from Fig. 2 in ref. 66 (Bentham Science Publishers)

Figure 1.10: Images from Fig. 6 in ref. 75 (American Chemical Society)

Figure 1.11: Images from Figs. 9-11 in ref. 74 (Advanstar Communications)

Figure 1.15: Image from Fig. 2 in ref. 86 (Wiley-VCH)

Figure 1.16: Images from Fig. 1d, 2a in ref. 90 (Wiley-VCH)

Figure 1.17: Image from Fig. 4 in ref. 92 (American Chemical Society)

Figure 1.18: Image from Fig. 8 in ref. 92 (American Chemical Society)

Figure 1.19: Image from Fig. 10 in ref. 92 (American Chemical Society)

Figure 1.20: Spectra from Fig. 1 in ref. 97 (American Chemical Society)

Figure 1.21: Spectra from Fig. 1 in ref. 99 (Elsevier)

Figure 1.22: Spectra and graph from Fig. 1, 2 in ref. 102 (American Chemical Society)

Figure 1.23: Diagram from Fig. 1 in ref. 105 (Society for Applied Spectroscopy) and Diagram from Fig. 1 in ref. 106 (American Chemical Society)

Figure 1.24: Spectra from Fig. 1a,b in ref. 111 (American Chemical Society)

Figure 1.25: Image and spectra from Fig. 5, 6 in ref. 112 (Wiley-VCH)

Figure 1.26: Image from Fig. 1 in ref. 113 (American Chemical Society)

Figure 1.27: Image from Fig. 3a in ref. 115 (Society for Applied Spectroscopy)

Figure 1.28: Image from Fig. 6 in ref. 115 (Society for Applied Spectroscopy)

Figure 1.29: Spectra from Fig. 1, 2 in ref. 119 (Society for Applied Spectroscopy)

Figure 1.30: Graph from Fig. 9 in ref. 119 (Society for Applied Spectroscopy)

Figure 1.31: Spectra from Fig. 2b in ref. 111 (American Chemical Society)

Figure 1.32: Image from Fig. 2 in ref. 121 (Wiley-VCH)

Figure 1.33: Image from Fig. 5b,c in ref. 89 (American Chemical Society)

Figure 1.34: Image from Fig. 6b,c in ref. 89 (American Chemical Society)

Figure 1.35: Spectra from Fig. 4 in ref. 122 (American Chemical Society)

Figure 1.36: Graph from Fig. 6 in ref. 122 (American Chemical Society)

Scheme 1.14: Inset image from Fig.2 in ref. 48 (American Chemical Society)

Figure 4.4 Image from Fig. 2 in ref. 170 (American Chemical Society)

Figure 5.2 Spectra from Fig. 1 in ref. 211 (Elsevier)

Scheme 5.2 Scheme and figure from Sch. 1 and Fig. 2 in ref. 210 (American Chemical Society)

Table of Contents

| | |
|---|-----------|
| 1 Introduction: Analytical Methods for Solid Phase Organic Synthesis..... | 1 |
| 1.1 Colorimetric Tests for Solid Phase Organic Synthesis | 2 |
| 1.1.1 Detection of Amines | 2 |
| 1.1.2 Detection of Hydroxyl and Phenol Groups..... | 7 |
| 1.1.3 Detection of Thiols | 9 |
| 1.1.4 Detection of Aldehydes and Ketones..... | 10 |
| 1.1.5 Detection of Carboxylic Acids | 11 |
| 1.1.6 Detection of Aliphatic Halides | 11 |
| 1.1.7 Bead-based self-indicating colorimetric sensors..... | 12 |
| 1.2 Nuclear Magnetic Resonance Spectroscopy | 14 |
| 1.2.1 Gel Phase NMR Spectroscopy | 14 |
| 1.2.2 Magic Angle Spinning NMR Spectroscopy..... | 17 |
| 1.3 Mass Spectrometry | 18 |
| 1.3.1 Matrix Assisted Laser Desorption Ionisation MS | 19 |
| 1.3.2 Secondary Ion MS | 20 |
| 1.3.3 Electron Impact MS | 23 |
| 1.3.4 Dual Linker Analytical Constructs for MS | 23 |
| 1.4 Optical Microspectroscopy..... | 25 |
| 1.4.1 Fluorescence Microspectroscopy | 25 |
| 1.4.1.1 Fluorescent confocal scanning microscopy..... | 25 |
| 1.4.1.2 Two-photon fluorescence laser scanning microscopy | 28 |
| 1.4.2 Infra-Red Microspectroscopy..... | 30 |
| 1.4.2.1 Single-bead reaction monitoring and kinetics | 31 |
| 1.4.2.2 Combinatorial library identification and mapping..... | 34 |
| 1.4.2.3 Functional group distribution mapping on single beads | 38 |
| 1.4.3 Raman Microspectroscopy..... | 39 |
| 1.4.3.1 Solid phase batch analysis..... | 39 |
| 1.4.3.2 Raman microscopy for single-bead analysis | 42 |
| 1.4.3.3 Confocal Raman microscopy..... | 43 |
| 1.5 Aims of the Research: UV-Visible Microspectrometry for Solid Supports..... | 46 |
| 2 On-bead UV-Visible Microspectrometry..... | 48 |
| 2.1 Design and Operation of UV-Vis Microspectrometer..... | 48 |
| 2.2 Results and Discussion..... | 49 |
| 2.2.1 Initial Testing and Observations..... | 49 |
| 2.2.2 Qualitative Analysis..... | 52 |
| 2.2.3 Quantitative Analysis..... | 55 |
| 2.2.4 UV-Visible Profiling of Solid Supported pH Indicator Dyes | 57 |
| 2.2.5 Analysis of pH-Indicating Resins..... | 61 |
| 2.2.6 Real-Time Reaction Monitoring and Reaction Kinetics..... | 63 |
| 2.3 Conclusions | 65 |

| | |
|--|------------|
| 3 Development of Fibre Optic UV-Visible pH Sensors | |
| Utilising Tethered Indicator Dyes..... | 66 |
| 3.1 Introduction: Fibre Optic pH Sensing..... | 66 |
| 3.2 Sensors Bearing Carboxy-Functionalised Indicator Dyes..... | 70 |
| 3.2.1 Attachment of Carboxy-Functionalised Dyes to Macroporous Glass Beads | 70 |
| 3.2.2 Construction and Testing of Sensor Assembly | 72 |
| 3.3 Sensors Bearing Aniline-Functionalised Indicator Dyes | 75 |
| 3.3.1 Investigation of Attachment Methods for Aniline-Functionalised Dyes.. | 76 |
| 3.3.2 Assessment of Sensors | 79 |
| 3.4 Conclusions | 82 |
| 4 UV-Visible Microspectrometry for the Analysis of Solid-Supported Peptide-Metal Complexes | 83 |
| 4.1 Introduction: Combinatorial Generation of Peptide-Metal Complexes | 83 |
| 4.2 Combinatorial Generation of the Peptide Library | 87 |
| 4.3 Microscopic and UV-Visible Microspectrometric Analysis of Metal Complexed Peptide Libraries | 89 |
| 4.3.1 Microscopic Analysis of Supported Complexes | 89 |
| 4.3.2 UV-Vis Microspectrometry of Stained Members of Library..... | 91 |
| 4.3.2.1 Analysis of copper-binding beads..... | 92 |
| 4.3.2.2 Analysis of nickel-binding beads..... | 95 |
| 4.3.2.3 Analysis of cobalt-binding beads..... | 95 |
| 4.4 Sequencing of Metal-Binding Peptides and Correlation with UV-Visible Spectra | 98 |
| 4.5 Conclusions | 101 |
| 5 On-bead Determination of Enantiomeric Excess by UV-Visible Microspectrometry..... | 102 |
| 5.1 Introduction: Kinetic Resolution of Chiral Compounds | 102 |
| 5.2 Syntheses of Pseudoenantiomeric Chiral Probes | 108 |
| 5.3 Chiral Resolution of On-bead Amino Acids and UV-Visible Microspectrometric Analysis | 111 |
| 5.4 Conclusions | 114 |
| 6 Experimental Procedures | 115 |
| 6.1 General | 115 |
| 6.1.1 Instrumentation..... | 115 |
| 6.1.2 Chemicals & Materials | 116 |
| 6.1.3 Solid Phase Resin Tests | 117 |
| 6.1.3.1 Quantitative Ninhydrin Test..... | 117 |
| 6.1.3.2 Quantitative Fmoc Test..... | 118 |
| 6.1.3.3 Chloranil Test for Secondary Amines..... | 118 |
| 6.2 Experimental procedures for chapter 2..... | 118 |
| 6.2.1 UV-Visible Microspectrometer Specifications | 118 |
| 6.2.2 Solid-Phase UV-Visible Spectra Acquisition and Processing | 119 |

| | |
|---|------------|
| 6.2.3 Assessment of Lensing Effect | 119 |
| 6.2.4 Coupling of Indicator Dyes to Solid Supports | 120 |
| 6.2.4.1 Coupling of <i>para</i> -Methyl Red to Aminomethyl Polystyrene or TentaGel | 120 |
| 6.2.4.2 Coupling of 4-Carboxyphenyl-Bromophenol Blue to TentaGel | 120 |
| 6.2.4.3 Coupling of Alizarin Yellow GG or Mordant Orange 1 to TentaGel | 121 |
| 6.2.4.4 Coupling of 3-Nitrotyrosine to Aminopropyl Controlled Pore Glass | 121 |
| 6.2.5 UV-Visible Analysis of Post-Reaction Solutions..... | 121 |
| 6.2.6 UV-Visible pH Profiling of Indicators | 122 |
| 6.2.6.1 4'-(4-Dimethylamino-phenylazo)-N-methyl benzamide (<i>para</i> -Methyl Red methyl amide) | 122 |
| 6.2.6.2 UV-Visible absorbance measurements | 123 |
| 6.2.7 Experimental Procedure for Kinetics Measurements | 123 |
| 6.3 Experimental procedures for chapter 3..... | 124 |
| 6.3.1 Construction of fibre optic assembly | 124 |
| 6.3.2 General methods for CPG chemistry | 125 |
| 6.3.2.1 Procedure A: Microwave assisted amide bond formation..... | 125 |
| 6.3.2.2 Procedure B: Fmoc deprotection with piperidine | 125 |
| 6.3.3 Fmoc- ϵ Ahx-CPG | 125 |
| 6.3.4 ϵ Ahx-CPG | 126 |
| 6.3.5 Fmoc- ϵ Ahx- ϵ Ahx-CPG..... | 126 |
| 6.3.6 ϵ Ahx- ϵ Ahx-CPG..... | 126 |
| 6.3.7 Partial Capping of Amino Termini | 127 |
| 6.3.8 Sensor Beads Bearing <i>para</i> -Methyl Red, 3.1 | 128 |
| 6.3.9 Sensor Beads Bearing (4-carboxyphenyl)-Bromophenol Blue, 3.2 | 128 |
| 6.3.10 Adipoyl Dichloride ¹³² | 129 |
| 6.3.11 Attachment of Adipic Acid to Partially Capped CPG | 129 |
| 6.3.12 Sensor Beads Bearing Disperse Black 3, 3.3 | 130 |
| 6.3.13 Sensor Beads Bearing Pararosaniline, 3.4..... | 130 |
| 6.3.14 Sensor testing..... | 130 |
| 6.4 Experimental procedures for chapter 4..... | 131 |
| 6.4.1 Generation of Split-and-Mix Tripeptide Library on TentaGel..... | 131 |
| 6.4.1.1 Procedure C: Amino acid coupling on TentaGel..... | 131 |
| 6.4.1.2 Procedure D: Fmoc deprotection on TentaGel | 131 |
| 6.4.1.3 Split-and-Mix Tripeptide Library, 4.1 | 131 |
| 6.4.2 Partial Boc-Protection of Tripeptide Library, 4.2..... | 132 |
| 6.4.3 <i>S</i> -Trityl-2-Mercaptoacetic Acid (<i>S</i> -Trityl-thioglycolic acid) | 132 |
| 6.4.4 <i>S</i> -Trityl-thioglycolic Acid-Capped Tripeptide Library, 4.3a | 133 |
| 6.4.5 2-(Diphenylphosphino)benzoic Acid-Capped Tripeptide Library, 4.3b | 133 |
| 6.4.6 Removal of Side-Chain Protection, Terminal Boc Groups and <i>S</i> -trityl Groups, 4.4a & 4.4b | 133 |
| 6.4.7 Metal Chelation and Staining of Tripeptide Libraries | 134 |
| 6.4.8 Selection and Microspectrometry of Stained Beads | 134 |
| 6.4.9 Preparation of Beads for Edman Sequencing..... | 135 |
| 6.5 Experimental procedures for chapter 5..... | 135 |
| 6.5.1 Synthesis of Chiral Probes | 135 |
| 6.5.1.1 pMR- ϵ Ahx, 5.8 | 135 |

| | |
|---|-----|
| 6.5.1.2 ϵ Ahx-OMe \cdot HCl..... | 136 |
| 6.5.1.3 MO1- ϵ Ahx-OMe..... | 136 |
| 6.5.1.4 MO1- ϵ Ahx, 5.9..... | 137 |
| 6.5.1.5 Fmoc-(D/L-Pro)-O-Clt-PS..... | 138 |
| 6.5.1.6 <i>p</i> MR- ϵ Ahx-Pro-O-Clt-PS..... | 139 |
| 6.5.1.7 <i>p</i> MR- ϵ Ahx-Pro, 5.6..... | 139 |
| 6.5.1.8 MO1- ϵ Ahx-D-Pro-O-Clt-PS..... | 140 |
| 6.5.1.9 MO1- ϵ Ahx-D-Pro-OH, 5.7..... | 141 |
| 6.5.2 Synthesis of Resin-Bound Amino Acid Substrates..... | 141 |
| 6.5.2.1 Partial capping of amino termini..... | 141 |
| 6.5.2.2 Attachment of <i>N</i> -Fmoc-(D/L-Leucine or D/L-Phenylalanine) to polystyrene at specified enantiomeric ratios..... | 142 |
| 6.5.3 Chiral Resolution of Resins with Pseudoenantiomeric Probes..... | 143 |
| 6.5.4 UV-Vis Microspectrometry of Resins Post-Resolution..... | 143 |

References..... 144

1 Introduction: Analytical Methods for Solid Phase Organic Synthesis

Organic synthesis on solid supports is an active area of research which has developed from the relatively straightforward stepwise synthesis of oligomers (*e.g.* peptides, oligonucleotides), to the synthesis of small molecules and has reached a stage where the solid phase organic synthesis (SPOS) of relatively complex natural products now is possible.¹⁻³ SPOS has grown in conjunction with the development of combinatorial chemistry since several strategies such as “split-and-mix” synthesis^{4,5} and the application of multicomponent reactions⁶ allow large collections (“libraries”) of products to be produced in a small number of synthetic steps. Additionally, the solid support offers a mechanism by which individual members of the library can be conveniently manipulated and it provides a location where various “tags” may be attached for the identification of the library members.⁷

Correspondingly, there has been much interest in the development of new tools for the analysis of compounds attached to solid supports, as this circumvents the need for cleavage of the product from the support prior to conventional analysis. Furthermore, investigations into the supports themselves provide insights into the physicochemical environment of the resins, an important aspect in efforts to improve and widen the scope of SPOS.

Apart from classical methods such as elemental analysis⁸ and titrimetry,⁹ a variety of analytical technologies have been applied to SPOS for the direct analysis of materials on the supports, and range from visually assessed colorimetric assays to the more modern techniques of nuclear magnetic resonance (NMR) and mass spectrometry (MS), as well as a number of optical microspectroscopy techniques.¹⁰⁻¹⁴

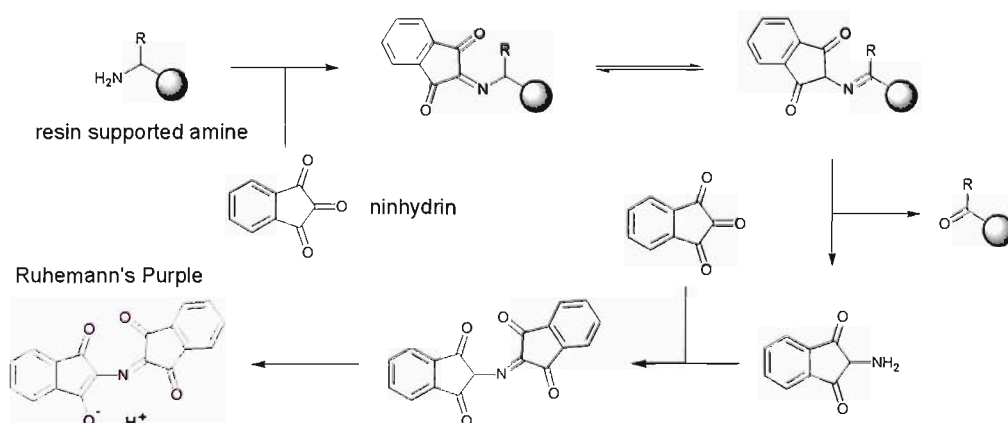
1.1 Colorimetric Tests for Solid Phase Organic Synthesis

Colorimetric tests on solid supports rely on the generation of a visually observable colour change when a specific functional group is present on the resin and are often used in SPOS to monitor the progress of reactions carried out on solid supports. These tests are widely used as they are generally rapid and simple to conduct.

1.1.1 Detection of Amines

Many colorimetric tests for the detection of solid-supported amines were originally developed for use during solid phase peptide synthesis and one of the first and most widely used of all the colorimetric SPOS tests is the ninhydrin (Kaiser) test employed for the qualitative detection of primary aliphatic amines.¹⁵ The colorimetric basis of this test is the formation and release of the chromophore Ruhemann's Purple by reaction of ninhydrin with the resin-bound amine. (**Scheme 1.1**) This test is highly sensitive, generating a visually observable purple solution from resins with an amine loading of at least $5 \mu\text{molg}^{-1}$. This test can also be used for the quantification of resin-bound amines by UV-Visible (UV-Vis) analysis of the Ruhemann's Purple generated by this reaction.¹⁶

Scheme 1.1 Formation of Ruhemann's Purple with ninhydrin and a resin-supported amine.

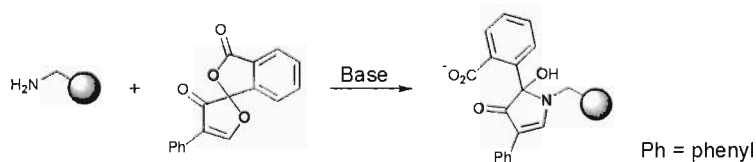


As can be seen from the reaction scheme, this test is not suitable for tertiary amines or when there are no H-atoms at the α -position to the amine (including anilines). Ambiguous results are also sometimes obtained with Arg, Asp, Asn, Cys and Ser residues with free side chains^{14,17} while secondary amines give a red-brown colour.¹⁵ As the test procedure requires the heating of the sample to ~ 100 °C, false positives are also occasionally observed when heat labile protecting groups such as the *tert*-butyloxycarbonyl (Boc) or trityl (Trt) are used.¹⁸

A modified version of the ninhydrin test has been used for the visualisation of resin-supported aliphatic azides, which consists firstly of the reduction of the azide to an amine *via* the Staudinger reaction with triphenylphosphine and water followed by visualisation of the amine.¹⁹ By adding triphenylphosphine and water to the reagent mixture for the ninhydrin test, the conversion could be performed *in situ* without the need for a separate step.

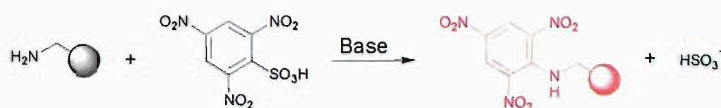
An alternative test that was developed specifically for the detection of solid supported primary amines employs the chromatographic derivatising agent fluorescamine.²⁰ Unlike the ninhydrin test where the observed chromophore is released into solution, this test attaches the derivatising agent to the support, resulting in fluorescent beads. (**Scheme 1.2**) This test is more straightforward to conduct than the ninhydrin test, requires no heating and is more sensitive, producing fluorescent beads with amine loadings as low as $0.6 \mu\text{mol g}^{-1}$. However, it has not been adapted to allow quantitative analysis.

Scheme 1.2 Reaction of fluorescamine with resin supported primary amines.



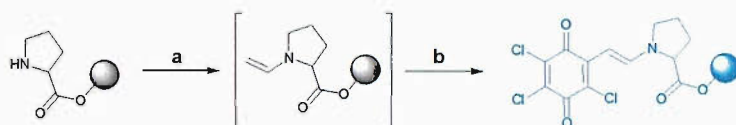
2,4,6-Trinitrobenzenesulfonic acid (TNBS) is another widely used colorimetric reagent that was developed for monitoring amino acid couplings in solid phase peptide synthesis.²¹ (**Scheme 1.3**) This reagent reacts with both primary and secondary amines to give red beads and is not affected by most other functional groups.¹⁷ It is as sensitive as the ninhydrin test in terms of resin loading²¹ although it may give erroneous results with sterically hindered amines.²²

Scheme 1.3 Reaction of TNBS with resin bound amines.



Due to the importance of Pro residues in amino acid synthesis and the substrate limitations of some of the previously mentioned tests, the chloranil test is often used for secondary amines.²³ This test gives blue beads in a pale yellow solution even with highly hindered secondary amines such as *N*-cyclohexylglycine and *N*-methylisoleucine at resin loadings as low as 2.8 μmolg^{-1} . The formation of the chromophore in this test is a two-step process, the initial formation of an enamine, followed by attack on to the electron deficient chloranil. (**Scheme 1.4**)

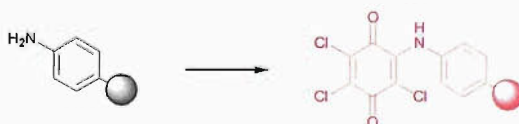
Scheme 1.4 Two-step formation of resin-bound chromophore in the chloranil test.



Reagents & conditions: (a) 2 % MeCHO, DMF, 5 min; (b) 2 % *p*-chloranil, DMF, 5-10 min. (Me = methyl, DMF = N,N-dimethylformamide)

The chloranil reagent can also be used for the detection of anilines.²⁴ (**Scheme 1.5**) This test generates red beads after heating and can detect supported anilines at loadings as low as 5 μmolg^{-1} although it does not react with *N*-alkylated anilines.

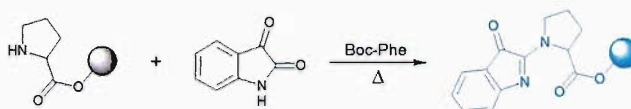
Scheme 1.5 Chloranil test for the detection of anilines.



Reagents & conditions: 2 % *p*-chloranil, DMF, 100 °C, 5 min.

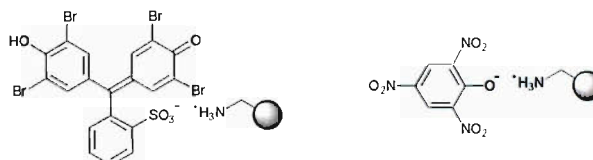
One reagent that is specific only for Pro is isatin,²⁵ which gives deep blue coloured beads when this residue is present, (**Scheme 1.6**) although this reagent does react with other secondary amines and anilines where it gives an orange or yellow colour.²⁶

Scheme 1.6 Reaction of solid supported proline with isatin.



Other tests are also employed which take advantage of the basicity of the amino group and non-specifically detect primary, secondary or tertiary amines. The most well known of these involves the use of Bromophenol Blue²⁷ or 2,4,6-trinitrophenol (picric acid)²⁸ which form ion pairs with amines. (**Figure 1.1**)

Figure 1.1 Ion pairs of a resin supported amine with Bromphenol Blue (left) or 2,4,6-trinitrophenol (right).

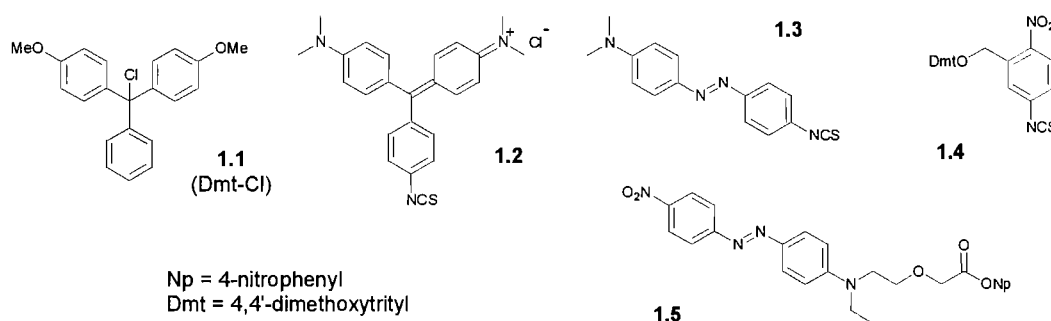


The indicator dye Bromophenol Blue is yellow under acidic conditions but becomes blue under neutral or basic conditions. As this dye is chemically unreactive to peptide acylation conditions, it may be added directly to the reaction mixture so reactions can be monitored by direct visual observation. The mixture is initially blue due to the presence of the amine but gradually changes to yellow as the acylation progresses and the amine is consumed. This *in situ* monitoring has also been adapted to allow automated feedback control of peptide synthesis.²⁹ For picric acid, a procedure has been developed to allow quantitation of the amino groups by eluting the bound yellow anion from the resin with an *N*-ethyl-diisopropylamine (DIPEA) solution and UV-Vis spectrometric quantification of the eluted anion.

Additionally, there are a number of other tests which exploit the nucleophilicity of the amines. These tests typically employ an activated chromophore which is attacked by the amine, forming a covalent bond which binds

the chromophore to the bead. Amongst the many variants are 4,4'-dimethoxytrityl (Dmt) chloride **1.1**,³⁰ Malachite Green isothiocyanate **1.2**, *N,N'*-dimethylaminoazobenzene-4-isothiocyanate **1.3**,²⁶ the “NPIT” reagent **1.4**³¹ and the “NF31” reagent **1.5**.²² (**Figure 1.2**)

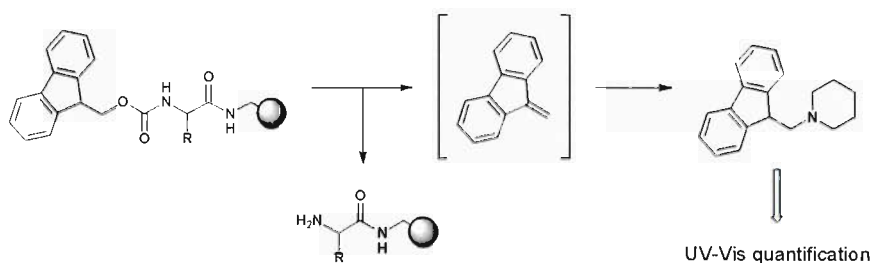
Figure 1.2 Activated chromophores employed in colorimetric tests for amines.



The reagents **1.1** and **1.4** are notable as they are only weakly coloured before and after attachment to the resin but upon treatment with trifluoroacetic acid (TFA), release the red 4,4'-dimethoxytrityl cation, which can be eluted and quantified by UV-Vis spectrometry to allow determination of the resin amine loading. Due to its bulkiness, **1.1** is poorly reactive towards hindered amines and the NPIT reagent **1.4** was conceived to overcome this limitation by having a more reactive isothiocyanate group and having the Dmt group distant from the site of coupling. This latter reagent reacts rapidly with primary and secondary amines as well as those with no α -H atoms, including anilines. The main disadvantage of reagent **1.4** is that it is not commercially available and requires a multistep synthesis to produce it.

The UV-Vis quantification of the fulvene-piperidine adduct produced by the deprotection of 9-fluorenylmethoxycarbonyl (Fmoc) protected amines (**Scheme 1.7**) is extensively used in the determination of the coupling efficiency of Fmoc-protected amino acids in solid phase peptide synthesis.³² After the acylation reaction, the Fmoc group is cleaved from a sample of resin, the solution eluted, and the adduct quantified and used to calculate the amount of amino acid attached to the resin. Real-time deprotection monitoring by UV-Vis detection of the adduct in the waste stream during the deprotection cycle is also commonly used in continuous flow synthesizers.¹⁴

Scheme 1.7 Fmoc deprotection with piperidine.

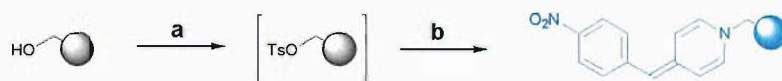


Reagents & conditions: 20 % v/v piperidine, DMF.

1.1.2 Detection of Hydroxyl and Phenol Groups

The expansion of SPOS to non-peptide synthesis generated the need for colorimetric tests for a larger variety of functional groups and one of the first non-amine tests developed was for the detection of resin bound hydroxyl groups. This test involved the *in situ* tosylation of the hydroxyl group followed by displacement with *para*-nitrobenzylpyridine (PNBP) to form blue coloured beads.³³ (Scheme 1.8) This test was able to detect hydroxyl groups down to a loading of 16 μmolg^{-1} and was not affected by amines or carboxylic acids. Halogenated substrates provided a positive test due to direct substitution by PNBP.

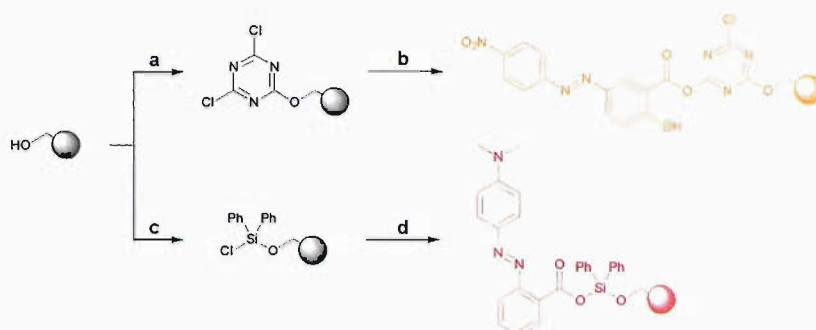
Scheme 1.8 PNBP test for the detection of resin bound hydroxyl groups.



Reagents & conditions: (a) TsCl, pyridine, toluene, Δ ; (b) PNBP, pyridine, toluene, Δ . (Ts = tosyl)

Another method of visualising hydroxyl and phenol groups is *via* the attachment of an activating agent such as 2,4,6-trichlorotriazine^{34,35} or diphenyldichlorosilane³⁶ followed by attachment of a carboxy-functionalised dye. (Scheme 1.9) However, as these tests rely on initial nucleophilic attack on to the activating agent, positive results are also generated by other groups such as amines and thiols and both tests also appear to be less sensitive compared to the PNBP test.

Scheme 1.9 Dye attachment *via* 2,4,6-trichlorotriazine and diphenyldichlorosilane to supported hydroxyl groups.

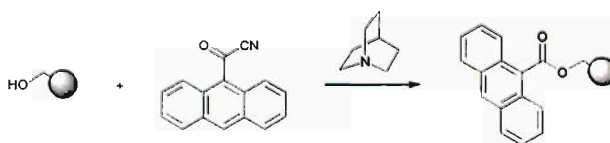


Reagents & conditions: (a) 2,4,6-trichlorotriazine, NMM, DMF, 70 °C, 20 min; (b) Alizarin R, NMM, DMF/NMP, 5 min; (c) Diphenyldichlorosilane, Et₃N, DCM, 10 min; (d) Methyl Red, DMF, 10 min. (NMM = *N*-methylmorpholine, NMP = *N*-methyl-2-pyrrolidinone, Et = ethyl, DCM = dichloromethane)

A test which differentiates between phenols and aliphatic alcohols using FeCl₃ has been described and is able to detect solid supported phenols with a loading > 80 μmolg⁻¹.³⁷ This test gives purple coloured beads by formation of iron-phenoxide complexes.

In terms of quantification, the reagent Dmt-Cl **1.1** also reacts with hydroxyl groups and can therefore be used for their quantification in a similar method as described for amines.³⁴ Another reagent that has been reported for the quantification of solid supported hydroxyl groups is 9-anthrolylnitrile (although absorbing only in the UV region).³⁸ (**Scheme 1.10**) Here, a known amount of the reagent and resin are mixed and after the reaction, the remaining unreacted 9-anthrolylnitrile is quantified by UV-Vis analysis. The amount of bound chromophore (*i.e.* the resin loading) is calculated by the difference in the amount of the reagent in solution pre- and post-reaction. Since this reagent is an activated carboxylic acid, it can also be used for measuring amine and phenol resin loadings though it is susceptible to steric interference and hindered substrates are not accurately quantified.

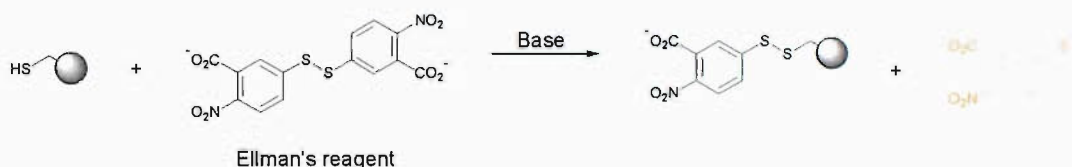
Scheme 1.10 Reaction of 9-anthrolylnitrile with supported hydroxyl groups.



1.1.3 Detection of Thiols

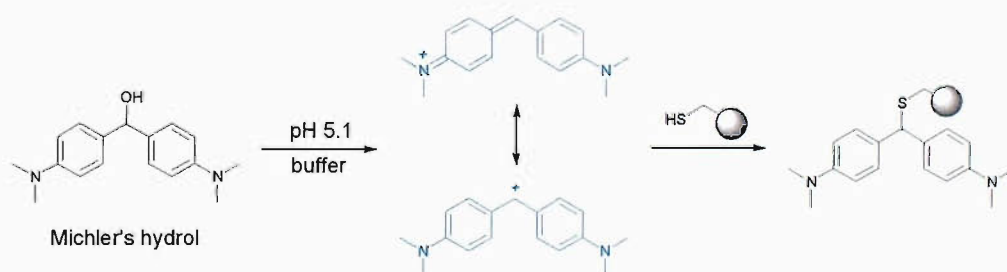
The most widely used selective colorimetric test for the detection and quantification of solid supported thiols involves the use of Ellman's reagent, 5,5'-dithio-bis(2-nitrobenzoic acid) (DTNB), that exploits the formation of disulfide bonds. Two different procedures are available, depending on the type of resin to be analysed although in both cases, the presence of thiols is indicated by the release of the bright yellow or orange dianion which can be eluted and quantified to determine resin loading.^{39,40} (**Scheme 1.11**)

Scheme 1.11 Reaction of solid supported thiols with Ellman's reagent.



A more recently described colorimetric test for thiols utilises Michler's hydrol, 4,4'-bis(dimethylamino)diphenylcarbinol.⁴¹ This reagent forms a deep blue carbonium-immonium species in an acidic solution that is decolourised by the addition of the thiol. (**Scheme 1.12**) This test can be applied for quantification of resin loading by measuring the decrease in the UV-Vis absorbance of the chromophore after reaction with a known amount of resin.

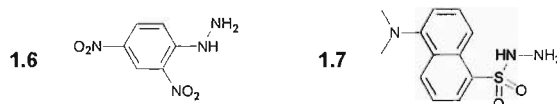
Scheme 1.12 Reaction of solid supported thiols with activated Michler's hydrol.



1.1.4 Detection of Aldehydes and Ketones

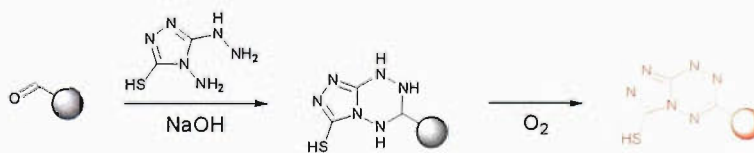
Aldehydes and ketones play an important role in the application of SPOS for small molecule generation since they are versatile intermediates in the formation of a range of compounds. In spite of this, the development of colorimetric tests for these groups on solid supports has occurred only relatively recently. These groups can be selectively detected by their ability to form hydrazones and the two most widely used reagents for this purpose are 2,4-dinitrophenylhydrazine (DNP)⁴² **1.6** and dansyl hydrazine⁴³ **1.7**. (**Figure 1.3**) DNP has been used in qualitative colorimetric tests, producing a visually detectable red colour with loadings as low as 18 μmolg^{-1} while a quantitative procedure has been described that utilises dansyl hydrazine and fluorometric quantification of this reagent in the supernatant solution.

Figure 1.3 Hydrazine-derived carbonyl derivatising reagents.



One reagent that is specific for supported aldehydes is purpald, which produces a red or brown colour in beads with an aldehyde loading of $> 20 \mu\text{molg}^{-1}$.⁴⁴ This colour is generated first by formation of a cyclic intermediate followed by aromatisation by air oxidation to give the chromophore. (**Scheme 1.13**) Although only tested with aromatic aldehydes, aliphatic aldehydes are also expected to give a positive result while no colour is produced with ketones or other functional groups. One drawback of the test is that solutions of purpald are unstable and must be freshly prepared. The brown colour is also sometimes difficult to observe if the resin loading is low and the colour faint.

Scheme 1.13 Reaction of solid supported aldehydes with purpald



Using a procedure modified from classical thin-layer chromatography (TLC) spot tests, solid supported aldehydes can also be detected upon heating with acidic solutions of *para*-anisaldehyde.⁴⁵ This test generates red or orange beads when aldehydes are present although the mechanism of chromophore formation is unclear. This test is reported to be compatible with both amine and hydroxyl groups.

1.1.5 Detection of Carboxylic Acids

The only reported and widely used visual test for supported carboxylic acids exploits the acidity of this functional group and its ion pairing with the indicator dye Malachite Green.⁴⁶ (Figure 1.4) This test gives green beads in the presence of aliphatic, aromatic and hindered carboxylic acids, however the results are time dependent with the colour fading after 15 min.¹⁷

The amount of carboxylic acid in a batch of resin can be quantified by its esterification with the UV-absorbing 1-pyrenyldiazomethane (Figure 1.5) in a similar manner to the quantification of alcohols with 9-anthrolynitrile, with measurement of the amount of remaining reagent used to calculate the loading of the resin.³⁸ Although not specifically tested, it is expected that this reagent would also alkylate phenols.

Figure 1.4 Ion pairing between Malachite Green and resin supported carboxylic acids.

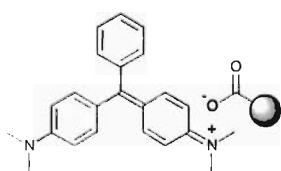
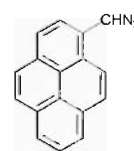


Figure 1.5 Carboxylic acid derivatising agent 1-pyrenyldiazomethane

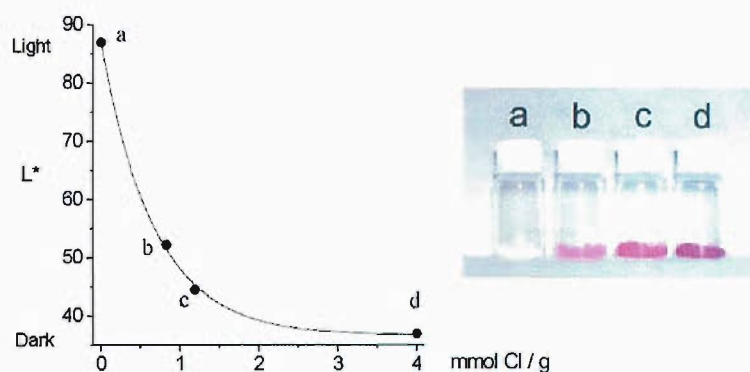


1.1.6 Detection of Aliphatic Halides

As previously noted, *para*-nitrobenzylpyridine (PNBP) used for the visual detection of alcohols can also be applied for the detection of resin bound aliphatic halides and this was recently explored with chloromethyl polystyrene (Cl-PS).⁴⁷ The sensitivity of this test was estimated to be $\sim 12 \mu\text{molg}^{-1}$ and these PNBP-stained beads were also subjected to analysis by diffuse reflectance UV-Vis spectroscopy

and colour analysis to determine its Commission Internationale de L'Eclairage (CIE) parameters. The UV-Vis reflectance spectra of the on-bead chromophore had a λ_{\max} value of ~ 540 nm that was similar to its solution phase analogue while the L^* colour CIE parameter (indicating brightness/lightness) could be correlated to the loading of the resins. (Figure 1.6)

Figure 1.6 Graph of the color parameter L^* after treatment with PNBP against chloride content of the resins.

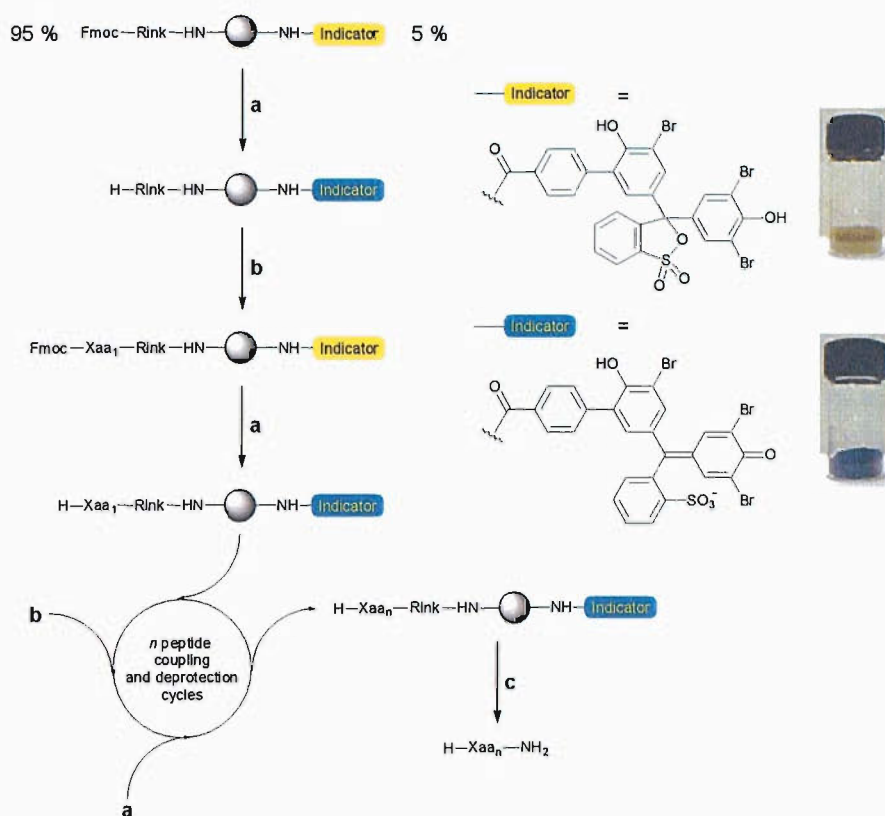


1.1.7 Bead-based self-indicating colorimetric sensors

Recently, the concept of *in situ* reaction monitoring with an indicator dye was extended with the introduction of “self-indicating” resins. Here, the indicator dye was bound to the resin enabling it to act as a sensor of the chemistry being carried out on the bead or to monitor reactions taking place in the solution around it.⁴⁸

The monitoring of on-bead reactions with these resins was first demonstrated in the synthesis of a peptides using AM-PS in which 5 % of the amine sites ($12 \mu\text{molg}^{-1}$) had been loaded with (4-Carboxyphenyl)-Bromophenol Blue (4CBPB).⁴⁸ (Scheme 1.14) In a similar way to the externally added Bromophenol Blue, this internal “sensor” dye gave a blue resin when amine groups were present but gradually converted to yellow as the peptide coupling progressed. Complete colour change only occurred when > 99 % of the amine groups were coupled.

Scheme 1.14 Solid-phase peptide synthesis on self-indicating resins.

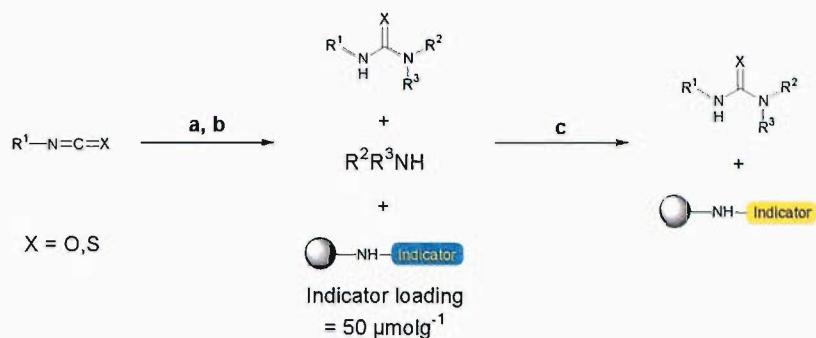


Reagents & conditions: (a) 20 % v/v piperidine, DMF; (b) Fmoc-Xaa-OH, DIC, HOBT, DMF; (c) 90 % v/v TFA, DCM.

Such self-indicating resins were useful in detecting and monitoring cases where the coupling of a specific residue was sluggish or incomplete since the colour change required prolonged reaction times or repeat couplings.

For the detection of amines in solution, the use of an indicator resin bearing 4CBPB has been described for the purification of a library of ureas prepared by reaction of a selection of isocyanates and amines.⁴⁸ (**Scheme 1.15**) In this example the indicator resin, added to the mixture after the reaction, immediately became blue due to the excess of amine present. Methylisocyanate resin was then added to scavenge the amines and the indicator resin gradually returned to a yellow colour once the removal of the amines was complete. The remaining ureas in solution could be isolated in high purity by removal of the resins and evaporation of the solvent. Tests with benzylamine showed the detection limit of this amine sensor was ~ 100 μM.

Scheme 1.15 Indicator resins for monitoring amines in solution.



Reagents & conditions: (a) $\text{R}^2\text{R}^3\text{NH}$ (1.25 mol. eq.), DCM, 2 h; (b) Indicator resin; (c) Methylisocyanate resin.

This concept was further developed with self-indicating scavenger resins where, rather than having the indicator and isocyanate on separate resins, the two were incorporated on to a single support.⁴⁹

1.2 Nuclear Magnetic Resonance Spectroscopy

NMR spectroscopy is a non-destructive technique that is potentially able to provide detailed information regarding the structure and intermolecular interactions of compounds. Thus, a significant amount of research has been directed at adapting NMR to the direct analysis of compounds on solid supports.

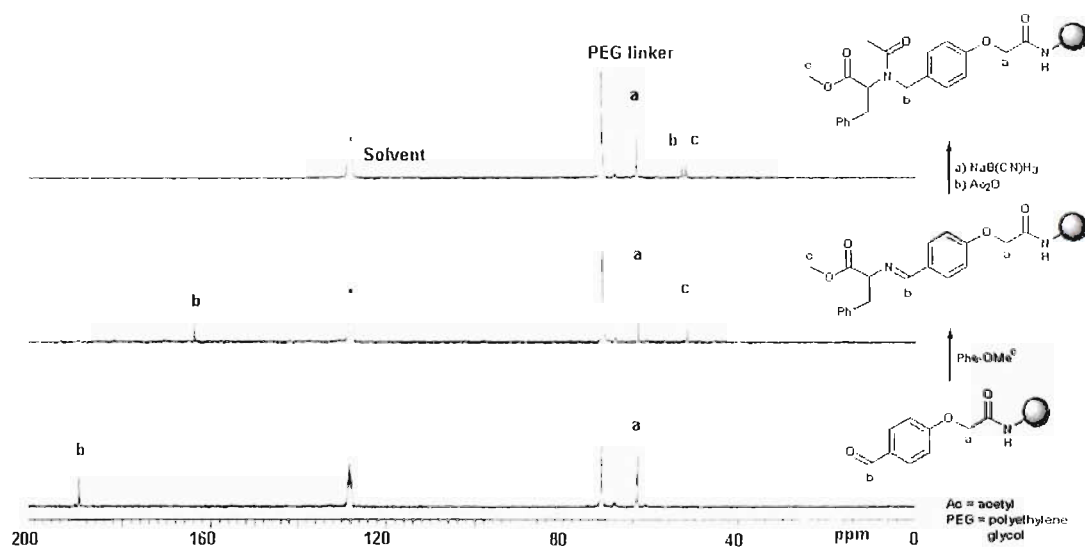
1.2.1 Gel Phase NMR Spectroscopy

Gel phase NMR was the first NMR method to be described for SPOS analysis where the spectrum was acquired from a slurry of the resin in an appropriate solvent (the “gel phase”) with a conventional liquid sample probe. Although this technique is widely available since no specialised equipment is required, it suffers from several drawbacks such as the need for a relatively large amount of resin and a broadening of the peaks in the spectra. The latter being the result of the reduced mobility of the compounds attached to the solid support and magnetic field inhomogeneities at the resin-solvent interfaces.^{11,50} In ^1H NMR, peakwidths of 100-300 Hz in this technique are too wide to afford meaningful data and this method is only applicable to nuclei with a low susceptibility to line broadening and a wide

dispersion of chemical shift values such as ^{13}C . Although ^{13}C gel phase NMR provides interpretable spectra with peakwidths of 25-75 Hz, the low natural abundance of this isotope requires prolonged data acquisition times.^{12,51} Large peaks from the resin polymer as well as impurities within the resin, which can vary between batches, can often complicate the interpretation of the spectra.¹⁰

In efforts to address these issues, ^{13}C -enriched building blocks have been used to allow gel-phase NMR spectra to be acquired in the same amount of time as a standard ^1H NMR, and without the interference of peaks from the polymer support.⁵² Complete isotopic labelling of all the C-atoms in the product was not necessary as most reactions can be monitored by the labelling of a small number of atoms at key locations. (**Figure 1.7**) In this example, the peak corresponding to the benzylic ^{13}C -atom “b” at 190 ppm is gradually lost as the reaction progressed, to be replaced with a new peak at 164 ppm corresponding to the imine. Subsequent reduction and acetylation resulted in the appearance of a new peak at 52 ppm and the loss of the previous peak.

Figure 1.7 ^{13}C Gel phase NMR monitoring of stepwise reaction sequence with ^{13}C -labelling.

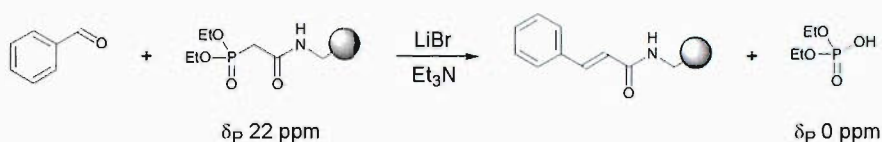


Other nuclei such as ^{31}P and ^{19}F have also been analysed by gel phase NMR to monitor the progress of reactions. Here, the nuclei under observation may be an integral part of the reaction, such the ^{31}P atom in a solid phase Horner-Wadsworth-Emmons reaction⁵³ (**Scheme 1.16**), or the observed nuclei may be present as a

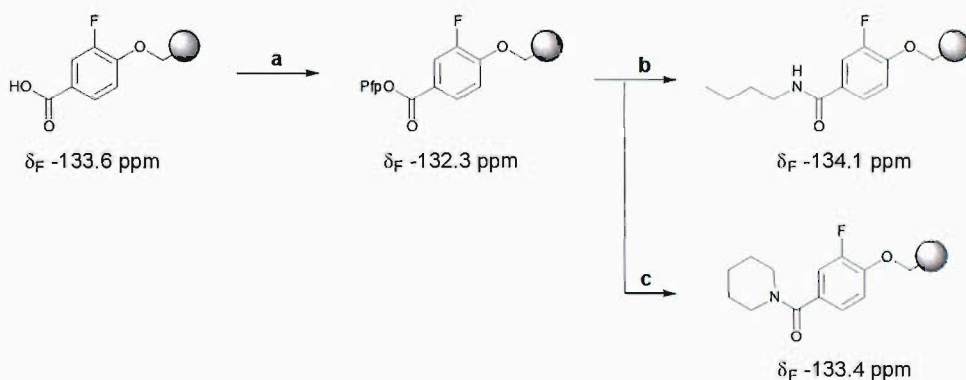
“reporter” that is peripheral to the reaction, such as in the synthesis of resin-bound 3-fluoro-4-hydroxybenzoic acid derivatives.⁵⁴ (**Scheme 1.17**)

Quantitative gel phase ^{19}F NMR has also been demonstrated by comparing the intensities of the peak from a resin-bound F-atom and the peak from a known amount of fluorobenzene that has been added to the solvent mixture.⁵⁵

Scheme 1.16 Solid phase Horner-Wadsworth-Emmons reaction and chemical shifts of ^{31}P nuclei used to observe reaction progress.



Scheme 1.17 Amidation of solid-supported 3-fluoro-4-hydroxybenzoic acid and chemical shifts of ^{19}F nuclei used to observe reaction progress.



Reagents & conditions:

(a) HOPfp, DIC, EtOAc; (b) HOBt, *n*-butylamine, EtOAc; (c) HOBt, piperidine, EtOAc. (HOPfp = pentafluorophenol, Pfp = 4-pentafluorophenyl, DIC = *N,N'*-diisopropylcarbodiimide, HOBt = 1-hydroxybenzotriazole)

The overall utility of gel phase NMR is limited by the unavailability of ^1H NMR and the moderate spectral resolution of ^{13}C NMR that is not always sufficient for structural determination. Furthermore, relatively long data acquisition times are required due to the poor signal-to-noise ratio of this technique. As a result, it is more often relegated to the role of monitoring the progress of reactions, a task that may be performed more conveniently by other analytical methods.

1.2.2 Magic Angle Spinning NMR Spectroscopy

In order to address the poor resolution of gel phase NMR, a previously developed technique for the NMR analysis of heterogeneous samples termed magic-angle-spinning (MAS) NMR was applied to SPOS resins. By spinning the slurried resin at an angle of 54.7° relative to the magnetic field (the “magic angle”), the effects of reduced sample mobility can be offset and the homogeneity of the magnetic field improved, giving rise to narrower peakwidths. In practical terms, the improved resolution and sensitivity from this has allowed reduced acquisition times as well as the accessibility of ^1H NMR for solid supported compounds. MAS probes designed specifically for small amounts of SPOS resins (~ 5 mg) are also now commercially available.^{50,51,56}

Various studies aimed at optimising MAS NMR for SPOS have noted that the choice of resin and solvent are the most important factors in determining the overall quality of the spectra. In general, the improved mobility provided by supports with long flexible polyethylene glycol (PEG) tethers such as TG (TentaGel) or polyoxyethylene-polyoxypropylene (POEPOP) resins provided the sharpest peaks. For solvents, best results were obtained when good solvation was provided to both the support as well as the attached product, which did not necessarily correlate to the degree of resin swelling.^{57,58}

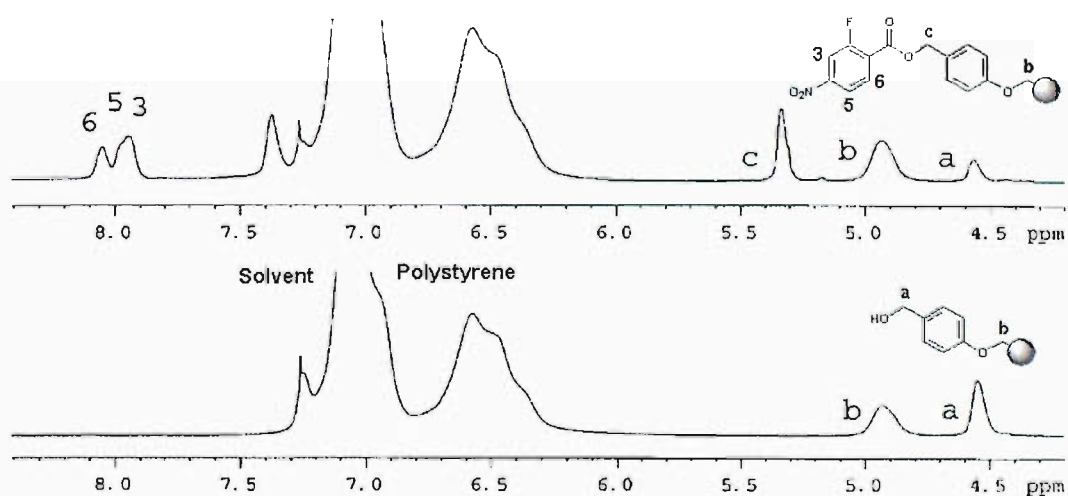
It has since been demonstrated that ^1H MAS NMR spectra of a quality approaching that of solution phase samples are possible with the appropriate choice of resin and solvent and the application of signal acquisition techniques that attenuate the peaks generated by the polymer backbone and the solvent. Peak resolution in one dimensional spectra is sometimes still insufficient for the determination of coupling constants for the assignment of individual peaks, particularly with less flexible resins such as polystyrene (PS), but this is overcome by the availability of a variety two-dimensional correlation experiments.^{50,56}

The availability of high resolution MAS NMR has in turn allowed the development of accurate quantitative experiments for the determination of resin loading and reaction yields. In a recent example, ^1H MAS NMR was used to study the attachment of 2-fluoro-4-nitrobenzoic acid to Wang PS resin.⁵⁹ (**Figure 1.8**) After the acylation reaction, a new peak corresponding to the benzylic protons “c” attached to the ester bond was observed. However, a residual peak corresponding to

the α -hydroxy protons “a” were also still present, indicating the reaction was not complete. The degree of conversion could then be calculated by comparison of the integrated peak areas for protons “a” and “c”. The peak area of “b” that was unchanged by the reaction provided an internal standard to allow the calculation of the absolute loading of the acid. Likewise, quantitative experiments involving ^{13}C and ^{19}F MAS NMR have also been reported.^{60,61}

Apart from product characterisation and quantitative reaction monitoring, many other MAS NMR applications analogous to those in solution phase NMR have since been described. These include the measurement of through-space couplings to enable conformational studies of resin-bound compounds, enantiomeric excess measurements after derivatisation with Mosher’s acids, analysis of the diffusion rates of amino acids into resins and a study of peptide aggregation on resin.^{50,56,62}

Figure 1.8 ^1H MAS NMR spectra of Wang resin pre- (bottom) and post-acylation (top) with 2-fluoro-4-nitrobenzoic acid.



1.3 Mass Spectrometry

The use of MS for direct “on-bead” analysis of supported compounds has received relatively little attention compared to its applications in the high throughput analysis of samples in solution.⁶³⁻⁶⁶ This is partly due to the fact that there are few MS ionisation methods that are capable of accepting solid samples. Additionally, since MS relies on the detection of free ions, the products of interest must be cleaved from resin either immediately prior to or during the analysis process.

1.3.1 Matrix Assisted Laser Desorption Ionisation MS

One of the first ionisation methods described for solid supports was matrix-assisted laser desorption ionisation (MALDI).⁶⁷ In this report, the analyte (a peptoid) was attached to PS *via* an acid-labile Rink amide linker. A single bead was treated with gaseous TFA to cleave the linker and subsequently loaded on a MALDI sample plate with a dihydroxybenzoic acid matrix for analysis. The laser used to initiate the ionisation had a beam diameter of 10-20 μm , which allowed a small part of the bead to be selectively targeted and this produced a mass spectrum clearly displaying the molecular ion of the peptoid. Molecular ions of the product could also be detected in regions of the matrix away from where the bead was located suggesting that leaching of the cleaved product into the matrix had occurred. Further reports have also described TFA-mediated cleavage from the Wang linker and cleavage of peptides with C-terminal Met residues using CNBr prior to MALDI-MS analysis of the beads.^{68,69} These studies demonstrated that MALDI-MS systems were sufficiently sensitive to analyse product cleaved from a single bead, an important consideration in the analysis of “one-bead-one-compound” libraries from split-and-mix syntheses.

Following this, further advances were made into streamlining and improving the quality of MALDI-MS analysis. In efforts to eliminate the need for this separate cleavage step, photolabile linkers were utilised that allowed the laser to simultaneously cleave and ionise the product in the spectrometer.^{70,71} A recent report has further demonstrated that matrix-free ionisation and analysis of compounds attached *via* photolabile linkers was possible.⁷² This development would allow the analysis of small molecule libraries commonly produced for medicinal chemistry without interference from the ions generated by the matrix or the risk of cross-contamination caused by the leaching of the cleaved products into the matrix.

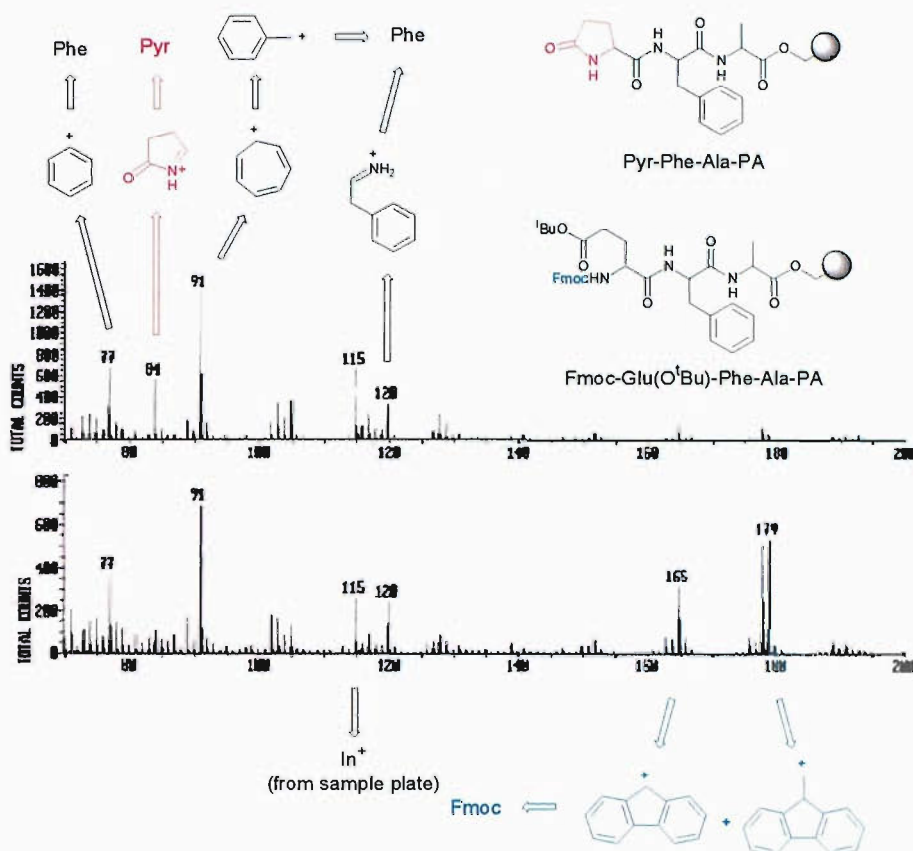
1.3.2 Secondary Ion MS

At the same time as the initial MALDI-MS report an alternative MS technique, secondary ion MS (SIMS) was described for on-bead analysis.⁷³ Instead of a laser, a tightly focused pulsed beam of inorganic ions was used to ionise and desorb compounds from the surface of the support. Although the equipment required for this type of ionisation was more technically complex, it offered a number of advantages over other MS systems which have been applied to SPOS analysis. Unlike MALDI, no matrix is necessary to aid ionisation, allowing easy analysis of small organic molecules and avoiding any risk of cross contamination associated with leaching of the products out of the bead.

SIMS is a “hard ionisation” method where fragment ions are preferentially generated due to the harsh ion bombardment of the analyte. As a result, it is often impossible to identify the molecular (or pseudomolecular) ion of the original product.⁷⁴ Nevertheless, as this ionisation method results in the breaking of bonds, it has been harnessed for the analysis of supported compounds without the need for any specific linker moiety or the need for prior cleavage from the support. In one example, two supported peptides attached to hydroxymethyl-functionalised polyacrylamide (PA) resin were analysed without prior cleavage and could be differentiated on the basis of their fragmentation patterns since the *N*-terminal pyroglutamate (Pyr) generated the immonium ion at m/z 84 while the Fmoc-peptide displayed the ion fragments from this protecting group at m/z 165 & 179.⁶⁶ (**Figure 1.9**)

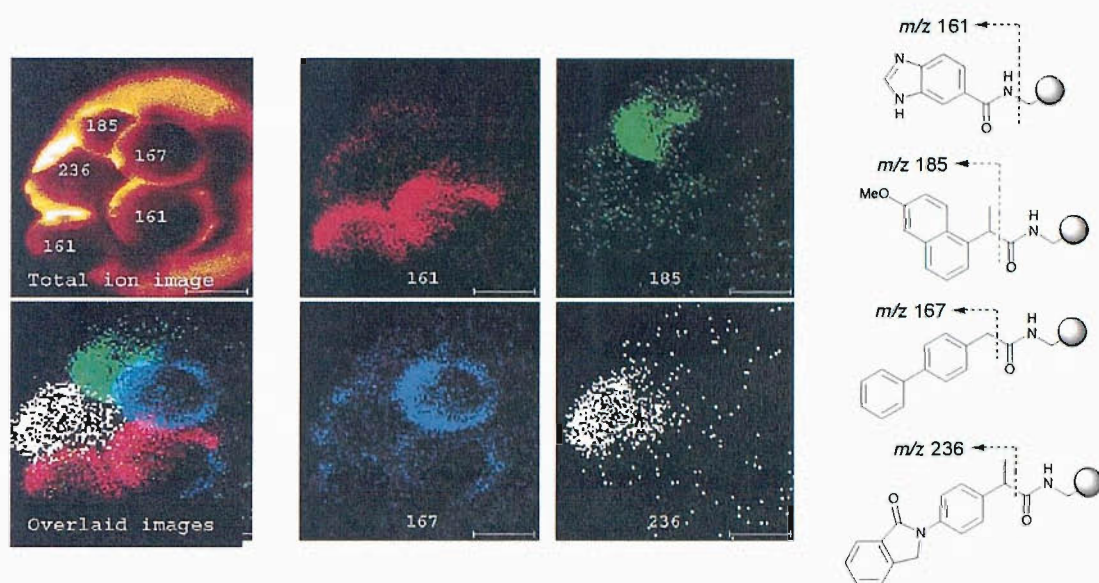
It was later realised that by careful control of ionisation parameters, it was possible to selectively rupture the weaker ester or amide bonds linking the product to the support. Using an improved procedure, unambiguous identification of individual members of a non-peptidic small molecule library from individual beads was demonstrated.⁷⁵ Separately, it was also discovered that the generation of molecular ions was possible if the peptides were first cleaved from the resin (with gaseous TFA) before analysis since the freed products were more easily desorbed without excessive bond breaking.⁷⁴

Figure 1.9 SIMS spectra from two resin bound peptides differentiated by their fragmentation patterns.



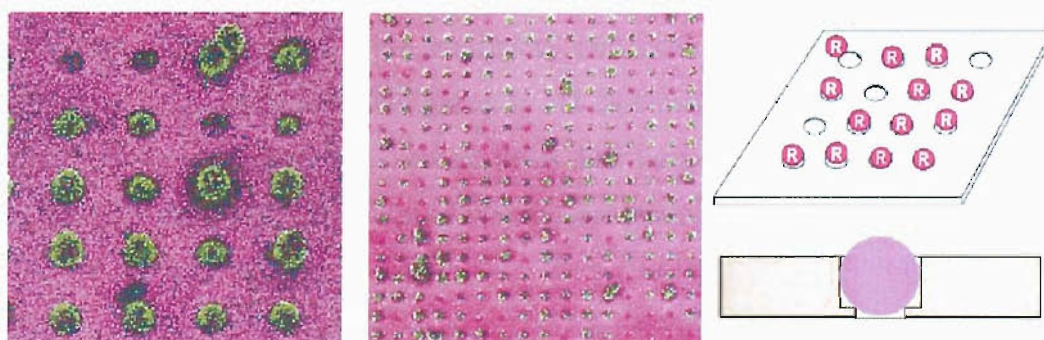
A major advantage of SIMS is the facility to image the surface of the sample under analysis where two-dimensional maps based on the abundance of various ion species can be generated.^{66,73,74,76} This was elegantly illustrated in the analysis of a test library of carboxylic acids attached to aminomethyl PS resin (AM-PS).⁷⁵ (**Figure 1.10**) Individual mass spectra were recorded sequentially for each location corresponding to a pixel in the analysed area and the final images were constructed by extracting from these spectra the intensities for the ions of interest. The area imaged was $395 \times 395 \mu\text{m}^2$ in size and took 30 min to complete (12 ms/spectra). Such molecule-specific imaging allows the identification of individual members from a split-and-mix library from several beads at once. The typical spatial resolution in these experiments is extremely high ($< 1 \mu\text{m}$) due to the high accuracy of the ion beam focusing.

Figure 1.10 SIMS ion intensity images of PS beads from a combinatorial library of carboxylic acids.



Among the more recent developments, the use of microfabricated SIMS chips has been described for arraying individual beads in a spatially addressable format which would streamline the characterisation of split-and-mix libraries.⁷⁴ (Figure 1.11) A comparative study on the analysis of compounds supported on PS and TG beads with a range of acid-, base-, thermo- and photolabile linkers has also been made. In comparing the amount of product on the surface of the beads available for analysis after cleavage, new analysis protocols were devised with improved spectral quality and reproducibility.⁷⁷

Figure 1.11 SIMS images of an array of beads on a microfabricated SIMS chip (left & middle) and schematic diagrams of the beads in individual wells (right).



1.3.3 Electron Impact MS

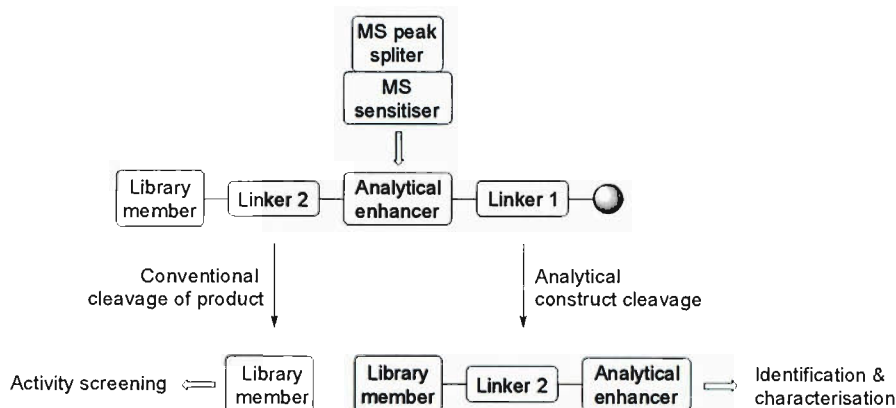
In addition to MALDI-MS and SIMS, there have been two reports on the use of electron impact MS (EIMS) for on-bead analysis by the ionisation-fragmentation-degradation of whole beads at high temperatures (300-400 °C).^{78,79} This hard ionisation technique produced predominantly fragment ions of the products without prior cleavage from the support.

Although EIMS facilities are wide available, these reports highlight a number of disadvantages to this technique. Unlike MALDI-MS or SIMS where several samples may be arrayed on a plate for analysis, samples can only be processed individually in EIMS and the ability to analyse a single bead was not demonstrated. Moreover, the harsh conditions employed make the detection of diagnostic molecular ions difficult and is unsuitable for heat-sensitive samples.

1.3.4 Dual Linker Analytical Constructs for MS

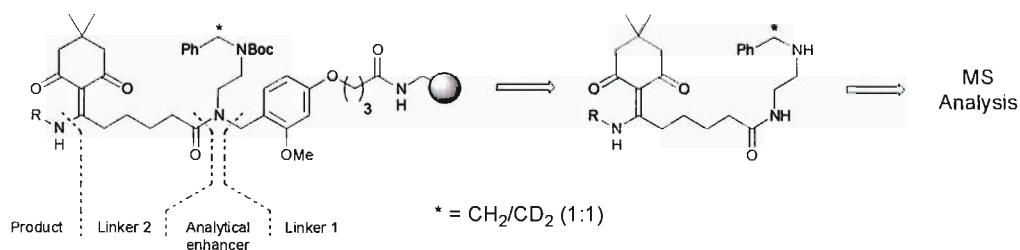
All MS systems suffer from a number of problems when used for the characterisation of libraries of compounds; the uneven susceptibility to ionisation between different members of a library complicates the quantification or even detection of individual members and in cases of poorly detectible products, identification of relevant peaks from background noise can also be troublesome. To address these issues, the concept of “analytical constructs” was introduced, in which the solid-supported compound and linker is anchored to the resin through an “analytical enhancer” group and a second orthogonally cleaved linker.⁸⁰ (**Figure 1.12**) Cleavage at linker 2 yields the library member in the usual way while cleavage at linker 1 releases the member together with the analytical enhancer which facilitates MS detection. This analytical enhancer group is composed of two components, an easily ionisable group to aid detection by MS and an isotopic mass label, which produces a characteristic mass distribution pattern of peaks in the mass spectrum to aid the identification of the relevant peaks.

Figure 1.12 Components of a generic analytical construct



One example of such a construct consists of a Boc-protected secondary amine as a masked MS sensitizer and a 1:1 isotopic mixture of H and D-atoms at its benzylic methylene groups provides the MS spectrum peak splitter. The first of the two orthogonal linkers employed was acid-labile (linker 1) and the second was hydrazine-labile (linker 2).⁸¹ (**Figure 1.13**) Treatment with TFA cleaved the analytical fragment with the product from the resin together with removal of the Boc group, revealing the readily ionisable amine group. In subsequent MS analysis, the construct was easily identified in the mass spectra by a characteristic doublet $2 m/z$ units apart.

Figure 1.13 An example of an analytical construct.



A number of other analytical constructs have been described in the literature⁸⁰ incorporating various features including photocleavable linkers for direct MALDI-MS analysis⁷¹ and ^{15}N isotope labels.⁸² Constructs that include chromophores to allow chromatographic UV-Vis detection and quantification in tandem liquid chromatography MS have also been described.⁸³

1.4 Optical Microspectroscopy

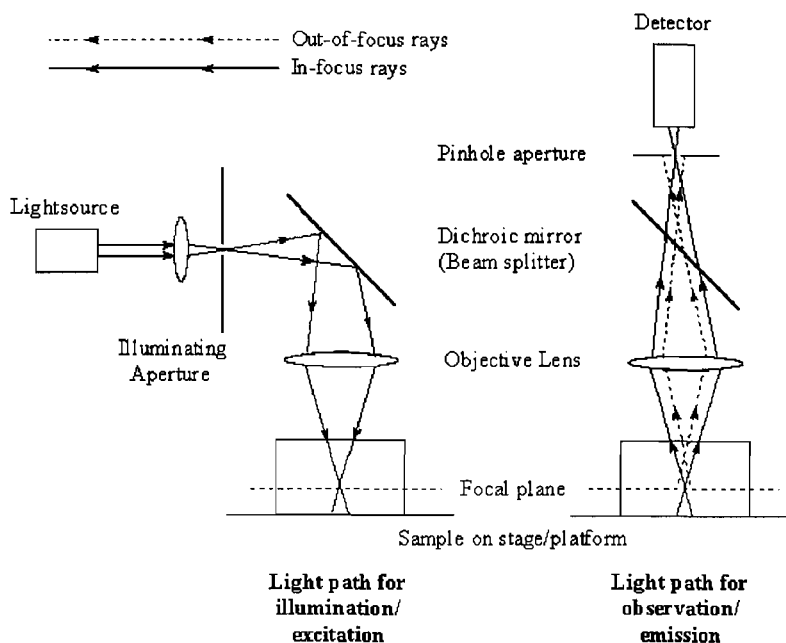
Optical microspectroscopy aims to couple the spatial resolution of optical microscopy with the analytical capability of fluorescence, IR or Raman spectroscopic methods. Such facilities are appealing in the field of SPOS for several reasons;⁸⁴ They are non-destructive, and the rates at which spectra can be recorded are sufficiently rapid that “real time” reaction monitoring is a possibility. Sample preparation is often a trivial matter of placing beads on an appropriate microscope slide and the equipment is relatively uncomplicated to operate compared to NMR or MS instruments. The high sensitivity of such microspectrometers allows analysis of a minute amount of sample (a single polymer bead). Often, sufficiently high resolution can be obtained to allow the spatial mapping of the interior of a variety of supports, providing information regarding the distribution of various chemical moieties within beads, a feature that is unique to microscopy. This is particularly important in the study of the physicochemical properties within them such as homogeneity of the functional site distribution and the rates of diffusion of reagents into the beads.

1.4.1 Fluorescence Microspectroscopy

1.4.1.1 Fluorescent confocal scanning microscopy

In early efforts to study the interior of resin beads, confocal microscopy techniques were applied in combination with fluorescence microscopy to study the distribution of fluorophores within individual beads. Unlike conventional light microscopy, confocal microscopy is capable of depth discrimination and is able to generate images from within a thick sample. It does so primarily by generating images from a small focal volume, ignoring light from points on the sides, above or below this volume.⁸⁵ To achieve this, a highly collimated light source is tightly focused to the small focal volume to provide illumination. In the detection process, any remaining light from other areas outside this volume is excluded from the detector by a pinhole aperture. (**Figure 1.14**)

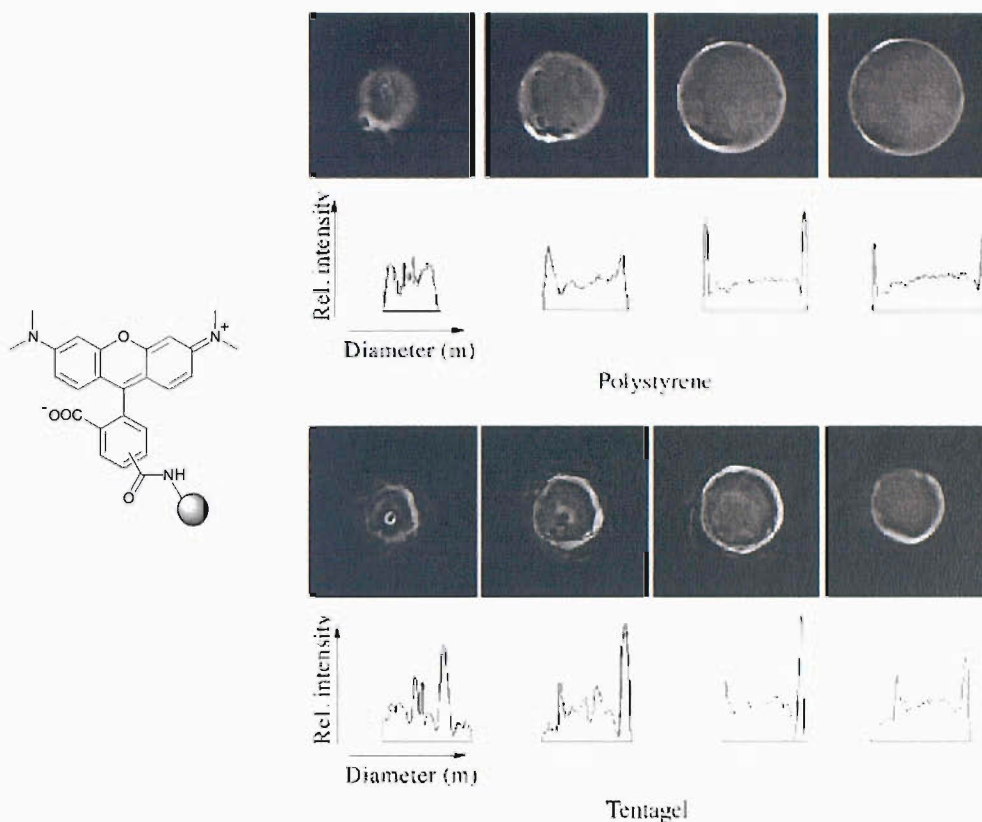
Figure 1.14 Schematic of a confocal microscope



By moving the detector laterally over the sample, it is possible to measure the light intensity at various points on the focal plane and scanning over the whole focal plane allows two-dimensional images of the sample to be constructed, termed “optical sectioning”. Raising or lowering the sample relative to the focal plane allows measurements at different depths. Multiple sections, when combined, allow the generation of three-dimensional maps. Thus, confocal microscopy avoids the need for physical sectioning which is tedious and may damage the original structure of the sample.

In fluorescence confocal microscopy, the lightsource (usually a laser) is set to the appropriate excitation wavelength of the fluorophore and the fluorescence spectra, or more commonly the fluorescence intensities at a specific wavelength, are recorded. The first experiments employing such systems for the examination of solid supports studied AM-PS and TG resins which had their functional sites coupled with carboxytetramethyl Rhodamine. Unexpectedly, the results from the optical cross-sectioning of these beads appeared to indicate a non-uniform functional site distribution with an increased degree of fluorescence on the outer layer of the bead.^{86,87} (**Figure 1.15**)

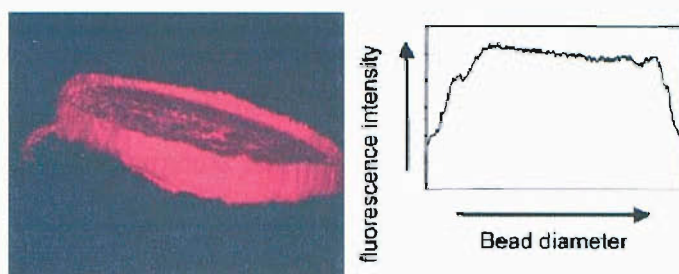
Figure 1.15 Optical sections of resin beads and relative fluorescence intensities across the diameters of four consecutive optical sections of beads.



However, these results were unconvincing for a number of reasons: In all cases the beads were exhaustively coupled to give high on-bead concentrations of Rhodamine. This dye displays a significant amount of fluorescence self quenching⁸⁸ and thus at high concentrations, would actually result in a lower amount of fluorescence than would be expected from a linear relationship between fluorescence intensity and the amount of fluorophore. Additionally, resins with high loadings would result in light absorption by the fluorophores to such a degree that nearly all the light would be absorbed by the outer layers of the bead and there would be no significant light penetration into the interior of the bead.^{89,90}

These concerns prompted further investigations into the distribution of resin functional groups in more detail and a later study using physically sectioned PS beads similarly loaded with Rhodamine demonstrated that the fluorescence was uniformly distributed throughout the interior of the beads.⁹⁰ (**Figure 1.16**)

Figure 1.16 Fluorescence microscopy image of a physically sectioned resin bead (left) and relative fluorescence intensities across the diameter (right).



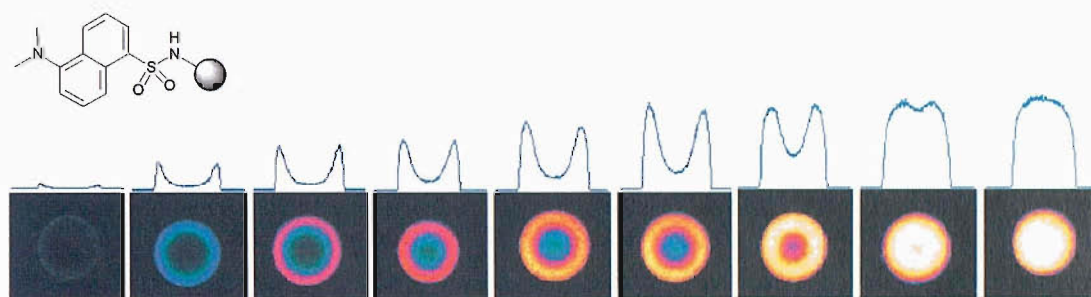
Another study observed this non-uniform effect even with Rhodamine loadings of as low as 1% of the functional sites of AM-PS ($\sim 10 \mu\text{molg}^{-1}$) and also noted that prolonged irradiation of the beads resulted in gradual a reduction of fluorescence due to photodegradation of the Rhodamine.⁸⁹ In light of this, other microscopy methods were sought to overcome these issues.

1.4.1.2 Two-photon fluorescence laser scanning microscopy

Two-photon microscopy⁹¹ (TPM) has also been applied to the study of bead interiors. These systems could be considered an extension of confocal microscopy in that the optics are designed such that excitation and detection were limited to a small focal volume. However unlike conventional fluorescence confocal microscopy, a pulsed laser with a long wavelength emission (visible or near-IR) is used with the combination of laser and fluorophore chosen such that the wavelength of maximum emission intensity of the source is approximately twice the wavelength of maximum absorption of the fluorophore. In this way, excitation of the fluorophore (and subsequent fluorescence emission) occurs only when two photons are absorbed simultaneously, and the probability of such an occurrence is high only at the focal point of the laser where the concentration of photons is high. Hence any fluorescence detected originates only from this focal point. The advantage of TPM is that there is no significant absorption of the excitation beam above or below the focal point as individual photons have an associated wavelength that is outside the absorption range of the fluorophore, allowing beam penetration deep into the beads. Also, the degree of photodegradation is reduced since the intervals between the laser pulses permits recovery of the fluorophore.

In the first report of a TPM study of solid supports,⁹² the distribution of functional sites on TG beads was revisited. Dansyl chloride labelling was employed as it (1) reacted readily with the amine functional groups of the beads, (2) is nonfluorescent before reaction with amines and (3) is less susceptible to self quenching.⁹³ By treatment of the beads with successive sub-stoichiometric aliquots of dansyl chloride, the gradual reaction of the functional sites within the beads was demonstrated in a series of optical sections culminating in the labelling of all the sites on the bead. (**Figure 1.17**) At complete labelling, uniform site distribution was observed.

Figure 1.17 False colour TPM optical sections of 90 μm TG beads (with fluorescence intensity traces above the sections) after successive dansyl labelling reactions.



By careful application of similar reactions to produce these fluorescent “shells”, beads with a series of five-layers could be produced and analysed (**Figure 1.18**) as well as beads with three different fluorophore shells; Dansyl, Rhodamine and Coumarin 343 (**Figure 1.19**).

Figure 1.18 False colour optical sections of five-shelled TG beads with fluorescence intensity traces above the sections.

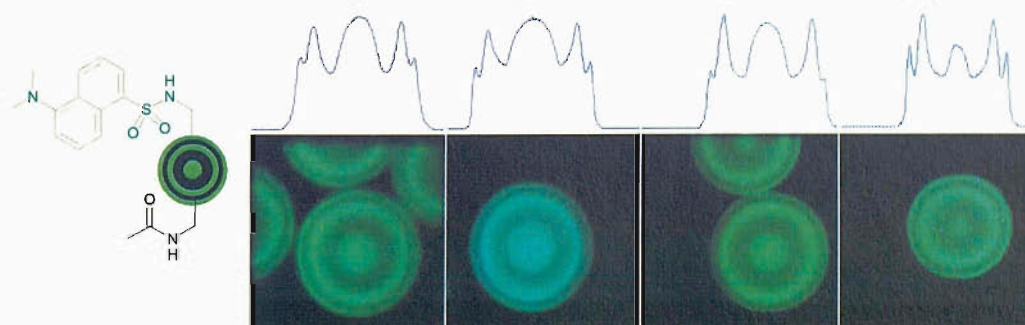
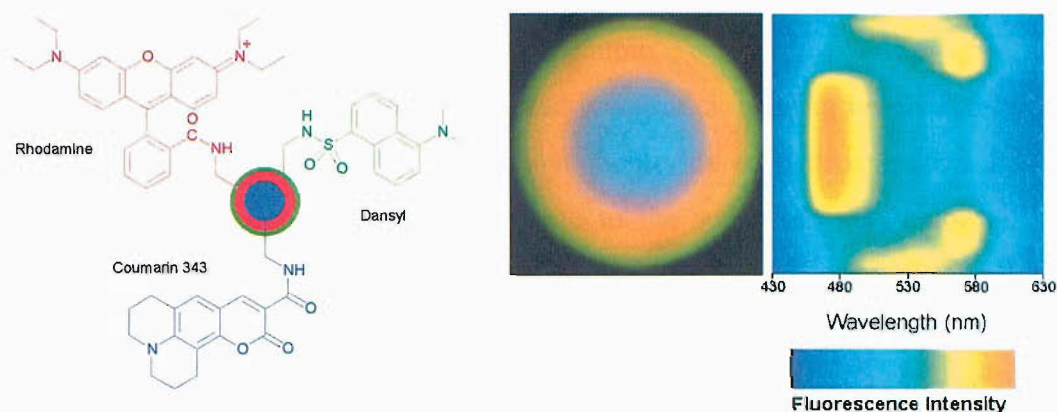


Figure 1.19 Optical section of three fluorophore layered TG beads, with a false colour plot of fluorescent intensity of a vertical line scan through the centre of the bead at various wavelengths (left).



Another TPM study with exhaustively dansyl-labelled PEGA indicated this resin also had a homogenous site distribution.⁹⁴ Some attenuation of the signal intensity was noted in this study, which was dependent on the pathlength from the top of the slide coverslip to the focal point, regardless of whether the path was entirely through the bead or partly through the surrounding solvent. However, this could be corrected mathematically to give a semi-quantitative linear relationship between fluorophore loading and fluorescence intensity.

1.4.2 Infra-Red Microspectroscopy

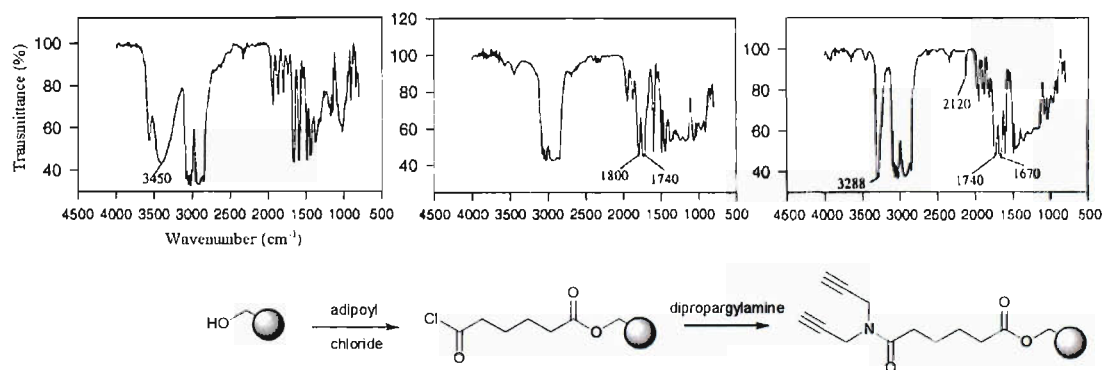
Once research into SPOS began in earnest, it was soon realised that IR spectroscopy would be very useful for the analysis of resin supports. Since this technique provided information regarding the presence of functional groups, it was a highly suitable tool for monitoring chemical transformations without excessive signal interference from the support material. Initial efforts made use of conventional Fourier transform IR (FT-IR) transmission spectrometers with bead samples pressed into KBr discs though measurement of IR spectra from solid supports has since been demonstrated with a number of different instruments making use of physical phenomena such as attenuated total reflectance (ATR) FT-IR, diffuse reflectance infra-red Fourier transform spectroscopy (DRIFTS) and photoacoustic FT-IR spectroscopy.^{95,96} However, further efforts to exploit instrumentation for single-bead IR spectroscopy led to use of transmission FT-IR microscopes.^{97,98}

1.4.2.1 Single-bead reaction monitoring and kinetics

Initial research with single-bead IR microspectroscopy aimed at the acquisition of IR spectra from a single bead at comparable quality to other IR methods which required larger amounts of sample.

The earliest example of single-bead reaction monitoring involved a two-step reaction scheme, the coupling of adipoyl dichloride to hydroxymethyl PS resin followed by coupling of dipropargylamine to the supported acyl chloride.⁹⁷ The diagnostic IR absorption bands for the functional groups were observed to be generated or lost after each reaction. (Figure 1.20) The first stage of the reaction scheme could be monitored by the loss of the hydroxyl band at 3450 cm^{-1} and the appearance of the carbonyl bands at 1800 and 1740 cm^{-1} corresponding to the acid chloride and ester moieties respectively. Similarly, the reaction with the amine was monitored by the conversion of the acid chloride carbonyl band to amide band at 1670 cm^{-1} as well as the appearance of bands for the terminal alkyne at 2120 and 3288 cm^{-1} corresponding to C–H and C≡C stretching vibrations respectively.

Figure 1.20 Single bead IR spectra of hydroxymethyl resin (left), after coupling of adipoyl chloride (middle) and after dipropargylamine (right).

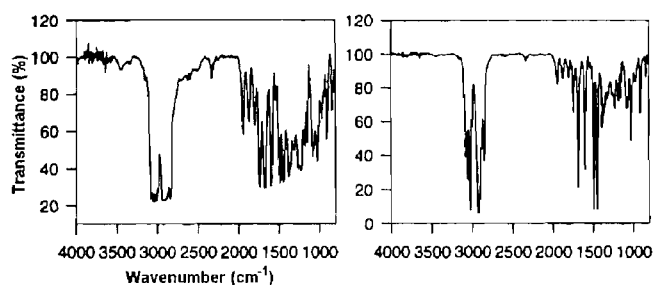


Two other important observations were also made: Firstly, by normalising the absorption intensities relative to the resin aryl ring absorbance at 1945 cm^{-1} it was possible to generate semi-quantitative data that was comparable between different beads. Secondly, analysis of 30 beads in each batch gave data that were identical within experimental error ($\pm 5\%$), suggesting that single bead analysis was representative of the entire batch.

IR spectra from spherical beads did however suffer from several deficiencies that were related to the relatively long pathlength of the IR beam through the bead and the curved surface.⁹⁹ This resulted in broad peaks and significant interfering bands caused by atmospheric CO₂ and water. These effects could be ameliorated by flattening the bead(s) between two IR sampling windows. (**Figure 1.21**) Preparation of the samples in this way made analysis less straightforward but allowed the implementation of experiments requiring higher resolution spectra and many chemical conversions monitored by this improved method have since been detailed.¹⁰⁰

The use of deuterium-labelled protecting groups has also been reported since the absorption bands for C-D bonds appear at different wavenumbers to the C-H bonds for the analogous functional groups. This can avoid the overlap of otherwise closely related bands and allowed improved quantification. These protecting groups were later cleaved so labelling did not alter the final product.¹⁰¹

Figure 1.21 IR Transmittance spectra of a single chloromethyl-PS bead without flattening (left) and when flattened between NaCl windows (right)

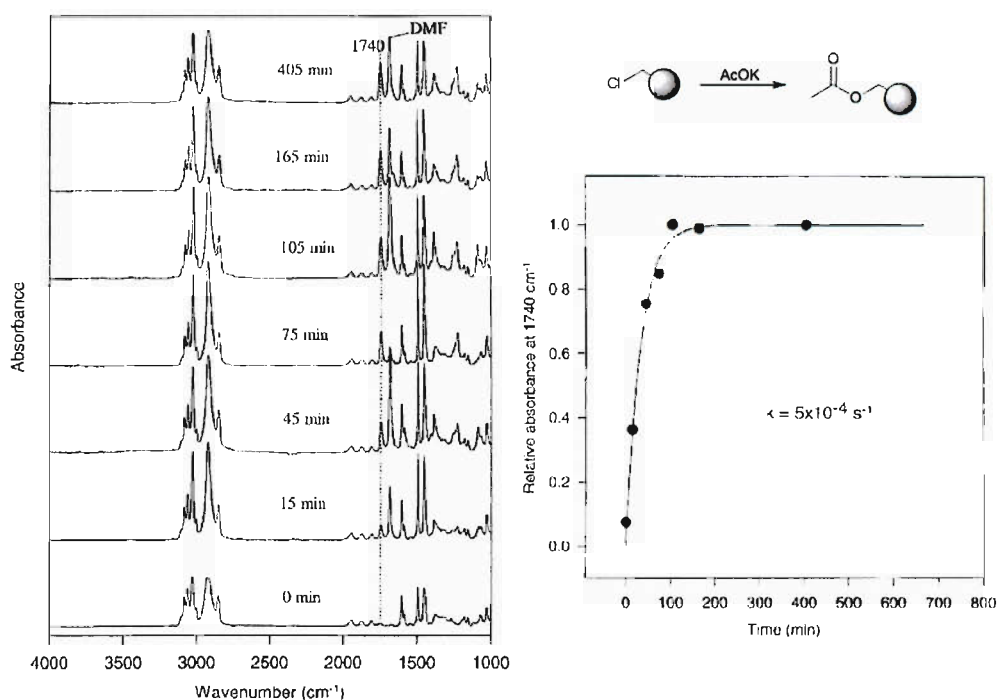


Time-resolved IR spectra have also been used in the study of on-bead reaction kinetics. In the first report of this, the nucleophilic substitution of Cl-PS with potassium acetate was monitored by the intensity of the ester carbonyl band (1740 cm⁻¹) at various time intervals.¹⁰² Since an excess of acetate was employed, the only limiting component was the number of resin chloromethyl sites and a pseudo-first order reaction rate constant could be calculated. (**Figure 1.22**) Using this procedure, a number of other esterifications and an aromatic nucleophilic substitution were similarly studied. Overall, the reaction rates calculated were surprisingly rapid and challenged the widely held assumption that solid-phase

reactions always proceeded more slowly than their counterparts in solution. The study also estimated the detection limit of IR microscopy to be ~ 125 fmol/bead.

The differences in reaction kinetics between PS and TG beads were compared in another series of reactions and demonstrated that reactions on TG were not always more rapid than on PS, again contradicting popular belief and implied that no single polymer support is favoured for all reactions. Rather, the choice of support and solvent should be dictated by the requirement for a polar or non-polar medium.¹⁰³ Another report using IR microspectroscopy to investigate the relationships between bead size and reagent size on reaction kinetics suggested a general trend that smaller bead size and less bulky reagents gave quicker reactions, but only where the rate of diffusion rather than the rate of reaction was the limiting step.¹⁰⁴

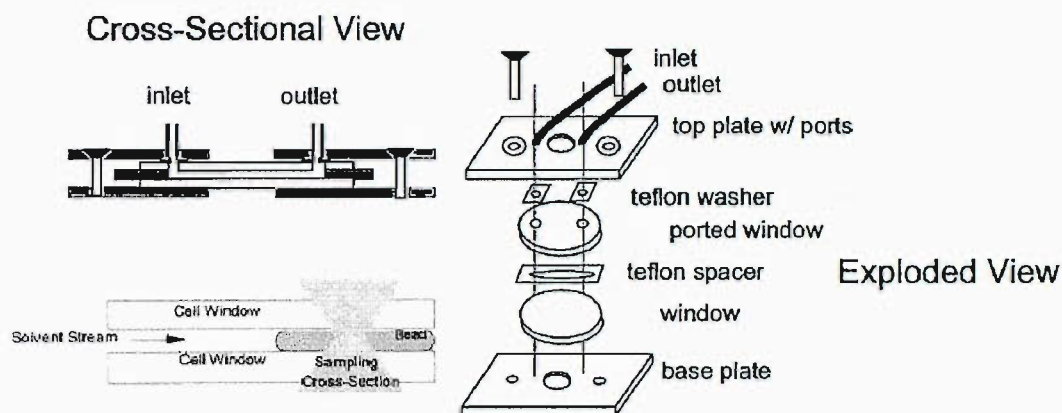
Figure 1.22 Time-resolved IR spectra for substitution of Cl-PS with potassium acetate (left) and time course of reaction (right).



In order to study on-bead reactions with real-time monitoring, the trapping of beads in a flow cell coupled to an IR microscope has been described.¹⁰⁵ (Figure 1.23) Using such an apparatus, reagent partitioning into beads,¹⁰⁶ amino acid coupling reactions¹⁰⁷ and resin linker photocleavage¹⁰⁸ reactions have been studied *in situ*. Although good quality quantitative data has been derived from these

experiments, they should be viewed with some caution as the effect of compressing the beads in the flow cell whilst conducting the reactions has not been fully evaluated. In these cases, the bead is no longer spherical and there is no solvent flow above or below the bead which would alter the diffusion characteristics of the reactants and products.

Figure 1.23 Schematics of the IR microspectrometry flow cell.



The most recent developments in this area have focused on improving calibration and processing methods for further enhancing the standard of data from IR spectra to give accurate absolute quantitation^{108,109} and for the analysis of severely overlapped absorption bands.¹¹⁰

1.4.2.2 Combinatorial library identification and mapping

The ability of IR microscopy to detect various combinations of functionalities meant that it could be harnessed for the identification of individual members of a combinatorial library. This principle was demonstrated by using a library of a PS-bound lysine-derived products where individual members could be identified on the basis of the presence of various absorbance bands from single-bead IR spectra.¹¹¹ Starting with lysine resin with orthogonal Fmoc and *N*^ε-(4,4-dimethyl-2,6-dioxocyclohex-1-ylidene)ethyl (Dde) amino protection, the amines were deprotected and coupled with a combination of IR active groups; 4-Cyanobenzoic acid, 3,5-di-*tert*-butyl-4-hydroxybenzoic and 4-pentynoic acid that absorbed at 2231, 3624 and 2120 cm⁻¹ respectively. (**Table 1.1**) The presence of these bands in the IR

spectra of the individual beads was used to identify the library members. (Figure 1.24)

Table 1.1 Substituents of the library members.

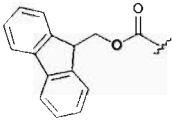
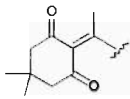
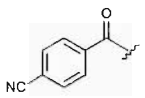
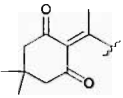
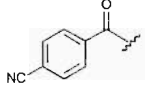
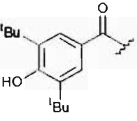
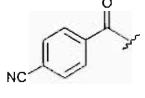
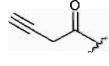
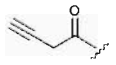
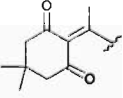
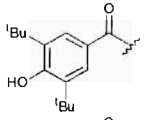
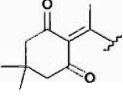
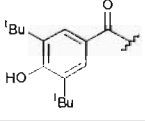
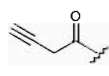
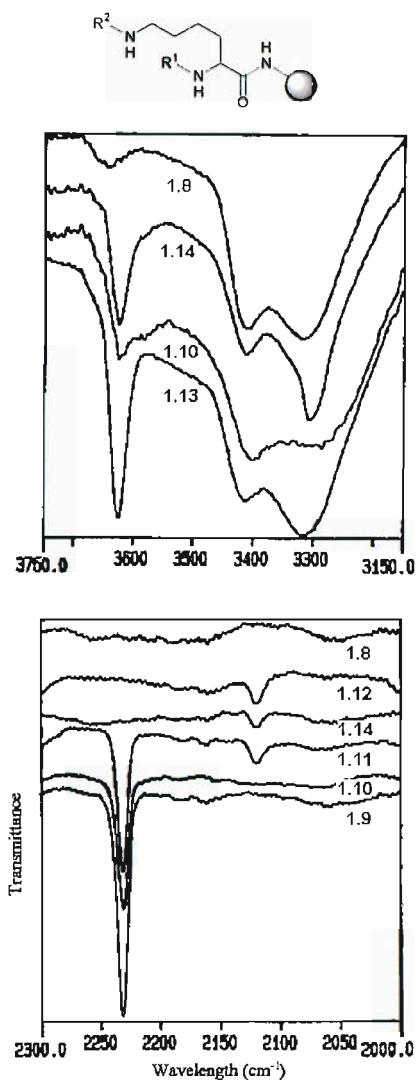
| Compound | R ¹ | R ² |
|----------|---|--|
| 1.8 |  = Fmoc |  = Dde |
| 1.9 |  |  |
| 1.10 |  |  |
| 1.11 |  |  |
| 1.12 |  |  |
| 1.13 |  |  |
| 1.14 |  |  |

Figure 1.24 IR spectra of the library members at 3150-3750 (top) and 2000-2300 cm⁻¹ (bottom).



A notable advantage of IR microscopes is the ability to collect data from a large spatial area by mapping arrays of beads. The two basic approaches for the generation of maps are the scanning (“step-and-collect”) method and the imaging method.

In a scanning method, the sample array is scanned in a stepwise manner and spectra from numerous small areas are acquired and combined to construct the final

complete map. Thus in one example, a split-and-mix library of isoxazolidines (**Scheme 1.18**) was arrayed between two KBr windows and the area scanned with an IR microscope equipped with a motorised stage.¹¹² This method offered spectra of good spectral and spatial resolution (4 cm⁻¹ and 50 μm respectively), but was somewhat time consuming with a 60 x 60 (3600 spectra) map requiring 5 h to generate. The collected spectra could be filtered to generate a series of intensity maps for the wavenumbers of interest. These maps were superimposed to identify the product on each bead by the combination of IR absorbance bands which represented each functionality. (**Figure 1.25**)

Scheme 1.18 Generation of supported isoxazolidine library.

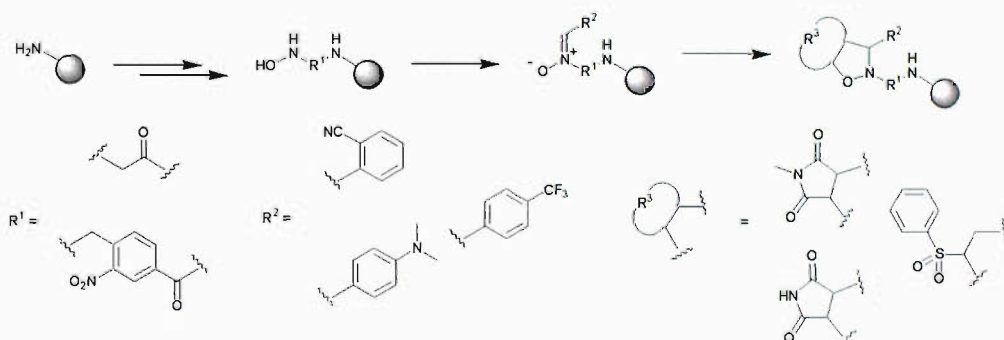
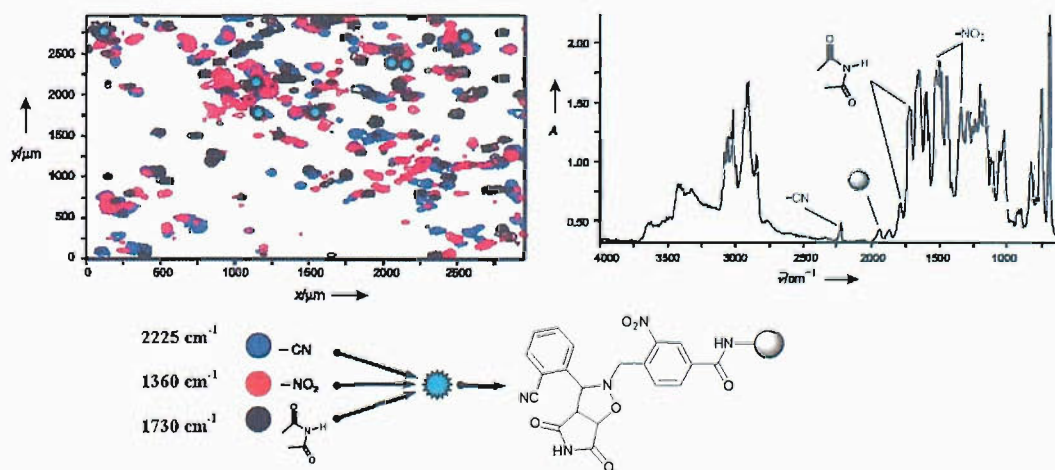
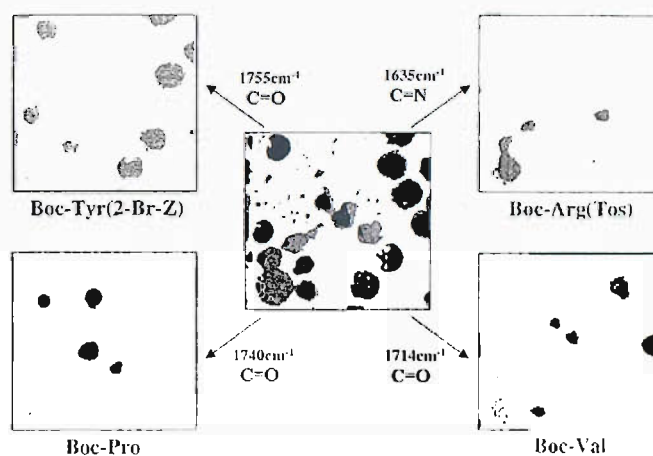


Figure 1.25 Superimposed IR intensity maps for the isoxazolidine bead library array (left) and an example of the full spectra of an identified product (right).



In the imaging experiment, using an IR microscope with a large array of numerous individual detectors the entire map with spectral and spatial information was collected simultaneously as a single “snapshot”. Using an instrument with a 64 x 64 detector assembly, maps of a 25-bead array could be generated in 20 s, satisfying the need for high throughput analysis of combinatorial libraries.¹¹³ In this particular example, a test library of four resin-bound amino acids with characteristic IR bands were imaged and it was demonstrated that the identity of amino acids bound to each bead could be determined. (Figure 1.26)

Figure 1.26 IR maps of supported amino acid library generated by plotting bands specific to each amino acid, with the central image being a composite of all of the individual images, showing the location of all beads in the field of view.



However, such imaging systems suffer from a number of drawbacks, poorer spectral range (1360-2720 cm⁻¹) and spectral resolution (8 cm⁻¹) as well as the high cost of large detector arrays. The inferior spectral resolution is a particularly serious disadvantage since combinatorial libraries often make use of components with very similar functional groups with accordingly small differences in IR absorption bands.

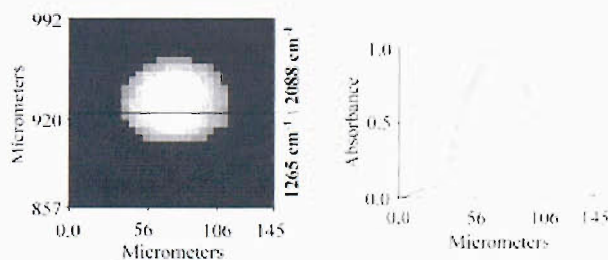
More recently, systems with 1 x 16 detector arrays which are able to conduct rapid scanning measurements with good spectral resolution have become available and offer an intermediate between scanning and imaging systems.¹¹⁴

1.4.2.3 Functional group distribution mapping on single beads

The ability of IR spectroscopy to detect functional groups makes this system ideal for the assessment of functional group distribution within each bead. However, a major difficulty in this endeavour is the long wavelength of the IR emissions themselves that limits spatial resolution since aperture sizes smaller than the wavelength would result in diffraction of the emissions. (*e.g.* at 500 cm^{-1} , the aperture would need to be $\geq 20\text{ }\mu\text{m}$) In practice a $25\text{ }\mu\text{m}$ aperture is used to allow spectra to be measured within a reasonable timescale with good signal-to-noise quality.¹¹⁵

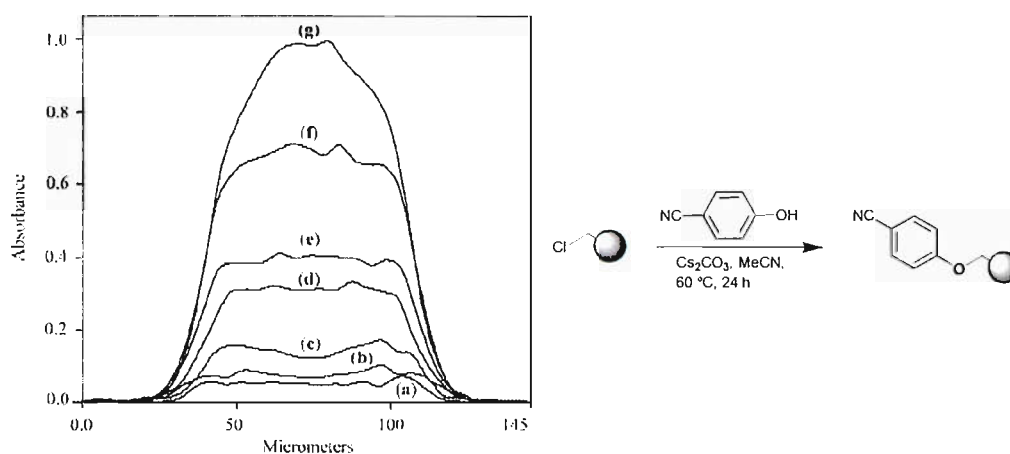
An elegant approach to circumvent this limitation was to generate maps by interpolating successive spectral measurements using a $5\text{ }\mu\text{m}$ step-width between each measurement.¹¹⁵ The chloride site distribution of Cl-PS resin was investigated in this way by mapping the chloromethyl absorbance at 1265 cm^{-1} with the beads in both their natural spherical shape as well as when flattened. Analysis of preliminary maps with spherical beads noted that the overall absorbance at the periphery of the beads was higher compared to the centre due to the curvature of the beads. To compensate for this, the chloromethyl absorbances were normalised against the weakly absorbing baseline region at 2088 cm^{-1} to generate “true intensity” maps and these demonstrated a uniform functional group distribution within the beads. (Figure 1.27)

Figure 1.27 IR maps of chloromethyl PS after baseline correction (left) and absorbance intensity profile through equatorial plane (right).



Further experiments mapping Cl-PS resins in which the chloride sites had been substituted with various amounts of 4-cyanophenol demonstrated a uniform site reactivity suggesting the rate of diffusion of the phenol into the beads was more rapid than the rate of reaction. (Figure 1.28)

Figure 1.28 Cyano IR absorption profiles of beads containing (a) 0.01, (b) 0.04, (c) 0.08, (d) 0.22, (e) 0.31, (f) 0.54 or (g) 0.84 mmol N/g of resin.



1.4.3 Raman Microspectroscopy

Similar to IR microspectrometry, Raman microspectrometry provides information regarding the presence of various functional groups in the sample. However it offers complimentary functional group selectivity to IR spectroscopy, moieties with permanent dipoles (*e.g.* carbonyl, hydroxyl, amine functionalities) generally give strong IR absorption while being very weak or completely absent from Raman spectra. Conversely, relatively non-polar groups (*e.g.* alkynes, aryl systems, nitriles) which are weakly IR absorbing give rise to strong Raman signals. Furthermore, functionalities that give broad or overlapped absorbance bands in IR spectra may be well resolved in Raman spectroscopy.^{100,116}

Raman spectroscopy is also somewhat less susceptible to variations in thickness of the sample or excessive absorption due to long pathlengths through the spherical bead. This is a valuable factor in SPOS since it sidesteps then need to compress or section the beads prior to analysis.

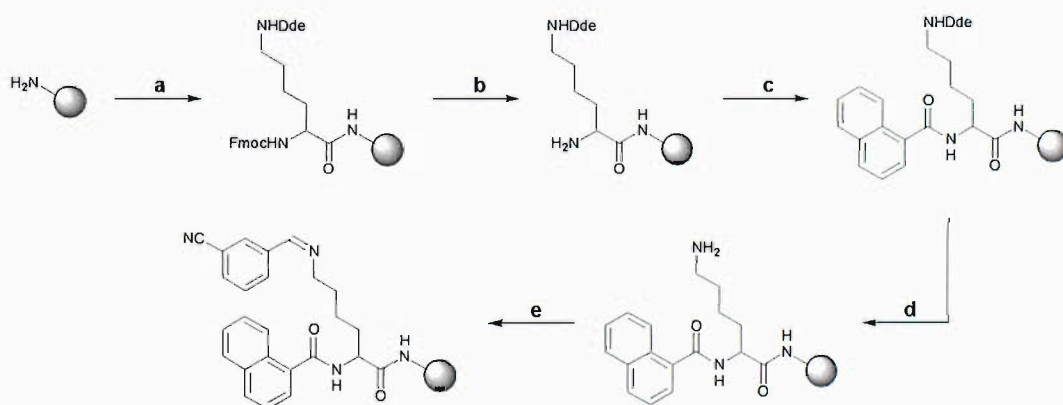
1.4.3.1 Solid phase batch analysis

Early Raman microspectroscopy experiments made use of milligram amounts of beads which were reasoned to be more representative of the entire batch. These initial experiments produced spectra of relatively low quality but confirmed the utility of this technique in following the progress of reactions in a similar way to

IR microscopy, and provided insights into the secondary structures of peptides (such as β -sheet formation) on solid supports.^{117,118} These early experiments also highlighted the importance of the choice of laser used for the generation of the Raman emissions since the use of short laser wavelengths resulted in fluorescence of the support that obscured the Raman signals.¹¹⁷ It was subsequently shown that the use of a NIR laser eliminated fluorescent emission on TG beads.¹¹⁸

More recently, the use of reaction flow cells have allowed real-time monitoring of the reactions with the beads retained in the flow cell by two small cotton plugs that avoided compression of the beads, unlike the previously described IR flow cell.¹¹⁹ (Scheme 1.19) Its use was demonstrated with a series of SPOS reactions in DMF, which could not be monitored by IR spectrometry as the carbonyl absorption band from the DMF obliterated the region between 1550-1750 cm^{-1} of the IR spectra. (This band was completely absent in the corresponding Raman spectra.) The Raman spectrum taken before the start of the reaction sequence was subtracted from the subsequent spectra so spectral changes during the reactions could be more clearly visualised. (Figure 1.29) Time resolved plots of the wavenumbers specific to the reactions of interest could also be generated (Figure 1.30), demonstrating the strength of this “on-line” analysis method. Furthermore, recent developments in data processing and calibration has allowed quantitation of the results at a quality equivalent to that of IR spectroscopy.¹⁰⁹

Scheme 1.19 Attachment and modification of lysine on AM-PS monitored by Raman microspectrometry.



Reagents & conditions: (a) Fmoc-Lys(Dde)-OH, DIC, HOBT, DMF, 1.5 h; (b) 2 % DBU, DMF, 15 min; (c) 2-naphthoic acid, DIC, HOBT, DMF, 1.5 h; (d) 2 % hydrazine, DMF, 15 min; (e) 3-cyanobenzaldehyde, DMF, 1.5 h. (DBU = 1,8-Diazabicyclo(5.4.0)undec-7-ene)

Figure 1.29 Total Raman data set for reaction sequence (top left) and data set after subtraction of Raman spectrum taken before start of sequence (bottom right).

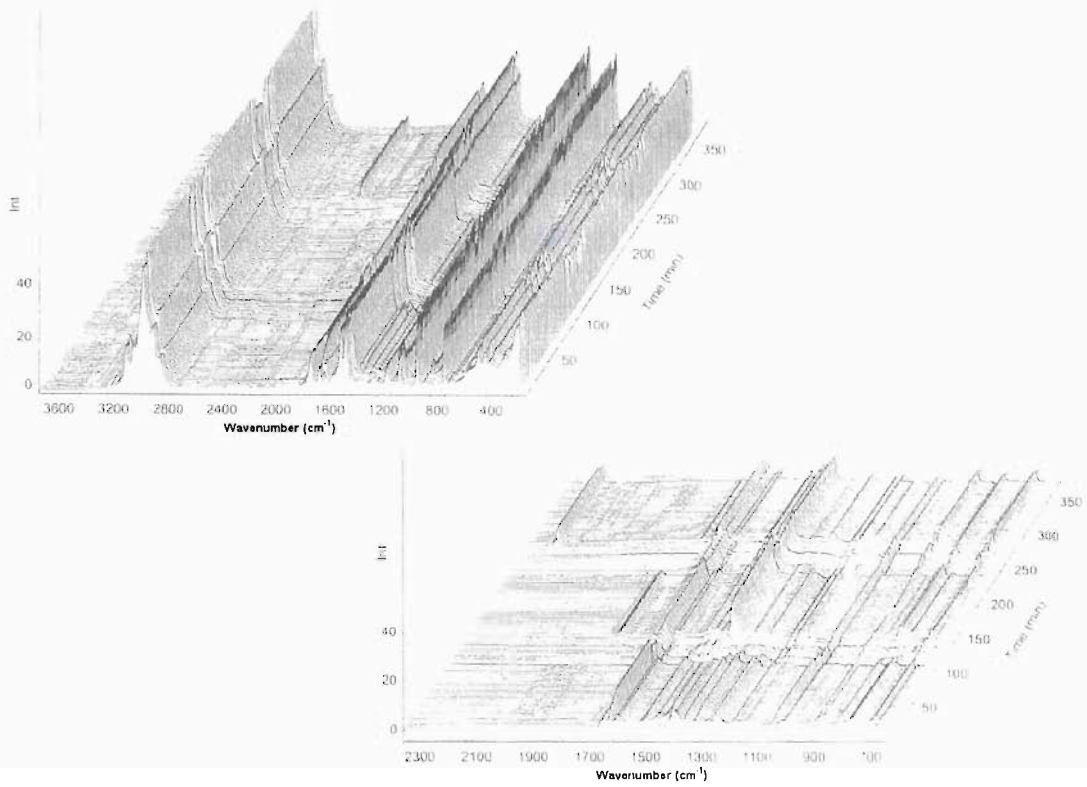
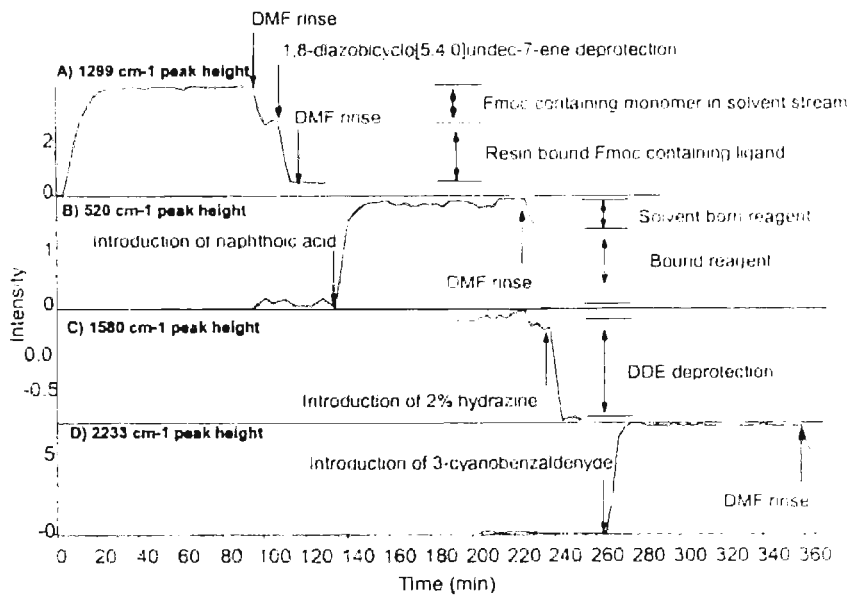


Figure 1.30 Time-resolved plots of group specific Raman intensities.

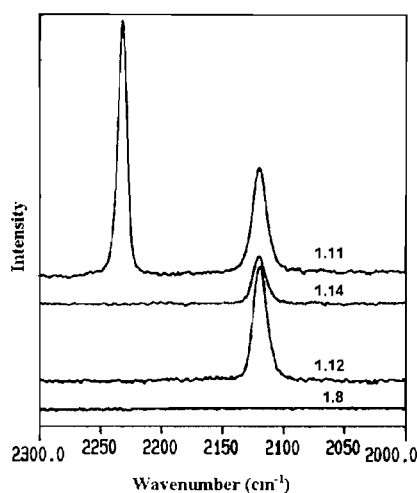


1.4.3.2 Raman microscopy for single-bead analysis

As previously noted, the capability to conduct single-bead analysis is desirable as it enables the characterisation of individual members of split-and-mix combinatorial libraries and investigations of reactions at the single bead level.

In the case of library member identification, the principle was demonstrated by subjecting a previously synthesised library of solid-supported lysine coupled with various Raman- and IR-active tags (**Table 1.1**) to Raman analysis.¹¹¹ As with the IR analysis, the presence of characteristic Raman bands in the spectra of the individual beads was used to identify the library members. (**Figure 1.31**)

Figure 1.31 Raman spectra at 2000-2300 cm^{-1} of a library of solid-supported lysine coupled with various Raman-active tags.



The practical utility of IR microscopy has been compared against Raman microscopy and highlighted several apparent disadvantages of Raman spectroscopy.¹²⁰ Chief amongst these were the low speed of analysis (10-20 min for single-bead analysis), the need for high powered lasers (1000 mW) and liquid nitrogen cooling, as well as high cost of the instrumentation. However, these limitations should be viewed with some scepticism since these conclusions were drawn from comparing a state-of-the-art IR microscope against a relatively old model Raman microscope. Newer Raman instruments such as the Renishaw *inVia* series have no need for liquid nitrogen cooling, make use of lasers with power outputs as low as 17 mW and are capable of collecting spectra in seconds.

1.4.3.3 Confocal Raman microscopy

Confocal microscopy has also been applied in conjunction with Raman spectroscopy in a similar arrangement to a fluorescence confocal microscope although instead of measuring fluorescence, the detector is configured to record the Raman emissions. Unlike IR microscopes, Raman instruments do not rely on the actual detection of long wavelength emissions and are therefore able to use very small apertures to achieve lateral resolutions similar to that of fluorescent confocal microscopes.

In this respect, scanning confocal Raman microscopy has been used for the optical sectioning of solid supports to verify their internal functional site distribution while avoiding the problems associated with fluorescence confocal microscopy.¹²¹ To increase the quality of data collected, the Raman active 4-cyanobenzoic acid was coupled to AM-PS resin and two-dimensional intensity maps of the nitrile peak (2230 cm^{-1}) intensity were generated with the beads swollen in 1,4-dioxane. The maps displayed a uniform intensity within the bead, suggesting uniform site distribution. (**Figure 1.32**) Similar results were attained with dry PS beads as well as wet and dry cyano-labelled TG beads. In these experiments, the lateral spatial resolution of the Raman confocal system was estimated at $1 \times 1\ \mu\text{m}^2$ with a depth resolution of $3\ \mu\text{m}$ for the wet beads and $6\ \mu\text{m}$ in the case of dry beads.

This technique was then extended for the study of functional site reactivity during the coupling of a low concentration of 4-cyanobenzoic acid to AM-PS and TG resins.⁸⁹ At various intervals the reactions were quenched and the beads subjected to mapping as above. In the case of AM-PS, there was a gradual increase of the cyanobenzoic acid throughout the bead as the reaction progressed (**Figure 1.33**), which suggested that the rate of coupling was slower than the rate of diffusion of the reagents into the bead. However, in the case of TG beads, the outer layer reacted first followed by a gradual increase in the interior of the bead until a uniform intensity was produced at the end of the reaction. (**Figure 1.34**) This suggested the opposite rate-limiting step to the AM-PS, here the diffusion of the reagents was slower than the rate of coupling.

Figure 1.32 Raman intensity map of the 2230 cm^{-1} nitrile peak of a AM-PS bead coupled with 4-cyanobenzoic acid (top left), the cross-section through the bead along the x-axis (bottom left) and the y-axis (top right), and the Raman spectra for the nitrile 2230 cm^{-1} peak (bottom right).

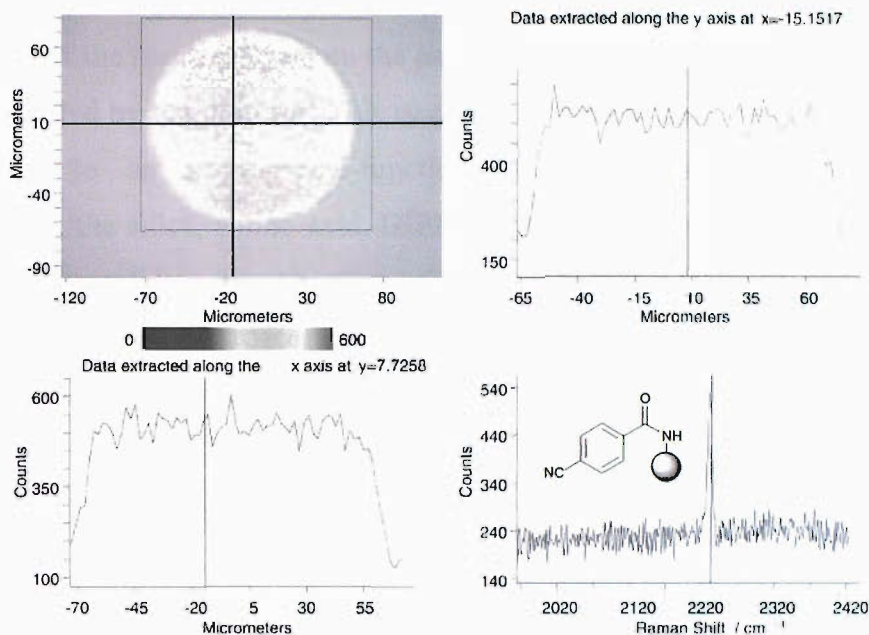


Figure 1.33 Intensity of Raman signal at 2230 cm^{-1} across AM-PS beads at various time intervals (left) and three dimensional representation of the nitrile distribution after 2 min (right).

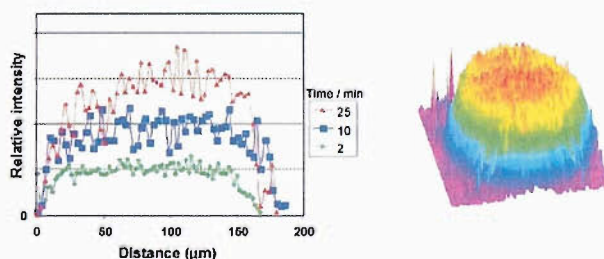
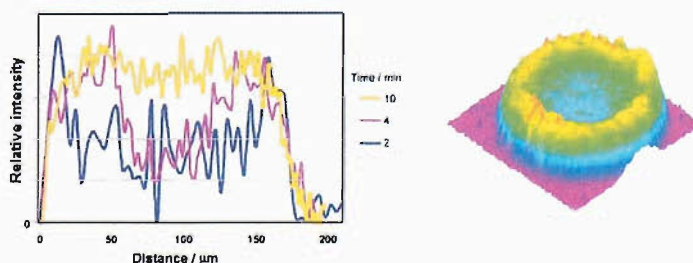


Figure 1.34 Intensity of Raman signal at 2230 cm^{-1} across TG beads at various time intervals (left) and three dimensional representation of the nitrile distribution after 2 min (right).



Confocal Raman real-time reaction monitoring has also been described on a single silica particle. Instead of using a flow cell, the phenomena of optical trapping was used to immobilise the particle of interest during spectral analysis.¹²² Optical trapping employs a tightly focused laser and the momentum of the light itself is used to physically manipulate and isolate the particle of interest.¹²³ At the same time, the scattering of the incident beam on the particle produces the Raman emissions which were recorded by the detector. This system was used to study the attachment of *N*-Fmoc-Phe to an aminopropyl-functionalised HPLC silica particle. In this experiment, the silica, amino acid, DIPEA and the coupling agent benzotriazole-1-yl-oxy-tris-pyrrolidino-phosphonium hexafluorophosphate (PyBOP) and were mixed and injected into the microscope sample cell. One particle was trapped and lifted $\sim 7 \mu\text{m}$ above the cell surface by “optical levitation”.¹²³ This levitation would allow diffusion of the reagents without the interference from the surface of the sample cell and more accurately simulated particles dispersed in a solution. Again, the Raman spectra were recorded and processed by subtraction of the first spectra collected so only the changes during the reaction were visualised. (**Figure 1.35**) From this, the rate constants of the reaction could be calculated. (**Figure 1.36**) Overall, this system was capable of detecting as little as 0.8 fmol of sample and had a focal volume of 2 fL, similar to the previously described confocal system, although the great advantage of this system was the ability to manipulate individual particles *in situ* by optical trapping and optical levitation.

Figure 1.35 Time dependent Raman spectra of Fmoc-Phe coupling to a single silica particle: Raw data (left) and after background correction (right).

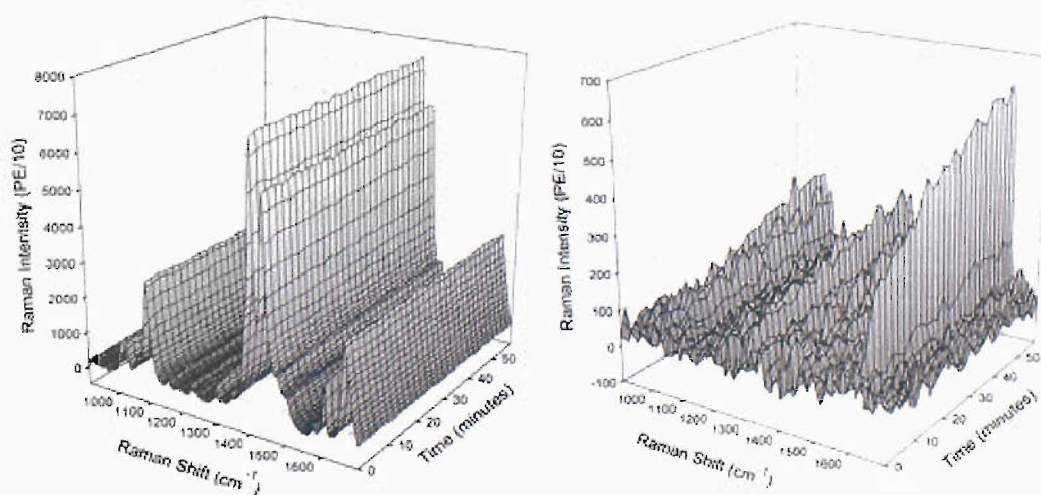
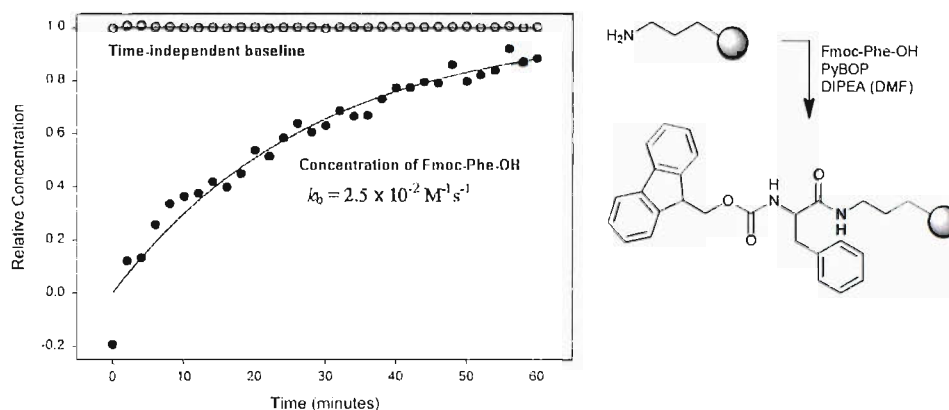


Figure 1.36 Graph of relative concentration of Fmoc-Phe-OH on particle over time.



1.5 Aims of the Research: UV-Visible

Microspectrometry for Solid Supports

The application of UV-Vis absorption spectrometry to SPOS has previously been limited to a few quantitative colorimetric tests described earlier for the determination the amounts of various chromophores related to the supported functional groups.

These quantitative measurements make use of an empirical relationship, the Beer-Lambert Law, which states that the fraction of incident light absorbed is independent of the intensity of the source (Lambert's Law) and the absorption is proportional to the number of absorbing molecules (Beer's Law).^{124,125} (**Equation 1.1**)

$$A = \log\left(\frac{I}{I_0}\right) = \epsilon \cdot c \cdot l \quad \text{Equation 1.1}$$

Where:

| | |
|------------|--|
| A | absorbance of sample |
| I | intensity of transmitted light |
| I_0 | intensity of incident light (or reference) |
| ϵ | molar absorption coefficient |
| c | concentration of sample |
| l | pathlength of light through sample |

The absorbance (A) is an expression of the fraction of light that is absorbed by the sample at a particular wavelength, and in practice is the value most often reported. The molar absorption coefficient (ϵ) is a representation of the UV-Vis “absorptivity” of the sample at a particular wavelength; this is affected by a number of factors such as the structure of the chromophore and the environment surrounding the chromophore (*e.g.* solvent used). There are deviations from the Beer-Lambert law, most commonly observed at high concentrations when the absorbing molecules interact with each other. The formation of dimers or other aggregates also results in the deviation from the Beer-Lambert Law for the same reason.¹²⁵ Deviations may also be due to equipment factors since low light levels (*i.e.* high absorbances) are less accurately measured.

The various optical microspectroscopy methods have been demonstrated to be highly applicable to SPOS for gaining insights into chemical reactions and the physicochemical properties of the supports as well as for the identification of individual members of combinatorial libraries. In this respect, the application of UV-Vis spectroscopy to the study of SPOS supports would further support these activities.

The aims of this research are therefore to explore the feasibility of using UV-Vis microspectrometry for direct analysis of solid-supported chromophores at the single-bead level together with the application of the Beer-Lambert Law for the development quantitative experiments. This could then be exploited to investigate a variety of bead-bound chromophoric species and to develop bead-bound sensors.

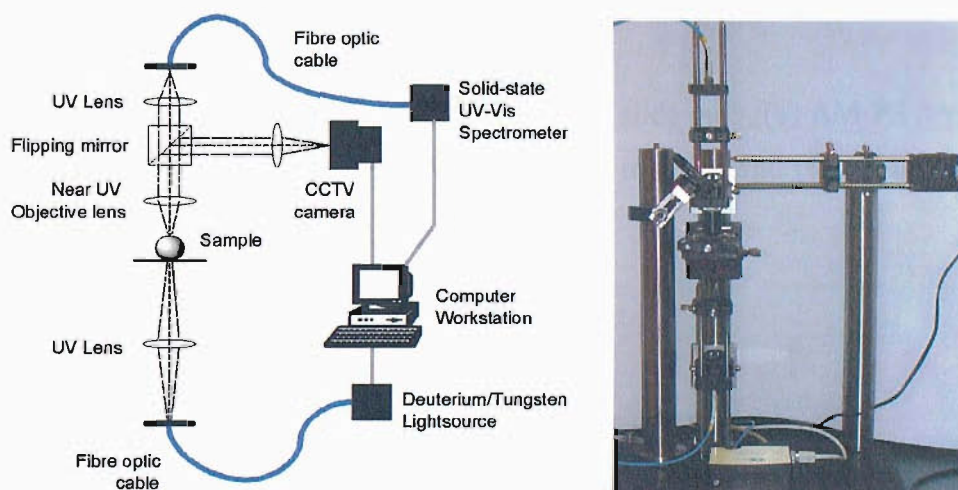
2 On-bead UV-Visible Microspectrometry

The aims of this initial part of the PhD project were to establish the feasibility and applicability of UV-Vis microspectrometry in the analysis of a variety of chromophores on solid supports. To this end a microscope coupled to a UV-Vis spectrometer was constructed in-house and tested in a series of experiments to demonstrate basic qualitative, quantitative and time-resolved UV-Vis spectroscopy on single beads.

2.1 Design and Operation of UV-Vis Microspectrometer

The microspectrometer was built by Dr. Fabrice Birembaut under the supervision of Prof. Mark Bradley, Dr. Jeremy G. Frey and Dr. William S. Brocklesby using UV transmitting fused silica lenses and coupled to a commercially available solid-state fibre optic UV-Vis spectrometer. (**Figure 2.1**)

Figure 2.1 The custom built UV-Vis microspectrometer



In this apparatus, the light was directed into the bottom of the microscope and focused on the sampling area of the microscope stage with the diameter of the focused beam at the sampling area set to 25 μm . This served both as the lightsource for the spectrometer and for visual observation. The light leaving the stage was then either refocused into a fibre optic cable above the microscope leading to the

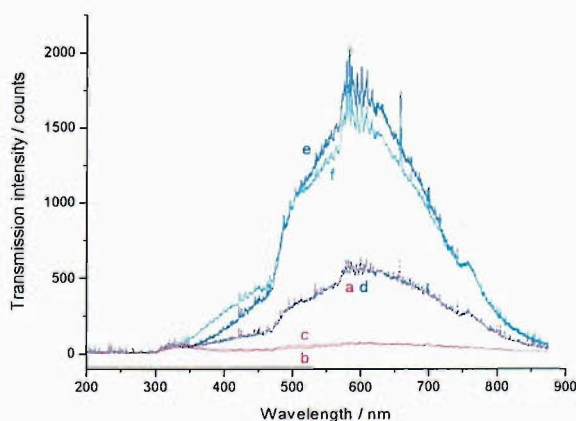
spectrometer, or redirected *via* a manually operated flipping mirror to a television camera for visual observation. Both the spectrometer and camera were interfaced to a personal computer where the data could be displayed and processed. In a typical analysis procedure, the sample beads were placed on a microscope slide on the stage and brought into sharp visual focus. The flipping mirror was then switched so that the lightpath was directed to the fibre optic cable and the UV-Vis spectra recorded.

2.2 Results and Discussion

2.2.1 Initial Testing and Observations

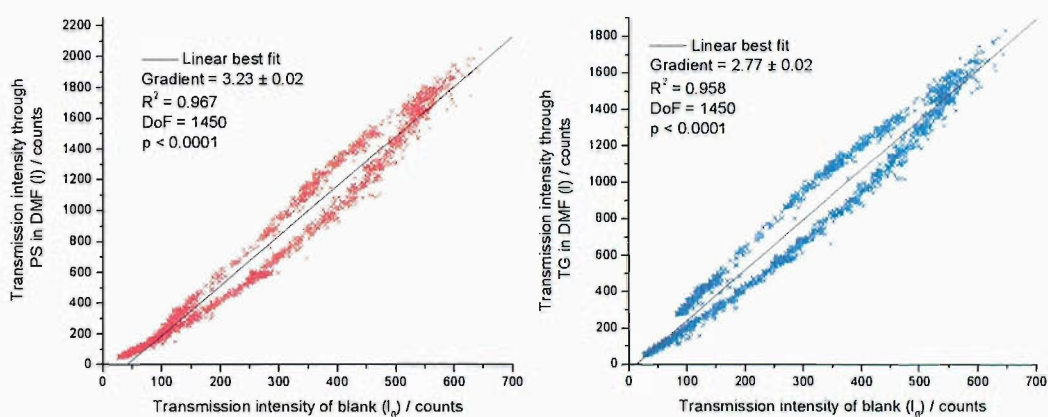
Two types of beads were studied, aminomethyl polystyrene (AM-PS) and TentaGel (TG). Upon examination of the dry beads, an overall reduced transmission of light was observed since the opaque beads scattered the light. When swollen in solvent, beads swelled to ~ 5 times their initial volume (with the volume of the swollen bead being 80-90 % solvent⁸⁹) and became “optically transparent”, allowing the transmission of light (**Figure 2.2**). Further microscopy was therefore carried out using only swollen beads in solvents and to account for the size differences between individual beads in a batch, the averaged spectra from eight different beads were used.

Figure 2.2 UV-Vis transmission spectra: (a) glass slide only, (b) AM-PS dry, (c) TG dry, (d) DMF on glass slide, (e) AM-PS swollen in DMF and (f) TG in swollen in DMF.



An interesting feature observed in this initial testing was that above 400 nm, there was an increase in the transmitted light (or increased focusing of light into the collecting objective) through the swollen beads compared to the light beam passing through the solvent alone. To visualise the degree of magnification over the wavelength range, the transmitted intensity through the beads in DMF against the intensity through DMF alone for both AM-PS and TG was plotted. This gave a near linear relationship between 400-900 nm with approximately 3-fold signal amplification. (**Figure 2.3**) Below 400 nm the absorption of the polymer support itself reduced the transmitted light, which is thus a limitation inherent to working with polymer supports.

Figure 2.3 Plots of transmission intensity through beads in DMF against DMF alone for AM-PS (left) & TG (right) from 400-900 nm.



One possible reason for these observations is that the difference in the refractive index between the solvent and the swollen beads was causing the bead to act as a lens, concentrating the light into the detector. Solvents commonly used in SPOS were evaluated to determine the extent of this effect and if it was possible to eliminate it. (**Table 2.1**) However, complete matching of the transmittance through the bead and through solvent alone was not possible using any of the tested solvents. The relationship between the degree of signal amplification and the type of solvent used was complex since it involved not only the refractive indices of the solvents but also the solvent's effect on the swelling of the beads. For AM-PS, the "lens effect" was apparent in solvents which caused good swelling of the beads while poor swelling solvents resulted in reduced light transmission. To compensate for this

effect, spectra were recorded from swollen beads and used as the reference (I_0 in Equation 1.1) for further experiments.

Table 2.1 Percentage light transmission through resins in different solvents compared to solvents alone.*

| Solvent | Solid Support | | |
|-------------------|---------------|-----|--------|
| | AM-PS | TG | AP-CPG |
| 1,4-dioxane | 401 | 359 | 199 |
| DMF | 347 | 313 | 199 |
| DCM | 365 | 266 | 180 |
| THF | 420 | 367 | 246 |
| MeOH | n.d. | 387 | 323 |
| Toluene | 350 | 162 | 111 |
| DMSO | 40 | 257 | 87 |
| MeCN | n.d. | 507 | 291 |
| H ₂ O | n.d. | 115 | 240 |
| CHCl ₃ | 339 | 237 | 127 |

* Measured at 625 nm, 100 % = no change in absorbance compared to solvent alone, > 100 % indicates increased light transmittance (n.d. = not determined)

DMF = *N,N*-dimethylformamide, DCM = dichloromethane, THF = tetrahydrofuran, MeOH = methanol, DMSO = dimethylsulfoxide, MeCN = acetonitrile

At this point, only glass slides were used to mount the samples but to determine if spectral transmittance at the lower wavelengths could be improved, quartz slides and coverslips were tested. Since only flat slides were commercially available, holes were drilled into glass coverslips and were used as improvised wells when placed between the quartz slide and coverslip.

Testing was carried out to compare the quartz and glass mountings and some improvement in transmission was noted around 300 nm. (**Figure 2.4**) It was hoped that this improvement would allow the detection of the Fmoc chromophore on-bead, which would be very useful since this protecting group is widely used in solid phase peptide synthesis.¹²⁶ Accordingly, spectra of AM-PS and Fmoc-protected glycine attached to AM-PS (Fmoc-Gly-PS) beads were measured on the quartz slides

(**Figure 2.5**). However even when using these slides, the spectral transmission through the beads gradually diminished from 450 nm downwards due to absorption from the resin and the transmission was so weak at the expected absorbance of the Fmoc chromophore that no significant difference could be detected between the AM-PS and the beads loaded with the Fmoc chromophore.

Figure 2.4 UV-Vis transmission through: (a) glass or (b) quartz slides and coverslips compared to (c) lightsource alone.

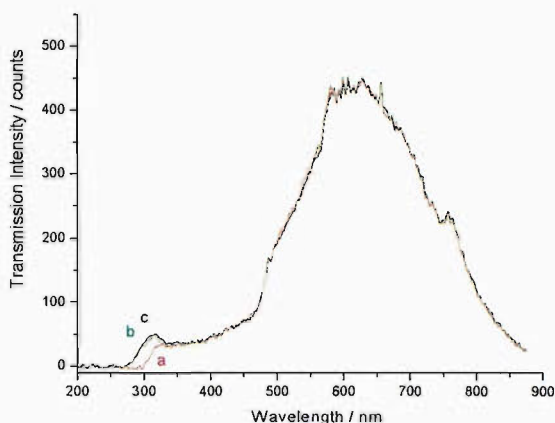
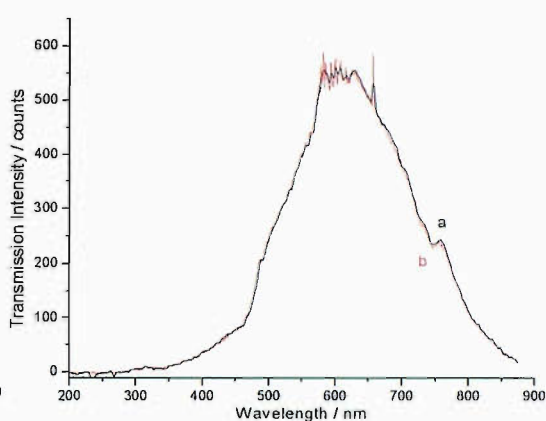


Figure 2.5 UV-Vis transmission through: (a) Fmoc-Gly-PS and (b) AM-PS resins on quartz slides and coverslips.

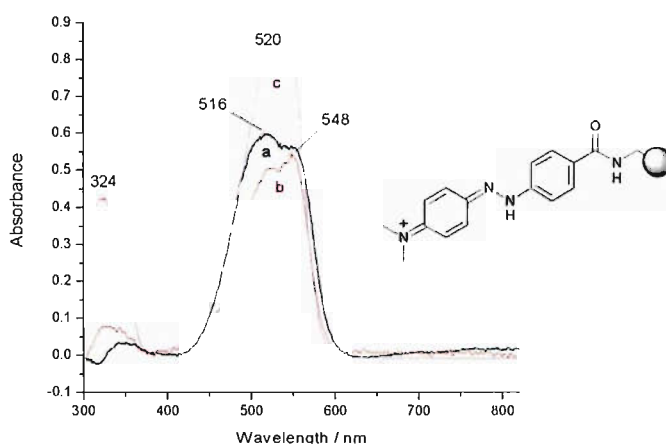


2.2.2 Qualitative Analysis

Having identified the optical issues related to collecting UV-Vis spectroscopic data from the beads, attempts were then made at a qualitative analysis of supported chromophores. The dye *para*-Methyl Red (*p*MR, also known as “dabcyI”) was coupled to AM-PS resin and the UV-Vis spectra of the beads were measured. Initially, beads exhaustively coupled with *p*MR were examined but there was no significant light transmission through the bead due to the intense colouration. A series of much lower dye loadings was then prepared by coupling with substoichiometric amounts of dye (1-10 % of resin amino loading). These were analysed under the UV-Vis microscope and a batch with a nominal loading of 7 % was found to transmit sufficient light for spectra to be measured with a good signal-to-noise ratio. This was compared with the dye in solution and both were observed to be similar although there was some alteration in the value of λ_{\max} . (**Figure 2.6**)

This change may be the result of alteration of the chromophore by its attachment to the solid phase since this involved the conversion of the carboxylic acid to an amide and the physicochemical environment around the chromophore caused by the presence of the polymer.

Figure 2.6 UV-Vis absorption spectra of *para*-Methyl Red in 160 mM HCl in 1,4-dioxane: (a) on AM-PS (7% loading), (b) in solution on the microspectrometer (100 μ M, 3 mm cell) and (c) in solution on a conventional spectrometer (25 μ M, 10 mm cell). (The ionised dye exists as a mixture of tautomers in solution¹²⁷ but for simplicity only the most abundant is shown here.)



A range of structurally diverse chromophores was then examined and compared with the dyes in solution and included (4-Carboxyphenyl)-Bromophenol Blue⁴⁸ (4CBPB) (**Figure 2.7**), Mordant Orange 1 (MO1) (**Figure 2.8**) and Alizarin Yellow GG (**Figure 2.9**) all on TG, as well as 3-nitrotyrosine on aminopropyl functionalised controlled pore glass (AP-CPG). (**Figure 2.10** & **Figure 2.11**) In all cases, an increase in the λ_{max} (*i.e.* a bathochromic shift) was observed, which was relatively small with Bromophenol Blue and nitrotyrosine but was significant with the two azo dyes. This is in agreement with the premise that a more polar solvent would result in a bathochromic shift due to the stabilisation of the more polar excited state¹²⁵ since the environment provided by the polyethylene glycol (PEG) chains on TG would be relatively more polar compared to the solvent alone.

Figure 2.7 UV-Vis spectra of 4CBPB in 72 mM Et₃N in 1,4-dioxane: (a) on TG (7% loading), (b) in solution in the microspectrometer (35 μM, 3 mm cell) and (c) in solution in a conventional spectrometer (10 μM, 10 mm cell).

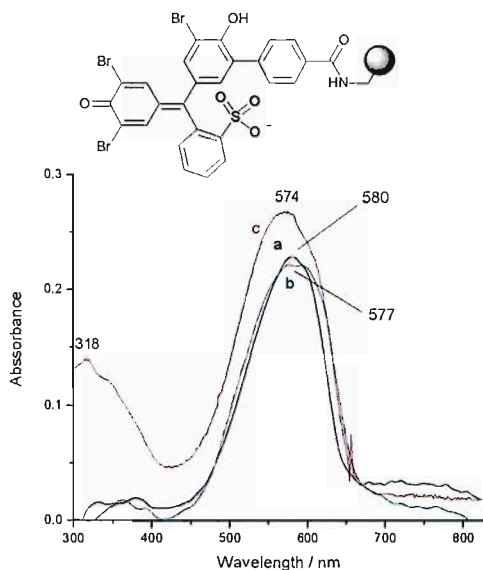


Figure 2.8 UV-Vis spectra of MO1 in 160 mM HCl in 1,4-dioxane: (a) on TG (10% loading), (b) in solution in a conventional spectrometer (33 μM, 10 mm cell).

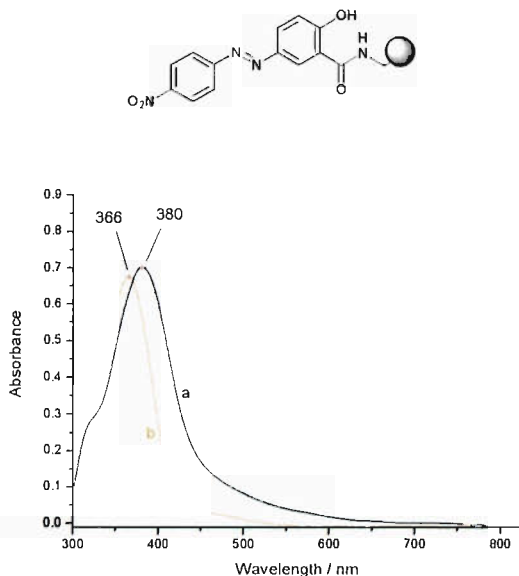


Figure 2.9 UV-Vis spectra of Alizarin Yellow GG in 160 mM HCl in 1,4-dioxane (a) on TG (10% loading), (b) in solution in a conventional spectrometer (56 μM, 10 mm cell).

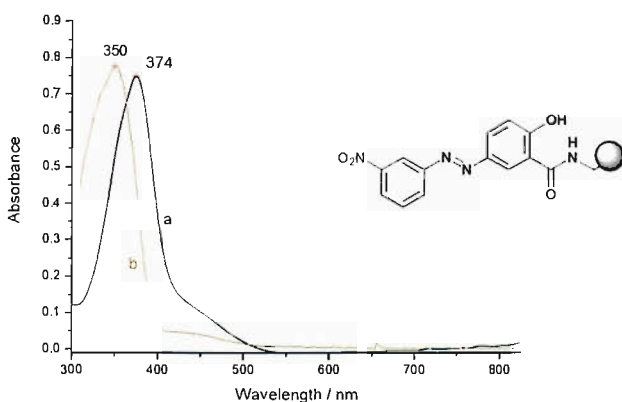


Figure 2.10 UV-Vis spectra of 3-nitrotyrosine in 1M NaOH: (a) on AP-CPG (61 μmolg^{-1}), (b) in solution in a conventional spectrometer (135 μM , 10 mm cell).

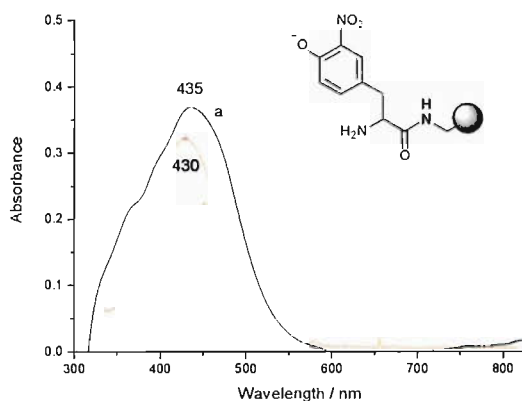
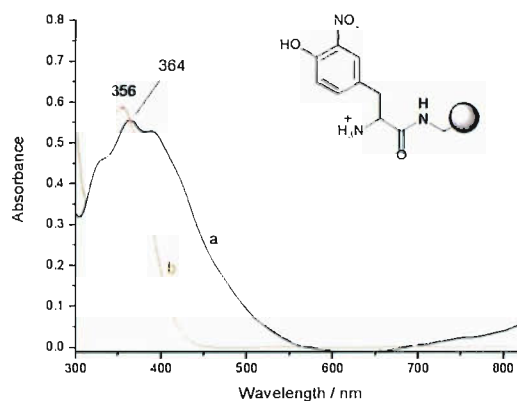


Figure 2.11 UV-Vis spectra of 3-nitrotyrosine in 1M aq. HCl: (a) on AP-CPG (61 μmolg^{-1}), (b) in solution in a conventional spectrometer (75 μM , 10 mm cell).



In summary, these test samples demonstrated that UV-Vis microspectroscopy was applicable to solid supports, although some changes in the spectra could be expected when compared to the solution phase equivalents. The main limiting factor was the poor light transmission at lower wavelengths which would not allow the study of UV only chromophores. This was a limitation inherent to the supports and therefore not addressable by the use of improved equipment.

2.2.3 Quantitative Analysis

Steps were now taken towards quantitative analyses with the study of dyes coupled beads at various loadings and the UV-Vis spectra of AM-PS coupled with *p*MR (1-10 % loadings) were recorded. Attempts were then made to quantify, in absolute terms, the relationship between loading and absorbance by applying the Beer-Lambert Law. However, the actual amount of dye coupled to the resins could not be accurately measured by either elemental analysis or other standard tests due to the low loading levels involved. To address this issue, the amount of coupled dye was determined indirectly through UV-Vis analysis of the reaction solutions. Thus for selected samples, the amount of dye in the reaction solution were measured pre- and post-coupling, and the difference was then used to calibrate the loading value.

(**Figure 2.12**) By applying the Beer-Lambert Law (**Equation 1.1**), the ϵ_{\max} for the dye attached to the beads was calculated using the diameter of the bead as the pathlength and the concentration of dye per bead (based on loading per bead and the volume of the swollen bead). For pMR, this gave a value of $\sim 7700 \text{ M}^{-1}\text{cm}^{-1}$. There was a similar linear relationship between loading and absorbance for 4CBPB on TG with 1-20 % nominal loadings, with a calculated ϵ_{\max} of $\sim 8500 \text{ M}^{-1}\text{cm}^{-1}$. (**Figure 2.13**)

The values of ϵ_{\max} calculated were approximately 2.5 times lower than those of the solution phase analogues for both dyes ($\epsilon_{548} = 18266$ for pMR, $\epsilon_{595} = 21233$ for 4CBPB, in the same solvents as used for the beads). The reason for this is unclear but ϵ_{\max} may be affected by the lower polarity of the surrounding environment within the polymer matrix and the high concentration of dye within the bead. This may also be the result of the previously mentioned “lensing” optical effect on the beads, although no obvious relationship could be inferred between the degree of reduction in the ϵ_{\max} and the degree of increased light intensity detected.

Figure 2.12 UV-Vis absorbance spectra of pMR on AM-PS beads at various loadings in 10 mM HCl in 1,4-dioxane with nominal loadings of (a) 10 %, (b) 9 %, (c) 8 %, (d) 7 %, (e) 6 %, (f) 5 %, (g) 4 %, (h) 3 %, (i) 2% and (j) 1% (left). Linear fit of absorbance vs. loading. (right)

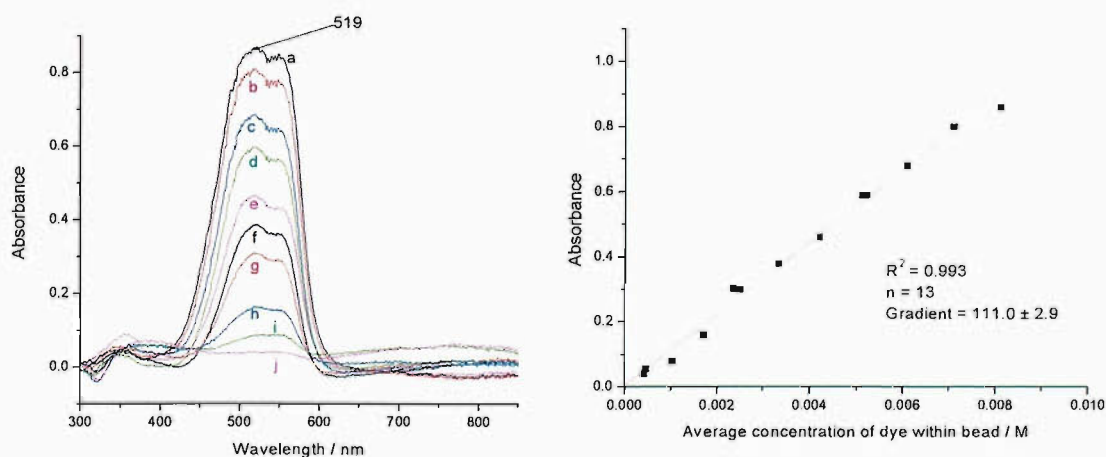
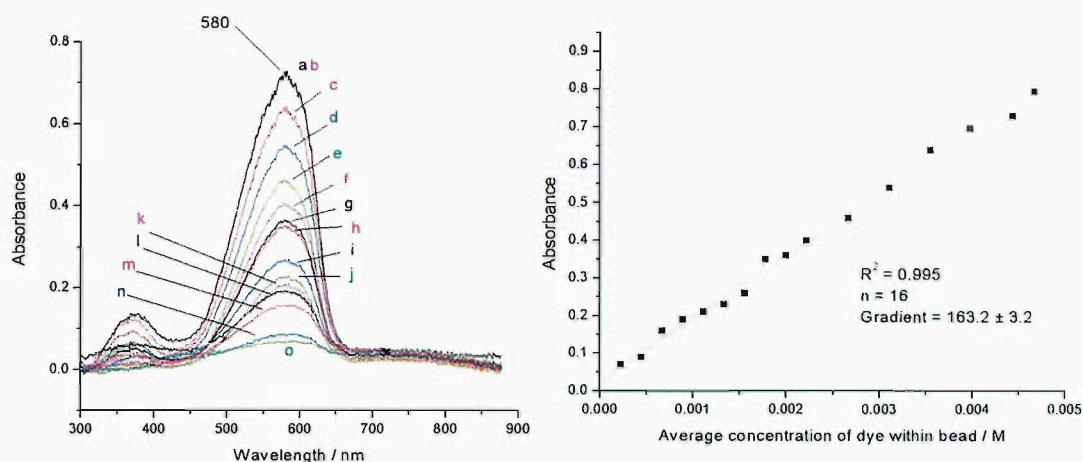


Figure 2.13 UV-Vis absorbance spectra of 4CBPB on TG beads at various loadings in 72 mM Et₃N in 1,4-dioxane with nominal loadings of (a) 20 %, (b) 18 %, (c) 16 %, (d) 14 %, (e) 12 %, (f) 10 %, (g) 9 %, (h) 8 %, (i) 7%, (j) 6 %, (k) 5 %, (l) 4 %, (m) 3 %, (n) 2 % and (o) 1 %. (left) Linear fit of absorbance vs. loading. (right)

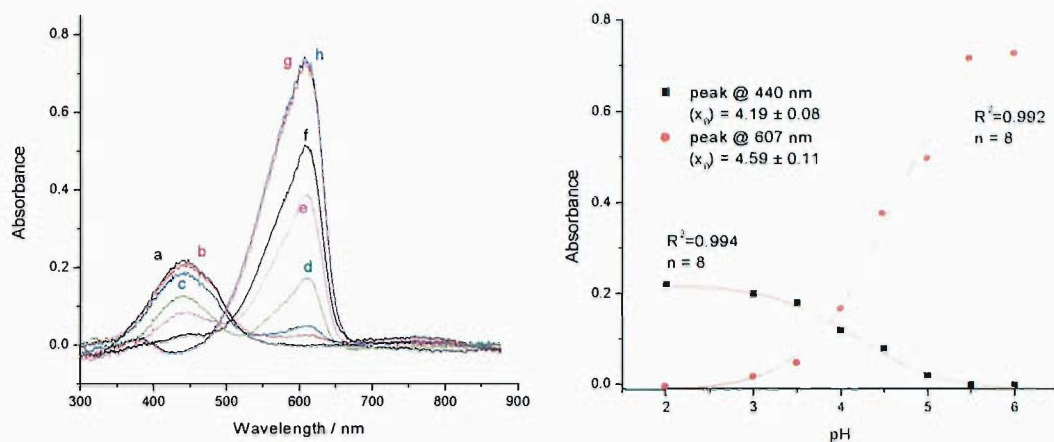


Nevertheless, both supported chromophores displayed linear relationships between the absorbance and amount of dye, and confirmed the validity of using the Beer-Lambert Law for these calculations.

2.2.4 UV-Visible Profiling of Solid Supported pH Indicator Dyes

Both *p*MR and Bromophenol Blue are used as pH indicators, and the pK_i of a dye in solution can be determined by UV-Vis spectrometry by quantifying the pH-dependent colorimetric changes.¹²⁸ To test the applicability of this on the solid-supported indicators, the spectra of 4CBPB loaded on TG (20 % nominal loading) were measured at various pH's. The intensities of the two peaks corresponding to the acid and base forms of the dye were plotted against pH with the best-fit Boltzmann sigmoidal curve. (**Figure 2.14**)

Figure 2.14 UV-Vis absorption spectra of 4CBPB-TG beads in aqueous solutions at various pH's: (a) 2 , (b) 3, (c) 3.5, (d) 4, (e) 4.5, (f) 5, (g) 5.5 and (h) 6. (left) Sigmoidal fit of absorbance against pH. (right)



From these plots, the pH at the inflection point between the maximum and minimum absorbance intensity (x_0) were determined. Thus, the pK_i was estimated to be between 4.2 (based on measurements at 440 nm) and 4.6 (based on measurements at 607 nm). For comparison, the spectra of a solution of (4-carboxyphenyl)-Bromophenol Blue were recorded at various pH's (**Figure 2.15**) and the pK_i values obtained (3.94 for the peak at 440 nm and 4.29 for the peak at 594 nm) were very similar to literature values for unmodified Bromophenol Blue in solution (~ 4.00).¹²⁸ Both were somewhat lower than for the resin-bound indicator signifying that the deprotonation of the indicator on TG required more basic conditions.

A similar experiment was conducted with *p*MR linked to TG (10% loading). The spectra in this case were more difficult to interpret due to the close overlap of the two possible absorbance bands, so in order to extract the desired information, deconvolution calculations were necessary. Using a model of two Gaussian peaks, the calculated maxima for these deconvoluted peaks (at 480 and 520 nm respectively) were then plotted in a similar manner to the Bromophenol Blue derivative. (**Figure 2.16**)

Figure 2.15 UV-Vis absorption spectra of 4CBPB-TG in aqueous solutions at 141 μM at various pH's: (a) 1.5, (b) 2.5, (c) 3.0, (d) 3.5, (e) 4.0, (f) 5.0, (g) 5.5 (h) 6.0 and (i) 6.5. (left) Sigmoidal fits of absorbance vs. pH (right)

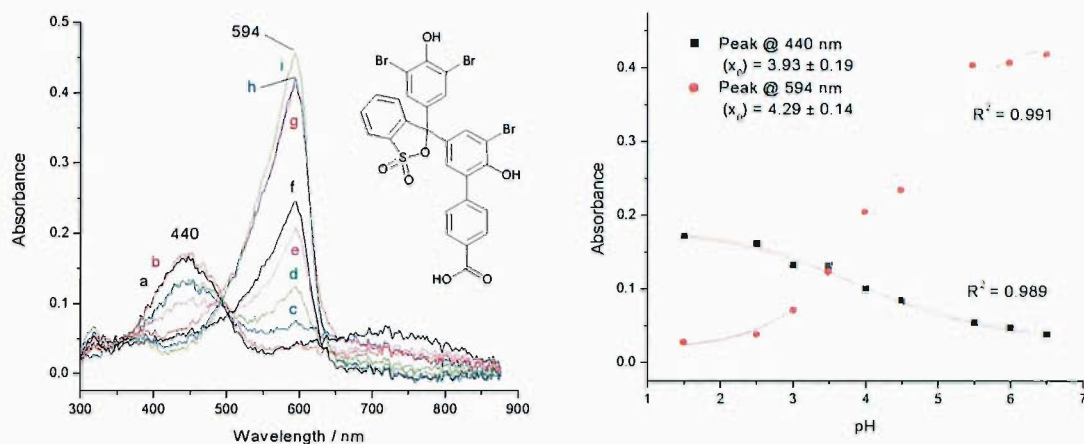
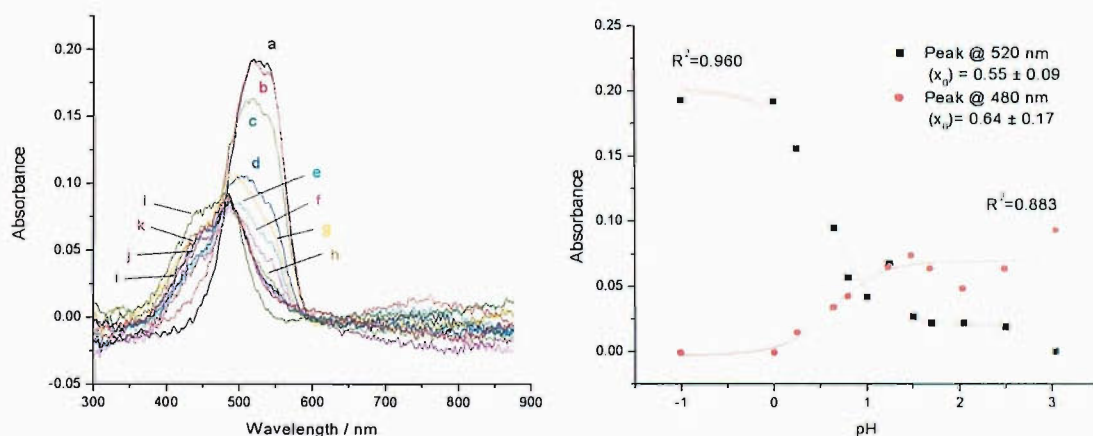


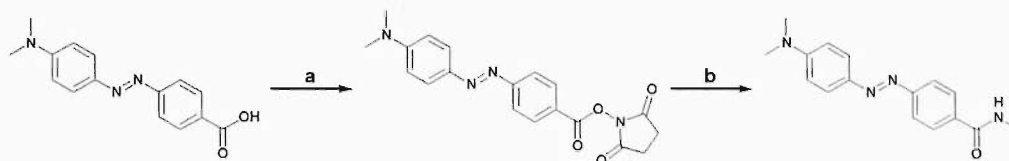
Figure 2.16 UV-Vis absorption spectra of *p*MR-TG beads in aqueous solutions at various pH's: (a) -1.00, (b) 0.00, (c) 0.25, (d) 0.65, (e) 0.80, (f) 1.00, (g) 1.25, (h) 1.50, (i) 1.70, (j) 2.05, (k) 2.50, (l) 3.05. (left) Sigmoidal fits of absorbance vs. pH (right).



From the plots, the estimated pK_i values in this case were 0.55 (from 520 nm) and 0.64 (from 480 nm) and were supported by a visually observed colour change in this pH range. This differed significantly from the known pK_i of ~ 1.78 for *p*MR in solution.¹²⁹ In order to determine if amide bond formation may have been the cause of this, *p*MR was coupled to methylamine *via* its succinimide ester.¹³⁰ (Scheme 2.1) The solution-phase spectra of this modified indicator were then measured at various pH's and the pK_i determined to be 1.66, similar to the

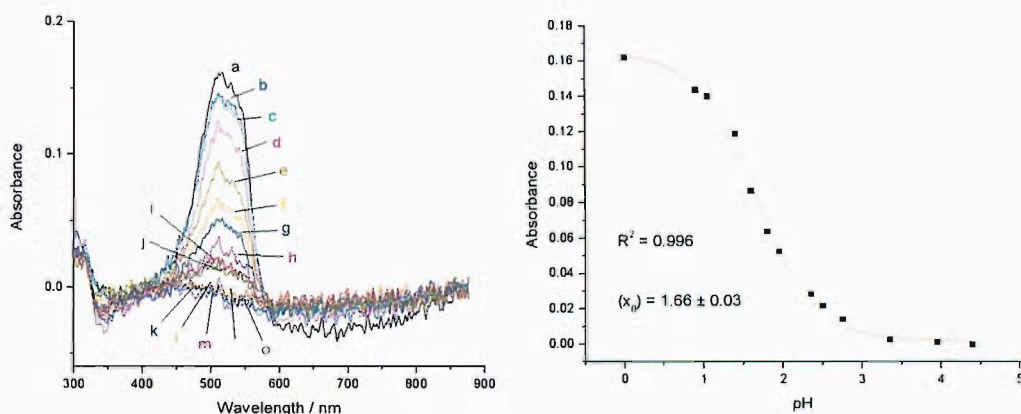
unmodified *p*MR but again significantly different to the solid-phase version. (**Figure 2.17**) This implies that much higher H_3O^+ concentrations were needed to protonate the indicator moieties that were within the polymer matrix of TG.

Scheme 2.1 Synthesis of *p*MR methyl amide.



Reagents & conditions: (a) HOSu, DCCl, DMF, 16 h; (b) $\text{MeNH}_2 \cdot \text{HCl}$, DIPEA, DMF, 16 h. 31 % over 2 steps. (HOSu = *N*-hydroxysuccinimide, DCCl = *N,N'*-dicyclohexylcarbodiimide, MeNH_2 = methylamine)

Figure 2.17 UV-Vis absorption spectra for *p*MR methyl amide in an aqueous solutions at various pH's (a) 0.00, (b) 0.90, (c) 1.05, (d) 1.40, (e) 1.60, (f) 1.80, (g) 1.95, (h) 2.35, (i) 2.50, (j) 2.75, (k) 3.20, (l) 3.35, (m) 3.50, (n) 3.95, (o) 4.40. (left) Sigmoidal fit of absorbance (at 516 nm) against pH. (right)



In both of these cases, more extreme conditions were needed for ionisation, increased pH for deprotonation and reduced pH for protonation. This may be caused by the high local concentration of indicator moieties within the bead (~ 2.5 mM) which decreases their likelihood of ionisation. The alteration of ion stability of reactants or products is an important factor in many chemical reactions and these results suggest that when transferring solution phase reactions to SPOS, equivalent outcomes should not be assumed.

2.2.5 Analysis of pH-Indicating Resins

In collaboration with Dr. J. K. Cho (Centre for Combinatorial Excellence), the concept of pH indicating beads was explored where a combination of two visual indicator dyes on TG were prepared with the intention of using these for sensing and monitoring applications. These resins made use of carboxyphenyl derivatives of sulfthalein dyes similar to 4CBPB, (4-carboxyphenyl)-Bromocresol Purple (4CBCP) and (4-carboxylphenyl)-Bromothymol Blue (4CBTB), which both change from yellow in acidic conditions to dark blue when ionised in basic conditions. *p*MR was used in conjunction with these, which changes from yellow under basic conditions to red (ionised) as the pH is decreased. (Figure 2.18 & Table 2.2) The combination of colours from the two indicators resulted in resins which changed from orange to a deep yellow and finally to a blue-black as the pH was increased. (Figure 2.19) To test the utility of the UV-Vis microspectroscopy on “real world” samples, the spectra of these beads were recorded at different pH’s.

Figure 2.18 General structure of pH indicating resins.

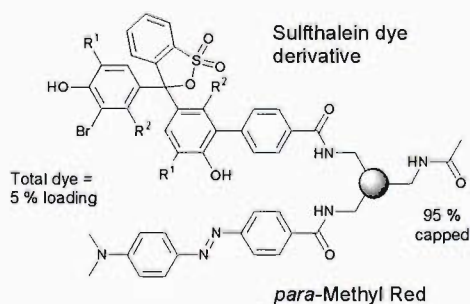
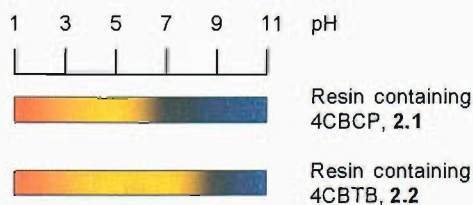


Table 2.2 Substituents of supported sulfthalein indicators.*

| | R ¹ | R ² | Originating dye |
|-----|-----------------|----------------|--------------------|
| 2.1 | Me | H | Bromocresol Purple |
| 2.2 | ⁱ Pr | Me | Bromothymol Blue |

* Me = methyl, ⁱPr = *iso*-propyl

Figure 2.19 Visually observed colour change for 2.1 & 2.2 in aqueous solutions.



For resin **2.1** (**Figure 2.20**) at pH 1, this was an orange colour and corresponded with the UV-Vis spectra which appeared to consist of two overlapped absorbance bands, a major band at ~450 nm which corresponds to the yellow colour of pMR and 4CBCP at this pH and a shoulder which corresponded to the red colour of ionised pMR. The latter was a minor component of the spectra since at this pH only a small proportion of pMR was in the red ionised form. At pH 5, the yellow unionised forms of both dyes gave only one major peak at 481 nm. Finally at pH 9, the dark blue colour of 4CBCP dominated the spectra giving a λ_{max} of 613 nm, though the yellow unionised form of pMR contributed to the shoulder at 400-500 nm.

For resin **2.2** (**Figure 2.21**) at pH's 1 & 5, the major absorbance was at ~460 nm peak corresponding to both yellow unionised dyes, although again a small shoulder was observed at pH 1 which corresponded to a small amount of ionised pMR. At pH 9, an additional absorbance peak at 622 nm appeared that was consistent with the blue colour component of the Bromothymol Blue derivative. At pH 11, this peak was so intense that the quality of the UV-Vis spectra was distorted and noisy, with extremely high absorbance values indicating the beads were no longer entirely optically transparent and was supported by the very dark colouration of the beads by visual observation.

Figure 2.20 UV-Vis absorbance spectra of resin **2.1** at (a) pH 1, (b) pH 5 & (c) pH 9.

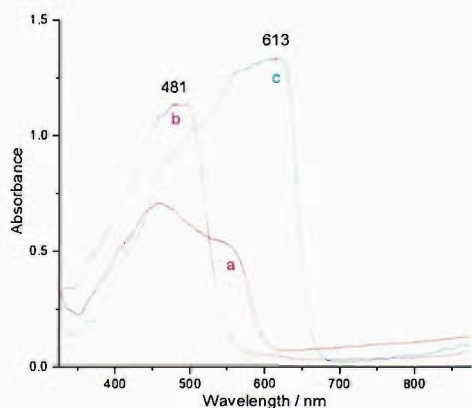
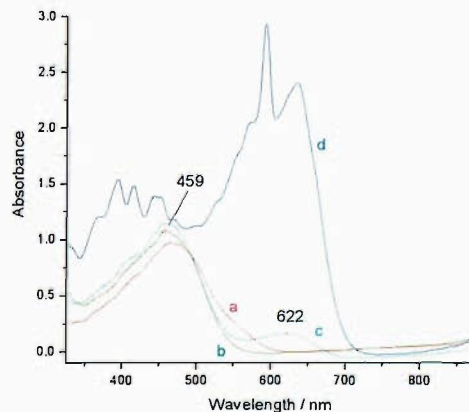


Figure 2.21 UV-Vis absorbance spectra of resin **2.2** at (a) pH 1, (b) pH 5, (c) pH 9 & (d) pH 11.



In summary, the results of the UV-Vis microspectrometry were used to supplement and confirm the otherwise rather subjective visual observations of the resin colour changes at different pH's. Additionally, the spectra indicated that even at pH 1 only minor amounts of ionised *p*MR were present, which supported earlier observations of the unusually low pK_i value of TG-supported *p*MR.

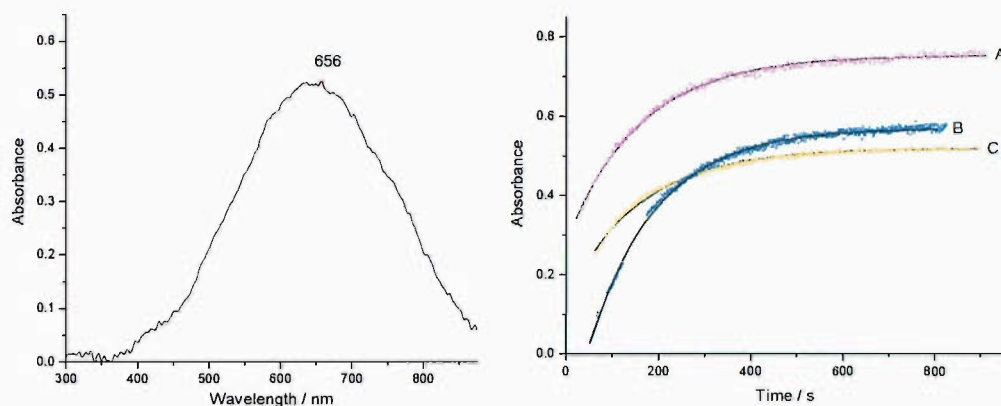
2.2.6 Real-Time Reaction Monitoring and Reaction Kinetics

The use of the microspectrometer as a tool for real-time reaction monitoring was also investigated as another possible application of this system, taking advantage of the solid-state design and associated software of the spectrometer which enables spectra to be measured far more quickly than a conventional split-beam spectrometer.

Thus, the main aim for this part of the research was to determine if quantitative data could be acquired for reaction kinetics. To demonstrate this, the chloranil test²² for secondary amines was studied. (**Scheme 1.4**) The secondary amine used in the study was proline attached *via* a 2-chlorotriptyl (Clt) linker¹³¹ to PS beads. The amine was first pre-reacted with a large excess of acetaldehyde before the addition of the chloranil so only the colour-producing step was studied. The UV-Vis spectra of a single bead were measured over time after the addition of the chloranil at a rate of 1 spectra/s and the absorbance at 550 nm was plotted against time (**Figure 2.22**). The high absorbance at the λ_{max} of the spectra was not used so as to avoid low light intensities and so the absorbance values fell within the range where the Beer-Lambert linear relationship between concentration and absorbance was likely to be maintained.

In these experiments, the amount of chloranil used for each reaction was also in excess so the only limiting factor was the amount of amine sites on the beads. Thus, the data could be modelled against a pseudo-first order reaction (**Equation 2.1**) and the kinetic parameters calculated. (**Table 2.3**)

Figure 2.22 UV-Vis absorbance spectra of a bead during the reaction (left) and UV-Vis absorbance at 550 nm plotted against time for 3 beads (right)



$$A = A_{\max} [1 - e^{-k(t-t_0)}]$$

Equation 2.1

Where:

- A absorbance
- A_{\max} maximum absorbance
- t time
- t_0 time when $A = 0$
- k rate constant

Table 2.3 Calculated parameters of the reactions.

| Figure | R^2 | A_{\max} | t_0 / s | k / s^{-1} |
|-----------|-------|------------|-----------|--------------|
| 2.22 ref. | | | | |
| A | 0.994 | 0.754 | -74.3 | 0.0063 |
| B | 0.997 | 0.572 | 44.2 | 0.0069 |
| C | 0.994 | 0.522 | -46.6 | 0.0064 |

Overall, the data fitted very well with the model equation, with variations in A_{\max} between different beads, likely due to variations in the size of the individual beads. Similarly, individual variations in the t_0 values were the result of the time differences between the addition of the chloranil solution and the commencement of

data acquisition. Nevertheless, the rate constant k demonstrated good reproducibility despite the differences in the bead sizes with an average value of 0.00653 s^{-1} .

Thus these experiments showed that the microspectrometer could be used for on-bead determination of reaction kinetics and real-time monitoring. Additionally, these studies into the chloranil test confirm that a reaction time of 5 min was sufficient for the positive determination of amines on-bead since the majority of the sites reacted within this time frame.

2.3 Conclusions

The aims of this section of the research were achieved in that qualitative, quantitative and time-resolved UV-Vis spectrometry at a single bead level were demonstrated. Issues such as the UV-Vis absorption of the beads and the “lens effect” were addressed by the use of appropriate reference samples although a lower spectral limit of $\sim 350 \text{ nm}$ was imposed by the beads. The quantitative experiments demonstrated this was a sensitive method with a linear response range over bead loadings of 1-20 % (in the pmol/bead range), depending on the resin and dye used. In terms of time-resolved analysis, the high rate of spectra collection allowed a large amount of data to be collected, allowing kinetic calculations to be made.

In all cases, the sampling of a larger number of beads would provide more representative information regarding each batch and in this respect, the system would benefit from automation of spectra collection, either by automatic detection of beads or a scanning system where data from an entire array of beads could be collected.

3 Development of Fibre Optic UV-Visible

pH Sensors Utilising Tethered Indicator

Dyes

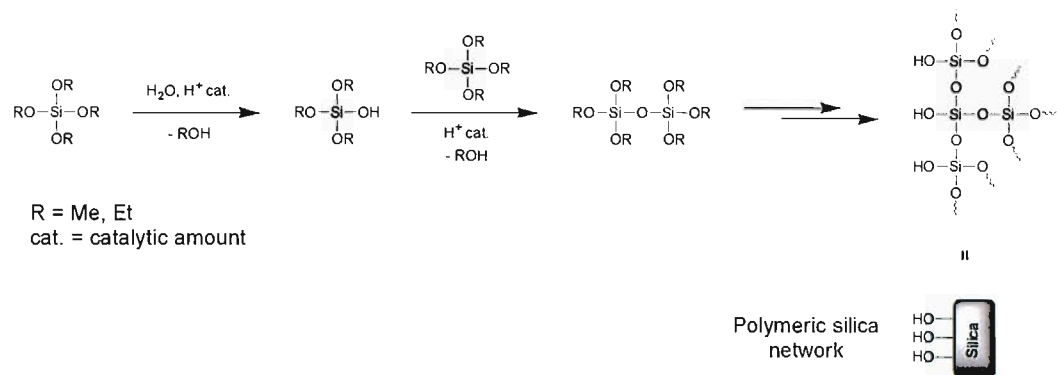
3.1 Introduction: Fibre Optic pH Sensing

Due to the importance of pH measurement in many fields of environmental, chemical and medical sciences, considerable efforts have focused on the development of organic-inorganic “functional hybrids” as pH sensing devices.¹³²⁻¹³⁵ In these devices, an organic indicator dye is immobilised on a polymeric matrix and is interfaced with a UV-Vis spectrometer, allowing colorimetric changes with pH to be measured.

Such solid-state sensors offer several advantages over standard electrochemical glass pH meters:^{134,136} (1) Fibre optic sensors do not rely on electrical currents and are therefore not affected by strong electrical fields, (2) light transmission through the fibres is extremely efficient and signals can be transmitted over long distances (up to several kilometres), allowing remote monitoring, (3) simultaneous sensing of multiple analytes is possible using a number of immobilised reagents and (4) fibre optic sensors can be produced in relatively small size. In terms of biomedical applications, the lack of electrical components in the sensor, small size and use of biologically inert materials make such sensors highly appealing.

Sol-gel glass is the most commonly used support for the indicator dyes in sensor applications. These glasses are optically transparent and have a porous silica polymeric network that is produced by the hydrolysis and polycondensation of silicon alkoxides in solution during the so-called “sol-gel process”.¹³⁵ (**Scheme 3.1**) By adjusting various parameters during synthesis, the fine structure (*e.g.* pore size) of the final sol-gel can be controlled and the glass itself may be prepared in a variety of shapes and sizes (*e.g.* particles, blocks, films).

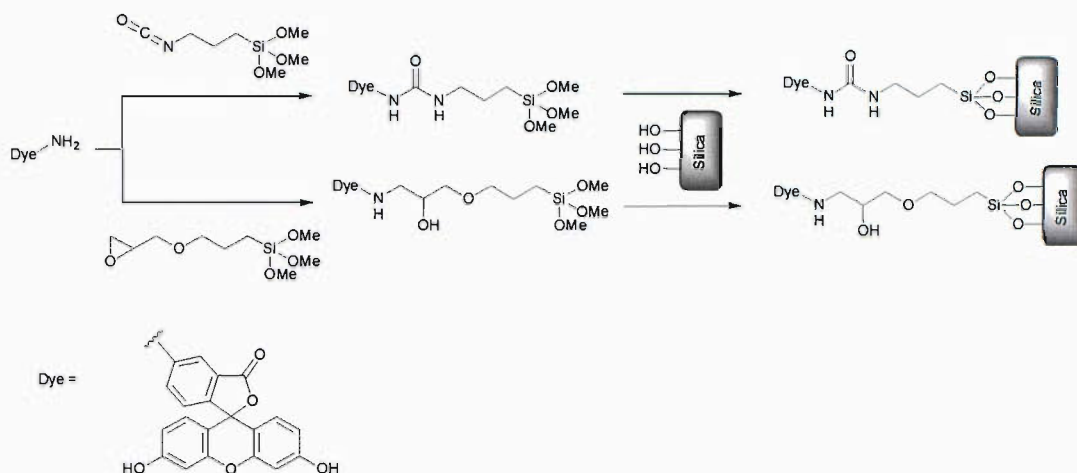
Scheme 3.1 Polymerisation of silicon alkoxides into a silica matrix.



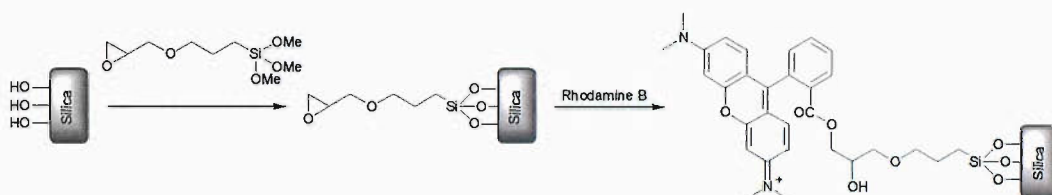
Often, the dyes are incorporated by non-covalent entrapment within the sol-gel matrix by addition of the dye to the mixture during the polymerisation process. However in sensors prepared in this way, there is often a gradual leaching of the dyes out of the matrix and into the media¹³⁷ resulting in contamination of the media as well as degradation of the sensor over time. This can be addressed by producing matrices of small pore size¹³⁷ to prevent the escape of the dyes or by incorporating hydrophobic monomers into the matrix during polymerisation such as Phenyl-, *iso*-butyl- or methyl-trimethoxysilane.¹³⁸⁻¹⁴⁰ However, this reduces access by the aqueous solutions to the indicator molecules and increases sensor response time.

Alternatively, the indicator dyes (both chromophores and fluorophores) can be covalently linked to prevent leaching and procedures for the attachment of indicators to silica-based sol-gel supports have been described using various activating agents as attachment moieties. An indicator may be attached to the activating agent and the activated dye moiety attached to the support, or the activating agent may first be attached to the support followed by the dye. The attachment of 4-aminofluorescein to sol-gel matrices with (glycidyoxypropyl)trimethoxysilane or 3-(trimethoxysilyl)propylisocyanate are examples of the former case.¹³⁸ (**Scheme 3.2**) The alternative strategy, attachment of (glycidyoxypropyl)trimethoxysilane first to the matrix followed the dye (Rhodamine B) has also been reported.¹⁴¹ (**Scheme 3.3**)

Scheme 3.2 Attachment of 4-aminofluorescein to sol-gel matrices via epoxides and isocyanates.

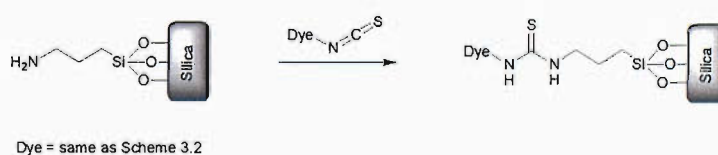


Scheme 3.3 Attachment of Rhodamine B to sol-gel matrices via epoxides.



Intermediates between these two strategies have also been described, with the silica matrix prefunctionalised with aminopropyl groups followed by attachment of isothiocyanate-functionalised dyes.^{142,143} (**Scheme 3.4**)

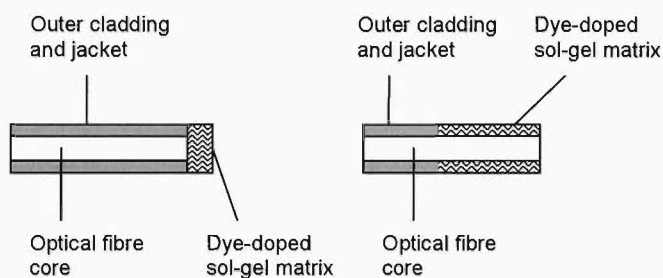
Scheme 3.4 Attachment of fluorescein isothiocyanate to the prefunctionalised silica matrix.



The use of cellulose has also been described as a support for indicator dyes in optical sensing applications. Although these have not used in conjunction with fibre optics, they demonstrate a number of chemical strategies that can be used for the attachment of dyes to solid supports including *via* imines,^{144,145} esters (formed with a water soluble carbodiimide)¹⁴⁶ and vinyl sulfones.¹⁴⁷

The sol-gels containing the indicator are then interfaced to the optical fibre either at the distal end of the fibre or by “side coating” the core of an unclad portion of a fibre.¹³⁵ (**Figure 3.1**)

Figure 3.1 Configurations of fibre optic sensing elements where the sol-gel is at the distal end (left) or side coated. (right)



Since issues such as self-quenching^{93,142} and photodegradation^{89,132} are a concern when using immobilised fluorophores; non-fluorescent dyes may be more suitable as spectrometric sensors. The work described in the previous chapter on UV-Vis spectrometric pH profiling of bead-supported indicator dyes suggested that routinely used SPOS procedures could be applied to the development of new sensors.

Instead of sol-gel glass, macroporous controlled pore glass (CPG) beads could be used as the support for the dyes since they possessed a number of characteristics that were desirable from sol-gel glasses such as functional group accessibility that was solvent-independent, rigidity (non-compressible and non-swelling), chemical inertness (except to strong alkalis), physical robustness and a large pore size. However unlike sol-gel materials, CPG beads are amenable to SPOS.¹⁴⁸ The spherical beaded consistency of this CPG was also convenient as a single “sensor bead” could be integrated into a fibre optic sensor assembly coupled to a solid-state UV-Vis spectrometer.

To this end, work was conducted on the attachment of various indicator dyes to CPG beads and the integration of these beads into a pH sensor assembly that was coupled with the fibre-optic UV-Vis spectrometer. The pH profile, response time and durability of the prepared sensors could then be examined.

3.2 Sensors Bearing Carboxy-Functionalised

Indicator Dyes

Based on the work associated with the initial testing of the UV-Vis microspectrometer, two solid-supported, covalently-linked pH indicators were first considered, *p*MR and 4CBPB.

3.2.1 Attachment of Carboxy-Functionalised Dyes to Macroporous Glass Beads

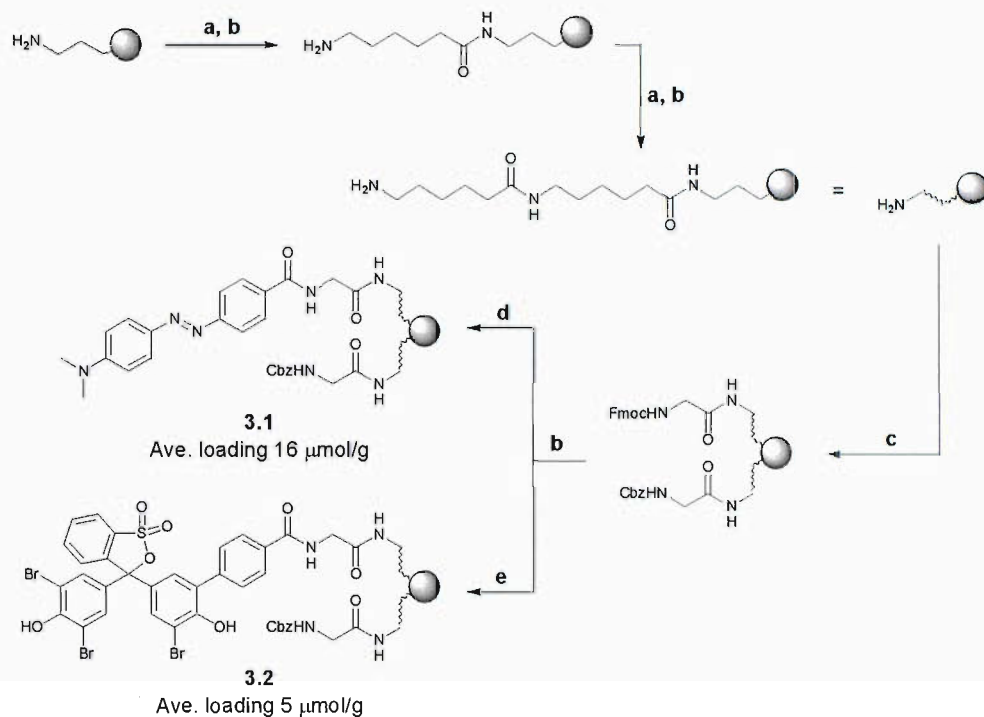
In addition to the good accessibility of the media to the indicators offered by the large pore size of the CPG, a di- ϵ Ahx spacer/tether was incorporated between the dyes and surface of the support to improve the flexibility and the exposure of the indicator. Prefunctionalised AP-CPG with a base amino loading of $171 \mu\text{molg}^{-1}$ was used as the starting support material and a stepwise strategy was adopted for the attachment of the spacer moieties followed by the dyes. An additional step was included to allow accurate control of the amount of dyes finally attached to the beads. (**Scheme 3.5**)

Due to the low reactivity of the amine close to the surface of the silica, the attachment of the first ϵ Ahx residue required microwave heating with a small excess of coupling agent. However, even under optimum conditions a yield of only $88 \mu\text{molg}^{-1}$ was achieved (by Fmoc quantification after ϵ Ahx coupling), although all batches gave a negative ninhydrin test result indicating all the readily accessible amine had been reacted.

Taking into consideration the low reactivity of this support, the Fmoc deprotection with piperidine was extended to 30 min and examination of the beads by IR microspectroscopy indicated complete deprotection was achieved in this time by loss of the carbamate absorbance band at $\sim 1700 \text{ cm}^{-1}$. The coupling of the next ϵ Ahx residue under the optimised microwave conditions gave the CPG with an average Fmoc loading of $75 \mu\text{molg}^{-1}$. Various ratios of benzyloxycarbonyl (Cbz) and Fmoc protected Gly were then attached to provide CPG with a range of Fmoc loadings. (**Table 3.1**) (This procedure was found to be superior to coupling sub-

stoichiometric amounts of amino acid which were sluggish and rarely went to completion due to the low concentrations of the reactants.)

Scheme 3.5 Attachment of tethered carboxy-functionalised indicators to AP-CPG.



Reagents & conditions: (a) Fmoc- ϵ Ahx-OH, DIC, THF, 140 °C microwave, 45 min; (b) 20% piperidine *v/v* in DMF, 30 min; (c) Cbz/Fmoc-Gly-OH, DIC, HOBt, DMF, 4 h; (d) *p*MR, DIC, HOBt, DMF, 4.5 h; (e) 4CBPB, TFFH, DIPEA, DMF, 6 h.

(TFFH = *N,N,N',N'*-tetramethylfluoroformamidinium hexafluorophosphate)

Table 3.1 Fmoc loading of CPG after co-acylation with Cbz- and Fmoc-Gly.

| Molar ratio Cbz- : Fmoc-Gly | Fmoc loading post-reaction / μmolg^{-1} |
|-----------------------------|--|
| 99:1 | 0.7 (0.9 %) |
| 97:3 | 2.8 (3.7 %) |
| 94:6 | 5.1 (6.8 %) |
| 9:1 | 16 (21 %) |
| 3:1 | 25 (33 %) |
| 1:1 | 56 (75 %) |
| 0:1 (control) | 75 (100 %) |

Based on the original quantitative experiments with the UV-Vis microspectrometer, a loading of between 5-20 % of the functional sites was thought to be appropriate to give good UV-Vis absorbance intensities while remaining within the linear range of the Beer-Lambert Law. Accordingly, *p*MR was coupled to CPG with a loading of 16 μmolg^{-1} to give **3.1** while 4CBPB was coupled CPG with a lower loading of 5 μmolg^{-1} (due to its higher molar absorption coefficient) to give **3.2**.

3.2.2 Construction and Testing of Sensor Assembly

In order to test the prepared beads, a sensor assembly was constructed with a transmission configuration where the bead was placed between the optical fibre providing the lightsource and the fibre leading to the spectrometer. The assembly was constructed from readily available components and held in place with cyanoacrylate glue. The ends of the optical fibre were cut with a ultrasonic fibre cleaver to give smooth perpendicular ends for uniform light transmission (**Figure 3.2 & Figure 3.3**) and the design enabled the sensor bead to be interchanged so different beads could be examined.

Figure 3.2 Schematic of sensor assembly.

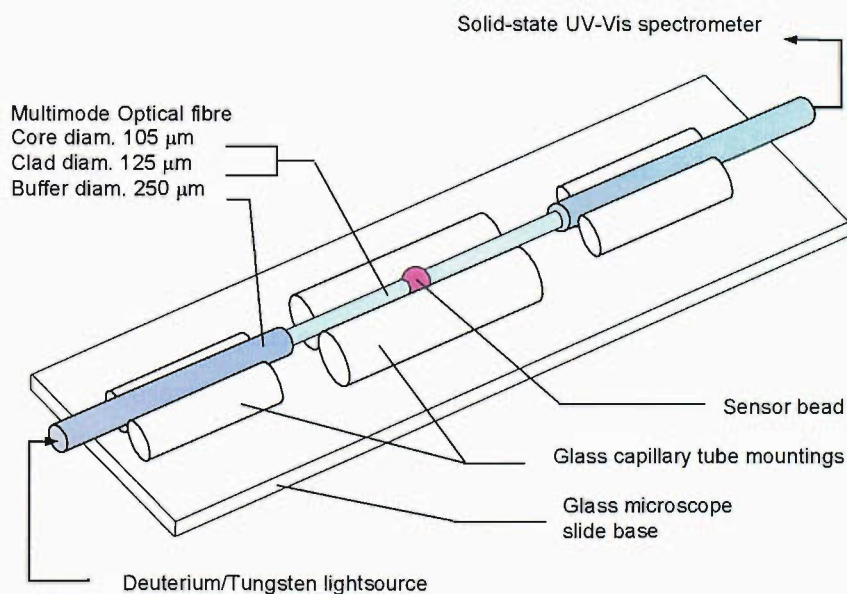
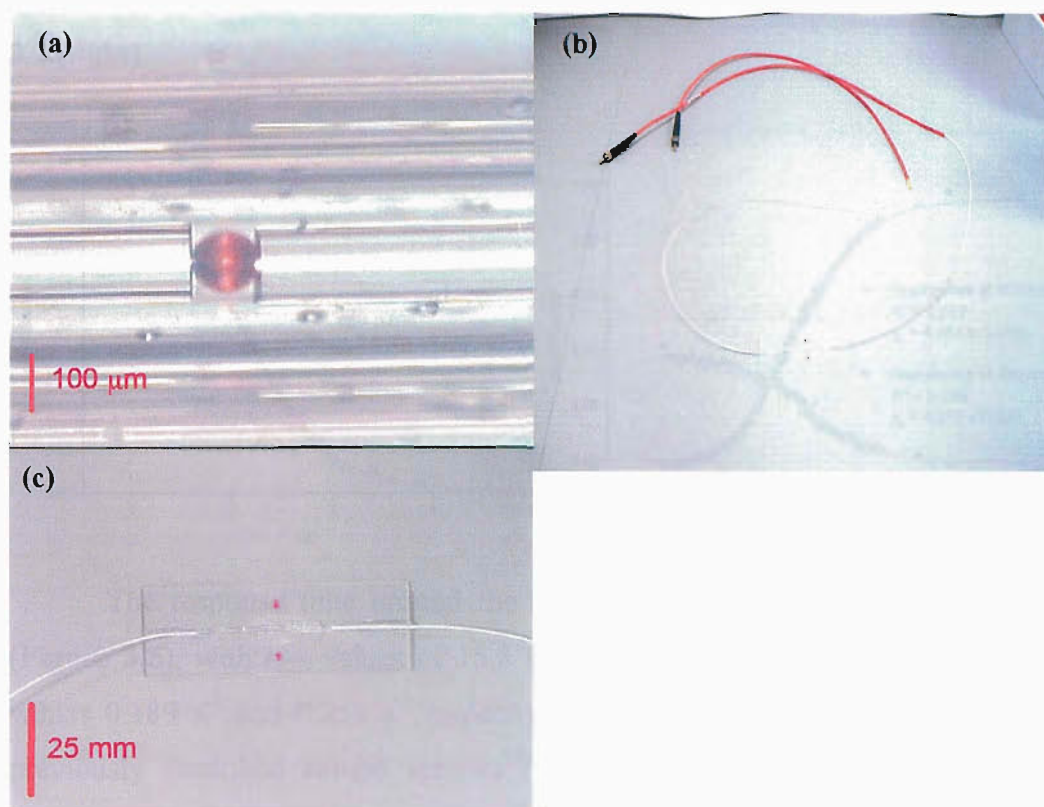


Figure 3.3 Photographs of sensor assembly: (a) Placement of sensor bead between two optical fibres within the assembly, (b) the entire device with connectors and (c) the sensor assembly (bottom left).

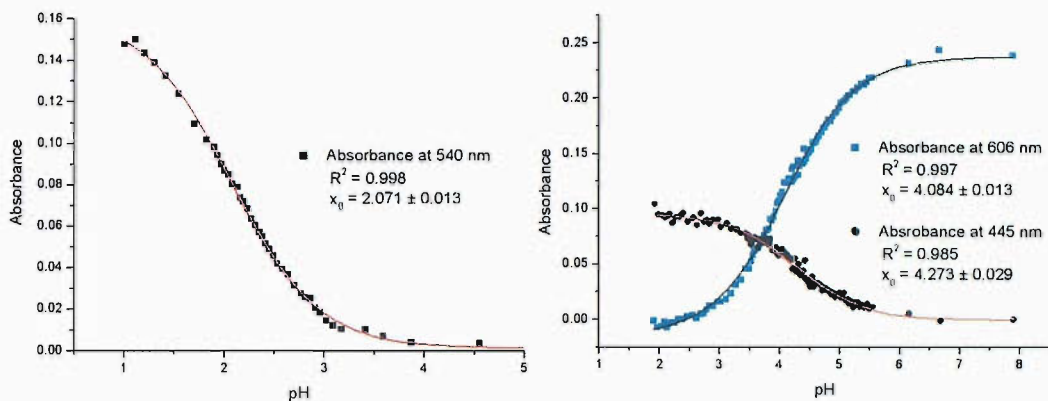


To determine the pH profile and dynamic range of the sensors, they were immersed in a 1 M HCl/NaOH aq. system and UV-Vis transmission spectra were recorded over a range of pH's with the CPG starting material used as a reference for the absorbance calculations.

In both cases, the selected dye loadings were found to be sufficient for sensing purposes and attention was focused on the λ_{max} of each dye, which for **3.1** was 540 nm (corresponding to the red colour of the protonated form) and for **3.2** were 606 nm (blue, ionised) and 445 nm (yellow, unionised). The dynamic ranges of the plots were observed to be pH 1.0-3.5 for sensor **3.1** and pH 2.0-6.0 in the case of **3.2**. (**Figure 3.4**) These ranges were relatively broad in contrast to the indicators in solution but concurred with the initial experiments involving the resin supported indicators as well as previous reports on sensors and are thought to be due to the heterogeneous microenvironment around the chromophores afforded by the supports.¹³⁸ The data were found to be in good agreement with the classical sigmoidal curves with R^2 values of 0.998 for sensor **3.1**, and 0.997 (at 606 nm) or

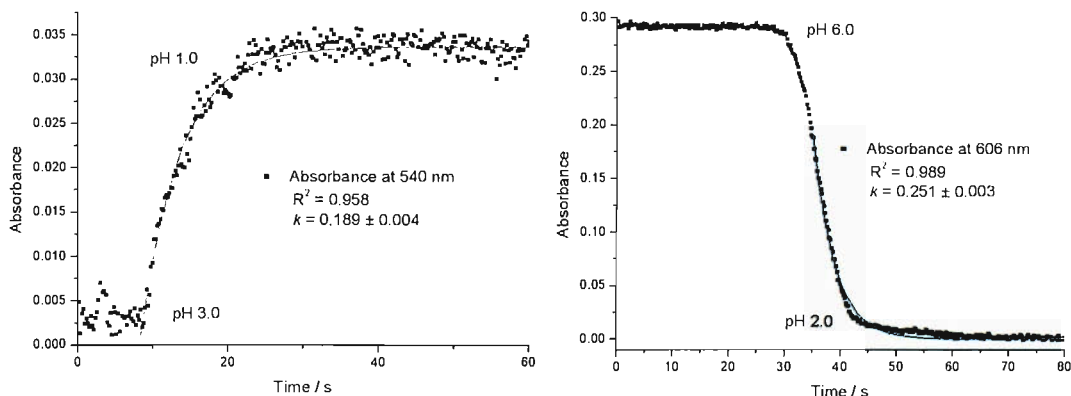
0.985 (at 445 nm) for **3.2**. From this, the pK_i of **3.1** was calculated to be 2.07. In the case of sensor **3.2**, this was between 4.08 (measured at 445 nm) and 4.27 (606 nm).

Figure 3.4 Graphs of UV-Vis absorbance at λ_{\max} against pH for sensor **3.1** (left) and **3.2** (right).



The response time around the pK_i of the sensors was found to be rapid (**Figure 3.5**), with $t_{95\%}$ values of 15.8 s and 11.9 s for **3.1** and **3.2** respectively (k values 0.189 s^{-1} and 0.251 s^{-1} respectively). These were as fast or faster than all previously described sol-gel sensors¹³⁸⁻¹⁴⁰ and 3-4 fold faster than conventional electrochemical pH meters.

Figure 3.5 Graph of UV-Vis absorbance at λ_{\max} against time for sensor **3.1** (left) and **3.2** (right).



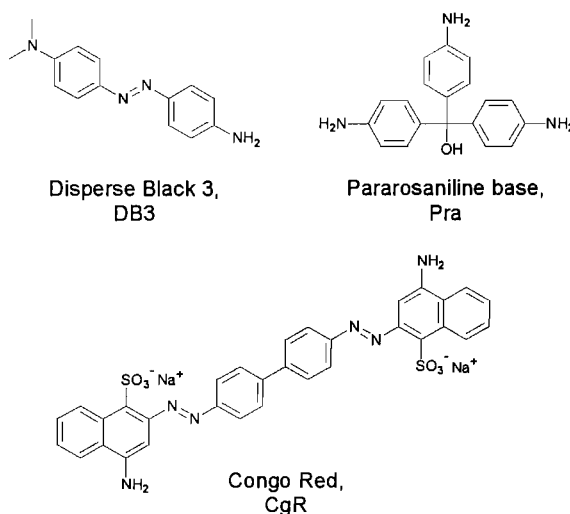
The UV-Vis spectra of both the dyes were measured before and after 12 h of continuous immersion at low pH (pH 1.0 for **3.1** and pH 1.3 for **3.2**) and no significant changes in the spectra were detected by the ANOVA statistical test, indicating dye stability and lack of leaching.

3.3 Sensors Bearing Aniline-Functionalised Indicator Dyes

The results obtained with the CPG beads in conjunction with the custom built sensor assembly suggested that other dyes could be similarly anchored to the beads and tested as novel sensors.

As many of the indicators available are aniline derivatives the development of procedures that allow the covalent attachment of dyes *via* these moieties at specified loadings would be useful. In this section, the attachment of three structurally diverse dyes; Disperse Black 3 (DB3), Pararosaniline base (Pra) and Congo Red (CgR) to CPG was explored. (**Figure 3.6**) DB3 could be compared to the structurally analogous *p*MR sensor while the triphenylmethane dye Pra displays two colorimetric changes at pH 1-3 & 11-14¹⁴⁹ and offered the opportunity to extend the dynamic range of dye-based sensors. Meanwhile, CgR gives an intense blue to red colour change¹⁵⁰ which may impart improved signal quality to the sensors.

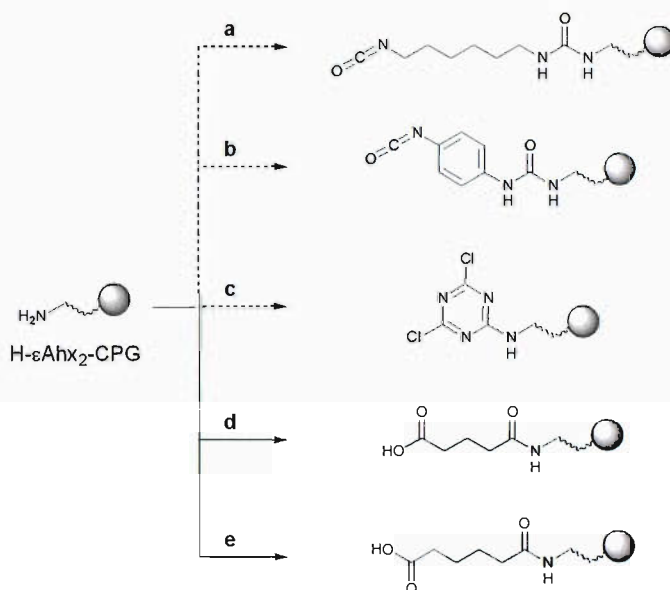
Figure 3.6 Structures of aniline-based indicator dyes



3.3.1 Investigation of Attachment Methods for Aniline-Functionalised Dyes

The Pararosaniline base and Congo Red were initially used to test the various possible attachment methods since these dyes were likely to be the most difficult cases. CPG with the di- ϵ Ahx spacers were therefore functionalised with various moieties for attachment to the dyes and the couplings attempted. (Scheme 3.6)

Scheme 3.6 Attachment of reactive spacers to the di- ϵ Ahx-CPG.



Reagents & conditions: (a) 1,6-diisocyanatohexane, N_2 , DCM, 3 h; (b) 1,4-phenylenediisocyanate, N_2 , NMP, 1 h; (c) 2,4,6-trichlorotriazine, DIPEA, DCM, 1 h; (d) glutaric anhydride, THF, 4 h; (e) adipoyl dichloride, DIPEA, DCM, 3 h, then 50 % v/v H_2O/THF .

Isocyanates had been previously described for the attachment of dyes to sol-gels¹³⁸ and thus di- ϵ Ahx-CPG was reacted with two diisocyanates (1,6-diisocyanatohexane and 1,4-phenylenediisocyanate) with the aim of generating supported isocyanates. As this functional group was unstable to heat, a modified ninhydrin test with a shorter heating time¹⁷ was used to monitor reaction progress and gave a negative test result with both the CPG-supported isocyanates. However, subsequent addition of the dyes did not give significant coupling to either of the isocyanates and IR microspectroscopy failed to detect the presence of the isocyanate absorbance band at $\sim 2275\text{ cm}^{-1}$. This may be due to cross-linking of the sites

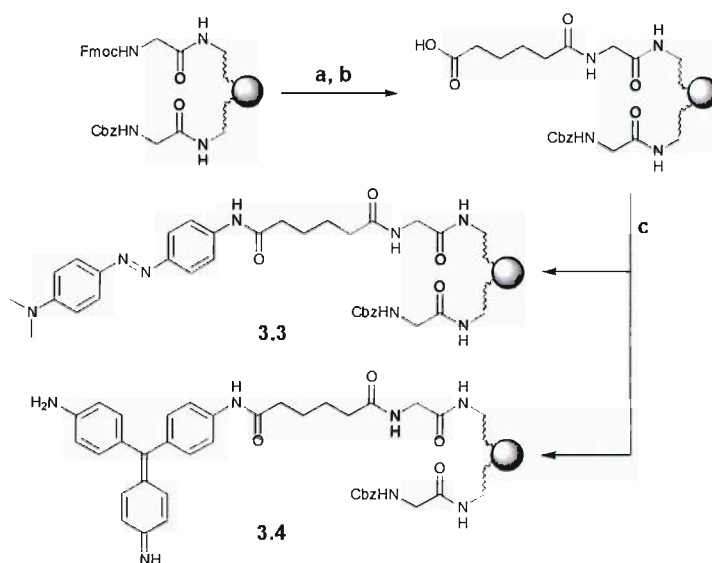
although this seems unlikely given the large excess of reagent applied. (20 mol. eq., 0.2 M)

Another method of anchoring was *via* triazines¹⁵¹ and 2,4,6-trichlorotriazine was used to give the CPG-supported dichlorotriazine but subsequent reaction with the two dyes also gave no significant loading.

Attention was then turned to the use of carboxylic acids with a view to using peptide coupling agents to attach the dyes to the CPG *via* amide bonds. Glutaric anhydride was first employed followed by coupling of the dyes with PyBOP but again no significant loading was detected. Adipoyl dichloride, freshly synthesised according to a literature procedure,¹⁵² was coupled to the CPG and the reaction quenched with water once complete coupling of the amine sites was observed (by ninhydrin test). The dyes were coupled to this batch of CPG using either PyBOP or bromo-tris-pyrrolidino-phosphonium hexafluorophosphate (PyBroP) and in both cases, coupling of Pararosaniline was finally achieved. However, no still no coupling was observed with Congo Red. Microscopic scrutiny of the Pra-coupled beads revealed that the colour intensity of the CPG coupled with PyBOP was stronger than with PyBroP coupling, suggesting that powerful activation of the carboxylic acid may be resulting in cyclisation or cross-linking of the diacid with consequently reduced yield.

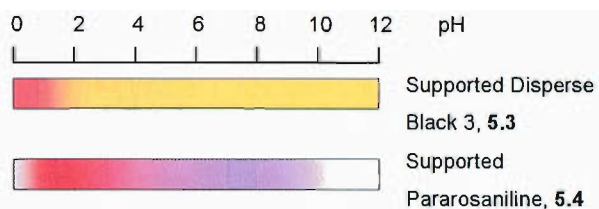
Using this knowledge, the sensor beads were then synthesised using the dyes DB3 and Pra only and the partially Fmoc-protected CPG ($5 \mu\text{molg}^{-1}$). (**Scheme 3.7**) The reactions proceeded as expected for both dyes to furnish the sensor beads **5.3** and **5.4** which were uniformly coloured under microscopic examination. The supported dyes continued to respond to pH variations in aqueous solutions. (**Figure 3.7**) For **5.3**, a single transition was observed as expected while with **5.4**, three transitions were seen, with decolourisation occurring at the extremes of the pH range due to addition to the central methine C-atom, interrupting extended conjugation.¹⁴⁹ (**Scheme 3.8**)

Scheme 3.7 Attachment of aniline-derived dyes to CPG.

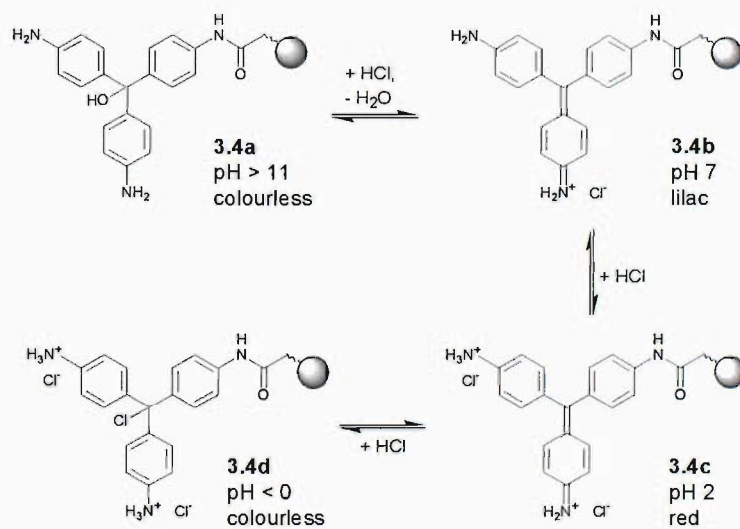


Reagents & conditions: (a) 20 % v/v piperidine, DMF, 30 min; (b) adipoyl dichloride, DIPEA, DCM, 3 h, then 50 % v/v H₂O/THF; (c) Pra or DB3, PyBOP, DIPEA, NMP, 16 h.

Figure 3.7 Visually observed colour change for **3.3** & **3.4** in aqueous solutions.



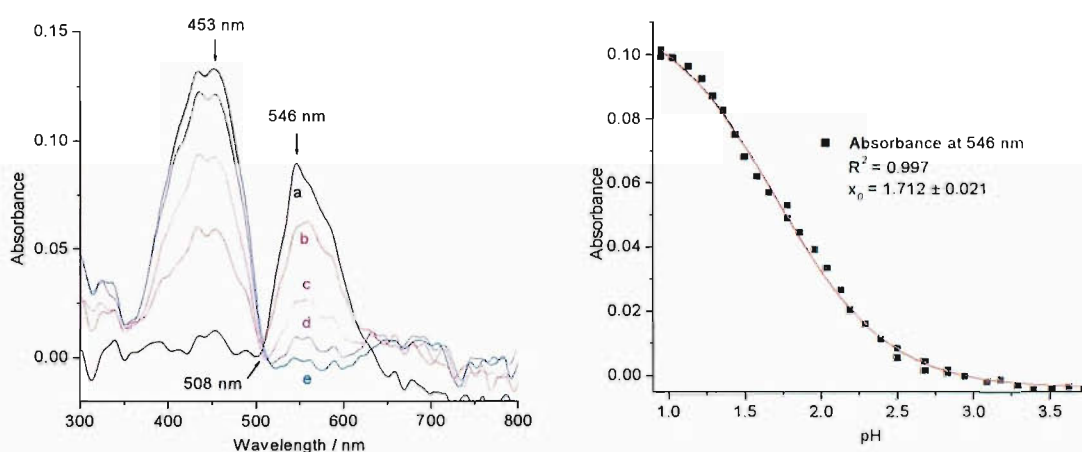
Scheme 3.8 Ionisation pattern of sensor **3.4** in an HCl/NaOH aq. system.



3.3.2 Assessment of Sensors

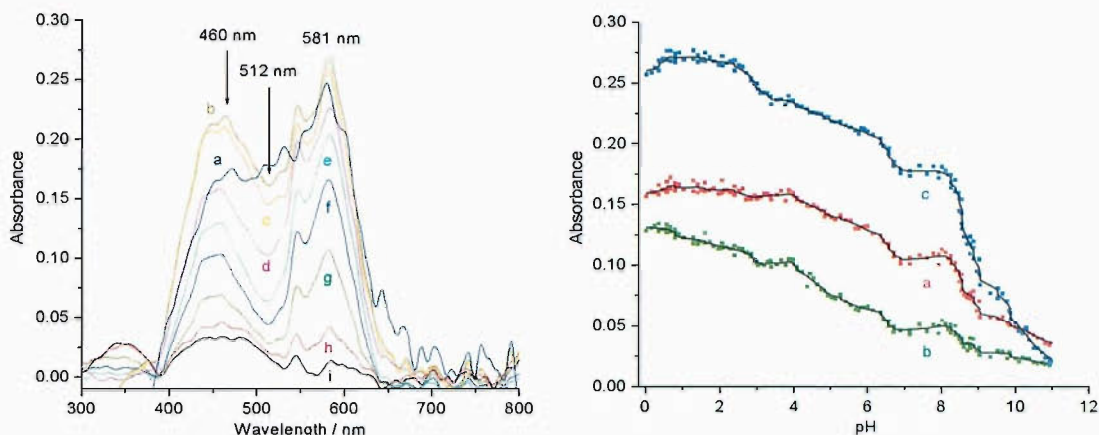
A single bead for each dye was inserted into the sensor assembly as before and the UV-Vis spectra, pH profile and response times were examined. In both cases of the sensor beads with a loading of $5 \mu\text{molg}^{-1}$ were found to be sufficient for sensing purposes. For **3.3**, the absorbance at λ_{max} (546 nm) corresponding to the protonated indicator was plotted against pH and the best-fit sigmoid curve provided a pK_i of 1.71 (**Figure 3.8**), similar to DB3 in solution (pK_i 1.78)¹²⁹ and the *p*MR sensor **3.1** (λ_{max} 540 nm, pK_i of 2.07). The dynamic range of **3.3** was observed to be between pH 1.0-3.0, also similar to the *p*MR-bearing **3.1**.

Figure 3.8 UV-Vis absorbance at pH's: (a) 1.0, (b) 1.5, (c) 2.0, (d) 2.5, (e) 3.1 (left) and absorbance at 546 nm against pH for DB3 sensor **3.3** (right).



For Pararosaniline, the single peak of the spectra in aqueous solution,¹⁴⁹ was resolved into two peaks in the supported dye **3.4**. (**Figure 3.9**) Plots of absorbance intensities of the peaks (460 and 581 nm) and the depression between them (512 nm) did not indicate any obvious pK_i transition points, nevertheless the sensor had a large pH response range, in regions where one or two of the observed wavelengths was unresponsive (pH 3-4 at 460 and 512 nm, pH 1-2 at 460 nm), the other wavelength(s) continued to change. However, there was a completely unresponsive region between pH 7-8 while at the extremes of the range the absorbance dropped as the dye became decolourised.

Figure 3.9 UV-Vis absorbance at various pH's: (a) 0.0, (b) 1.0, (c) 2.1, (d) 4.0, (e) 5.7, (f) 7.2, (g) 8.7, (h) 9.9, (i) 11.0 (left) and absorbance against pH for Pra sensor **3.4** at: (a) 460 nm, (b) 512 nm, (c) 581 nm. (right)



The response time of sensor **3.3** around its pK_i was comparable to that of the previously cited CPG-based sensors, with a $t_{95\%}$ of 8.7 s and a k of 0.348 s^{-1} . (**Figure 3.10**) The response speed measurements of **3.4** were more complicated due to the lack of transition points. Initial measurements covering a large part of the dynamic range did not give the classical exponential curve, the initial part of the plot was somewhat uneven followed by a well defined curve. (**Figure 3.11**) The overall $t_{95\%}$ was $\sim 2870 \text{ s}$ and a best-fit exponential curve of this latter stage provided a k value of $3.47 \times 10^{-3} \text{ s}^{-1}$. The initial phase could be attributed mainly to formation of the cation to give **3.4b**, while the second phase was the protonation of the second N -atom to give **3.4c**. The conversion from **3.4b** to **3.4c** was examined in more detail and unexpectedly, gave a $t_{95\%}$ of $\sim 7560 \text{ s}$ and a k of $6.50 \times 10^{-4} \text{ s}^{-1}$, significantly slower than the response over the whole range. (**Figure 3.11**) In either case, the response rates for sensor **3.4** were several orders of magnitude slower than the other CPG- or sol-gel glass-based sensors.

Figure 3.10 Graph of UV-Vis absorbance at 546 nm against time for sensor **3.3**.

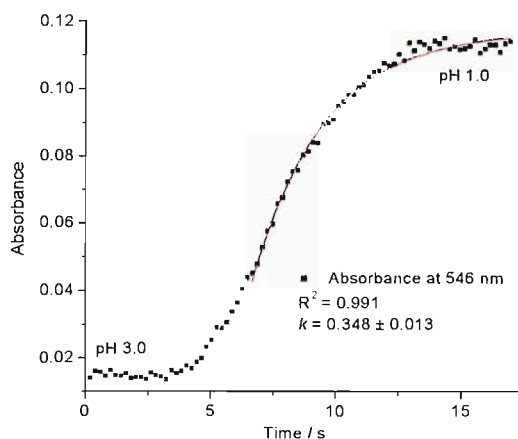
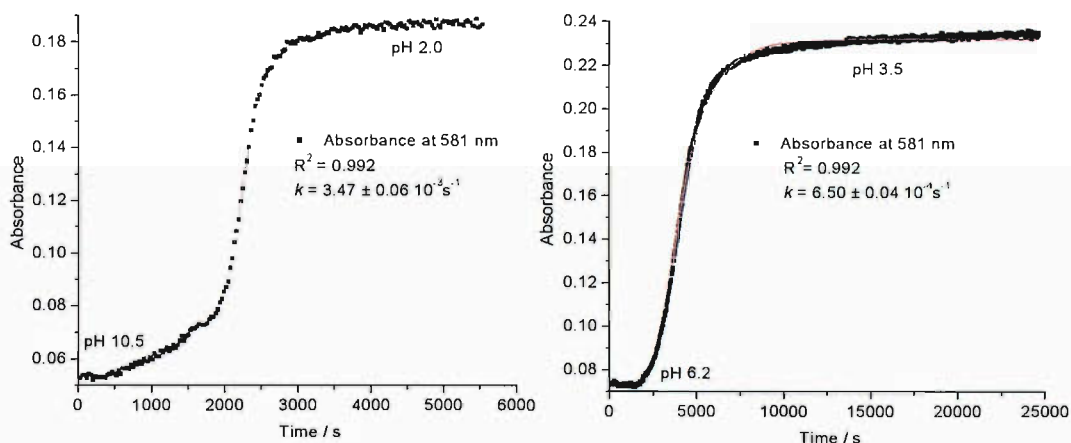


Figure 3.11 Graph of UV-Vis absorbance at 546 nm against time for sensor **3.4** from pH 10.5 to 2.0 (left) and pH 6.2 to 3.5 (right).



Overall, the attachment of two aniline-functionalised chromophores to CPG and their testing as pH sensors are described. Synthetic methods for covalent attachment were developed for Pra and DB3 although none of the tested methods were successful for CgR. The assessment of the sensors demonstrated that the supported DB3 gave a similar performance to *p*MR in terms of response time and dynamic range. On the other hand, the Pararosaniline-bearing sensor gave extremely slow response times but a large sensing range and demonstrating that by observing several wavelengths, nearly the entire pH range could be measured.

3.4 Conclusions

In conclusion, the covalent attachment of carboxy- and aniline-functionalised dyes to CPG and the assessment of these materials as pH sensors was successfully conducted. To this end, a sensor array was constructed which allowed the beads to be easily interchanged for testing purposes and procedures for the attachment of these dyes at specified loadings to CPG were developed. Spherical CPG beads were found to be a suitable material for optical applications although the low reactivity in SPOS was inconvenient. In the case of *p*MR-, DB3- and 4CBPB-based sensors, all had rapid response times while the CPG-bound Pra was extremely slow. However, the latter did display a wide sensing range, hitherto a major limitation of spectrometric sensors which usually operate only within ± 2 units of the pK_i of the dyes used.¹⁵³

The relationships between the structure, UV-Vis spectra and pK_i have been well studied for phthalein,^{154,155} triarylmethane¹⁵⁶⁻¹⁵⁸ and azo^{127,159} dyes and would allow the tuning of these sensors' structures to achieve the desired colour and dynamic sensing ranges for individual applications. The newly described strategies for the synthesis of a diverse range of these phthalein,¹⁶⁰ triarylmethane¹⁶¹ and azo^{162,163} dyes opens the possibility of applying combinatorial strategies to the development of new sensors.

Several avenues for future work are possible from here. It was observed during the synthesis of the sensors that DB3 was a highly solvatochromic dye and may have potential applications in solvent detection and measurement. Improvements in data processing would also be advantageous, such as the application of more complex formulae for the determination response times which take into account diffusion parameters,¹⁶⁴ as well as the ability to calculate an average pH value measured from several wavelengths to provide increased accuracy.

4 UV-Visible Microspectrometry for the Analysis of Solid-Supported Peptide-Metal Complexes

4.1 Introduction: Combinatorial Generation of Peptide-Metal Complexes

Peptides and amino acids can be very effective and specific ligands for a range of metal ions as they contain a variety of potential coordinating sites and thus peptide-metal complexes have long been the subject of research. In the area of bioinorganic chemistry, an understanding of metal-peptide interactions is crucial in the study of cellular signalling, the function of metalloenzymes, the toxicology of metallic environmental contaminants and the metabolic processes by which metal ions are transported and incorporated into living systems.¹⁶⁵⁻¹⁶⁹ In relation to this, work has also been conducted on the development of synthetic metallopeptides as potential medical imaging and therapeutic agents.¹⁷⁰⁻¹⁷² Another area where metal-ligand complexes are important is in the search for new homogenous catalysts.¹⁷³ Here, the incorporation of chiral amino acids or their derivatives into catalytically active transition metal complexes affords a simple and economical way of accessing potential enantioselective catalysts.¹⁷⁴ The specificity of metal-peptide binding has also been harnessed for the development of metal ion sensors for use in environmental monitoring.¹⁷⁵

Work in all these areas would benefit from the discovery of new peptide-derived receptors with high metal affinity and several attempts at harnessing combinatorial chemistry for this purpose have been reported. The earliest example of this was the development of a split-and-mix library of peptides based around a TG-supported cyclen core.¹⁷⁶ (**Figure 4.1**) This library was exposed to Cu^{2+} or Co^{2+} in aqueous solutions and selective metal binding was observed by the generation of a blue (in the case of Cu^{2+}) or red (Co^{2+}) colour on the beads “containing” peptide sequences that were metal ion specific. These were then analysed to determine the residues that promoted metal binding and a strong preference was found for the

Asp(O^tBu) residue at the *N*-terminal position when binding Cu²⁺ regardless of the length of the peptide arms (**Figure 4.2**). The same residue preferred a position one residue removed from the terminus for the binding of Co²⁺.

Figure 4.1 Generic structure of solid-supported cyclen-peptide library

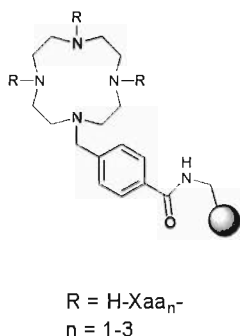
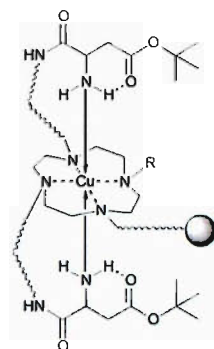
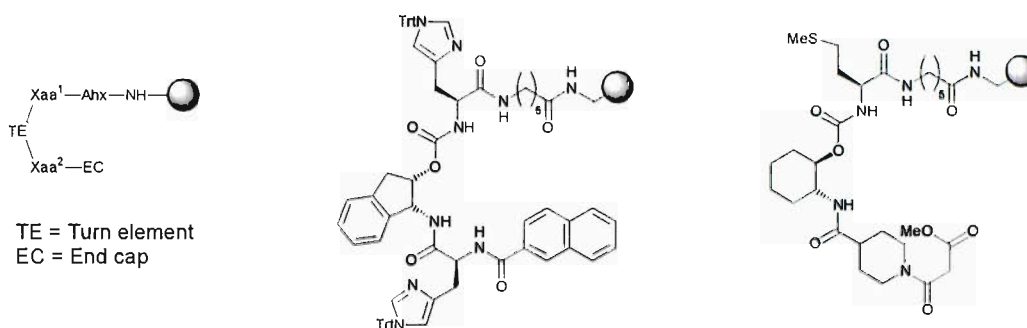


Figure 4.2 Possible structure of Cu²⁺ binding receptor



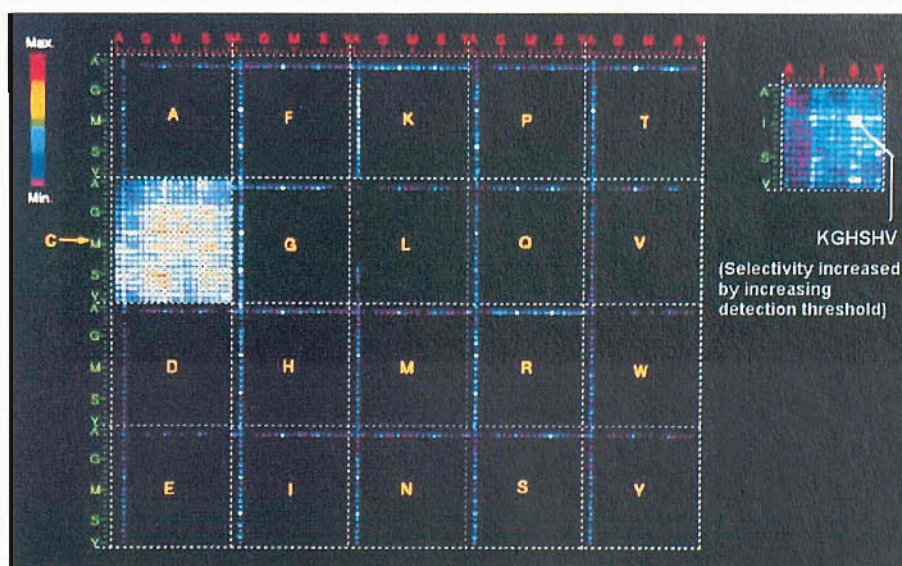
As the cyclen core used was already recognized to be a powerful tetradentate ligand for both these metal ions, this study could therefore be considered an optimisation of the selectivity of a known ligand. The use of combinatorial methods for the discovery of entirely novel ligands was only later demonstrated, again by using a split-and-mix library where 12,000 potential metal binders were synthesised, with each member consisting of four variable components, two amino acid residues interspaced with a variable “turn element” and a number of *N*-terminal end caps.¹⁷⁷ (**Figure 4.3**) The library members, supported on TG, were exposed to methanolic solutions of a variety of metals followed by treatment with staining reagent solutions. These staining reagents gave intensely coloured complexes within the beads where the metal cations were present and allowed the “hits” (the active members) to be selected. From this library, two high affinity binders were identified for Ni²⁺ and Fe³⁺. (**Figure 4.3**)

Figure 4.3 Structure of novel metal binding ligands: Generic structure of library members (left), high affinity Ni²⁺ binder (middle) and high affinity Fe³⁺ binder (right).



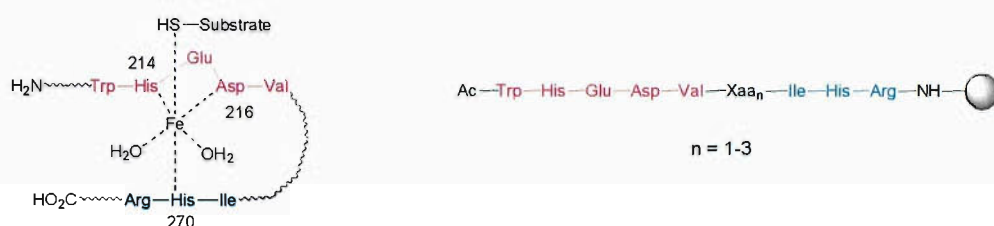
In the search for new radiopharmaceutical agents, another combinatorial method was used where spatially addressed cellulose-bound hexapeptide libraries were screened for binding to ^{99m}Tc.¹⁷⁰ A library of defined and randomised positions (Lys-Xaa¹-His/Met-Xaa²-His-Xaa³) were synthesised by spot synthesis at specific locations on a cellulose sheet and subsequently exposed to ^{99m}TcO₄⁻. The amount of ^{99m}Tc bound to various parts of the cellulose was visualised by autoradiography and the positions with greatest activity were correlated to the peptide sequence. (**Figure 4.4**) Two strong binders were subsequently identified from this library as having the sequences Lys-Gly-His-Ser-His-Val and Lys-Ala-Met-Tyr-His-Gly.

Figure 4.4 An example of autoradiography results from the spatially addressed peptide library



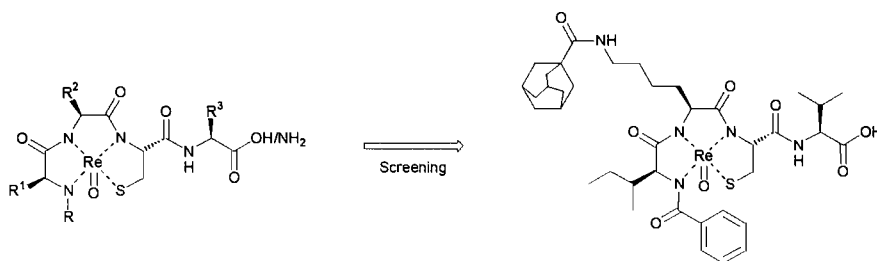
The active site of a metalloenzyme, isopenicillin *N* synthase, containing a Fe^{II} atom has also been used as a model for the generation of metal-binding ligands.¹⁷⁸ Two sequences important for coordination were conserved and the split-and-mix methodology was used to generate a TG-supported library of peptides where the amino acid residues between the two sequences were varied. (**Figure 4.5**) The library was then exposed to Fe^{2+} , Cu^{2+} or Co^{2+} and the actively binding members could be identified as they were coloured by complexation with the metal ions. However, no strategy for determining the peptide sequence of the active beads was incorporated so no further information could be gained, apart from demonstrating that selective binding was possible from a library of these peptides.

Figure 4.5 Active site of isopenicillin *N* synthase (left) and the supported peptide library designed to mimic active site (right).



The most recent example of combinatorial generation of metallopeptides is the development of a “metal-ion induced distinctive array of structures” (MIDAS) which was a library of tetrapeptides with a locked conformation caused by complexation with a Re^{V} atom.¹⁷¹ Here, a library of 60 *N*-terminally capped peptides with the general formula $\text{R-Xaa}^1\text{-Xaa}^2\text{-Cys-Xaa}^3\text{-OH/NH}_2$ were synthesised by standard SPOS methods followed by on-resin complexation with the metal transfer reagent $\text{ReOCl}_3(\text{PPh}_3)_2$. These peptide complexes were cleaved from the supports and screened as inhibitors against human neutrophil elastase and porcine pancreatic elastase and from this library, the peptide sequence Bz-Ile-Lys(Adam)-Cys-Val was found to give selective inhibition of the former enzyme with a K_i of $9.7 \mu\text{M}$. (**Figure 4.6**)

Figure 4.6 Generic structure of MIDAS compounds (left) and structure of active inhibitor of human neutrophil elastase (right).



This example together with non-combinatorial work in the area of bioinorganic chemistry¹⁷⁹⁻¹⁸¹ suggested that potential ligands with high metal affinity could be generated from relatively small peptides (3-4 residues) without the need for more complex non-proteogenic components described in the first two examples.

The aim of this part of the thesis was therefore to generate a solid supported combinatorial library of tripeptides, which would be tested with a number of transition metal solutions and the actively binding members visualised by treatment with staining reagents. The colour intensity of the stained beads would be analysed on-bead by UV-Vis microspectrometry to provide an indication of the binding strength of the individual peptides. Once the spectra were recorded, the beads could be subjected to Edman degradation to determine the binding peptide sequence.

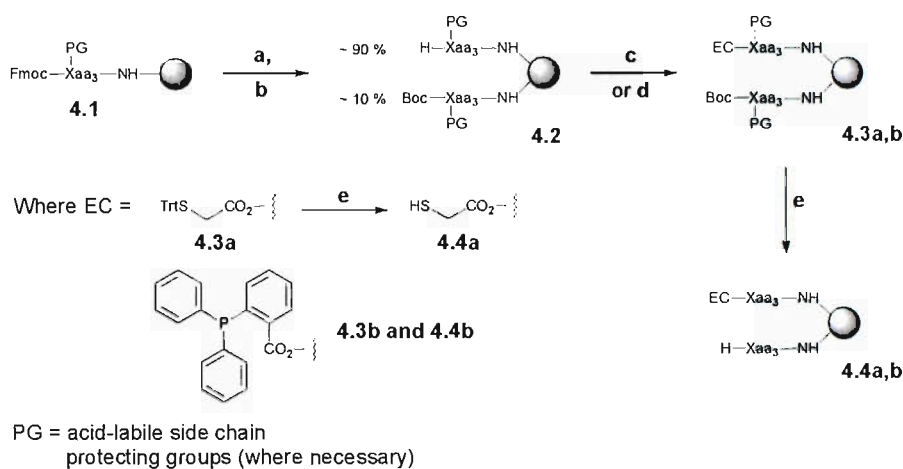
4.2 Combinatorial Generation of the Peptide Library

The library of tripeptides was synthesised using standard split-and-mix protocols and the Fmoc synthetic strategy with 10 protected amino acid residues; Fmoc-Asp(O^tBu), Fmoc-Glu(O^tBu), Fmoc-Gln, Fmoc-Tyr(^tBu), Fmoc-Ser(^tBu), Fmoc-Pro, Fmoc-Gly, Fmoc-Val, Fmoc-His(Trt) and Fmoc-Lys(Boc). The majority of these residues also included heteroatoms, which it was hoped would provide increased affinity for the metals. Three peptide coupling cycles provided a 1000-member library **4.1** with one compound per bead on TG, which was compatible with the methanolic solutions of the metal ions that would be used during screening.

For identification purposes, the tripeptide library *N*-terminal was deblocked and 10% of the free sites were re-protected with di(*tert*-butyl)dicarbonate (Boc₂O) to give **4.2**, allowing Edman sequencing of the hits. The remaining free termini were

coupled with two *N*-terminal capping units, which introduced additional potential co-ordination sites for the metals. (**Scheme 4.1**) Finally, the acid-labile side-chain protection for libraries **4.3a** & **4.3b** was removed with TFA to afford the libraries **4.4a** & **4.4b** with the various end caps. In the case of **4.4a**, the terminal Trt group was also removed at this step.

Scheme 4.1 Synthesis of capped tripeptide library.



Reagents & conditions: (a) 20% v/v piperidine, DMF, 2 x 5 min; (b) Boc₂O (10% mol eq.), DIPEA, DCM, 2 h; (c) *S*-trityl-thioglycolic acid, PyBOP, DIPEA, DMF, 4.5 h; (d) 2-(diphenylphosphino) benzoic acid, DIC, HOBt, DMF, 4.5 h; (e) 95% TFA, 2.5% H₂O, 2.5% TIPS, 3h. (TIPS = tri(*iso*-propyl)silane, Xaa = Asp(O^tBu), Glu(O^tBu), Gln, Tyr(^tBu), Ser(^tBu), Pro, Gly, Val, His(Trt) or Lys(Boc))

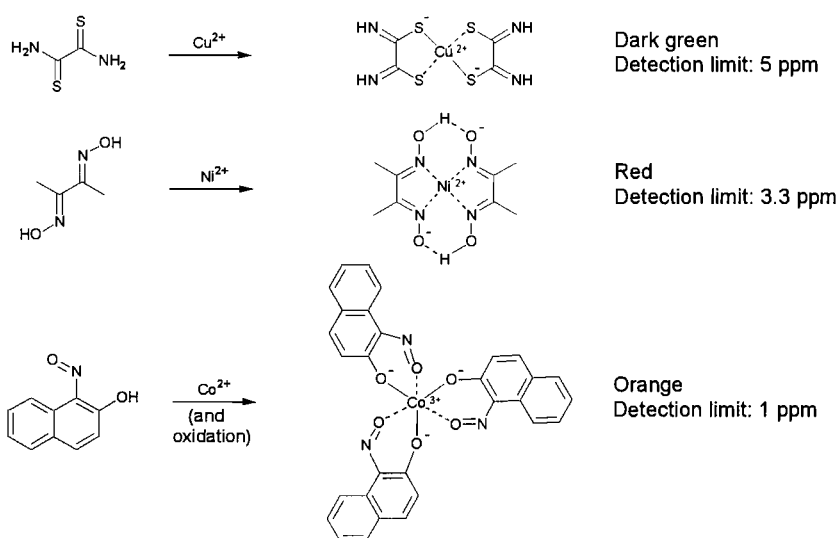
4.3 Microscopic and UV-Visible Microspectrometric Analysis of Metal Complexed Peptide Libraries

4.3.1 Microscopic Analysis of Supported Complexes

Batches from the four libraries **4.3a**, **4.3b**, **4.4a**, & **4.4b** were mixed with methanolic solutions of CuCl_2 , CoCl_2 or $\text{Ni}(\text{OAc})_2$ to produce the peptide-metal complexes. In all cases 5 mg of each library was used for screening, providing approximately 5 copies of library (~ 1000 beads/mg) that was statistically calculated to give a 95-99 % coverage of all possible library members.¹⁸²

After exposure to the metal solutions, the beads were visually inspected and collectively observed to have a pale blue (with Cu^{2+}), pink (Co^{2+}) or orange (Ni^{2+}) colour. However under light microscopy, the colour on the individual beads were too faint to allow differentiation between hits and non-active beads and necessitated the use of staining reagents for the detection of the metal cations. For the three metals investigated, the reagents used were dithio-oxamide for Cu^{2+} , dimethylglyoxime for Ni^{2+} and 1-nitroso-2-naphthol for Co^{2+} .¹⁸³ (**Figure 4.7**)

Figure 4.7 Metal detection reagents: dithio-oxamide (top), dimethylglyoxime (middle) and 1-nitroso-2-naphthol (bottom)



The amounts of the metal salts added were varied with 0.01, 0.1, 1.0 or 10 mol. eq. relative to the resin loading (corresponding to 0.01, 0.1, 1.0 or 10 mM solutions) to determine the optimum amount required for detection of the active beads. In all cases, the beads were allowed to equilibrate overnight in the solutions and then examined under a conventional microscope before and after staining.

The *S*-Trt capped library **4.3a** was first examined with 0.1 mM CuCl₂ which was found to be sufficient for the selective detection of active ligands after staining. (**Figure 4.8**) There was no benefit from further increasing the concentration and at 10 mM, non-selective binding was observed as all beads were stained, although even at this concentration the active beads could still be differentiated from the non-selective binding by having a more intense colouration. Similar behaviour was noted for Co²⁺ but for Ni²⁺ the minimum concentration required for detection was an order of magnitude higher at 1 mM. (**Table 4.1**) In the case of the thiol deprotected library **4.4a**, the concentrations of cations required for the detection of active ligands were lower for Ni²⁺ and Co²⁺ at 0.1 mM and 0.01 mM respectively.

Figure 4.8 Photograph of selectively stained beads after treatment with 0.1 mM CuCl₂ and dithio-oxamide.



In comparing the phosphine-capped library **4.3b** to the *S*-Trt-capped library **4.3a**, greater affinity was observed for Co²⁺ with the cation being detected after treatment with only 0.01 mM CoCl₂. In the case of the deprotected library **4.4b**, activity was detected with similar concentrations of cations in all cases (0.1 mM).

Table 4.1 Concentration of cation required for selective staining of tripeptide libraries under microscopic observation.

| Library | Capping group | Cation tested | Concentration / mM* |
|-------------|-----------------------|------------------|---------------------|
| 4.3a | -S-Trt | Cu ²⁺ | 0.10 |
| | | Ni ²⁺ | 1.00 |
| | | Co ²⁺ | 0.10 |
| 4.4a | -SH (d) | Cu ²⁺ | 0.10 |
| | | Ni ²⁺ | 0.10 |
| | | Co ²⁺ | 0.01 |
| 4.3b | -PPh ₃ | Cu ²⁺ | 0.10 |
| | | Ni ²⁺ | 1.00 |
| | | Co ²⁺ | 0.01 |
| 4.4b | -PPh ₃ (d) | Cu ²⁺ | 0.10 |
| | | Ni ²⁺ | 0.10 |
| | | Co ²⁺ | 0.10 |

(d) = peptide side-chain(s) deprotected

* Concentration of solutions also correspond to the mol. eq. relative to resin loading.

4.3.2 UV-Vis Microspectrometry of Stained Members of Library

Five beads from each batch were picked under a light microscope, two beads of greatest colour intensity, two of moderate intensity and one of weak colour intensity to give a range of samples and these were individually analysed under UV-Vis microspectrometry.

Unlike previous experiments, the spectra were now measured from a single bead rather than an average from a number of different beads and some adjustment in the methodology was needed to compensate for the variation in bead sizes. The size of each bead was measured by analysis of images of the beads taken under the microscope after collection of the spectra and the raw UV-Vis transmission spectra were then processed by scaling them against an averaged reference spectrum from each library without the chelated metal. The absorbance spectra were calculated from these intensity adjusted transmission spectra and the references then normalised to a pathlength (*i.e.* bead diameter) of 150 μm .

4.3.2.1 Analysis of copper-binding beads

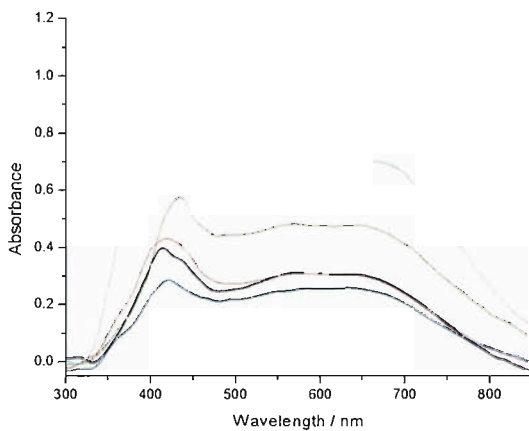
Initially the side-chain-protected libraries **4.3a** & **4.3b** chelated with Cu^{2+} and stained with dithio-oxamide were studied. (**Figure 4.9a-f**, **Figure 4.10a,b**) The broad absorbance band at ~ 650 nm corresponding to the dark green colour of the metal-stain complex could be clearly observed and dominated the spectra at high absorbance although due to the differing physicochemical environments within each bead due to the attached peptides, variations in λ_{max} were observed. There was a general correlation between the visually observed colour intensity and the spectral intensity of the individual beads and a good spread of absorbance intensities could be observed. (**Figure 4.9a** & **Figure 4.10b**) However in one of the picked batches, despite having deliberately selected a range of visually different colour intensities, the beads exhibited similar absorbance spectra. (**Figure 4.9e**) This may be due to the variations in the sizes of individual beads in which the smaller beads appeared to have a weaker colour intensity while this size variation was compensated during the calculations for the absorbance spectra. In some cases, a weaker absorbing band at ~ 420 nm could also be observed.

In nearly all the cases, the most intensely coloured beads from each screen had absorbance values higher than 1.0. Therefore a linear relationship between the amount of cation present and absorbance intensity could not be assumed, though in general terms a higher intensity would still correlate to higher concentrations of the cations.

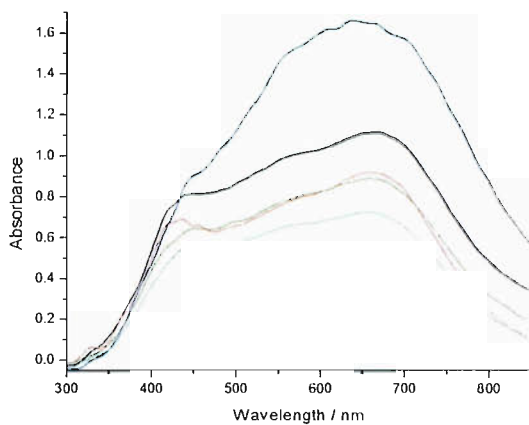
In comparing the effect of changing the amount of Cu^{2+} added to each screen, it was observed that the most intensely stained beads all had similar absorbance values regardless of the amount of Cu^{2+} added, ~ 1.2 for the *S*-Trt libraries (**Figure 4.9c** & **e**) and ~ 1.5 for the phosphine libraries (**Figure 4.9d** & **f**). These values may represent the maximum absorbances for the individual beads where all the binding sites for the metal ions are occupied.

Figure 4.9 UV-Vis absorbance spectra of single Cu^{2+} -binding side-chain protected beads stained with dithio-oxamide.

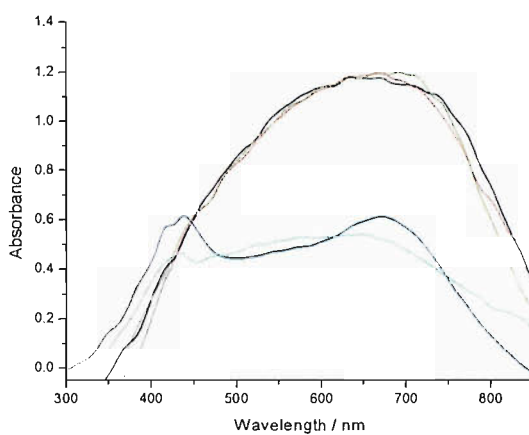
a) *S*-Trt-capped, 0.10 mM Cu^{2+}



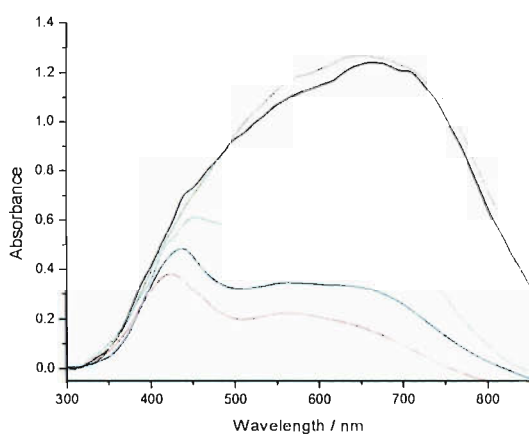
b) Phosphine-capped, 0.10 mM Cu^{2+}



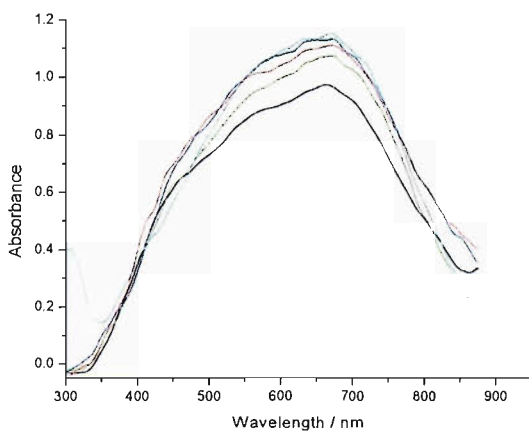
c) *S*-Trt-capped, 1.00 mM Cu^{2+}



d) Phosphine-capped, 1.00 mM Cu^{2+}



e) *S*-Trt-capped, 10.00 mM Cu^{2+}



f) Phosphine-capped, 10.00 mM Cu^{2+}

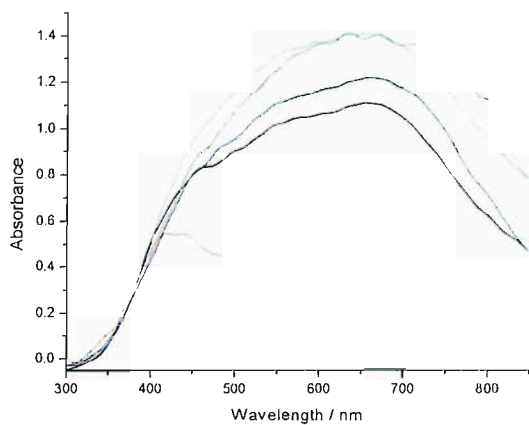
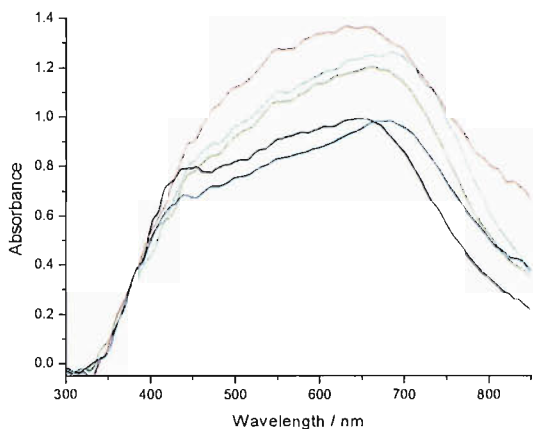
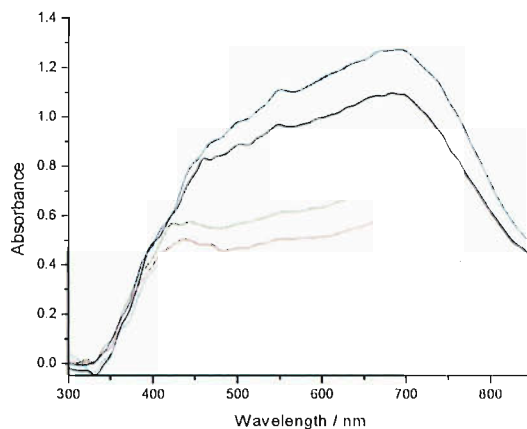


Figure 4.10 UV-Vis absorbance spectra of Cu²⁺-binding side-chain deprotected beads stained with dithio-oxamide

a) Thiol-capped, 0.10 mM Cu²⁺



b) Phosphine-capped, 0.10 mM Cu²⁺



Attention was focused on the screens which used the minimum amount of cation required to produce stained beads and a good spread of spectral intensities were obtained with the *S*-Trt-capped library (**Figure 4.9a**) with 0.1 mM (representing 0.1 mol. eq.) of Cu²⁺ although a similar concentration with the phosphine-capped beads still gave very high absorbances (**Figure 4.9b**). Another interesting observation was that some beads displayed markedly different spectra even at similar absorbance intensities (**Figure 4.9c**). These spectra could indicate the presence of a different spectrometric species, perhaps a mixed stain-cation-peptide complex. In the case of the deprotected libraries **4.4a** & **4.4b** (**Figure 4.10a,b**), similar maximum absorbance intensities and λ_{max} were obtained for the beads with the highest metal affinities.

In a few cases (**Figure 4.9d,f** & **Figure 4.10b**), the difference in absorbance between weakly and strongly stained was greater than 1.0 absorbance units, which suggests the amount of metal present and the affinities of individual members of the libraries differed by at least an order of magnitude.

4.3.2.2 Analysis of nickel-binding beads

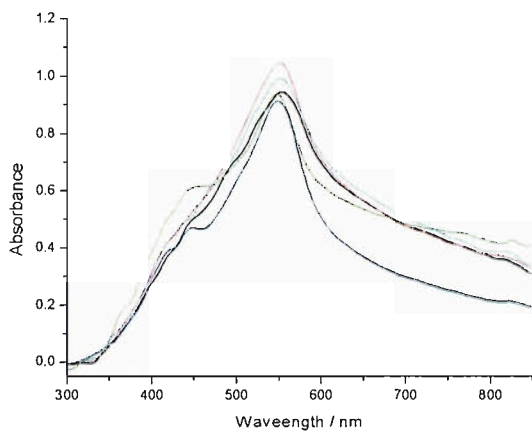
The UV-Vis absorbance spectra for the Ni-binding beads stained with dimethylglyoxime were then scrutinised (**Figure 4.11a-f**). The red colour of the stain-cation complex clearly correlated to λ_{max} at ~ 550 nm although in some cases another absorption peak at ~ 420 nm could be observed. In common with the Cu-binding screen, the most actively binding beads gave absorbance values greater than 1.0 with the most intensely stained members having an absorbance value of 1.1-1.2 for the protected libraries **4.3a** & **4.3b** regardless of the capping group or the amount of Ni(OAc)₂ originally added. (**Figure 4.11a-d**) In the deprotected libraries **4.4a** & **4.4b** (**Figure 4.11e,f**) the maximum absorbances were higher at ~ 1.4 .

4.3.2.3 Analysis of cobalt-binding beads

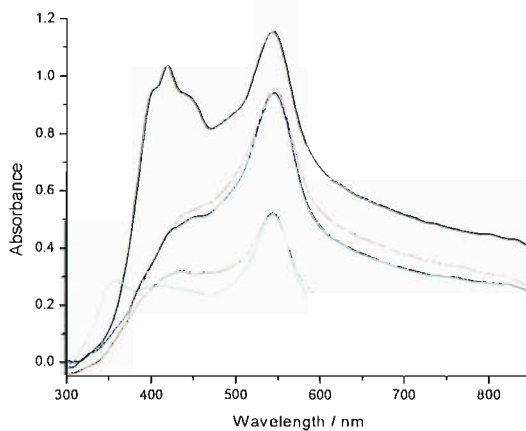
Finally, the Co²⁺-binding beads were analysed (**Figure 4.12a-e** & **Figure 4.13a-c**). The λ_{max} between 430-440 nm correlated to the visually observed orange colour (**Figure 4.12d**) although broadening of the absorbance bands and larger deviations in λ_{max} were seen as the absorbance increased above 1.0 when 10 mM CoCl₂ was used (**Figure 4.12c,e**). This change in λ_{max} suggests a significant change in the chromophoric species and appeared to be related to the detection of non-specifically bound Co²⁺ from the 10-fold excess (relative to resin loading) of CoCl₂ used. In general, the high sensitivity of the stain allowed the use of much smaller amounts of CoCl₂ (0.01 mol. eq.) and the UV-Vis absorbance intensities of the peaks were lower than 1.0. (**Figure 4.12a,b,d** & **Figure 4.13a-c**)

Figure 4.11 UV-Vis absorbance spectra of Ni²⁺-binding beads stained with dimethylglyoxime

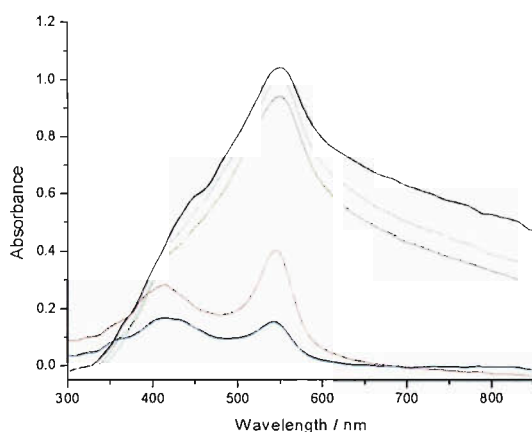
a) *S*-Trt-capped, 1.00 mM Ni²⁺



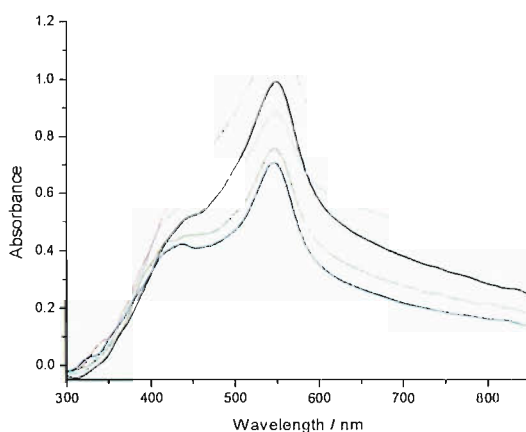
b) Phosphine-capped, 1.00 mM Ni²⁺



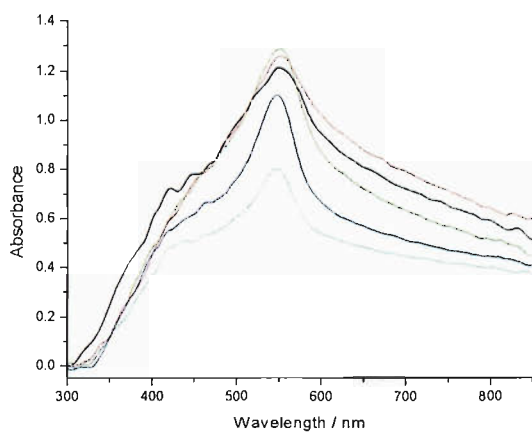
c) *S*-Trt-capped, 10.00 mM Ni²⁺



d) Phosphine-capped, 10.00 mM Ni²⁺



e) Thiol-capped, side-chain deprotected, 0.10 mM Ni²⁺



f) Phosphine-capped, side-chain deprotected 0.10 mM Ni²⁺

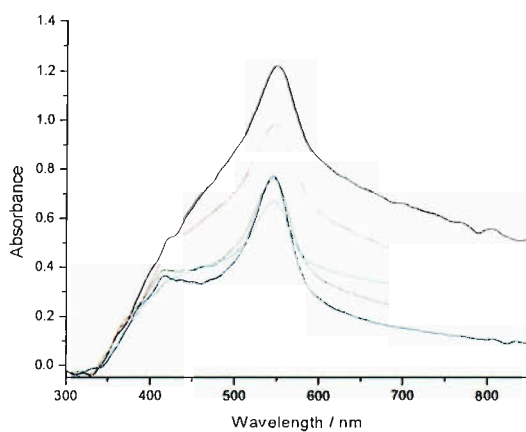
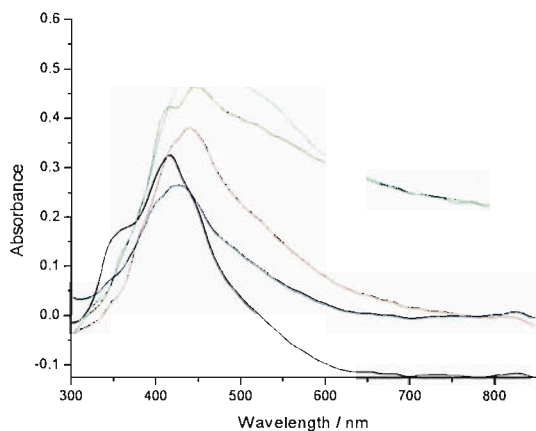
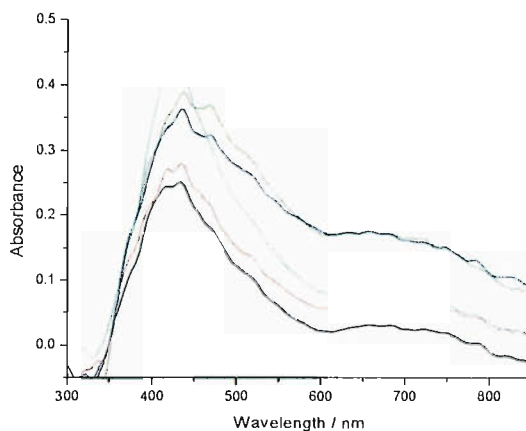


Figure 4.12 UV-Vis absorbance spectra of Co^{2+} -binding beads stained with 1-nitroso-2-naphthol.

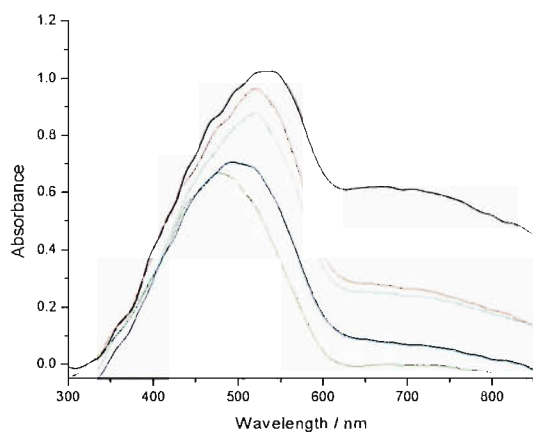
a) *S*-Trityl-capped, 0.10 mM Co^{2+}



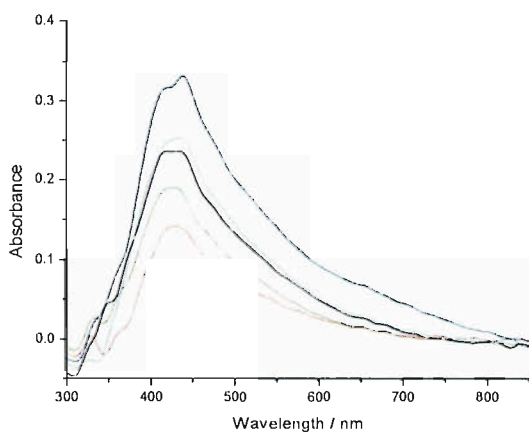
b) Phosphine-capped, 0.01 mM Co^{2+}



c) *S*-Trityl-capped, 10.00 mM Co^{2+}



d) Phosphine-capped, 0.10 mM Co^{2+}



e) Phosphine-capped, 10.00 mM Co^{2+}

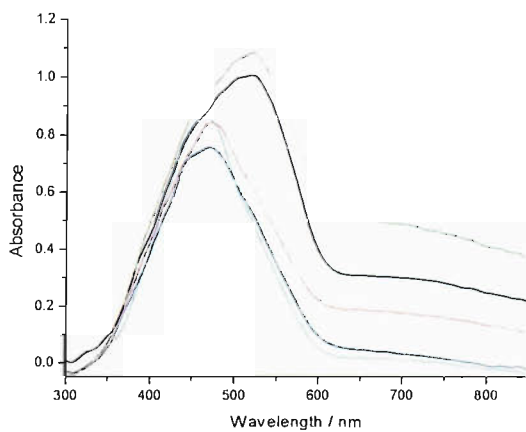
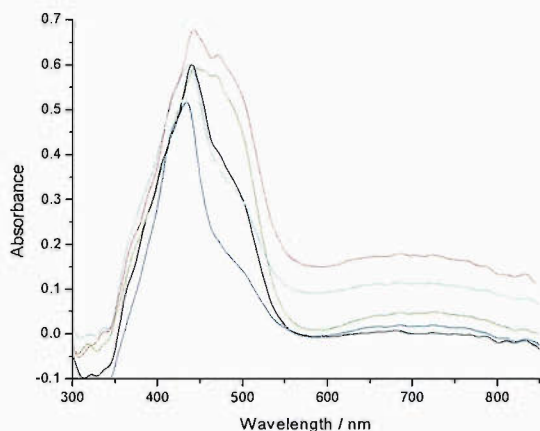
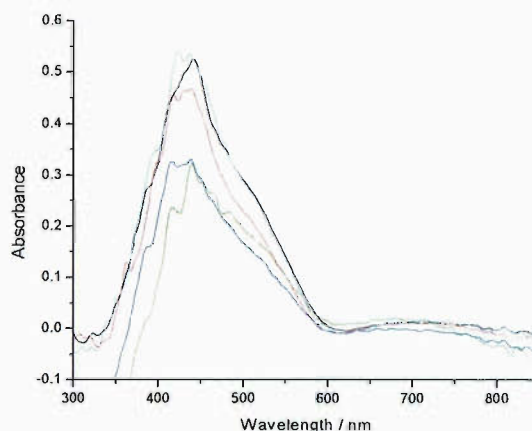


Figure 4.13 UV-Vis absorbance spectra of side-chain deprotected Co^{2+} -binding beads stained with 1-nitroso-2-naphthol

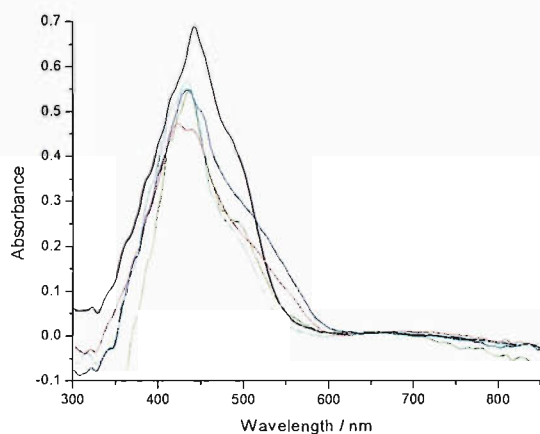
a) Thiol-capped, 0.01 mM Co^{2+}



b) Phosphine-capped, 0.10 mM Co^{2+}



c) Thiol-capped, 0.10 mM Co^{2+}



4.4 Sequencing of Metal-Binding Peptides and Correlation with UV-Visible Spectra

From the UV-Vis analysed beads, attention was focused on the beads from *S*-Trt capped tripeptides treated with 0.1 mM CuCl_2 since the selected beads gave a good range of spectral intensities. (**Figure 4.9a**) These beads were treated with TFA to remove the terminal Boc group from the identification arm of the beads (and the side-chain protection) and submitted for Edman degradation to determine the peptide sequences. (**Table 4.2**)

Table 4.2 Absorbance intensities of stains and corresponding peptide sequences.

| UV-Vis spectra ref. | Wavelength measured / nm | Absorbance at wavelength measured | Sequence |
|--|--------------------------|-----------------------------------|-------------------|
| Figure 4.9a Cu-(dithio-oxamide) | 655 | 0.71 | EC-Pro-His-His-TG |
| | | 0.48 | EC-Ser-His-Lys-TG |
| | | 0.30 (red)* | EC-Lys-His-Lys-TG |
| | | 0.30 (black)* | EC-Pro-His-Pro-TG |
| | | 0.25 | EC-Tyr-His-Val-TG |
| Figure 4.11a Ni-(dimethylglyoxime) | 551 | 1.05 | EC-His-His-Pro-TG |
| | | 0.99 | EC-His-His-???-TG |
| | | 0.95 (black)* | EC-His-His-Gly-TG |
| | | 0.94 (green)* | EC-???-???-???-TG |
| | | 0.91 | EC-???-???-???-TG |
| Figure 4.12a Co-(1-nitroso-2-naphthol) | 443 | 0.52 | EC-His-His-His-TG |
| | | 0.46 | EC-Ser-His-His-TG |
| | | 0.38 | EC-His-His-???-TG |
| | | 0.24 (blue)* | EC-His-Lys-Lys-TG |
| | | 0.24 (black)* | EC-His-Pro-Pro-TG |

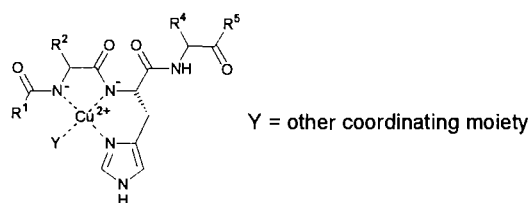
* Colour of corresponding lines in Figures 4.9a, 4.11a and 4.12a respectively

??? = No clear result from Edman sequencing

EC = end cap (*S*-Trt-thioglycolate), TG = TentaGel amino resin

All the active Cu-binding beads selected had at least one His residue while the bead with the highest measured absorbance contained two such residues in the sequence, in agreement with the fact that the imidazole ring of these residues are a powerful metal-coordinating moiety. In all cases, a His residue occupied position 2 in the sequences and at this position are likely to form stable complexes with Cu²⁺ at neutral pH with participation of two amide backbone N-atoms and the imidazole ring N^π-atom.^{179,180} (**Figure 4.14**) The Trt protection of the imidazole N^τ-atom did not appear to hinder this process.

Figure 4.14 Generic structure of Cu-peptide complex with a His residue at position 2.



Of the other residues in the sequences, no obvious conclusions could be drawn. Although the sequences with a higher number residues containing potentially coordinating heteroatoms (Lys, Ser) appeared to give somewhat higher absorbances, these were more difficult to rationalise since these side chains are usually considered to be either too distant (Lys) or unable to adopt the appropriate configuration (Ser) to contribute to coordination with the same Cu-atom as the amide backbone.¹⁷⁹ In these peptides, the formation of dimeric (or polymeric) species may be a possibility. The presence of Pro residues in the selected beads was unexpected since the secondary amide bonds formed by this residue do not possess a H-atom which can be exchanged with the metal to form Cu-N⁻ bonds.¹⁷⁹ However, Pro residues are known to promote β -turns in peptide chains¹⁸⁴ and may bring the end-capping S-atom into close proximity to the metal, promoting additional coordination. The similarity of the UV-Vis results between Pro-His-Pro and Lys-His-Lys suggests that the overriding factor in Cu-binding was the presence of the His, with only a small contribution from the other residues or the capping group.

For comparison, the beads from the *S*-Trt capped library which were screened with Ni were sequenced (**Figure 4.11a & Table 4.2**) although the quality of these results were much poorer with a significant number of sequencing failures. Of the sequences that were determined, all possessed two His residues and at least one occupying position 2. The UV-Vis absorbances of all the picked beads were all similarly high which suggested that the identity of the final residue was probably unimportant relative to the strong binding provided by the His residues. The sequencing results from the beads picked from the screening of Co²⁺ (**Figure 4.12a**) again demonstrated the importance of His residues with the number of these residues present being correlated to the absorbance measured. However, in these beads, the His residue did not always occupy position 2.

4.5 Conclusions

These results demonstrate that sequence-selective binding of metals is possible with tripeptides attached to a solid support. The affinity of the various sequences can be estimated with the aid of single bead UV-Vis microspectrometry by quantifying the amount of chromophore produced by individual beads when exposed to an appropriate staining reagent. However, the quality of the spectral data was reduced since they were reliant on a single measurement rather than an average taken from several beads.

All the sequenced beads contained at least one His residue and number of these residues present were positively correlated to the absorbance (and therefore the amount of metal bound). The presence of His residues thus appeared to be the overriding factor in binding, with minimal contribution from other residues. For all the metals screened, the presence of all the protecting groups did not hinder binding. Further sequencing results may provide more insights by comparing these fully protected peptides with the deprotected versions and comparing the two different end caps. Of the peptides that have already been sequenced, further investigations into the selectivity of these peptides to different metals may benefit from competition experiments with one peptide with several metals.

5 On-bead Determination of Enantiomeric Excess by UV-Visible Microspectrometry

5.1 Introduction: Kinetic Resolution of Chiral Compounds

For many years, the mainstay of enantiomeric excess (e.e.) determination has relied on polarimetry, NMR spectroscopy (in conjunction with chiral derivatising agents, lanthanide shift reagents or chiral solvating agents)^{185,186} and chromatography (HPLC or gas chromatography, with chiral derivatising agents or chiral stationary phases).^{187,188} However, more recently, the advent of “combinatorial asymmetric catalysis” has renewed interest in analytical techniques for the determination of e.e.¹⁸⁹⁻¹⁹¹ and to this end, a large number of methods for the measurement of e.e. have been described, which either allow high-throughput analysis or are novel methods of e.e. determination, or both. These include the application of spectrometric (fluorescence spectroscopy,^{192,193} NMR,^{194,195} MS,¹⁹⁶⁻¹⁹⁸ IR,¹⁹⁹ NIR,²⁰⁰ IR thermography,²⁰¹ UV-Vis anisotropy²⁰²) and non-spectrometric methods such as imaging polarimetry²⁰³ and electrophoresis.^{204,205}

Many non-chiral analytical tools have also been used in conjunction with kinetic resolution for e.e. determination where the target enantiomers are first resolved by a competitive kinetic reaction with a chiral reagent (or catalyst). Such kinetic resolutions can be subdivided into methods where a chiral catalyst (enzymatic^{206,207} or non-enzymatic¹⁹²) is used, or where the derivatising reagents themselves are chiral.

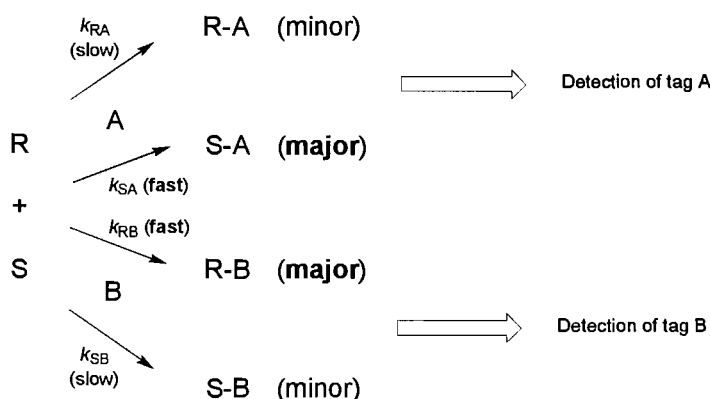
In a simple kinetic resolution where a mixture of the two enantiomers of the sample reacts simultaneously with a single chiral agent, the initial product ratio corresponds to the selectivity factor (s) of the agent, which is the ratio of the competing rate constants. However, the overall product ratio decreases as the reaction progresses since there is a continuous increase in the relative concentration (and therefore the relative rate of reaction) of the less reactive substrate as the faster reacting substrate is consumed. The end result is an e.e. value approaching zero as conversion approaches 100%.²⁰⁸ Exceptionally high s values are necessary if both

high e.e.'s and conversions are desired, for example at 50 % conversion (the theoretical maximum for each enantiomer) a 98 % e.e. value would require an s value of 500 while 96 % e.e. would require an s value of 200 and these are only currently possible with a small range of reactions. Thus in many cases the chemist is limited to a few highly selective reactions, or must compromise between yield and enantioselectivity, a far from perfect situation.

Ideally, a method is required where the less reactive enantiomer is removed by a complimentary reaction and the ratio of substrate enantiomers is maintained throughout the resolution process. In a technique termed parallel kinetic resolution (PKR),²⁰⁹ two resolving agents, each one with a preference for one of the enantiomers are employed. In this way, both enantiomers are consumed with the ratio of rates of reaction being constant. Accordingly, the ratio of the four products generated will also remain constant throughout the resolution. It is therefore possible to achieve high enantiomeric purity with concomitantly high conversion rates. In addition, the effect of using two resolving agents is synergistic, giving high e.e.'s even though the s value for the individual agents may be relatively low.

In an analytical context a pair of pseudoenantiomeric derivatising agents, each bearing an easily identifiable tag (*e.g.* a fluorophore, mass tag) which is correlated to the absolute configuration but remote from the chiral centre of the agent, is used. The analyte is reacted with a large excess (relative to the analyte) of an equimolar mixture of the derivatising agents, resulting in a four component reaction with four possible reaction rate constants. Accordingly, in a bimolecular reaction with an excess of one component (the derivatising agent), the pseudo first order rate constants are k_{SA} , k_{RA} , k_{RB} and k_{SB} . If analyte enantiomer **S** has a preference for agent **A**, and **R** for **B**, it follows that the rate constants k_{SA} and k_{RB} would respectively be greater than k_{RA} and k_{SB} . Correspondingly, the major products are **S-A** and **R-B**. (**Scheme 5.1**)

Scheme 5.1 Generalised reaction scheme of chiral analyte with pseudoenantiomeric resolving agents.



Where the resolving agents are structurally similar, it would be expected that $k_{SA} \approx k_{RB}$ and can be represented by a global rate of k_{fast} . Likewise, $k_{RA} \approx k_{SB}$ and can be represented by k_{slow} with the ratio of k_{fast}/k_{slow} now representing the s value for the overall resolution. After the resolution, the amounts of tag corresponding to **A** and **B** are quantified and the e.e. determined.^{197,210} (**Equation 5.1 & Equation 5.2**)

$$e.e.(\%) = \left[\frac{(x-1)(s+1)}{(x+1)(s-1)} \right] \cdot 100\% \quad \text{Equation 5.1}$$

$$x = z \cdot \frac{I_{tagA}}{I_{tagB}} \quad \text{Equation 5.2}$$

$$s = \frac{k_{fast}}{k_{slow}}$$

Where:

| | |
|------------|--|
| I_{tagA} | signal intensity from derivatives with A |
| I_{tagB} | signal intensity from derivatives with B |
| z | correction factor for signal intensities from A & B |
| x | corrected ratio of A:B |
| k_{fast} | rate constant for the faster reaction pair |
| k_{slow} | rate constant for the slower reaction pair |
| s | selectivity factor |

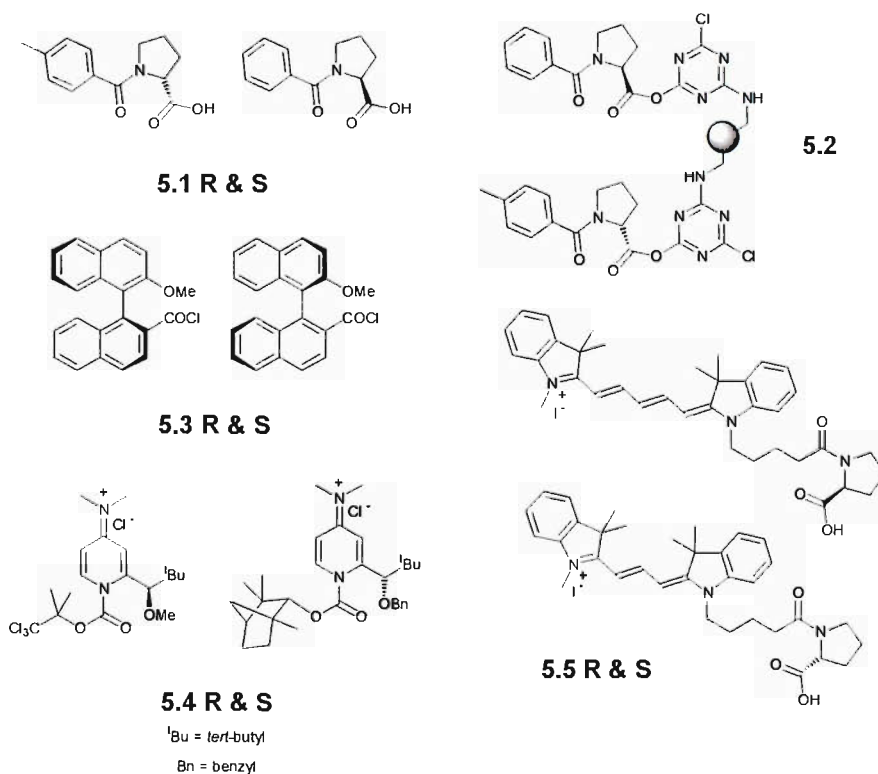
The expression z is included in the equation to account for any differences in signal intensities produced by equimolar amounts of the tags during quantification. During calibration, the z value can be determined by quantification of a racemic

mixture ($x = 1$) of the analyte with Equation 5.2, while a second calibration with another sample of known e.e. (usually a pure sample of one of analyte's enantiomers) is then used to determine the s value with Equation 5.1 and the previously determined z value.

Parallel kinetic resolution only relies on the product ratios, which are constant throughout the reaction, and it is thus unnecessary for the resolution to be continued to completion before analysis. Identical reactivities (where rate constants $k_{SA} \approx k_{RB}$, $k_{RA} \approx k_{SB}$) although desirable, are also probably unnecessary so long as the relative concentrations of the resolving agents are adjusted so the relative rates of the reactions are similar over the majority of the reaction.²⁰⁹

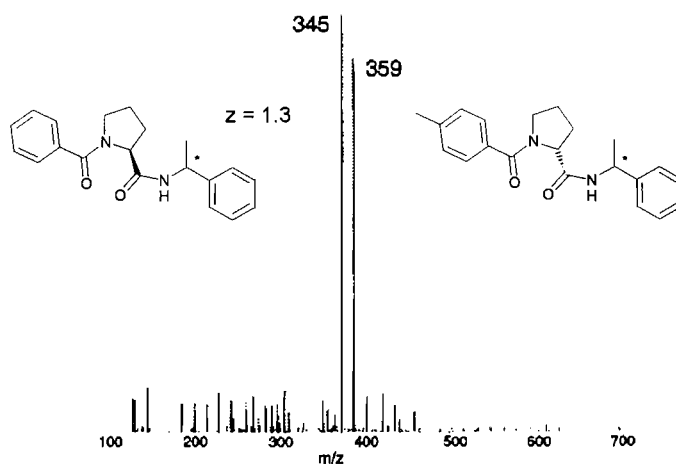
To this end, a number of pseudoenantiomeric resolving agents have been described, aimed mainly at the e.e. determination of chiral amines and alcohols since these are important components of many pharmaceuticals and fine chemicals.^{204,207} In these cases, the resolving agents are often carboxylic acids in a pre-activated form or are activated *in situ* with a coupling agent during the resolution. (**Figure 5.1**)

Figure 5.1 Examples of chiral resolving agents used in parallel kinetic resolutions.



Structurally, the most simple of these pseudoenantiomeric “probes” are pair **5.1** which are only differentiated by an additional methyl group distant from the chiral centre in **5.1R**. These probes have been used for the resolution of alcohols by coupling with DCCI and the acylation catalyst 4-dimethylaminopyridine (DMAP), or with amines by coupling with DCCI and HOBT.¹⁹⁷ The products of the resolution are quantified by MS, where they are differentiated by the mass of the additional methyl group. A solid supported version of this resolving pair (**5.2**) has also been developed on AM-PS where the beads contain a pseudoracemic mixture of **5.1 R & S** activated as chlorotriazine esters.²¹¹ These solid supported derivatising reagents were used for the resolution of chiral amines simply by adding a 20-fold molar excess of the reagent with a catalytic amount of DMAP to a solution of the amine followed by MS quantification. As an illustration, the resolution of a racemic mixture of 1-methylbenzylamine followed by MS analysis gave the ratio of the peak intensities (*i.e.* the intensity correction factor, *z*) as 1.3 since the products at *m/z* 359 were less easily ionised than the products at *m/z* 345. (**Figure 5.2 & Equation 5.3**) Calibration using a series of samples with known e.e. then gave an *s* value of 1.2.

Figure 5.2 Electrospray-MS analysis of the products derived from resolution of racemic 1-methylbenzylamine and resin **5.2**.



$$x = z \cdot \frac{I_{mass,A}}{I_{mass,B}} \quad \text{Equation 5.3}$$

Where $I_{mass,A}$ & $I_{mass,B}$ are the mass peak intensities for probes **A** & **B** respectively.

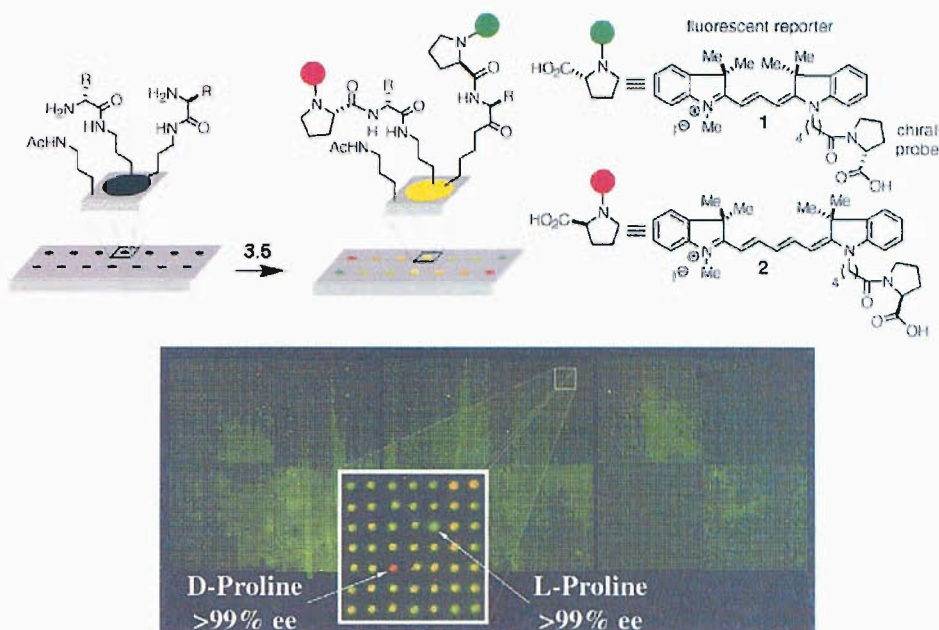
A variety of other amine test compounds were analysed using these mass-tagged probes and overall, these probes showed that even a modest excess of the resolving agents and relatively small *s* values gave analytical values that all fell within 10 % e.e. of the actual values.

Other examples include the use of binaphthyls **5.3** which were quantified post-resolution by CD spectroscopy,²¹² alkoxy-carbonylpyridinium acylating salts derived from chiral DMAP catalysts **5.4** which were analysed by NMR,²⁰⁹ and fluorophore-labelled probes **5.5** in which the ratio of the fluorescent intensities for each of the labels was measured. In the case of **5.4**, PKR was possible even when the resolving agents were quite different in structure.

The application of fluorophore-probes **5.5** was particularly interesting as these were used to resolve amino acids which were supported on a microarray.²¹⁰ The relative intensities of the fluorescent emission at their respective λ_{max} values was quantified by an automated laser scanner to provide the *x* values and demonstrated that at least 15552 separate resolutions were possible on each chip with pmol/spot quantities of analyte. (**Scheme 5.2 & Equation 5.4**)

However, all these methods with the exception of the microarray were aimed at e.e. determination of samples in solution while the expansion of combinatorial chemistry has increased the development of chiral synthetic chemistry on solid supports,²¹³ and thus a method of directly assessing e.e. of resin-supported products was proposed using a pair of pseudoenantiomeric chromophores for parallel kinetic resolution on solid-supports. The intensity of the UV-Vis absorption of the two chromophores on-bead could then be determined using the UV-Vis microspectrometer and subsequently used to calculate e.e.

Scheme 5.2 Chiral resolution of chip-bound amino acids with probes **3.5**.



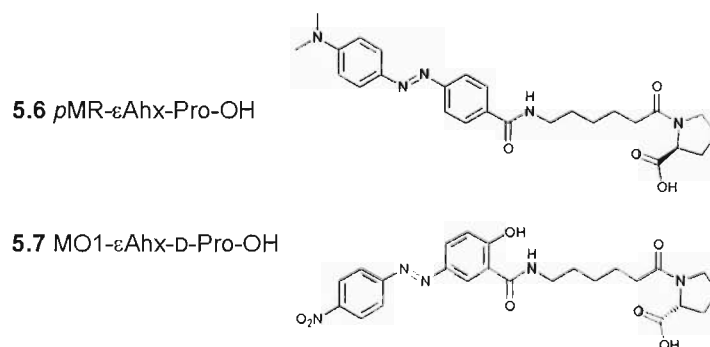
$$x = z \cdot \frac{I_{fluor,A}}{I_{fluor,B}} \quad \text{Equation 5.4}$$

Where $I_{fluor,A}$ & $I_{fluor,B}$ are the fluorescence intensities at λ_{max} for probes **A** & **B** respectively.

5.2 Syntheses of Pseudoenantiomeric Chiral Probes

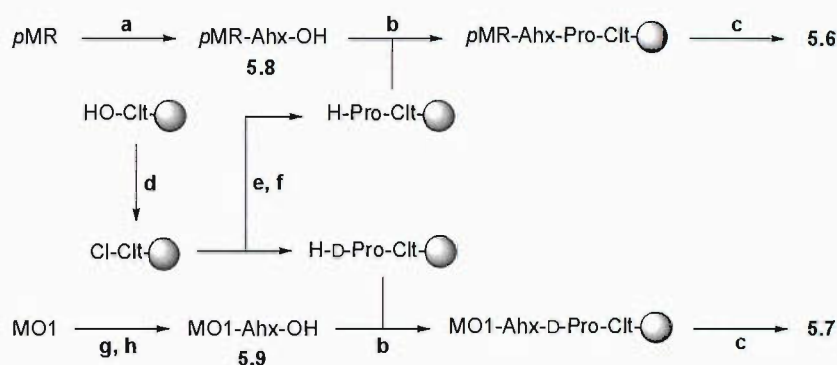
The intended chiral probes employed a design similar to the previously described fluorescent probes **5.5**, consisting of a chromophore (dye), a spacer (ϵ Ahx residue) and a chiral selector (D- or L-Pro residue). The previously used dyes *p*MR and MO1 were employed to give **5.6** & **5.7** respectively. (**Figure 5.3**)

Figure 5.3 Structures of the chromophoric pseudoenantiomeric chiral probes



A combination of solution and solid phase procedures were used for the synthesis of the probes. (**Scheme 5.3**) Beginning with the synthesis of **5.8**, a “one pot, two step” procedure was adopted where the dye-succinimide active ester was pre-formed with DCCI and HOSu followed by addition of ϵ Ahx. The attachment of the amino acid was found to be sluggish, requiring up to 48 h to reach completion and was thought to be due to the poor reactivity of the highly conjugated dye.

Scheme 5.3 Overview of pseudoenantiomeric probe synthesis



Reagents & conditions: (a) DCCI, HOSu, DMF, 48 h; then ϵ Ahx, DMF, 27 h, 70 %; (b) PyBOP, DIPEA, DCM/DMF, 3 h, quant.; (c) 1% TFA, DCM, 5 min x 5 cycles, quant.; (d) SOCl_2 , DCM, 2 h; (e) Fmoc-(D or L)-Pro, DIPEA, DCM, 4 h, 48 %; (f) 20 % piperidine, DMF, 10 min x 3 cycles; (g) SOCl_2 , THF, 4.5 h; then ϵ Ahx-OMe, 1,4-dioxane, 16 h; (h) NaOH, aq/acetone, 4 h, 33 % over two steps.

For the synthesis of **5.9**, no literature precedents could be found for the synthetic manipulation of MO1 (apart from its commercial production) and several DCCI mediated coupling reactions with either HOSu, HOBt, 1-hydroxy-7-azabenzotriazole (HOAt) or a catalytic amount of DMAP were attempted but none produced significant amounts of the desired product (conversions by HPLC < 20 % in all cases). This low reactivity was thought to be due to the electron withdrawing effect of the nitro group and the high degree of conjugation of MO1. The conversion to the highly activated MO1 acyl chloride was carried out by treatment with SOCl_2 and complete conversion to the desired acyl chloride was observed after 4 h. Evaporation of the excess SOCl_2 followed by coupling with ϵ Ahx-OMe gave the desired product although in poor overall yield. Saponification of the methyl ester gave the free acid **5.9**.

In the solid phase component of the synthesis, proline was attached to the acid-labile 2-chlorotrityl (Clt) linker on PS using standard procedures with DIPEA.¹³¹ **5.8** and **5.9** were then attached to the deprotected proline-resin under basic conditions with PyBOP/DIPEA. (The DIC/HOBt coupling procedure resulted in premature cleavage and re-attachment of probes to give a mixture of products with 2-3 proline residues, **Figure 5.4**) Cleavage from the supports with dilute TFA produced the desired probes in excellent purity by HPLC. (**Figure 5.5**)

Figure 5.4 HPLC of chromatogram of crude mixture after DIC/HOBt coupling of **3.8** (top) & **3.9** (bottom).

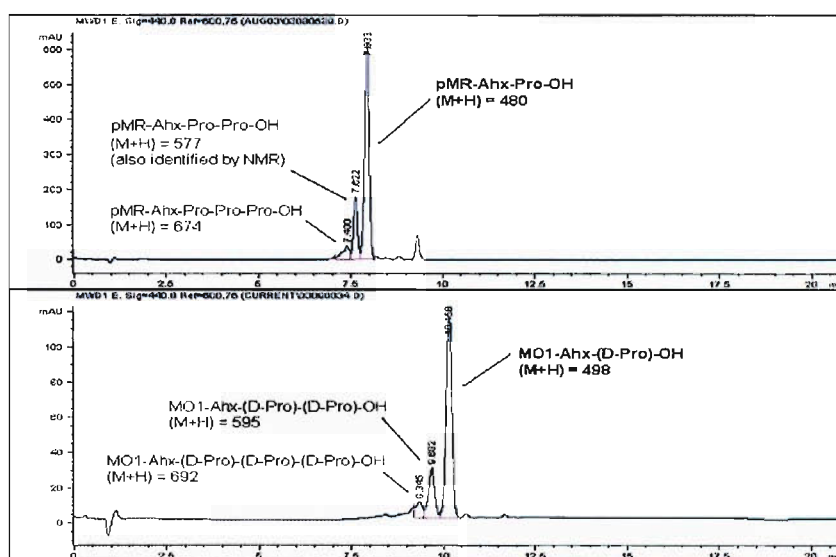
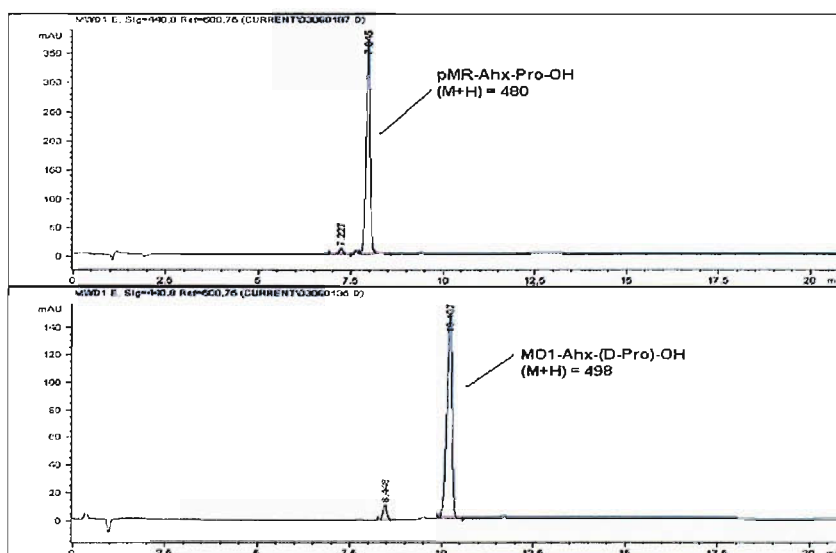


Figure 5.5 HPLC chromatogram of crude mixture after PyBOP/DIPEA coupling of **3.8** (top) & **3.9** (bottom).

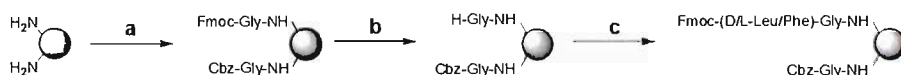


In both cases, the cleaved hydroxy-Clt resin was reconverted to the chloride with SOCl_2 ²¹⁴ so sufficient amounts of each chiral probe could be synthesised.

5.3 Chiral Resolution of On-bead Amino Acids and UV-Visible Microspectrometric Analysis

For the test substrates two amino acids, Leu and Phe, representing aliphatic and aromatic substrates were coupled to polystyrene resin. To prevent the possibility of excessively high absorbances and to demonstrate the sensitivity of the UV-Vis microspectrometer, the polystyrene resin was first partially capped to give a loading of $\sim 0.04 \text{ mmol g}^{-1}$ of the chiral amino acids. (**Scheme 5.4**) The reduced loadings were produced by coupling an excess of mixtures of Fmoc- and Cbz-Gly in a similar way to the CPG sensor beads in Section 3.2.1. (**Table 5.1**) The Fmoc protecting group was then removed and followed by the coupling of various ratios of Fmoc-Leu or Fmoc-Phe enantiomers.

Scheme 5.4 Synthesis of low-loading PS resins with a range of enantiomeric ratios of Leu and Phe.



Reagents & conditions: (a) Cbz/Fmoc-Gly-OH, DIC, HOBt, DCM/DMF, 3 h; (b) 20% piperidine, DMF, 5 min \times 2 cycles; (c) Fmoc-(D and/or L)-Leu or Fmoc-(D and/or L)-Phe, DIC, HOBt, DCM/DMF, 19 h.

Table 5.1 Fmoc loading of resins after co-acylation with Cbz- and Fmoc-Gly.

| Molar ratio Cbz- : Fmoc-Gly | Fmoc loading post-reaction / $\mu\text{mol g}^{-1}$ |
|-----------------------------|---|
| 99:1 | 9 (0.8 %) |
| 98:2 | 15 (1.3 %) |
| 97:3 | 24 (2.0 %) |
| 94:6 | 41 (3.7 %) |
| 91:9 | 78 (7.1 %) |
| 0:100 (control) | 1099 (100 %) |

Using the synthesised pseudoenantiomeric probes, experiments were conducted to attempt the chiral discrimination of resin supported leucine. A number of coupling procedures were tested with the aim of *in situ* generation of the HOPfp active ester using pentafluorophenyl diphenylphosphinate (FDPP)^{210,215} or DIC, (Table 5.2) while a 30- or 50-fold excess of probe, relative to the sites on the beads was used, depending on resin loading. Overall, the best conditions gave a modest but detectible chiral discrimination. (entry C, Table 5.2)

Table 5.2 Tested conditions for chiral resolution with pseudoenantiomeric probes.

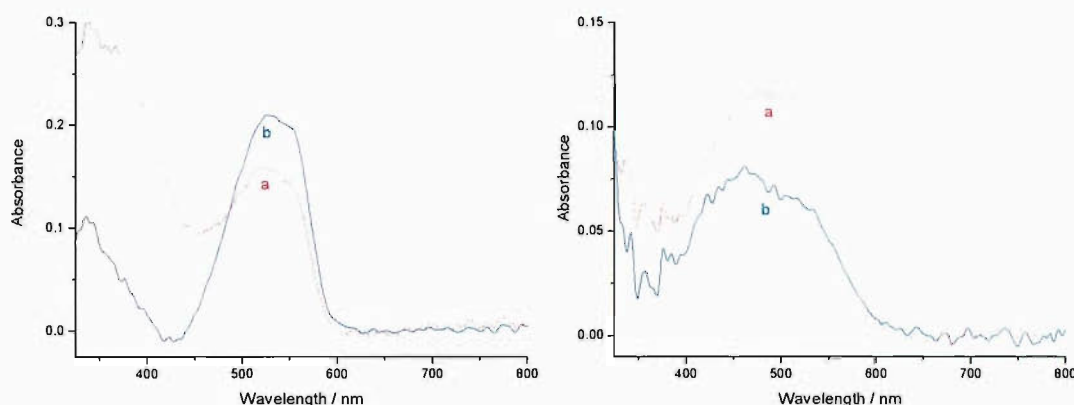
| Ref. | Conditions* | | | | Spectral intensity | Quality of resolution |
|------|-----------------|---------------------------------------|----------------------|------------------------|--------------------|-----------------------|
| | Coupling agents | Resin loading / μmolg^{-1} | Reaction volume / mL | Temperature range / °C | | |
| A | DIC, HOPfp | 24 | 20 | -25 – -10 | Strong | None |
| B | FDPP, HOPfp | 24 | 20 | -35 – -24 | Weak | Poor |
| C | FDPP, HOPfp | 41 | 20 | -35 – -24 | Moderate | Moderate |
| D | FDPP, HOPfp | 41 | 20 | -59 – -47 | None | – |
| E | FDPP, HOPfp | 41 | 60 | -59 – -47 | None | – |

* In all cases, 5 mg of resin (0.12 or 0.21 μmol of sites) and 6 μmol of probes were used. Reaction time: 8 h

Each sample of beads was analyzed under both acidic and basic conditions to maximize the quality of the UV-Vis data as the *p*MR gave an intense red colour under acidic conditions while MO1 produced a deep orange under basic conditions. This provided usable spectra even when only a fraction of the resin sites were loaded with dye. For supported Leu, the spectra gave complimentary results with the supported L-Leu giving a higher absorbance due to the *p*MR λ_{max} (518 nm) while

D-Leu resin gave a higher absorbance at the MO1 λ_{\max} (490 nm). (**Figure 5.6**) Identical resolution conditions were then used for the analysis of supported Phe.

Figure 5.6 UV-Vis absorbance spectra of (a) 100% D- and (b) 100% L-Leucine on PS after resolution using entry C on **Table 5.2** in 160 mM HCl in 1,4-dioxane (left) and 67 mM DBU in 1,4-dioxane (right).

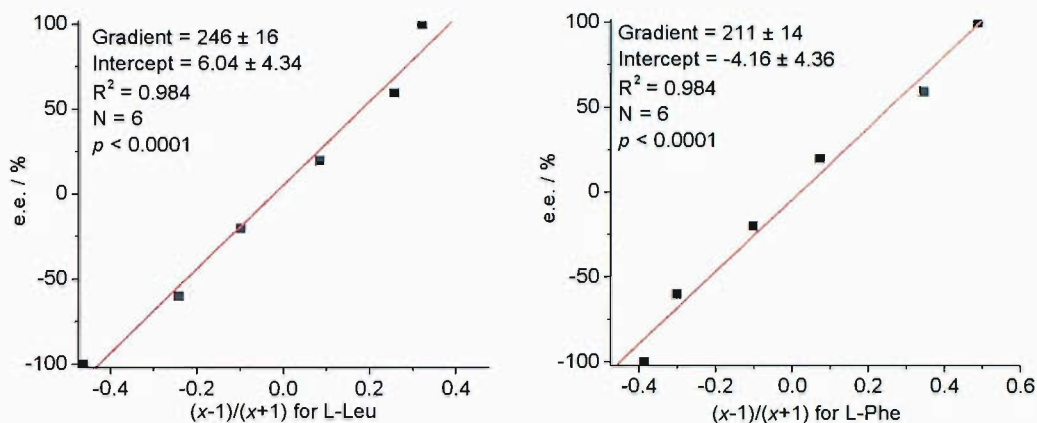


In both cases, the L-prolinyl probes had a preference for the L-residues of both the supported amino acids. To determine the z values (**Equation 5.5**), the appropriate absorption maxima of the spectra from two sets of samples, 20 % e.e. in favour of D-residue and 20 % e.e. in favour of the L-residue were used, rather than relying on a single value from the racemic sample, and gave a z value of 0.575 for the Leu substrate and 0.526 for Phe. These z values were used in Equation 3.5 to calculate the other x values that were then applied into Equation 3.1. From this, a linear plot of e.e. against $(x-1)/(x+1)$ provided $(s+1)/(s-1)$ as the gradient of the line (**Figure 5.7**) and the s values were calculated to be 2.37 and 2.80 for Leu and Phe respectively. On average, the experimental data fell within 7.6 and 7.5 % e.e. of the true values respectively. These were related to the s values since superior enantiomeric discrimination (*i.e.* higher s values) gave more accurate results.^{197,210}

$$x = z \cdot \frac{A_{pMR}}{A_{MO1}} \quad \text{Equation 5.5}$$

Where A_{pMR} and A_{MO1} are the on-bead absorbance intensities at the λ_{\max} of pMR and $MO1$ respectively.

Figure 5.7 Graphs of actual e.e. against $(x-1)/(x+1)$ for leucine (left) & phenylalanine (right). (100 % e.e. = pure L-enantiomer, -100 % e.e. = pure D-enantiomer)



5.4 Conclusions

In summary, the feasibility of direct determination of e.e. of supported amino acids by the application of chromophoric chiral probes with UV-Vis microspectrometry has been demonstrated. This was successful even with very low resin loadings while avoiding issues related to analyzing bead-supported fluorophores. In the process, the synthesis of a novel pair of chromophoric chiral derivatising agents was developed.

The results of the chiral resolution were comparable in accuracy to other analytical PKR methods (typically 5-10% e.e. of the true value) and sufficient for preliminary screening activities^{196,197,210} although greater accuracy is likely to be achieved by using lower temperatures and longer times for the resolutions, as well as taking a larger sample of beads for UV-Vis measurements.

6 Experimental Procedures

6.1 General

6.1.1 Instrumentation

Melting points were determined using an Electrothermal melting point apparatus. A Personal Chemistry Smith Synthesizer was used in reactions requiring microwave heating. Solution phase UV-Vis spectra were measured using a Hewlett Packard 8452A Diode Array Spectrophotometer. IR spectra were recorded from neat compounds with an ATR apparatus Bio-Rad Golden Gate FTS 135 spectrophotometer. The IR spectra for solid-supported materials were recorded using an FTIR Perkin-Elmer 2000 spectrophotometer coupled to an AutoIMAGE Fourier transform infrared microspectrophotometer with a resolution of $\pm 8 \text{ cm}^{-1}$. Mass spectra were obtained on a VG Platform single quadrupole electrospray mass spectrometer and a ThermoQuest TraceMS single quadrupole electron impact mass spectrometer. High resolution mass spectra were obtained on a Bruker Apex III FT-ICR-MS with electrospray ionisation. NMR spectra were recorded on a Bruker AV300 (at 300 MHz for ^1H and 75 MHz for ^{13}C) or a Bruker DPX400 (at 400 MHz and 100 MHz respectively) at 298K. The chemical shifts are quoted in ppm on the δ scale using residual protonated solvent as the internal standard. Coupling constants (J) were quoted in Hz. Interpretation of the spectra was aided by the spectra of the parent compounds, two-dimensional NMR techniques and a chemical shift estimation computer program (CS ChemNMR Pro Ver 6.0, Upstream Solutons, Hergiswil, Switzerland). Analytical HPLC was performed with an Agilent 1100 Series system with a multiple wavelength detector. The eluents A ($\text{H}_2\text{O} + 0.1 \text{ \% v/v}$ TFA) and B ($\text{MeCN} + 0.04 \text{ \% v/v}$ TFA) were used at a 10-90 % B gradient with an overall flow rate of 0.5 mLmin^{-1} . The columns and gradients used were: (1) S5OD: Supelco Discovery $5\mu \text{ C18}$, $50 \times 4.6 \text{ mm}$ column, 3 min gradient followed by 2 min isocratic 90 % B, (2) S15OD: Phenomenex Luna $3\mu \text{ C18}$, $150 \times 3 \text{ mm}$ column, 10 min gradient followed by 5 min isocratic 90 % B.

Elemental analyses were provided by Medac (Egham, UK) and Peptide sequencing by Edman degradation was provided by the School of Biological Sciences (University of Southampton).

6.1.2 Chemicals & Materials

All chemicals employed were of reagent grade and used without further purification unless otherwise stated. All DMF used was of peptide synthesis grade.

1% Crosslinked aminomethyl functionalised polystyrene resin beads had a dry diameter of 75-150 μm (100-200 mesh) and an amine loading of 1.11 mmol g^{-1} (Polymer Labs, Church Stretton, UK) or a trityl chloride loading of 1.50 mmol g^{-1} (Merck Biosciences, L aufelfingen, Switzerland). TentaGel-S Amino beads had a dry diameter of 130 μm and an amine loading of 0.25 mmol g^{-1} (Rapp Polymere, T ubingen, Germany). Trisoperl Amino, aminopropyl functionalised spherical controlled pore glass beads (VitraBio, Steinach, Germany) had an amine loading of 111 $\mu\text{mol g}^{-1}$ and a diameter of 100-200 μm (Trisoperl Amino-170, batch no. PMGK L 07/01) or 171 $\mu\text{mol g}^{-1}$ and 50-100 μm (Trisoperl Amino-163, batch no. PMGK L 30/92). TentaGel resins with the attached *para*-Methyl Red and (4-carboxyphenyl)-Bromocresol Purple or (4-carboxylphenyl)-Bromothymol Blue were provided by Dr. J. K. Cho (Centre for Combinatorial Excellence, University of Southampton).

para-Methyl Red purchased from TCI (Tokyo, Japan) and Fmoc-Tyr(3-NO₂) purchased from Advanced ChemTech (Louisville, Kentucky). (4-carboxyphenyl)-Bromophenol Blue was donated by Dr. J. K. Cho. All other dyes were purchased from Aldrich (Gillingham, UK).

Peptide coupling agents TFFH & FDPP were purchased from Advanced ChemTech and Aldrich respectively.

6.1.3 Solid Phase Resin Tests

6.1.3.1 Quantitative Ninhydrin Test¹⁶

Reagent A:

Solution 1: Phenol (40 g) was mixed with absolute ethanol (10 ml) with warming. This was then stirred with Amberlite mixed-bed resin MB-3 (4 g) for 45 min and filtered.

Solution 2: KCN (65 mg) was dissolved in water (100 ml). 2 ml of this was diluted to 100 ml with pyridine (freshly distilled) and stirred with Amberlite mixed-bed resin MB-3 (4 g). This was then filtered

Solutions 1 and 2 were mixed to produce reagent A.

Reagent B:

Ninhydrin (2.5 g) was dissolved in absolute ethanol (50 ml).

To a known mass of resin (5-20 mg), 6 drops of reagent A and 2 drops of reagent B were added and heated at 100 °C for 10 min. This was then cooled and 60% aqueous ethanol (2 ml) was added. The mixture was then filtered through glass wool to remove the beads. The filtrate was collected in a volumetric flask (5-50 ml). The beads were washed with a solution of Et₄NCl (0.5 M in DCM, 2 × 0.5 ml) and the washings collected with the earlier filtrate. This was made up to volume with 60% aqueous ethanol. The UV-Vis absorbance was then measured against a blank containing the Et₄NCl solution (2 × 0.5 ml) and made up to the same volume with 60% aqueous ethanol. The amount of free amino groups was calculated:

$$\text{Amount of amine (mmol g}^{-1}\text{)} = (A_{570} \times V \times 10^3) / (\epsilon_{570} \times W)$$

| | | |
|--------|------------------|--|
| Where: | A_{570} | UV-Vis absorption at 570 nm |
| | V (ml) | Volume of the final solution |
| | ϵ_{570} | Molar absorption coefficient suitable for most peptides at 570 nm ($1.5 \times 10^4 \text{ M}^{-1} \text{ cm}^{-1}$) |
| | W (mg) | Weight of solid support sample |

6.1.3.2 Quantitative Fmoc Test²¹⁶

To a known quantity of beads (5-10 mg) a solution of piperidine (20% v/v in DMF, 1 ml) was added and allowed to react for 15 min. The solution was filtered through glass wool to remove the beads. The filtrate was collected in a volumetric flask (5-25 ml). The beads was washed with 20% piperidine in DMF (2 x 2 ml) and the washings collected with the earlier filtrate. This was then made up to volume with 20% piperidine in DMF. The UV-Vis absorbance was then measured against a blank containing 20% piperidine in DMF. The amount of Fmoc groups was calculated:

$$\text{Amount of Fmoc (mmol g}^{-1}\text{)} = (A_{302} \times V \times 10^3) / (\epsilon_{302} \times W)$$

| | | |
|--------|------------------|--|
| Where: | A_{302} | UV-Vis absorption at 302 nm |
| | V (ml) | Volume of the final solution |
| | ϵ_{302} | Molar absorption coefficient for the piperidyl-fulvene adduct at 302 nm (8100 M ⁻¹ cm ⁻¹) |
| | W (mg) | Weight of solid support sample |

6.1.3.3 Chloranil Test for Secondary Amines²³

To a small sample of resin (1-3 mg) was added 2 drops of 2 % v/v acetaldehyde in DMF and 2 drops of 2 % w/v *p*-chloranil in DMF. The mixture was allowed to stand for 5 min before visual examination. The presence of secondary amines was indicated by a blue colouration of the beads.

6.2 Experimental procedures for chapter 2

6.2.1 UV-Visible Microspectrometer Specifications

The lightsource for the microscope and spectrometer was a Mini-D2T deuterium-tungsten fiber optic light source (Ocean Optics, Dunedin, Florida) and the Deuterium lamp had a spectral range of 200 to 410 nm while the tungsten lamp covered 360 to 1100 nm (ignition delay < 2 s). A fused silica lens (40 mm focal

length) was placed 80 mm from the lightsource and the sample stage was located 80 mm above the lens. Above this was placed the objective lens, an OFR LMU-40x-NUV (NA = 0.50) with a working distance of 1 mm and an effective focal length of 5 mm. The beam exiting the objective lens was then either refocused on to a fiber optic cable leading to the entrance slit of a USB2000-UV-Vis spectrometer (spectral range 200-850 nm, typical overall spectral resolution 1.5 nm, from Ocean Optics Inc.), or diverted to a CCTV camera using a flipping mirror. Another fused silica lens with a focal length of 40 mm was used to refocus the beam onto the fiber optic cable. The optic fibers used throughout had core diameters of 200 μm . (**Figure 2.1**) The magnification at the detector end was $\times 8$ and at the camera end, $\times 18$ while the microscope had a sampling area with a diameter of 25 μm . The spectrometer was connected to a PC which used OOIBase32 software (ver.1.0.3, Ocean Optics) configured to measure UV-Vis transmission.

The quartz slides (76 x 26 x 1 mm) and quartz coverslips (22 mm \O x 0.25 mm) were purchased from Agar Scientific (Stansted, UK). The glass coverslips (thickness # 1) had either 1.0 or 0.5 cm holes drilled through them to act as wells.

6.2.2 Solid-Phase UV-Visible Spectra Acquisition and Processing

The beads were soaked in the solution of interest for at least 1 h before being placed in a microscope slide well, the well filled with the solution and covered with a coverslip. The transmission spectra of 8 different beads were recorded with a 1 s acquisition time and were then converted and further processed with the statistical software package Origin version 6.1 (OriginLab, Northampton, Massachusetts) to produce the absorbance spectra using the Beer-Lambert Equation (**Equation 1.1**). In quantitative calculations, the concentration of the dye within the beads was used (c , was calculated from the known loading and volume of the beads), the diameter of the bead was used for l .

6.2.3 Assessment of Lensing Effect

Each batch of beads (5 mg) was moistened in the desired solvent (1 mL) for 2 h and the UV-Vis transmission spectra for 8 beads from each solvent were measured and averaged. The transmission spectra for the solvents alone were then

measured and the percentage change in transmission intensity at 625 nm was calculated.

6.2.4 Coupling of Indicator Dyes to Solid Supports

6.2.4.1 Coupling of *para*-Methyl Red to Aminomethyl Polystyrene or TentaGel

para-Methyl Red (27mg, 0.1 mmol) and HOBt (15 mg, 0.1 mmol) were dissolved in a solvent mixture of 25 % DMF in THF (3 mL). DIC (15.7 μ L, 0.1 mmol) was added and the mixture allowed to activate for 5 min before being made up to 10 mL with the solvent mixture. Each batch of either aminomethyl polystyrene or amino TentaGel resin (25 mg each batch) was wet with the solvent mixture (200 μ L), the volume of activated dye solution appropriate to the desired nominal dye loading was added and the mixtures were shaken for 6 h and drained. The resin was then washed successively with 25 % DMF *v/v* in THF, 5 % TFA *v/v* in DCM, DCM, MeOH and Et₂O (5 \times 1.5 mL each solvent) and dried overnight *in vacuo*.

6.2.4.2 Coupling of 4-Carboxyphenyl-Bromophenol Blue to TentaGel⁴⁸

(4-Carboxyphenyl)-Bromophenol Blue (71 mg, 0.1 mmol) was dissolved in 25 % DMF in THF (5 mL) and TFFH²¹⁷ (29 mg, 0.11 mmol) and DIPEA (34.6 μ L, 0.2 mmol) were added and allowed to stand for 5 min. This solution was then made up to either 100 or 20 mL with 25% DMF in THF. Each batch of TentaGel resin (25 mg each batch) was first wet with the solvent mixture (200 μ L). The volume of activated dye solution appropriate to the desired dye loading was added and the mixtures were shaken for 6 h. The beads were subsequently drained, washed and dried as described in the section above.

6.2.4.3 Coupling of Alizarin Yellow GG or Mordant Orange 1 to TentaGel

Alizarin Yellow GG (31mg, 0.1 mmol) or Mordant Orange 1 (29 mg, 0.1 mmol) and HOBt (31 mg, 0.2 mmol) were dissolved in a solvent mixture of 25 % DMF in THF (5 mL). DIC (15.7 μL , 0.1 mmol) was added and the mixture allowed to activate for 10 min before being made up to 10 mL with the solvent mixture. The activated dye solution (500 μL) was added to TentaGel resin (25 mg each batch, 0.29 mmol g^{-1}) and the mixtures were shaken for 6 h. The resin was washed and dried as described for the *para*-Methyl Red resins.

6.2.4.4 Coupling of 3-Nitrotyrosine to Aminopropyl Controlled Pore Glass

Trisoperl Amino-170 CPG (100 mg) was wet with THF (1 ml) and stirred with N-Fmoc-3-nitrotyrosine (224 mg, 0.5 mmol in 1 ml THF) for 10 min. DIC (63.1 μL , 0.5 mmol) was added and the mixture stirred under microwave heating at 140 °C for 45 min. The resin was then drained and washed with THF (10 \times 1 ml) and DCM (3 \times 3 ml) then dried. This yielded pale yellow beads with a negative ninhydrin test result and an Fmoc test loading of 61 $\mu\text{mol g}^{-1}$. The Fmoc protecting group was then removed by treatment with 20% piperidine *v/v* in DMF for 30 min. The resin was drained, washed with DMF (5 \times 3 ml), DCM (5 \times 3 ml) and dried.

6.2.5 UV-Visible Analysis of Post-Reaction Solutions

For the measurements involving *para*-Methyl Red, small aliquots of known volumes (100-200 μL) of the activated dye solution were diluted with the coupling solvent (25 % DMF in THF, 1 mL) and 10 mM HCl in 1,4-dioxane (to 100 mL). The UV-Vis absorbance was measured on a conventional UV-Vis spectrometer and the Beer-Lambert Law applied to determine ϵ_{max} value. The activated dye solution then was used in the coupling reactions as described above. After reaction, the reaction solution was drained from the beads and collected. These solution were each diluted with 10 mM HCl in 1,4-dioxane to a concentration suitable for analysis by UV-Vis (Abs < 1). Using the previously determined ϵ_{max} , the amount of dye remaining was

calculated. The beads were washed with 1,4-dioxane (8 mL), this solution collected, diluted as appropriate with 1,4-dioxane and 1 M aq. HCl achieve a concentration of 10 mM HCl in 1,4-dioxane and subjected to UV-Vis analysis. This washing process was repeated until no further dye was detectable by UV-Vis spectrometry (usually 3-4 cycles).

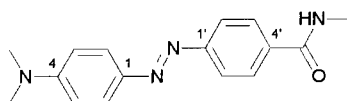
The total amount of dye recovered from the reaction solution and washings was deducted from the original amount of dye added to the coupling reactions to give the amount of dye remaining on the beads. Together with the number of beads per gram and the volume per bead (**Table 6.1**), the concentration of dye within the beads was calculated. This concentration value was used to calibrate the absorbance graphs.

Table 6.1 Physical dimensions of the beads used

| Bead type | Mean diameter measured by microscopy / μm | | Mean swollen volume of dry bead / nL | Number of beads ²¹⁸ / g |
|-------------------------|--|------------------------|--------------------------------------|------------------------------------|
| | Dry | Swollen in 1,4-dioxane | | |
| Aminomethyl-Polystyrene | 99.5 (n = 58) | 144 (n = 44) | 1.6 | 1.72×10^6 |
| TentaGel-S Amino (TG) | 125 (n = 49) | 192 (n = 47) | 3.7 | 0.78×10^6 |

6.2.6 UV-Visible pH Profiling of Indicators

6.2.6.1 4'-(4-Dimethylamino-phenylazo)-N-methyl benzamide (*para*-Methyl Red methyl amide)



To a solution of *para*-Methyl Red (135 mg, 0.5 mmol) and HOSu (65 mg, 0.56 mmol) in DMF (5 mL) was added DCCI (113 mg, 0.54 mmol) and stirred for

16 h to give the intermediate succinimide active ester. A suspension of methylamine hydrochloride (38 mg, 0.56 mmol) and DIPEA (87 μ L, 0.5 mmol) in DMF (4 mL) was added and the mixture stirred for a further 16 h. DCU was removed by filtration and the DMF was evaporated under reduced pressure. The residue was then purified by flash column chromatography using the eluent noted below to yield a red solid. This was recrystallized with MeOH/Hexane to give fine red needles of the product (87 mg, 31%). R_f 0.45 (Hexane:EtOAc:AcOH, 1:1:0.01); HPLC method S5OD: 220 nm, 3.44 min; mp 239 $^{\circ}$ C; (Found: C, 68.0; H, 6.4; N, 19.5. $C_{16}H_{18}N_4O$ requires C, 68.1; H, 6.4; N, 19.8%); ν_{max} (solid)/ cm^{-1} 3347 (CONH), 2898 (ArNMe₂), 1606 (CONH), 1546 (Ar), 1371 (ArNMe₂), 1137 (Ar), 824 (Ar); δ_H (400 MHz; CDCl₃) 3.03 (3H, d, J 5, NHCH₃), 3.10 (6H, s, N(CH₃)₂), 6.22 (1H, br d, J 4, CONH), 6.75 (2H, d, J 9, 3-Ar), 7.85-7.91 (6H, m, 2,2',3'-Ar); δ_C (100 MHz; CDCl₃) 27.0 (NHCH₃), 40.4 (N(CH₃)₂), 111.6 (3-Ar), 122.4 (2'-Ar), 125.5 (2-Ar), 127.9 (3'-Ar), 134.8 (4'-Ar), 143.8 (1-Ar), 153.0 (4-Ar), 155.2 (1'-Ar), 167.9 (CONH); m/z (ES⁺) 305 (100 %, (M+Na)⁺); (HRMS found 283.1550, (M+H)⁺ requires 283.1554).

6.2.6.2 UV-Visible absorbance measurements

Batches of resin (~ 5 mg each) were soaked overnight in 0.1 M sodium phosphate buffers (0.5 mL). The spectra were then measured in the solutions of the appropriate pH. For the pMR methyl amide, a stock solution of 5 mg in 1 mL 1M aq. HCl was prepared. 10 μ L aliquots of this solution were diluted and adjusted to the required pH with conc. HCl or aq. NaOH to the desired pH and a final volume of 1 mL (50 μ g/mL of dye). The UV-Vis spectra were recorded with 200 μ L placed in a well of a microscope slide and an average of 2 spectra taken against a reference solution of matching pH without the dye. The deconvolution calculations were conducted with Origin 6.1.

6.2.7 Experimental Procedure for Kinetics Measurements

Prolinyl-(2-chlorotriyl)-polystyrene resin (1 mg, 45 μ molg⁻¹, from Section 6.5.1.6) was placed in the microscope slide sample well and 2 % acetaldehyde solution in DMF (30 μ L) was added. The mixture was allowed to stand for 5 min and 2 % w/v *p*-chloranil in DMF (30 μ L) was added. The well was immediately

covered with a glass coverslip and a single bead was brought into focus under the UV-Vis microscope. The spectra were then recorded every 1.0 s for approximately 15 min.

The spectra were imported into Origin 6.1 and the transmittance at 550 nm was extracted with the appropriate time values. These transmittance values were then converted to absorbance values using the previously described formula using the transmittance from prolinyl-(2-chlorotrityl)-polystyrene resin beads in 60 μL of 2 % acetaldehyde solution as the reference. The absorbance was then plotted against time and a non-linear curve fitting was applied to achieve the best fit curve for Equation 2.1.

6.3 Experimental procedures for chapter 3

6.3.1 Construction of fibre optic assembly

A standard glass microscope slide (76mm x 26 mm) was used to mount the assembly. (**Figure 3.2**) Glass capillary tubes with a 1.85 mm external diameter were cut to 25 mm lengths and used as the central support for the bare optical fibre and bead, while smaller tubes (1.15 mm external diameter, 10 mm length) were used to support the buffer-insulated optical fibre. These tubes were aligned 5 mm apart and cemented to the glass slide with cyanoacrylate glue. A patch cable with SMA connectors (part no.: M15L02, ThorLabs, Newton, NewJersey, USA) was cut in half and approximately 30 cm of the outer jacket removed from each cut end. Approximately 30 mm of the plastic buffer was stripped to reveal the optical fibre, which was cleaved with an ultrasonic fibre cleaver to give smooth perpendicular termini approximately 18 mm from the buffer.

Under a microscope, one half of the cable was attached to the mountings by cementing the buffer and bare fibre to the capillary tubes taking care not to allow the glue to come in contact with the cut terminal. A single sensor bead of suitable size was then placed in contact with the end of the fibre. The end of the second half of the cable was used to wedge the bead firmly and was glued to the mountings in a similar manner to the first half of the cable. (**Figure 3.3a**) The cyanoacrylate cement was allowed to harden overnight to furnish the completed assembly (**Figure 3.3b & c**). The assembly was connected to a USB2000 miniature fibre optic spectrometer

and lightsource (Ocean Optics, Dunedin, Florida, USA) via the SMA connectors. The assembly was immersed in the aqueous solution of interest and in all cases the full UV–vis spectra were recorded.

To change the sensor bead in the assembly, the assembly was inverted and tapped gently to remove the previous bead. A new bead was placed between the optical fibres under a microscope.

6.3.2 General methods for CPG chemistry

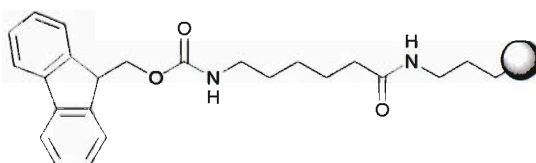
6.3.2.1 Procedure A: Microwave assisted amide bond formation.

Amino CPG (up to 300 mg) was stirred with the protected amino acid (0.5 mmol in 2mL THF) for 10–15 min. DIC (63.1 μ L, 0.5 mmol) was then added and the mixture heated in a sealed reaction vessel with microwave irradiation at 140 °C for 45 min. After reaction, the beads were drained, washed with THF (5 \times 5 mL) followed by DCM (5 \times 5 mL) and dried *in vacuo* overnight.

6.3.2.2 Procedure B: Fmoc deprotection with piperidine

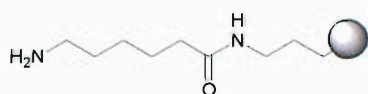
A solution of piperidine (2 mL, 20%, *v/v* in DMF) was added to the CPG beads (up to 375 mg) and shaken for 30 min. The beads were then washed with the 20% piperidine solution (5 \times 5 mL), DMF (5 \times 5 mL) and DCM (5 \times 5 mL) and dried *in vacuo*.

6.3.3 Fmoc- ϵ Ahx-CPG



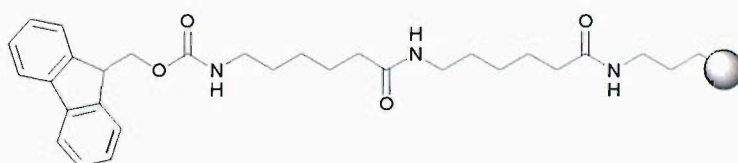
Fmoc- ϵ Ahx was coupled to the aminopropyl CPG (300 mg) according to Procedure A and gave a negative ninhydrin test and an Fmoc loading of 89 μ molg⁻¹. ν_{max} (microscope)/cm⁻¹ 3327br (CONH and OCONH), 2933 (alkyl), 1699 (OCONH), 1626 (CONH), 1543 (CONH and Ar).

6.3.4 ϵ Ahx-CPG



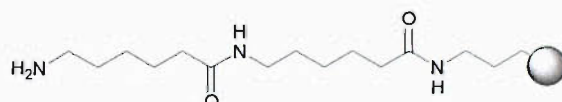
Fmoc- ϵ Ahx-CPG (290 mg) was deprotected with piperidine according to Procedure B to yield white ϵ Ahx-CPG beads. ν_{\max} (microscope)/ cm^{-1} 3307br (CONH), 2933 (alkyl), 1633 (CONH), 1557 (CONH).

6.3.5 Fmoc- ϵ Ahx- ϵ Ahx-CPG



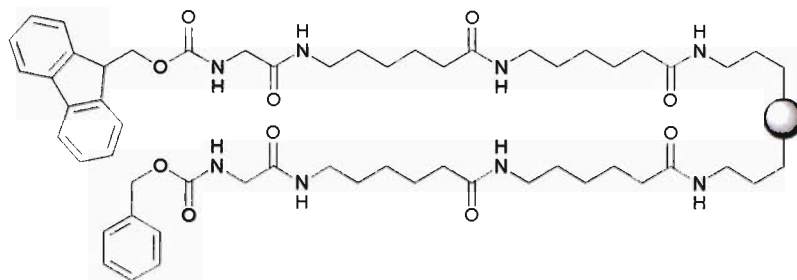
The deprotected ϵ Ahx-CPG (290 mg) was coupled again with Fmoc- ϵ Ahx using Procedure A. These beads had an Fmoc loading of $75 \mu\text{molg}^{-1}$ and a negative ninhydrin test result. ν_{\max} (microscope)/ cm^{-1} 3300br (CONH and OCONH), 2933 (alkyl), 1700 (OCONH), 1637 (CONH), 1550 (CONH or Ar).

6.3.6 ϵ Ahx- ϵ Ahx-CPG



Fmoc- ϵ Ahx- ϵ Ahx-CPG (100 mg) was deprotected using Procedure B to yield white beads. ν_{\max} (microscope)/ cm^{-1} 3300br (CONH), 2933 (alkyl), 1640 (CONH), 1550 (CONH).

6.3.7 Partial Capping of Amino Termini

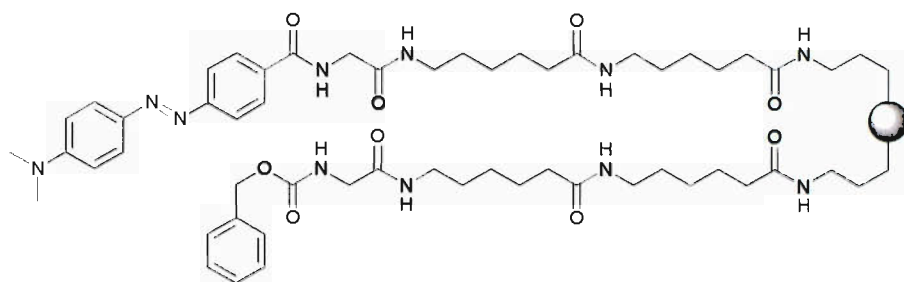


For nominal loadings of 10-100%: A stock solution of HOBt in DMF (208 mg, 1.375 mmol in 5 mL) was prepared and used to prepare stock solutions (2mL) of Cbz-Gly (105 mg, 0.5 mmol) and Fmoc-Gly (149 mg, 0.5 mmol). The appropriate amounts of each solution required to produce molar ratios of 10, 25 and 50% of Fmoc-Gly to Cbz-Gly were mixed to give solutions of 75 μ mol of total amino acid in 300 μ L. To each mixture was added DIC (11.8 μ L, 75 μ mol) and allowed to activate for 5 min before being added to ϵ Ahx₂-CPG (100 mg each batch, 7.5 μ mol) beads. The mixtures were shaken for 4 h, drained, washed with DMF (1.5 mL \times 5), DCM (1.5 mL \times 5) and dried.

For nominal loadings of 1-6%: The Fmoc-Gly stock solution above was further diluted in DMF (200 μ L to 2 mL) and using a combination of this and the Cbz-Gly stock solution above, solutions of the appropriate nominal molar ratio (1, 3, 6%) and amount of total amino acid (75 μ mol each batch) were prepared. These were activated with DIC (11.8 μ L, 75 μ mol) for 5 min, mixed with the ϵ Ahx₂-CPG (100 mg, 7.5 μ mol) and shaken for 4 h. The beads were then washed and dried as above.

All batches gave a negative ninhydrin test and the actual loadings were determined by quantitative Fmoc tests. (**Table 3.1**)

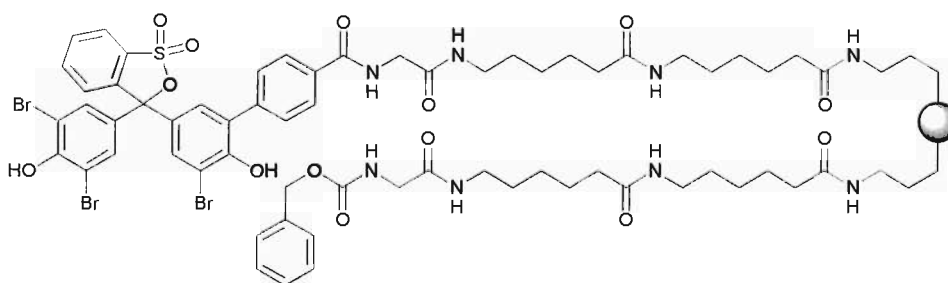
6.3.8 Sensor Beads Bearing *para*-Methyl Red, 3.1



The Fmoc groups were removed according to Procedure B from the partially capped beads with a loading of $16 \mu\text{molg}^{-1}$ (20 mg). A solution of *para*-Methyl Red (500 μL of 0.1M in DMF) was activated for 5 min with DIC (3.9 μL , 25 μmol), added to the deprotected beads and shaken for 3.5 h. The reaction was drained, the beads were washed with DMF ($5 \times 1.5 \text{ mL}$), 20% *v/v* piperidine in DMF ($5 \times 1.5 \text{ mL}$), 5% *v/v* TFA in DCM ($5 \times 1.5 \text{ mL}$) and DCM ($5 \times 1.5 \text{ mL}$). The washing cycle was repeated until no dye could be seen in the washings (usually two cycles) and the beads were dried *in vacuo*. The pink beads gave a negative ninhydrin test. ν_{max} (microscope)/ cm^{-1} 3301br (CONH and OCONH), 2935 (alkyl), 1703 (OCONH), 1638 (CONH), 1544 (CONH and/or Ar).

6.3.9 Sensor Beads Bearing (4-carboxyphenyl)-Bromophenol Blue, 3.2

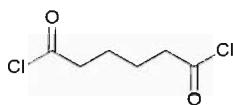
3.2



Fmoc groups were removed according to Procedure B from the partially capped beads with a loading of $5 \mu\text{molg}^{-1}$ (20 mg). (4-carboxyphenyl)-Bromophenol Blue (11.3 mg, 16 μmol) and TFFH²¹⁷ (4.2 mg, 16 μmol) were dissolved in DMF (750 μL) and DIPEA (5.6 μL , 32 μmol) was added. This dye mixture was added to the deprotected beads and shaken for 6 h. The CPG was drained, washed and dried

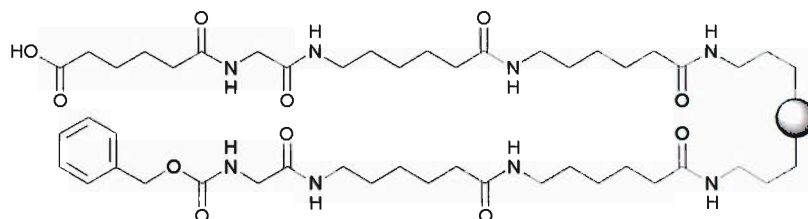
in a similar manner as for **3.1** above. This gave deep yellow beads with a negative ninhydrin test result. ν_{\max} (microscope)/ cm^{-1} 3301br (CONH and OCONH), 2935 (alkyl), 1710 (OCONH), 1642 (CONH), 1550 (CONH and/or Ar).

6.3.10 Adipoyl Dichloride¹⁵²



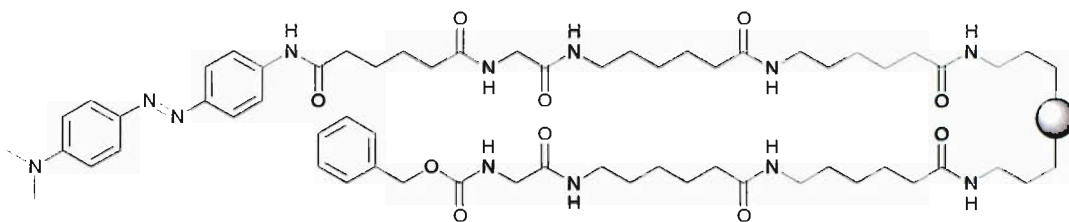
Adipic acid (5.0 g, 34.22 mol) was refluxed ($\sim 80\text{ }^{\circ}\text{C}$) in SOCl_2 (7.5 mL) for 2 h. SOCl_2 was evaporated under reduced pressure and the residue dried *in vacuo* overnight to give the desired product as a yellow oil (6.3 g, quantitative). R_f 0.25 (Hexane:Et₂O, 1:3); ν_{\max} (oil)/ cm^{-1} 1788 (COCl), 928 (COCl), 721 (alkyl); δ_{H} (300 MHz; C₆D₆) 0.78-0.89 (4H, m, 3,4-CH₂), 1.87-1.97, (4H, m, 2,5-CH₂); δ_{C} (75 MHz; C₆D₆) 23.4 (3,4-CH₂), 46.0 (2,5-CH₂), 172.7 (COCl); m/z (EI) 147 (90 %, (M-Cl)⁺), 119 (50 %, (M-COCl)⁺), 111 (100 %, (M-H-2Cl)⁺).

6.3.11 Attachment of Adipic Acid to Partially Capped CPG



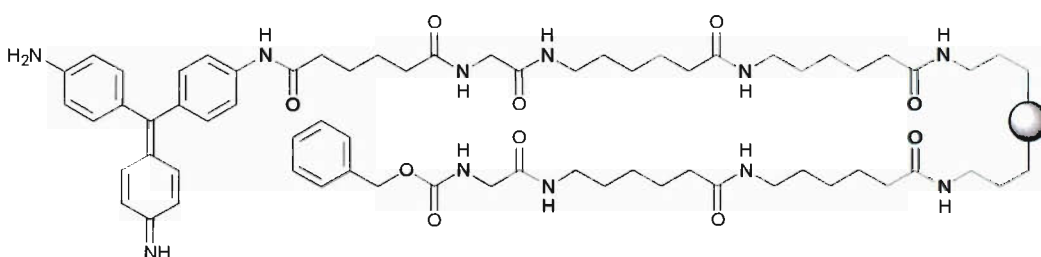
Partially capped Fmoc-protected CPG (60 mg, 5 μmolg^{-1} Fmoc loading) was deprotected according to Procedure B, placed in an air-tight vessel and the purged with N₂. Freshly prepared adipoyl dichloride (145 μL , 1 mmol) was dissolved in freshly distilled DCM (1 mL), cooled in an ice bath and DIPEA (346 μL , 2 mmol) was added. Aliquots of this solution (300 μL) were added to the deprotected CPG and the mixtures shaken under N₂ at RT for 3 h. The CPG was drained, washed with DCM (3 mL \times 3), 50 % v/v water in THF (3 mL \times 3), THF (3 mL \times 3), DCM (3 mL \times 3) and finally dried *in vacuo*. All batches gave a negative result to the ninhydrin test.

6.3.12 Sensor Beads Bearing Disperse Black 3, 3.3



A stock solution of PyBOP (208 mg, 400 μmol) in peptide synthesis grade NMP (2 mL) was prepared and a 300 μL aliquot was mixed with Disperse Black 3 (14.4 mg, 60 μmol) and DIPEA (20.8 μL , 120 μmol) then shaken with the carboxy-CPG (10 mg, from Section 6.3.11) for 16 h, drained and washed with NMP (1.5 mL \times 5), 5 % TFA *v/v* in DCM (1.5 mL \times 5), 5 % Et_3N *v/v* in DCM (1.5 mL \times 5) and DCM (1.5 mL \times 5). The beads were then soaked in NMP (1 mL) for 2 h and drained repeatedly until no further colour could be seen in the solution (usually 4 cycles). The CPG was rinsed again with NMP, TFA and Et_3N solutions and DCM as above and dried *in vacuo*. ν_{max} (microscope)/ cm^{-1} 3293br (CONH and OCONH), 2933 (alkyl), 1713 (OCONH), 1643 (CONH), 1550 (CONH and/or Ar).

6.3.13 Sensor Beads Bearing Pararosaniline, 3.4



The beads were prepared according to the procedure above (Section 6.3.12) except replacing the Disperse Black 3 with Pararosaniline (18.3 mg, 60 μmol). ν_{max} (microscope)/ cm^{-1} 3293br (CONH and OCONH), 2933 (alkyl), 1710 (OCONH), 1640 (CONH or Ar), 1553 (CONH and/or Ar).

6.3.14 Sensor testing

All testing was conducted in a vigorously stirred 1M NaCl bath (500 mL) adjusted to the desired pH by addition of aq. HCl or NaOH solutions. In the response

tests, the UV–vis spectra were recorded every 0.2 s until no further change was observed.

6.4 Experimental procedures for chapter 4

6.4.1 Generation of Split-and-Mix Tripeptide Library on TentaGel

6.4.1.1 Procedure C: Amino acid coupling on TentaGel

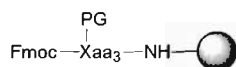
Individual stock solutions of each Fmoc-protected amino acid (600 μmol) in DMF (2 mL, except for Fmoc-Gln, 3 mL) and HOBt (529 mg, 3.5 mmol) in DMF (10 mL) were prepared. Where necessary, these were stored at $< 0\text{ }^{\circ}\text{C}$.

For each coupling cycle, the amino acid (250 μL , 75 μmol ; except for Fmoc-Gln, 375 μL) and HOBt solutions (250 μL , 87.5 μmol) solutions were mixed and DIC (11.8 μL , 75 μmol) added. The mixture was allowed to activate for 5 min before being added to the resin and shaken for 3 h. The resins were drained and washed with DMF (5 \times 3 mL), DCM (5 \times 3 mL), MeOH (3 \times 3 mL), Et₂O (2 \times 3 mL) then dried *in vacuo*. Complete coupling was determined by the ninhydrin test and where necessary, a repeat coupling was conducted.

6.4.1.2 Procedure D: Fmoc deprotection on TentaGel²¹⁶

Resins were shaken with 20 % v/v piperidine in DMF (7 mL) for 5 minutes twice then washed with 20 % v/v piperidine in DMF (5 \times 7 mL), DMF (5 \times 7 mL), DCM (5 \times 7 mL) and dried *in vacuo*.

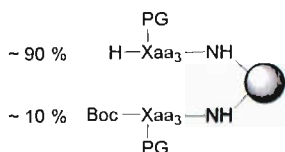
6.4.1.3 Split-and-Mix Tripeptide Library, 4.1⁶



TG resin (85 mg each batch, 0.25 mmol g⁻¹) was coupled to each amino acid according to Procedure C then combined and deprotected according to Procedure D. The combined batches of beads were divided to batches (85 mg each batch) for the next coupling cycle. Subsequent coupling and deprotection cycles according to

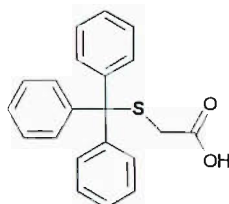
Procedure C & D were carried out until a total of 3 residues were coupled. All batches gave a negative ninhydrin test result after each coupling step.

6.4.2 Partial Boc-Protection of Tripeptide Library, 4.2²¹⁹



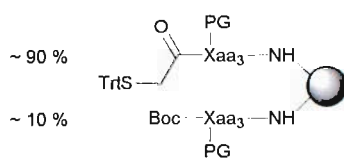
The Fmoc-protected TentaGel library **4.1** (640 mg, 121 μmol) was deprotected using Procedure D. Separately, Boc_2O (26 mg, 121 μmol) was dissolved in DCM (~ 5 mL), DIPEA (42 μL , 242 μmol) added and the solution made up to 10 ml with DCM. The wet resin was then suspended in DCM (5 mL) and 1 mL of the Boc_2O solution was added. The suspension was shaken for 2 h then washed with DCM (15 mL \times 5), MeOH (15 mL \times 5), Et_2O (15 mL \times 5) and dried *in vacuo*.

6.4.3 S-Tryl-2-Mercaptoacetic Acid (S-Tryl-thioglycolic acid)²²⁰



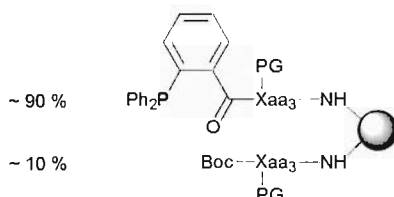
Trityl chloride (6.13 g, 22 mmol) dissolved in DCM (50 mL) and Et_3N (3.07 mL, 22 mmol) was added, followed by thioglycolic acid (1.4 mL, 20 mmol). The solution was stirred for 3 h then extracted twice with water (100 mL), dried with MgSO_4 and evaporated under reduced pressure to give a yellow oil. This oil was triturated with toluene at 40-50 $^\circ\text{C}$ and dried *in vacuo* to yield the desired product as an off-white, odourless solid (2.54 g, 37 %); R_f 0.47 (DCM:MeOH, 9:1) (lit.²²⁰ 0.43); mp 162 $^\circ\text{C}$ (lit.²²⁰ 162.5-163 $^\circ\text{C}$); ν_{max} (solid)/ cm^{-1} 3056br (COOH), 1704 (COOH), 1292 (SCH_2), 746 (Ar); δ_{H} (300 MHz; DMSO-d_6) 2.83 (2H, s, SCH_2), 7.15-7.50 (15H, m, Ph), 12.70 (1H, br s, COOH); δ_{C} (75 MHz; DMSO-d_6) 34.7 (SCH_2), 66.3 (Ph_3C), 127.0 (4-Ph), 128.2 (2-Ph), 129.1 (3-Ph), 144.0 (1-Ph), 170.3 (COOH); m/z (ES-) 447 (100%, (M-H+TFA) $^-$).

6.4.4 S-Tryl-thioglycolic Acid-Capped Tripeptide Library, 4.3a



The partially Boc-protected resin **4.2** (150mg, 26 μ mol free amine) was swollen in DCM (0.4 mL) and a solution of *S*-trityl-2-thioacetic acid (17.5 mg, 52 μ mol), PyBOP (27 mg, 52 μ mol) and DIPEA (18 μ L, 104 μ mol) in DMF (0.7 mL) was added. The suspension was shaken for 4 h, then washed with DMF (3 mL \times 5), DCM (3 mL \times 5), MeOH (3 mL \times 5), Et₂O (3 mL \times 5) and dried *in vacuo* to yield a pale yellow resin which gave a negative ninhydrin test result.

6.4.5 2-(Diphenylphosphino)benzoic Acid-Capped Tripeptide Library, 4.3b



The partially Boc-protected resin **4.2** (150mg, 26 μ mol free amine) was swollen in DCM (0.4 mL). Separately, 2-(diphenylphosphino)benzoic acid (16 mg, 52 μ mol) and HOBt (8 mg, 52 μ mol) was dissolved in DMF (0.7 mL) and DIC (8.1 μ L, 52 μ mol) was added and the mixture allowed to activate for 5 min before addition to the swollen resin. The resin suspension was shaken for 4 h then washed and dried as the *S*-Trityl capped resin. This gave a yellow resin which had a negative ninhydrin test result.

6.4.6 Removal of Side-Chain Protection, Terminal Boc Groups and S-trityl Groups, 4.4a & 4.4b

The resins **4.3a** or **4.3b** were deprotected in 5 mg batches as needed by shaking with 1 mL of a *v/v* mixture of 95% TFA, 2.5% H₂O and 2.5% TIPS for 3 h.

After which the resins were rinsed with TFA (1.5 mL x 3), DCM (1.5 mL x 5), MeOH (1.5 mL x 5), Et₂O (1.5 mL x 5) and dried *in vacuo*.

6.4.7 Metal Chelation and Staining of Tripeptide Libraries

Batches of the libraries **4.3a**, **4.3b**, **4.4a** or **4.4b** (5 mg each) were swollen in MeOH (1 mL) for 10 min and drained. To each batch was then added 1 mL of the metal salt solution at the desired concentration and allowed to mix overnight. The resins were drained and washed with MeOH (1.5 mL x 5) and 1 mL of the staining reagents in a solution of MeOH (either 0.5% *w/v* dithio-oxamide, 1% *w/v* dimethylglyoxime or 1% *w/v* 1-nitroso-2-naphthol) added to the resins. After 10 min, the staining reagents were drained and the resins washed with MeOH (1.5 mL x 5).

6.4.8 Selection and Microspectrometry of Stained Beads

The samples of resin were examined in MeOH under a Leica Leitz DM 1L inverted configuration microscope and the beads of interest from each batch picked with the aid of a 1 μ L micropipette.

The picked beads were then transferred in MeOH to a quartz slide and examined under the UV-Vis microspectrometer. The bead was brought into focus to achieve the maximum transmittance intensity and the spectra recorded as well as the bead size. The spectra of several amino TG beads in MeOH were also recorded for use as references.

The raw data was then processed with Origin 6.1. The transmission spectra of the individual beads were then scaled to an average transmittance spectra of 7 beads from the same library without the complexed metal in MeOH. The intensity of the spectra were adjusted to match the reference transmittance at 308 nm and if possible, at 758 nm. The absorbance was calculated with the corrected transmittances and then adjusted again according to the measured bead size.

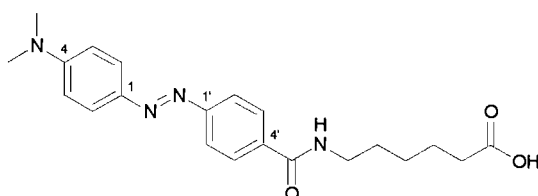
6.4.9 Preparation of Beads for Edman Sequencing

The individual beads selected for sequencing were treated with 5 μ L of a v/v mixture of 95% TFA and 5% H₂O for 1 h to remove the terminal Boc and side-chain protection then air dried.

6.5 Experimental procedures for chapter 5

6.5.1 Synthesis of Chiral Probes

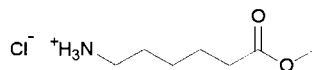
6.5.1.1 pMR- ϵ Ahx, 5.8



para-Methyl Red (1616 mg, 6 mmol) and HOSu (863 mg, 7.5 mmol) were dissolved in dry, degassed DMF (80 mL) with mild heating. DCCI (1279 mg, 6.2 mmol) dissolved in DMF (5 mL) was added dropwise to the dye/HOSu solution and stirred for 48 h. Water (0.5 mL) was added to mixture and stirred for 0.5 h to neutralize excess DCCI. The solution was filtered to remove precipitated DCU, ϵ Ahx (788 mg, 6 mmol) was added and the solution stirred for a further 24 h. The solution was then evaporated under reduced pressure and the red residue purified by flash column chromatography using the eluent noted below to give the product as a red solid (1595 mg, 70 %); R_f 0.40 (Hexane:EtOAc:AcOH, 1:1:0.01); HPLC method S5OD: 220 nm, 3.44 min, S15OD: 220 nm, 8.09 min; mp 205-208 °C; (Found: C, 65.9; H, 6.9; N, 14.4. C₂₁H₂₆N₄O₃ requires C, 65.9; H, 6.9; N, 14.6%); ν_{\max} (solid)/cm⁻¹ 3377br (CONH), 2929br (COOH), 1703 (COOH), 1597 (CONH), 1546 (CONH), 1366 (ArNMe₂), 1135 (Ar), 818 (Ar); δ_H (400 MHz; C₅D₅N) 1.53 (2H, m, γ -Ahx), 1.80 (4H, m, β,δ -Ahx), 2.50 (2H, t, J 7, α -Ahx), 2.85 (6H, s, N(CH₃)₂), 3.69 (2H, dt, J 6 & 7, ϵ -Ahx), 6.80 (2H, d, J 9, 3-Ar), 8.16 (2H, d, J 9, 2'-Ar), 8.19 (2H, J 9, 2-Ar), 8.47 (2H, d, J 9, 3'-Ar), 9.11 (1H, t, J 6, CONH); δ_C (100 MHz; C₅D₅N) 25.8 (β -Ahx), 27.5 (γ -Ahx), 30.5 (δ -Ahx), 35.2 (α -Ahx), 40.3 (N(CH₃)₂), 40.7 (ϵ -

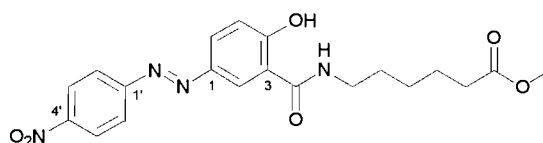
Ahx), 112.5 (3-Ar), 112.9 (2'-Ar), 126.3 (2-Ar), 129.4 (3'-Ar), 137.0 (4'-Ar), 144.5 (1-Ar), 153.7 (4-Ar), 155.6 (1'-Ar), 167.6 (CONH), 176.4 (COOH); *m/z* (ES-) 495 (100%, (M-H+TFA)⁻); (HRMS Found 383.2078, (M+H)⁺ requires 383.2078).

6.5.1.2 εAhx-OMe · HCl²²¹



SOCl₂ (16 mL) was added dropwise to MeOH (100 mL) in a cold water bath. εAhx (13.12 g, 0.1 mol) was then added to the mixture and stirred for 7.5 h at RT. The solution was then evaporated under reduced pressure and the residue triturated with Et₂O to yield the product (14.94 g, 94%) as a white crystalline solid; R_f 0.23 (DCM:MeOH:AcOH, 9:1:0.01); mp 116 °C (lit.²²¹ 120-121 °C); ν_{max} (solid)/cm⁻¹ 2943 (NH₃⁺), 1729 (COOR), 1517 (OMe), 1250, 1190 (all alkyl), 1152 (NH₂R); δ_H (400 MHz; D₂O) 1.45 (2H, tt, *J* 5 & 7, γ-Ahx), 1.65-1.77 (4H, m, β,δ-Ahx), 2.47 (2H, t, *J* 7, α-Ahx), 3.05 (2H, t, *J* 7, ε-Ahx), 3.75 (3H, s, OCH₃); δ_C (100 MHz; D₂O) 22.9 (β-Ahx), 24.2 (γ-Ahx), 25.5 (δ-Ahx), 32.6 (α-Ahx), 38.5 (ε-Ahx), 51.3 (OCH₃), 176.5 (COO); *m/z* (ES+) 209 (100%, (M+Na+MeCN)⁺).

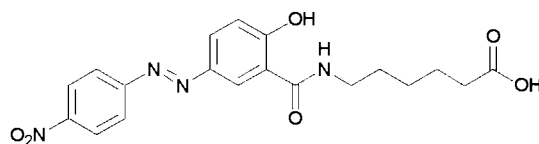
6.5.1.3 MO1-εAhx-OMe



SOCl₂ (3 mL) was added dropwise into THF (4 mL) in an ice bath followed by Mordant Orange 1 (862 mg, 3 mmol) and added and stirred at RT for 4.5 h. The excess SOCl₂ and THF were evaporated under reduced pressure and the brown solid was suspended in 1,4-dioxane (10 mL). DIPEA (1.5 mL) was added to the suspension, followed by εAhx-OMe·HCl (550 mg, 3 mmol) and the mixture was stirred overnight. The solvent was evaporated under reduced pressure and the residue was purified by column chromatography using the eluent noted below to yield the product (442 mg, 36%) as a bright orange solid of which a small sample was recrystallized in MeOH for further analysis; R_f 0.50 (Hexane:EtOAc:AcOH,

3:1:0.01); HPLC method S5OD: 220 nm, 4.62 min, S15OD: 220 nm, 12.16 min; mp 134 °C; (Found: C, 58.0; H, 5.4; N, 13.4. C₂₀H₂₂N₄O₆ requires C, 57.7; H, 5.4; N, 13.5%); ν_{\max} (solid)/cm⁻¹ 3418br (CONH), 2948 (alkyl), 1735 (COOR), 1581 (CONH), 1519 (CONH and Ar), 1494 (ArNO₂), 1340 (ArNO₂), 1172 (ArOH), 843 (Ar); δ_{H} (400 MHz; CDCl₃) 1.35-1.50 (2H, m, γ -Ahx), 1.69 (4H, tt, *J* 7 & 7, β , δ -Ahx), 2.35 (2H, t, *J* 7, α -Ahx), 3.51 (2H, dt, *J* 7 & 7, ϵ -Ahx), 3.65 (3H, s, OCH₃), 6.94 (1H, br s, CONH), 7.09 (1H, d, *J* 9, 5-Ar), 7.90 (2H, m, 2'-Ar), 8.03 (1H, dd, *J* 2 & 9, 6-Ar), 8.13 (1H, d, *J* 2, 2-Ar), 8.33 (2H, m, 3'-Ar), 13.21 (1H, br s, ArOH); δ_{C} (100 MHz; CDCl₃) 24.2 (β -Ahx), 26.3 (γ -Ahx), 28.9 (δ -Ahx), 33.8 (α -Ahx), 39.6 (ϵ -Ahx), 51.7 (OCH₃), 114.5 (3-Ar), 119.7 (5-Ar), 123.1 (2'-Ar), 123.7 (2-Ar), 124.8 (3'-Ar), 127.9 (6-Ar), 144.8 (1-Ar), 148.4 (4'-Ar), 155.9 (1'-Ar), 165.8 (4-Ar), 169.6 (CONH), 174.3 (COO); *m/z* (ES⁺) 851 (100%, (2M+Na)⁺); (HRMS Found 437.1433, (M+Na)⁺ requires 437.1431).

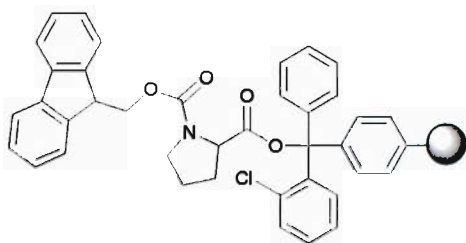
6.5.1.4 MO1- ϵ Ahx, 5.9



The methyl ester (1210 mg, 2.9 mmol) was dissolved in acetone (45 mL) and 1 M aq. NaOH solution (10 mL) was added dropwise with stirring. The dark red solution was stirred for 4 h, taken up in EtOAc (500 mL) and extracted twice with 1 M aq. HCl solution (200 mL), once with water (100 mL) and once with brine (200 mL). The organic phase was then dried with MgSO₄ and evaporated under reduced pressure to the yield an orange solid that was further triturated with hot CHCl₃ to give the desired product (1061 mg, 91 %); *R_f* 0.40 (Hexane:EtOAc:AcOH, 2:1:0.01); HPLC method S5OD: 220 nm, 4.18 min; mp 197 °C; (Found: C, 56.6; H, 5.0; N, 13.7. C₁₉H₂₀N₄O₆ requires C, 57.0; H, 5.0; N, 14.0%); ν_{\max} (solid)/cm⁻¹ 3416 (CONH and ArOH), 2935br (COOH), 1703 (COOH), 1642 (CONH), 1579 (CONH), 1520 (ArNO₂), 1494 (Ar), 1343 (COOH and ArNO₂), 1202 (ArOH), 845 (Ar); δ_{H} (400 MHz; C₅D₅N) 1.37-1.48 (2H, m, γ -Ahx), 1.64 (2H, tt, *J* 7 & 8, δ -Ahx), 1.70 (2H, tt, *J* 7 & 8, β -Ahx), 2.38 (2H, t, *J* 7, α -Ahx), 3.53 (2H, dt, *J* 6 & 7, ϵ -Ahx), 7.20

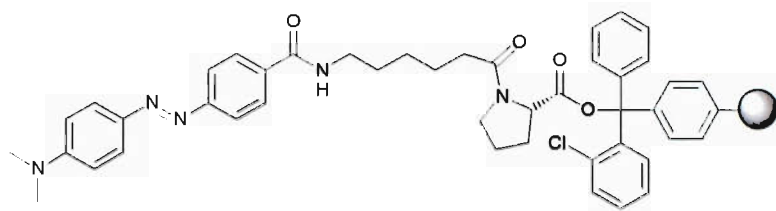
(1H, d, J 9, 5-Ar), 7.74 (2H, d, J 9, 2'-Ar), 8.07 (1H, dd, J 2 & 9, 6-Ar), 8.25 (2H, d, J 9, 3'-Ar), 8.87 (1H, d, J 2, 2-Ar), 9.75 (1H, t, J 6, CONH); δ_c (100 MHz; C_5D_5N) 25.8 (β -Ahx), 27.5 (γ -Ahx), 30.1 (δ -Ahx), 35.2 (α -Ahx), 40.5 (ϵ -Ahx), 117.3 (3-Ar), 119.9 (5-Ar), 124.5 (2'-Ar), 125.6 (3'-Ar), 126.3 (2-Ar), 128.8 (6-Ar), 145.8 (1-Ar), 149.1 (4'-Ar), 156.5 (1'-Ar), 166.5 (4-Ar), 170.3 (CONH), 176.3 (COOH); m/z (ES+) 401 (100%, (M+H)⁺), 801 (10%, (2M+H)⁺), 823 (10%, (2M+Na)⁺), 839 (10%, (2M+K)⁺); (HRMS Found 401.1456, (M+H)⁺ requires 401.1456).

6.5.1.5 Fmoc-(D/L-Pro)-O-Clt-PS



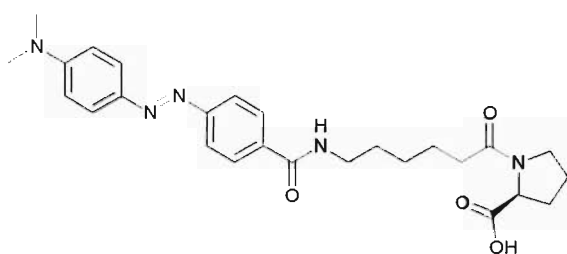
2-Chlorotrityl chloride resin (Cl-Clt-PS, 1 g, 1.5 mmol) was placed in a peptide synthesis vessel and purged with N_2 . Separately, either Fmoc-Pro-OH or Fmoc-D-Pro-OH (675 mg, 2 mmol, dried overnight *in vacuo*) was dissolved in freshly distilled DCM (6 ml) and DIPEA (692 μ l, 4 mmol, dried over KOH) added and mixed. This solution was then added to the resin and the mixture shaken under N_2 for 4 h. The resin was drained and washed with a capping mixture of DCM/MeOH/DIPEA (17:2:1, 4 x 6 ml), distilled DCM (4 x 6 ml), MeOH (4 x 6 ml) and dried *in vacuo*. This afforded a resin with a loading of 0.45 mmolg⁻¹ (Fmoc test) for L-Pro and 0.75 mmolg⁻¹ for D-Pro.

6.5.1.6 *p*MR- ϵ Ahx-Pro-O-Clt-PS



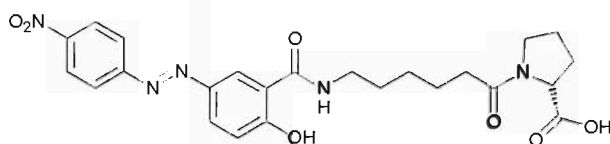
The Fmoc-Pro-O-Clt-PS resin (1g, 0.45 mmol) was shaken with 20% piperidine *v/v* in DMF (6 ml) for 5 min and drained. This was repeated 3 times and the resin washed with 20% piperidine *v/v* in DMF (4 x 6 ml), DMF (2 x 6 ml), distilled DCM and DMF (2 x alternating 6 ml), distilled DCM (4 x 6 ml). *p*MR- ϵ Ahx-OH, **5.8** (258 mg, 0.68 mmol) and PyBOP (351 mg, 0.68 mmol) were dissolved in DMF (4 ml) and DIPEA (234 μ l, 1.35 mmol) added. This solution was then added to the resin and shaken for 3 h. The resin was drained and rinsed with DMF (6 x 6 ml), distilled DCM and DMF (2 x alternating 6 ml), distilled DCM (4 x 6 ml), MeOH (2 x 6 ml), Et₂O (2 x 6 ml) and then dried under constant air flow. This afforded a red resin which showed a quantitative coupling by the chloranil test. ν_{\max} (solid)/cm⁻¹ 2926 (Alkyl), 1745 (COOR), 1656 (CON and CONH), 1600 (CON and CONH), 1446 (ArNMe₂), 1151 (COOR).

6.5.1.7 *p*MR- ϵ Ahx-Pro, **5.6**



The *p*MR- ϵ Ahx-Pro-O-Clt-PS resin (1 g) was swirled with 1 % TFA *v/v* in DCM (6 ml) for 5 min and the red filtrate collected. This was repeated until a colorless solution was eluted (usually 4-5 cycles). The cleavage solutions were combined and evaporated under reduced pressure and the red residue purified by flash column chromatography using the eluent below to yield a dark red solid (279 mg, 100% based on the Fmoc loading of the Fmoc-Pro-O-Clt resin); R_f 0.46

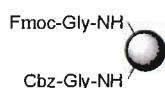
6.5.1.9 MO1- ϵ Ahx-D-Pro-OH, 5.7



The MO1- ϵ Ahx-D-Pro-O-Clt-PS resin (945 mg) was swirled with 1 % TFA *v/v* in DCM (6 ml) for 5 min and the rust red filtrate collected. This was repeated until a colorless solution was eluted (usually 4-5 cycles). These solutions were combined and evaporated under reduced pressure and the brown residue purified by flash column chromatography using the eluent below to yield an orange solid (375 mg, 100% based on the Fmoc loading of the Fmoc-D-Pro-O-Clt-PS resin); R_f 0.51 (EtOAc:DCM:MeOH:AcOH, 20:19:1:0.01); HPLC method S15OD: 220 nm, 10.20 min; ν_{\max} (solid)/ cm^{-1} 3405br (ArOH and COOH), 2935br (COOH), 1728 (COOH), 1640 (CONH and CON), 1586 (CONH and CON), 1522 (ArNO₂), 1342 (ArOH and COOH), 1176 (ArOH); δ_H (400 MHz; CDCl₃) 1.35-1.55 (2H, m, γ -Ahx), 1.55-1.90 (4H, m, β,δ -Ahx), 1.95-2.45 (6H, m, β,γ -Pro & α -Ahx), 3.40-3.70 (4H, m, δ -Pro & ϵ -Ahx), 4.35-4.65 (1H, m, α -Pro), 7.06 (1H, d, J 9, 5-Ar), 7.55 (1H, br s, CONH), 7.90-8.05 (3H, m, 6,2'-Ar), 8.25-8.45 (3H, m, 2,3'-Ar); δ_C (100 MHz; CDCl₃) 23.5 (β -Ahx), 24.9 (γ -Pro), 26.0 (γ -Ahx), 28.5 (β,δ -Pro), 34.0 (α -Ahx), 39.3 (ϵ -Ahx), 47.7 (δ -Pro), 59.4 (α -Pro), 114.7 (3-Ar), 119.7 (5-Ar), 123.2 (3'-Ar), 124.9 (2'-Ar), 125.4 (2-Ar), 126.9 (6-Ar), 144.9 (1-Ar), 148.4 (4'-Ar), 155.9 (1'-Ar), 165.9 (4-Ar), 169.6 (CONH), 173.8 (CON), 174.0 (COOH); m/z (ES-) 610 (100%, (M-H+TFA)⁻), 992 (20%, (2M-H)⁻), 1490 (10%, (3M-H)⁻); (HRMS Found 498.1984, (M+H)⁺ requires 498.1983).

6.5.2 Synthesis of Resin-Bound Amino Acid Substrates

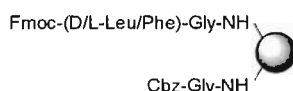
6.5.2.1 Partial capping of amino termini



Separately, Cbz-Gly (628 mg, 3 mmol) and Fmoc-Gly (892 mg, 3 mmol) were each dissolved in DMF (5 ml) with HOBt (504 mg, 3.33 mmol). The

appropriate volumes of each stock solution were mixed to produce the molar ratios described in Table 5.1 (0.5 mL, 0.3 mmol total amino acid each) and DIC (47 μL , 0.3 mmol) was added. These mixtures were allowed to react for 5 min and then added to batches of AM-PS (100 mg each batch, 1.11 mmol g^{-1}) which were pre-swollen with DCM (400 μL each batch). The reactions were then shaken for 3 h, drained, washed with DMF (8 \times 3 mL), DCM (5 \times 3 mL), MeOH (3 \times 3 mL), Et₂O (2 \times 3 mL) then dried *in vacuo*. All resins gave a negative result to the ninhydrin test and the Fmoc loading was determined. (Table 5.1)

6.5.2.2 Attachment of *N*-Fmoc-(D/L-Leucine or D/L-Phenylalanine) to polystyrene at specified enantiomeric ratios



Batches of low-loading resin from the previous section (50 mg each batch, $41 \mu\text{mol g}^{-1}$) were shaken with 20 % *v/v* piperidine in DMF (1 mL) for 5 min twice. The resins were then rinsed with the piperidine solution (3 \times 1 mL), DMF (3 \times 1 mL), DCM (5 \times 1 mL) and drained. For the leucine-loaded beads, Fmoc-Leu (70.7 mg, 200 μmol) and HOBt (33.3 mg, 220 μmol) was dissolved in DMF (\sim 0.5 mL). DIC (31.3 μL , 200 μmol) was added to the solution and allowed to mix for 10 min and then made up to 2 mL with DMF to give a 0.1 M solution of activated amino acid. A separate solution for the other Leu enantiomer was also prepared. From these two stock solutions of activated Fmoc-Leu, the appropriate volumes of were mixed to give the desired enantiomeric ratio (20.5 μmol of total activated amino acid enantiomers in 205 μL each batch). The mixture of enantiomers was added to the moist resins with an additional 100 μL DMF and shaken for 19 h. The resins were washed with DMF (5 \times 1 mL), DCM (3 \times 1 mL), MeOH (3 \times 1 mL), Et₂O (2 \times 1 mL) and dried *in vacuo*. All resins produced a negative ninhydrin test result.

The phenylalanine resins were produced in a similar procedure using Fmoc-Phe & Fmoc-D-Phe instead (77.5 mg, 200 μmol of each enantiomer).

6.5.3 Chiral Resolution of Resins with Pseudoenantiomeric Probes

Resins bearing each enantiomeric mixture (5 mg each batch) were deprotected by mixing with 20 % *v/v* piperidine in DMF (10 mL) for 10 min twice, then washed with DMF (5 × 1 mL). DMF (20 mL) was added to the beads and the mixtures cooled to approx. -30 or -50 °C in an acetone/water/NaCl bath with solid CO₂.

A mixture of the probes **5.6** and **5.7** (0.48 mmol each probe, 1:1 mol. ratio by NMR) and HOPfp (442 mg, 2.4 mmol) was made up with DMF (to 25 mL) to produce a stock solution of the probes and HOPfp. The coupling agents DIC (15.1 μL, 96 μmol) or FDPP²¹⁵ (36.9 mg, 96 μmol) was added to 2.5 mL (48 μmol of each probe) of the stock probe/HOPfp mixture. Where DIC was used, the solution was allowed to preactivate for 10 min before being made up to a final volume of 10 mL with DMF. With FDPP, DIPEA (62.3 μL, 360 μmol) was added and the solution immediately made up to 10 mL with DMF.

Aliquots of the activated probe solution (625 μL, 3 μmol each probe) were added to each batch of cooled resin and gently agitated for 8 h. During this time, the temperature was maintained within the desired range (**Table 5.2**) by intermittent addition of solid CO₂ to the bath. The resins were then drained and rinsed with DMF at -20 °C (10 × 2 mL), DMF at RT (10 × 2 mL), DCM (5 × 2 mL), MeOH (3 × 2 mL), Et₂O (2 × 2 mL) and allowed to dry at RT o.n.

6.5.4 UV-Vis Microspectrometry of Resins Post-Resolution

For detection of probe **5.6**, the resins were washed with 160 mM HCl in 1,4-dioxane (3 × 2 mL) and soaked for at least 1 h in the same solution (2 mL). The UV-Vis spectra from each batch were then taken in this acidic solution according to the usual method against reference spectra from Cbz-Gly-PS resin. For the detection of probe **5.7**, the resins were treated in a similar way as above but using 64 mM DBU in 1,4-dioxane instead.

Data processing and calculations for Equation 5.1 & 5.5 were conducted with Origin ver. 6.1.

References

- 1) K. C. Nicolaou, J. A. Pfefferkorn, in *Handbook of Combinatorial Chemistry: Drugs, Catalysts, Materials*, eds. K. C. Nicolaou, R. Hanco, W. Hartwig, Wiley-VCH, Weinheim, 2002, p. 613-642.
- 2) V. Krchňák, M. W. Holladay, *Chem. Rev.*, 2002, **102**, 61-91.
- 3) G. R. Marshall, *J. Peptide Sci.*, 2003, **9**, 534-544.
- 4) F. Sebestyén, G. Dibó, A. Kovács, Á. Furka, *Bioorg. Med. Chem. Lett.*, 1993, **3**, 413-418.
- 5) A. Furka, *Drug Discovery Today*, 2002, **7(Suppl.)**, 1-4.
- 6) A. Tuch, S. Wallé, in *Handbook of Combinatorial Chemistry: Drugs, Catalysts, Materials*, eds. K. C. Nicolaou, R. Hanco, W. Hartwig, Wiley-VCH, Weinheim, 2002, p. 685-705.
- 7) M. H. Todd, C. Abell, *Analyst*, 2002, **127**, 1399-1406.
- 8) B. Yan, C. F. Jewell Jr., S. W. Myers, *Tetrahedron*, 1998, **54**, 11755-11766.
- 9) L. C. Dorman, *Tetrahedron Lett.*, 1969, **10**, 2319-2321.
- 10) B. J. Egner, M. Bradley, *Drug Discovery Today*, 1997, **2**, 102-109.
- 11) M. A. Gallop, W. L. Fitch, *Curr. Opin. Chem. Biol.*, 1997, **1**, 94-100.
- 12) M. Dal Cin, S. Davalli, C. Marchioro, M. Passarini, O. Perini, S. Provera, A. Zaramella, *Farmaco*, 2002, **57**, 497-510.
- 13) J. J. Scicinski, M. S. Congreve, C. Kay, S. V. Ley, *Curr. Med. Chem.*, 2002, **9**, 2103-2127.
- 14) G. Sabatino, M. Chelli, A. Brandi, A. M. Papini, *Curr. Org. Chem.*, 2004, **8**, 291-301.
- 15) E. Kaiser, R. L. Colescott, C. D. Bossinger, P. I. Cook, *Anal. Biochem.*, 1970, **34**, 595-598.
- 16) V. K. Sarin, S. B. Kent, J. P. Tam, R. B. Merrifield, *Anal. Biochem.*, 1981, **117**, 147-157.
- 17) J. Vázquez, G. Qushair, F. Albericio, *Methods Enzymol.*, 2003, **369**, 21-35.
- 18) C. Kay, O. E. Lorthioir, N. J. Parr, M. Congreve, S. C. McKeown, J. J. Scicinski, S. V. Ley, *Biotechnol. Bioeng.*, 2001, **71**, 110-118.
- 19) S. Punna, M. G. Finn, *Synlett*, 2004, 99-100.
- 20) A. M. Felix, M. H. Jimenez, *Anal. Biochem.*, 1973, **52**, 377-381.

- 21) W. S. Hancock, J. E. Battersby, *Anal. Biochem.*, 1976, **71**, 260-264.
- 22) A. Madder, N. Farcy, N. G. C. Hosten, H. De Muynck, P. J. De Clercq, J. Barry, A. P. Davis, *Eur. J. Org. Chem.*, 1999, **1999**, 2787-2791.
- 23) T. Vojtkovsky, *Peptide Res.*, 1995, **8**, 236-237.
- 24) J. Mařík, A. Song, K. S. Lam, *Tetrahedron Lett.*, 2003, **44**, 4319-4320.
- 25) E. Kaiser, C. D. Bossinger, R. L. Colescott, D. B. Olsen, *Anal. Chim. Acta*, 1980, **118**, 149-151.
- 26) A. Shah, S. S. Rahman, V. de Biasi, P. Camilleri, *Anal. Commun.*, 1997, **34**, 325-328.
- 27) V. Krchňák, J. Vágner, P. Šafář, M. Lebl, *Collect. Czech. Chem. Commun.*, 1988, **53**, 2542-2548.
- 28) B. F. Gisin, *Anal. Chim. Acta*, 1972, **58**, 248-249.
- 29) M. Flegel, R. C. Sheppard, *Chem. Commun.*, 1990, 536-538.
- 30) M. P. Reddy, P. J. Voelker, *Int. J. Peptide Protein Res.*, 1988, **31**, 345-348.
- 31) S. S. Chu, S. H. Reich, *Bioorg. Med. Chem. Lett.*, 1995, **5**, 1053-1058.
- 32) P. D. White, W. C. Chan, in *Fmoc Solid Phase Peptide Synthesis: A Practical Approach*, eds. P. D. White, W. C. Chan, Oxford University Press, Oxford, 2000, p. 9-40.
- 33) O. Kuisle, M. Lolo, E. Quiñoá, R. Riguera, *Tetrahedron*, 1999, **55**, 14807-14812.
- 34) M. E. Attardi, A. Falchi, M. Taddei, *Tetrahedron Lett.*, 2000, **41**, 7395-7399.
- 35) M. E. Attardi, M. Taddei, *Tetrahedron Lett.*, 2001, **42**, 2927.
- 36) B. A. Burkett, R. C. D. Brown, M. M. Meloni, *Tetrahedron Lett.*, 2001, **42**, 5773-5775.
- 37) J. G. Breitenbucher, C. R. Johnson, M. Haight, J. C. Phelan, *Tetrahedron Lett.*, 1998, **39**, 1295-1298.
- 38) B. Yan, L. Liu, C. A. Astor, Q. Tang, *Anal. Chem.*, 1999, **71**, 4564-4571.
- 39) V. Swali, PhD Thesis, University of Southampton, 2000.
- 40) J. P. Badyal, A. M. Cameron, N. R. Cameron, D. M. Coe, R. Cox, B. G. Davis, L. J. Oates, G. Oye, P. G. Steel, *Tetrahedron Lett.*, 2001, **42**, 8531-8533.
- 41) C. E. Freeman, A. G. Howard, *Analyst*, 2001, **126**, 538-541.
- 42) S. K. Shannon, G. Barany, *J. Comb. Chem.*, 2004, **6**, 165-170.
- 43) B. Yan, W. Li, *J. Org. Chem.*, 1997, **62**, 9354-9357.

- 44) J. J. Cournoyer, T. Kshirsagar, P. P. Fantauzzi, G. M. Figliozzi, T. Makdessian, B. Yan, *J. Comb. Chem.*, 2002, **4**, 120-124.
- 45) J. Vázquez, F. Albericio, *Tetrahedron Lett.*, 2001, **42**, 6691-6693.
- 46) M. E. Attardi, G. Porcu, M. Taddei, *Tetrahedron Lett.*, 2000, **41**, 7391-7394.
- 47) F. Galindo, B. Altava, M. I. Burguete, R. Gavata, S. V. Luis. *J. Comb. Chem.*, 2004, **6**, 859-861.
- 48) J. K. Cho, P. D. White, W. Klute, T. W. Dean, M. Bradley, *J. Comb. Chem.*, 2003, **5**, 632-636.
- 49) J. K. Cho, P. D. White, W. Klute, T. W. Dean, M. Bradley, *Chem. Commun.*, 2004, 502-503.
- 50) H. Schröder, *Comb. Chem. High Throughput Screening*, 2003, **6**, 741-753.
- 51) P. A. Keifer, *Drug Discovery Today*, 1997, **2**, 468-478.
- 52) G. C. Look, C. P. Holmes, J. P. Chinn, M. A. Gallop, *J. Org. Chem.*, 1994, **59**, 7588-7590.
- 53) C. R. Johnson, B. Zhang, *Tetrahedron Lett.*, 1995, **36**, 9253-9256.
- 54) A. Svensson, T. Fex, J. Kihlberg, *Tetrahedron Lett.*, 1996, **37**, 7649-7652.
- 55) D. Stones, D. J. Miller, M. W. Beaton, T. J. Rutherford, D. Gani, *Tetrahedron Lett.*, 1998, **39**, 4875-4878.
- 56) M. J. Shapiro, J. S. Gounarides, *Biotechnol. Bioeng.*, 2001, **71**, 130-148.
- 57) P. A. Keifer, *J. Org. Chem.*, 1996, **61**, 1558-1559.
- 58) M. Grøtli, C. H. Gotfredsen, J. Rademann, J. Buchardt, A. J. Clark, J. Ø. Duus, M. Meldal, *J. Comb. Chem.*, 2000, **2**, 108-119.
- 59) J. Blas, A. Rivera-Sagredo, R. Ferritto, J. F. Espinosa, *Magn. Reson. Chem.*, 2004, **42**, 950-954.
- 60) R. Hany, D. Rentsch, B. Dhanapal, D. Obrecht, *J. Comb. Chem.*, 2001, **3**, 85-89.
- 61) M. Drew, E. Orton, P. Krolikowski, J. M. Salvino, N. V. Kumar, *J. Comb. Chem.*, 2000, **2**, 8-9.
- 62) Y. Yamane, M. Matsui, H. Kimura, S. Kuroki, I. Ando, *J. Appl. Polym. Sci.*, 2003, **89**, 413-421.
- 63) G. Siuzdak, J. K. Lewis, *Biotechnol. Bioeng.*, 1998, **61**, 127-134.

- 64) R. Süßmuth, A. Trautwein, H. Richter, G. Nicholson, G. Jung, in *Combinatorial Chemistry: Synthesis, Analysis, Screening*, ed. G. Jung, Wiley-VCH, Weinheim, 1999, p. 499-532.
- 65) D. B. Kassel, *Chem. Rev.*, 2001, **101**, 255-267.
- 66) C. Enjalbal, D. Maux, J. Martinez, R. Combarieu, J.-L. Aubagnac, *Comb. Chem. High Throughput Screening*, 2001, **4**, 363-373.
- 67) R. A. Zambias, D. A. Boulton, P. R. Griffin, *Tetrahedron Lett.*, 1994, **35**, 4283-4286.
- 68) B. J. Egner, G. J. Langley, M. Bradley, *J. Org. Chem.*, 1995, **60**, 2652-2653.
- 69) B. J. Egner, M. Cardno, M. Bradley, *Chem. Commun.*, 1995, 2163-2164.
- 70) M. C. Fitzgerald, K. Harris, C. G. Shevlin, G. Siuzdak, *Bioorg. Med. Chem. Lett.*, 1996, **6**, 979-982.
- 71) M. R. Carrasco, M. C. Fitzgerald, Y. Oda, S. B. H. Kent, *Tetrahedron Lett.*, 1997, **38**, 6331-6334.
- 72) J. M. Gerdes, H. Waldmann, *J. Comb. Chem.*, 2003, **5**, 814-820.
- 73) C. L. Brummel, I. N. W. Lee, Y. Zhou, S. J. Benkovic, N. Winograd, *Science*, 1994, **264**, 399-402.
- 74) N. Winograd, R. M. Braun, *Spectroscopy*, 2001, **16**, 14-27.
- 75) C. Enjalbal, D. Maux, R. Combarieu, J. Martinez, J.-L. Aubagnac, *J. Comb. Chem.*, 2003, **5**, 102-109.
- 76) J.-L. Aubagnac, C. Enjalbal, C. Drouot, R. Combarieu, J. Martinez, *J. Mass Spectrom.*, 1999, **34**, 749-754.
- 77) J. Y. Xu, R. M. Braun, N. Winograd, *Anal. Chem.*, 2003, **75**, 6155-6162.
- 78) K. Heinze, U. Winterhalter, T. Jannack, *Chem. Eur. J.*, 2000, **6**, 4203-4210.
- 79) D. Chávez, A. Ochoa, D. Madrigal, M. Castillo, K. Espinoza, T. González, E. Vélez, J. Meléndez, J. D. Garcia, I. A. Rivero, *J. Comb. Chem.*, 2003, **5**, 149-154.
- 80) M. S. Congreve, S. V. Ley, J. J. Scicinski, *Chem. Eur. J.*, 2002, **8**, 1768-1776.
- 81) P. J. Murray, C. Kay, J. J. Sciciński, S. C. McKeown, S. P. Watson, R. A. E. Carr, *Tetrahedron Lett.*, 1999, **40**, 5609-5612.
- 82) S. C. McKeown, S. P. Watson, R. A. E. Carr, P. Marshall, *Tetrahedron Lett.*, 1999, **40**, 2407-2410.

- 83) G. M. Williams, R. A. E. Carr, M. S. Congreve, C. Kay, S. C. McKeown, P. J. Murray, J. J. Scicinski, S. P. Watson, *Angew. Chem., Int. Ed.*, 2000, **39**, 3293-3296.
- 84) H-U Gremlich, *Biotechnol. Bioeng.*, 1998, **61**, 179-187.
- 85) R. H. Webb, *Methods Enzymol.*, 1999, **307**, 3-20.
- 86) S. R. McAlpine, S. L. Schreiber, *Chem. Eur. J.*, 1999, **5**, 3528-3532.
- 87) S. R. McAlpine, C. W. Lindsley, J. C. Hodges, D. M. Leonard, G. F. Filzen, *J. Comb. Chem.*, 2001, **3**, 1-5.
- 88) F. López Arbeloa, P. Ruiz Ojeda, I. López Arbeloa, *J. Lumin.*, 1989, **44**, 105-112.
- 89) J. Kress, R. Zanaletti, A. Rose, J. G. Frey, W. S. Brocklesby, M. Ladlow, M. Bradley, *J. Comb. Chem.*, 2003, **5**, 28-32.
- 90) J. Rademann, M. Barth, R. Brock, H.-J. Egelhaaf, G. Jung, *Chem. Eur. J.*, 2001, **7**, 3884-3889.
- 91) W. Denk, J. H. Strickler, W. W. Webb, *Science*, 1990, **248**, 73-76.
- 92) R. A. Farrer, G. T. Copeland, M. J. R. Previte, M. M. Okamoto, S. J. Miller, J. T. Fourkas, *J. Am. Chem. Soc.*, 2002, **124**, 1994-2003.
- 93) B. Yan, P. C. Martin, J. Lee, *J. Comb. Chem.*, 1999, **1**, 78-81.
- 94) R. V. Ulijn, I. Brazendale, G. Margetts, S. L. Flitsch, G. McConnell, J. Girkin, P. J. Halling, *J. Comb. Chem.*, 2003, **5**, 215-217.
- 95) W. Huber, A. Bubendorf, A. Grieder, D. Obrecht, *Anal. Chim. Acta*, 1999, **393**, 213-221.
- 96) B. Yan, H.-U. Gremlich, *J. Chromatogr. B*, 1999, **725**, 91-102.
- 97) B. Yan, G. Kumaravel, H. Anjaria, A. Wu, R. C. Petter, C. P. Jewell Jr., J. R. Wareing, *J. Org. Chem.*, 1995, **60**, 5736-5738.
- 98) J. E. Katon, *Micron*, 1996, **27**, 303-314.
- 99) B. Yan, G. Kumaravel, *Tetrahedron*, 1996, **52**, 843-848.
- 100) Y. R. de Miguel, A. S. Shearer, *Biotechnol. Bioeng.*, 2000, **71**, 119-129.
- 101) K. Russell, D. C. Cole, F. M. McLaren, D. E. Pivonka, *J. Am. Chem. Soc.*, 1996, **118**, 7941-7945.
- 102) B. Yan, J. B. Fell, G. Kumaravel, *J. Org. Chem.*, 1996, **61**, 7467-7472.
- 103) W. Li, B. Yan, *J. Org. Chem.*, 1998, **63**, 4092-4097.
- 104) B. Yan, Q. Tang, *Ind. Eng. Chem. Res.*, 2003, **42**, 5964-5967.

- 105) D. E. Pivonka, K. Russell, T. Gero, *Appl. Spectrosc.*, 1996, **50**, 1471-1478.
- 106) D. E. Pivonka, D. L. Palmer, *J. Comb. Chem.*, 1999, **1**, 294-296.
- 107) D. E. Pivonka, D. L. Palmer, T. W. Gero, *Appl. Spectrosc.*, 1999, **53**, 1027-1032.
- 108) D. E. Pivonka, T. R. Simpson, *Anal. Chem.*, 1997, **69**, 3851-3853.
- 109) D. E. Pivonka, *J. Comb. Chem.*, 2000, **2**, 33-38.
- 110) B. Yan, H. Yan, *J. Comb. Chem.*, 2001, **3**, 78-84.
- 111) S. S. Rahman, D. J. Busby, D. C. Lee, *J. Org. Chem.*, 1998, **63**, 6196-6199.
- 112) W. J. Haap, T. B. Walk, G. Jung, *Angew. Chem., Int. Ed.*, 1998, **37**, 3311-3314.
- 113) C. M. Snively, G. Oskarsdottir, J. Lauterbach, *J. Comb. Chem.*, 2000, **2**, 243-245.
- 114) G. S. Mandair, A. E. Russell, G. Aston, M. Bradley, *Mol. Divers.*, 2004, **8**, 135-139.
- 115) G. S. Mandair, Z. Yu, N. Galaffu, M. Bradley, A. E. Russell, *Appl. Spectrosc.*, 2004, **58**, 43-48.
- 116) J. R. Ferraro, K. Nakamoto, *Introductory Raman Spectroscopy*, Academic Press, Boston, 1994, p. 1-94.
- 117) B. Due Larson, D. H. Christensen, A. Holm, R. Zillmer, O. Faurskov Nielsen, *J. Am. Chem. Soc.*, 1993, **115**, 6247-6253.
- 118) J. Ryttersgaard, B. Due Larsen, A. Holm, D. H. Christensen, O. Faurskov Nielsen, *Spectrochim. Acta A*, 1997, **53**, 91-98.
- 119) D. E. Pivonka, R. B. Sparks, *Appl. Spectrosc.*, 2000, **54**, 1584-1590.
- 120) B. Yan, H.-U. Gremlich, S. Moss, G. M. Coppola, Q. Sun, L. Liu, *J. Comb. Chem.*, 1999, **1**, 46-54.
- 121) J. Kress, A. Rose, J. G. Frey, W. S. Brocklesby, M. Ladlow, G. W. Mellor, M. Bradley, *Chem. Eur. J.*, 2001, **7**, 3880-3883.
- 122) M. P. Houlne, C. M. Sjostrom, R. H. Uibel, J. A. Kleimeyer, J. M. Harris, *Anal. Chem.*, 2002, **74**, 4311-4319.
- 123) A. Ashkin, *Proc. Natl. Acad. Sci. USA*, 1997, **94**, 4853-4860.
- 124) D. H. Williams, I. Fleming, *Spectroscopic Methods in Organic Chemistry*, McGraw-Hill, London, 1995, p. 1-27.

- 125) J. B. Lambert, H. F. Shurvell, D. A. Lightner, R. G. Cooks, *Organic Structural Spectroscopy*, Prentice Hall, Upper Saddle River, 1999, p. 252-273.
- 126) G. B. Fields, R. L. Noble, *Int. J. Peptide Protein Res.*, 1990, **35**, 161-214.
- 127) E. Sawicki, *J. Org. Chem.*, 1957, **22**, 1084-1088.
- 128) D. Escolar, M. R. Haro, A. Saucedo, J. Ayuso, A. Jimenez, J. A. Alvarez, *Appl. Spectrosc.*, 1996, **50**, 1290-1294.
- 129) E. Şeclăman, A. Salló, F. Elenes, C. Crăşmăreanu, C. Wikete, S. Timofei, Z. Simon, *Dyes Pigments*, 2002, **55**, 69-77.
- 130) Z. Shen, Y. Zhang, Y. Chen, *Synth. Commun.*, 2000, **30**, 2525-2532.
- 131) K. Barlos, D. Gatos, W. Schäfer, *Angew. Chem., Int. Ed.*, 1991, **30**, 590-593.
- 132) M. J. P. Leiner, O. S. Wolfbeis, in *Fibre Optic Chemical Sensors and Biosensors*, ed. O. S. Wolfbeis, CRC Press, Boca Raton, 1991, vol. 1, p. 359-384.
- 133) C. Sanchez, B. Lebeau, F. Chaput, J.-P. Boilot, *Adv. Mater.*, 2003, **15**, 1969-1994.
- 134) M. Mehrvar, C. Bis, J. M. Scharer, M. Moo-Young, J. H. Luong, *Anal. Sci.*, 2000, **16**, 677-692.
- 135) J. Lin, C. W. Brown, *Trends Anal. Chem.*, 1997, **16**, 200-211.
- 136) J. M. López-Higuera, in *Handbook of Optical Fibre Sensing Technology*, ed. J. M. López-Higuera, John-Wiley, Chichester, 2002, p. 1-22.
- 137) T. M. Butler, B. D. MacCraith, C. McDonagh, *J. Non-Cryst. Solids*, 1998, **224**, 249-258.
- 138) A. Lobnik, I. Oehme, I. Murkovic O. S. Wolfbeis, *Anal. Chim. Acta*, 1998, **367**, 159-165.
- 139) R. Makote, M. M. Collinson, *Anal. Chim. Acta*, 1999, **394**, 195-200.
- 140) E. Wang, K.-F. Chow, V. Kwan, T. Chin, C. Wong, A. Bocarsly, *Anal. Chim. Acta*, 2003, **495**, 45-50.
- 141) T. Seçkin, A. Gültek, S. Kartaca, *Dyes Pigments*, 2003, **56**, 51-57.
- 142) H. E. Posch, M. J. P. Leiner, O. S. Wolfbeis, *Fresenius Z. Anal. Chem.*, 1989, **334**, 162-165.
- 143) G. E. Badini, K. T. V. Grattan, A. C. C. Tseung, *Analyst*, 1995, **120**, 1025-1028.
- 144) L. A. Saari, W. R. Seitz, *Anal. Chem.*, 1982, **54**, 821-823.

- 145) Y. Kostov, S. Tzonkov, L. Yotova, M. Krysteva, *Anal. Chim. Acta*, 1993, **280**, 15-19.
- 146) O. S. Wolfbeis, N. V. Rodriguez, T. Werner, *Mikrochim. Acta*, 1992, **108**, 133-141.
- 147) G. J. Mohr, O. S. Wolfbeis, *Anal. Chim. Acta*, 1994, **292**, 41-48.
- 148) R. Haag, A. Hebel, J.-F. Stumbé, in *Handbook of Combinatorial Chemistry: Drugs, Catalysts, Materials*, eds. K. C. Nicolaou, R. Hanco, W. Hartwig, Wiley-VCH, Weinheim, 2002, vol. 1, p. 24-58.
- 149) R. L. Heinemann, *Stain Technol.*, 1970, **45**, 165-172.
- 150) F. J. Green, *The Sigma-Aldrich Handbook of Stains, Dyes and Indicators*, Aldrich Chemical Company, Milwaukee, 1991, p. 220-221.
- 151) G. B. Harper, *Anal. Chem.*, 1975, **47**, 348-351.
- 152) H. Liu, T.-M. Cheng, H.-M. Zhang, R.-T. Li, *Arch. Pharm. Pharm. Med. Chem.*, 2003, **336**, 510-513.
- 153) O. S. Wolfbeis, C. Huber, T. Werner, in *Chemosensors of Ion and Molecule Recognition*, eds. J. P. Desvergne, A. W. Czarnik, Kluwer Academic, Dordrecht, 1996, p. 61-74.
- 154) M. C. Aragoni, M. Arca, G. Crisponi, V. M. Nurchi, R. Silvagni, *Talanta*, 1995, **42**, 1157-1163.
- 155) N. O. Mchedlov-Petrossyan, V. I. Kukhtik, V. D. Bezugliy, *J. Phys. Org. Chem.*, 2003, **16**, 380-397.
- 156) N. C. Deno, J. J. Jaruzelski, A. Schriesheim, *J. Org. Chem.*, 1954, **19**, 155-167.
- 157) H. B. Lueck, J. L. McHale, W. D. Edwards, *J. Am. Chem. Soc.*, 1992, **114**, 2342-2348.
- 158) S. A. Gorman, J. D. Hepworth, D. Mason, *J. Chem. Soc., Perkin Trans. 2*, 2000, 1889-1895.
- 159) S. Stoyanov, L. Antonov, T. Stoyanova, V. Petrova, *Dyes Pigments*, 1996, **32**, 171-185.
- 160) S. Cihelník, I. Stibor, P. Lhoták, *Collect. Czech. Chem. Commun.*, 2002, **67**, 1779-1789.
- 161) A. Noack, A. Schröder, H. Hartmann, *Dyes Pigments*, 2002, **57**, 131-147.
- 162) M. Caldarelli, I R. Baxendale, S. V. Ley, *Green Chem.*, 2000, 43-45.

- 163) J. Merrington, M. James, M. Bradley, *Chem. Commun.*, 2002, 140-141.
- 164) Y. Kostov, S. Tzonkov, L. Yotova, *Analyst*, 1993, **118**, 987-990.
- 165) H. Sigel, R. B. Martin, *Chem. Rev.*, 1982, **82**, 385-426.
- 166) B. Sarkar, *J. Indian Chem. Soc.*, 1982, **59**, 1403-1411.
- 167) S. K. Chapman, *Perspect. Bioinorg. Chem.*, 1991, **1**, 95-140.
- 168) W. Bal, M. Jeżowska-Bojczuk, K. S. Kasprzak, *Chem. Res. Toxicol.*, 1997, **10**, 906-914.
- 169) B. Bóka, A. Myari, I. Sóvágó, N. Hadjiliadis, *J. Inorg. Biochem.*, 2004, **98**, 113-122.
- 170) R. Malin, R. Steinbrecher, J. Janssen, W. Semmler, B. Noll, B. Johannsen, C. Frömmel, W. Höhne, J. Schneider-Mergener, *J. Am. Chem. Soc.*, 1995, **117**, 11821-11822.
- 171) Y. Shi, S. Sharma, *Bioorg. Med. Chem. Lett.*, 1999, **9**, 1469-1474.
- 172) J. A. Bravo, A. Gibson, K. Loughran, M. Bradley, *Chem. Commun.*, 2001, 837-838.
- 173) M. B. Francis, T. F. Jamison, E. N. Jacobsen, *Curr. Opin. Chem. Biol.*, 1998, **2**, 422-428.
- 174) K. Severin, R. Bergs, W. Beck, *Angew. Chem., Int. Ed.*, 1998, **37**, 1634-1654.
- 175) J. J. Gooding, E. Chow, R. Finlayson, *Aust. J. Chem.*, 2003, **56**, 159-162.
- 176) M. T. Burger, W. C. Still, *J. Org. Chem.*, 1995, **60**, 7382-7383.
- 177) M. B. Francis, N. S. Finney, E. N. Jacobsen, *J. Am. Chem. Soc.*, 1996, **118**, 8983-8984.
- 178) N. Shibata, J. E. Baldwin, M. E. Wood, *Bioorg. Med. Chem. Lett.*, 1997, **7**, 413-416.
- 179) L. D. Pettit, J. E. Gregor, H. Kozłowski, *Perspect. Bioinorg. Chem.*, 1991, **1**, 1-41.
- 180) H. Kozłowski, W. Bal, M. Dyba, T. Kowalik-Jankowska, *Coord. Chem. Rev.*, 1999, **184**, 319-346.
- 181) E. Farkas, I. Sóvágó, *Amino Acids, Peptides & Proteins*, 2002, **33**, 295-364.
- 182) K. Burgess, A. I. Liaw, N. Wang, *J. Med. Chem.*, 1994, **37**, 2985-2987.
- 183) G. Svehla, *Vogel's Qualitative Inorganic Analysis*, 6th. Ed, Longman, Harlow, 1987, p. 80, 119, 12.

- 184) P. D. Bailey, *An Introduction to Peptide Chemistry*, Wiley, Chichester, 1990, p. 187-191.
- 185) D. Parker, *Chem. Rev.*, 1991, **91**, 1441-1457.
- 186) T. J. Wenzel, J. D. Wilcox, *Chirality*, 2003, **15**, 256-270.
- 187) T. Toyo'oka, *J. Biochem. Biophys. Methods*, 2002, **54**, 25-56.
- 188) V. Schurig, *Trends Anal. Chem.*, 2002, **21**, 647-661.
- 189) M. T. Reetz, *Angew. Chem., Int. Ed.*, 2001, **40**, 285-310.
- 190) M. T. Reetz, *Angew. Chem., Int. Ed.*, 2002, **41**, 1335-1338.
- 191) M. G. Finn, *Chirality*, 2002, **14**, 534-540.
- 192) G. T. Copeland, S. J. Miller, *J. Am. Chem. Soc.*, 2001, **123**, 6496-9502.
- 193) Y. Xu, M. E. McCarroll, *J. Phys. Chem. A*, 2004, **108**, 6929-6932.
- 194) M. T. Reetz, A. Eipper, P. Tielmann, R. Mynott, *Adv. Synth. Catal.*, 2002, **344**, 1008-1016.
- 195) M. T. Reetz, P. Tielmann, A. Eipper, A. Ross, G. Schlotterbeck, *Chem. Commun.*, 2004, 1366-1367.
- 196) M. T. Reetz, M. H. Becker, H.-W. Klein, D. Stöckigt, *Angew. Chem., Int. Ed.*, 1999, **38**, 1758-1761.
- 197) J. Guo, J. Wu, G. Siuzdak, M. G. Finn, *Angew. Chem., Int. Ed.*, 1999, **38**, 1755-1758.
- 198) L. Wu, R. L. Clark, R. G. Cooks, *Chem. Commun.*, 2003, 136-137.
- 199) P. Tielmann, M. Boese, M. Luft, M. T. Reetz, *Chem. Eur. J.*, 2003, **9**, 3882-3887.
- 200) C. D. Tran, V. I. Grishko, D. Oliveira, *Anal. Chem.*, 2003, **75**, 6455-6462.
- 201) N. Millot, P. Borman, M. S. Anson, I. B. Campbell, S. J. F. Macdonald, M. Mahmoudian, *Org. Process Res. Dev.*, 2002, **6**, 463-470.
- 202) P. Horváth, A. Gergely, B. Noszál, *Talanta*, 1997, **44**, 1479-1485.
- 203) P. R. Gibbs, C. S. Uehara, P. T. Nguyen, R. C. Willson, *Biotechnol. Prog.*, 2003, **19**, 1329-1334.
- 204) M. T. Reetz, K. M. Kühling, A. Deege, H. Hinrichs, D. Belder, *Angew. Chem., Int. Ed.*, 2000, **39**, 3891-3893.
- 205) G. Gübitz, M. G. Schmid, *Electrophoresis*, 2004, **23**, 3981-3996.
- 206) P. Abato, C. T. Seto, *J. Am. Chem. Soc.*, 2001, **123**, 9206-9207.
- 207) Z. Li, L. Bütikofer, B. Witholt, *Angew. Chem., Int. Ed.*, 2004, **43**, 1698-1702.

- 208) H. B. Kagan, J. C. Fiaud, *Top. Stereochem.*, 1988, **18**, 249-330.
- 209) E. Vedejs, X. Chen, *J. Am. Chem. Soc.*, 1997, **119**, 2584-2585.
- 210) G. A. Korbel, G. Lalic, M. D. Shair, *J. Am. Chem. Soc.*, 2001, **123**, 361-362.
- 211) D. D. Diaz, S. Yao, M. G. Finn, *Tetrahedron Lett.*, 2001, **42**, 2617-2619.
- 212) T. Hattori, Y. Minato, S. Yao, M. G. Finn, S. Miyano, *Tetrahedron Lett.*, 2001, **42**, 8015-8018.
- 213) P. Arya, M.-G. Baek, *Curr. Opin. Chem. Biol.*, 2001, **5**, 292-301.
- 214) M. Harre, K. Nickisch, U. Tilstam, *React. Funct. Polym.*, 1999, **41**, 111-114.
- 215) S. Chen, J. Xu, *Tetrahedron Lett.*, 1991, **46**, 6711-6714.
- 216) J. Eichler, M. Bienert, A. Stierandova, M. Lebl, *Peptide Res.*, 1991, **4**, 296-307.
- 217) L. A. Carpino, A. El-Faham, *J. Am. Chem. Soc.*, 1995, **117**, 5401-5402.
- 218) W. Rapp, *Methods Org. Chem. (Houben-Weyl)*, 2002, **E22a**, 672-684.
- 219) I. Lingard, PhD Thesis, University of Southampton, 2002.
- 220) Z. Kupihár, Z. Schmél, Z. Kele, B. Penke, L. Kovács, *Bioorg. Med. Chem.*, 2001, **9**, 1241-1247.
- 221) Y.-M. Lin, M. J. Miller, *J. Org. Chem.*, 2001, **66**, 8282-8285.